

# **For Reference**

---

**NOT TO BE TAKEN FROM THIS ROOM**



Ex LIBRIS  
UNIVERSITATIS  
ALBERTAENSIS







Digitized by the Internet Archive  
in 2019 with funding from  
University of Alberta Libraries

<https://archive.org/details/Hawkins1977>









THE UNIVERSITY OF ALBERTA

RELEASE FORM

NAME OF AUTHOR ..... JAMES R. HAWKINS .....

TITLE OF THESIS ..... THE CATALYTIC OXIDATION OF ETHYLENE IN LOW  
..... CONCENTRATION OVER SUPPORTED PLATINUM CATALYSTS .....

DEGREE FOR WHICH THESIS WAS PRESENTED..... Ph. D. ....

YEAR THIS DEGREE GRANTED..... 1977 .....

Permission is hereby granted to THE UNIVERSITY OF ALBERTA LIBRARY to reproduce single copies of this thesis and to lend or sell such copies for private, scholarly or scientific research purposes only.

The author reserves other publication rights, and neither the thesis nor extensive extracts from it may be printed or otherwise reproduced without the author's written permission.





THE UNIVERSITY OF ALBERTA

THE CATALYTIC OXIDATION OF  
ETHYLENE IN LOW CONCENTRATION OVER  
SUPPORTED PLATINUM CATALYSTS

BY



JAMES R. HAWKINS

A THESIS

SUBMITTED TO THE FACULTY OF GRADUATE STUDIES AND RESEARCH  
IN PARTIAL FULFILMENT OF THE REQUIREMENTS FOR THE DEGREE  
OF DOCTOR OF PHILOSOPHY  
IN  
CHEMICAL ENGINEERING

DEPARTMENT OF CHEMICAL ENGINEERING

EDMONTON, ALBERTA

FALL, 1977





THE UNIVERSITY OF ALBERTA

FACULTY OF GRADUATE STUDIES AND RESEARCH

The undersigned certify that they have read, and  
recommend to the Faculty of Graduate Studies and Research,  
for acceptance, a thesis entitled ..... THE OXIDATION OF  
..... ETHYLENE IN LOW CONCENTRATION OVER SUPPORTED PLATINUM  
..... CATALYSTS.  
.....  
submitted by ..... JAMES R. HAWKINS  
.....  
in partial fulfilment of the requirements for the degree of  
Doctor of Philosophy in Chemical Engineering.





## DEDICATION

This thesis is dedicated to Iassac Kaila and Alvin G. MacDonald, two men, very different, but each of whom had certain qualities which helped shape my life.



## ABSTRACT

In the past ten years, a concern about the degradation of our environment has resulted in major efforts to reduce the rate at which pollutants are released into the air and water. The internal combustion engine used in automobiles was singled out as a villain, and automobile manufacturers responded with a number of methods to reduce the emissions of carbon monoxide, hydrocarbons and nitrogen oxides into the air. North American manufacturers chose to equip new automobiles with catalytic converters to meet the government standards. Some of the many aspects of the catalytic conversion of hydrocarbons to harmless carbon dioxide and water were studied here. The kinetics of the oxidation of ethylene over a 0.3% Pt/Al<sub>2</sub>O<sub>3</sub> surface-coated catalyst were studied in both low and high oxygen concentrations in a differential recycle reactor. Between 362 K and 472 K, the rate of ethylene oxidation was found to obey the rate function  $-r = k[O_2]/[C_2H_4]$  at low ethylene concentrations (less than 2 mole percent).

The predictions of the rate equation were independently tested against measurements of fractional conversion in an integral bed reactor. The predictions were generally lower than the measured values for three different reactor models. The selection of an inside wall heat transfer coefficient for the models indicated that heat transfer may be as important as the reaction kinetics in determining the effectiveness of the catalytic converters.

In both the integral bed and the recycle reactor, instabilities which were both cyclical and non-cyclical were observed. These instabilities usually caused a temporary increase in the activity of





of the catalyst. A number of possible explanations were presented, the most promising of which involved changes in the surface of the platinum during the reaction.

The structure sensitivity of the reaction was examined by comparing dispersion normalized rates against the dispersion for a series of sintered 0.5% Pt/Al<sub>2</sub>O<sub>3</sub> catalyst samples. The reaction was found to be demanding, but a concise relationship between catalyst activity and dispersion could not be developed. If, as was suspected, the surface morphology of the platinum changes during the reaction, this approach may not have been valid.

Three possible mechanisms for the reaction were considered. The most reasonable mechanism which resulted in a rate equation identical to the equation developed in the recycle reactor required that oxygen adsorption onto the platinum surface be the rate controlling step and that ethylene adsorb dissociatively. The other mechanisms were founded on similar assumptions, and the kinetic data did not provide a sufficient basis on which to differentiate between the three mechanisms.

Finally, the role of surface morphology changes was discussed. Possible changes in the surface structure of the platinum may have caused some of the uncertainties in the recycle and integral bed experiments as well as in the studies with sintered catalysts.



## ACKNOWLEDGEMENTS

The preparation of this thesis would have been extremely difficult, if not impossible, were it not for the assistance provided me by a number of individuals and organizations. For financial support, I would like to thank The Department of Chemical Engineering, The University of Alberta, The National Research Council of Canada, and K.E.H. For assistance in the design, fabrication, and prompt repair to all of my apparatus I would like to thank the gentlemen in the Instrument Shop and the Machine Shop. Many thanks are due to Dave Furnell for his tireless assistance in all aspects of the computerized computations I required. For their companionship and critical comments on my work at all stages, I would like to thank JM and JPM. To Bill Lye and R.A. 'Bud' White go my thanks for providing the incentive to attend The University of Alberta in the first place. Finally, the greatest debt of all is owed to my supervisor, Sieg Wanke, without whose patience, encouragement, and sense of humour, this thesis would never have been written.





## TABLE OF CONTENTS

	PAGE
CHAPTER 1 INTRODUCTION	1
1.1 Supported Metal Catalysts	1
1.2 Automotive Catalysts	2
1.3 Approach	4
1.4 Reactor Instabilities	5
 CHAPTER 2 SURVEY OF CATALYTIC OXIDATION AND REACTOR INSTABILITIES	 7
2.1 Carbon Monoxide Oxidation	7
2.2 Catalytic Hydrocarbon Oxidation	11
2.2.1 Surface Reactions	11
2.2.2 Adsorption Measurements	17
2.3 Reactor Analysis	26
CHAPTER 3 PROCEDURE AND EQUIPMENT	28
3.1 Differential Recycle Reactor	28
3.1.1 Equipment	28
3.1.2 Operation	33
3.2 Integral Bed Reactor	34
3.2.1 Equipment	34
3.2.2 Operation	38
3.3 Catalyst Activity Comparisons	39
3.3.1 Procedure	39
3.3.2 Catalyst Preparation and Analysis	39



	PAGE
CHAPTER 4 DIFFERENTIAL RECYCLE REACTOR	41
4.1 Introduction	41
4.2 Reactor Selection	41
4.3 Blank Runs	42
4.4 Catalyst Activation	43
4.5 Kinetic Runs - Fresh Catalyst	46
4.6 Kinetic Runs - Aged Catalyst	58
4.7 Adsorption Studies	62
4.8 Conclusions - Differential Recycle Reactor	66
CHAPTER 5 INTEGRAL BED REACTOR	68
5.1 Introduction	68
5.2 Blank Runs	69
5.3 Catalyst Pre-Treatment	72
5.4 Predictions of the Rate Equation - Isothermal Model	73
5.5 Predictions of the Rate Equation - Non-Isothermal Model	78
5.6 Predictions of the Rate Equation - Non-Homogeneous Model	85
5.7 Conclusions - Integral Bed Reactor	91
CHAPTER 6 REACTION INSTABILITIES	94
6.1 Instabilities in the Integral Bed Reactor	94
6.2 Instabilities in the Differential Recycle Reactor	101





	PAGE
6.3 Physical Models	107
6.3.1 Macroscopic CSTR Instabilities	107
6.3.2 Instabilities Due to the Nature of the Rate Equation	109
6.3.3 Multiple Types of Adsorbed Oxygen	110
6.3.4 Instabilities Due to Periodic Burn-Off	111
6.3.5 Instabilities Arising from Changes in the Catalyst Surface	112
6.4 Summary	115
CHAPTER 7 THE EFFECT OF PLATINUM DISPERSION ON ACTIVITY	116
7.1 Introduction	116
7.2 Results	118
7.3 Discussion of Results	120
7.4 Conclusions	129
CHAPTER 8 SOME COMMENTS ON THE CATALYTIC OXIDATION OF ETHYLENE	131
8.1 Possible Mechanisms for Ethylene Oxidation	131
8.2 Variations in Catalytic Activity	135
CHAPTER 9 CONCLUSIONS AND RECOMMENDATIONS	138
9.1 Conclusions	138
9.2 Recommendations	139



NOMENCLATURE	PAGE 141
REFERENCES	146
APPENDIX A MASS BALANCE EQUATIONS AND SAMPLE CALCULATIONS	153
A.1 Component Balances for a Differential Recycle Reactor	153
A.2 Sample Calculation for DRR	155
A.3 Carbon Balance	156
A.4 Mass and Energy Transfer Limitations	157
A.4.1 External Transfer Limitations	158
A.4.2 Internal Transfer Limitations	166
A.5 Integral Bed Reactor	174
A.5.1 Non-Isothermal Case	174
A.5.2 Isothermal Case	184
APPENDIX B EQUIPMENT CALIBRATIONS	187
B.1 Thermocouples	187
B.2 Temperature Controllers	189
B.3 Rotameters	189
B.4 Mass Flowmeters	191
B.5 Gas Chromatographs	200
APPENDIX C GAS CHROMATOGRAPHY ANALYSIS	207
C.1 Chromatographic Operating Conditions	207
C.2 Signal Analysis	209



APPENDIX D	MEASURED AND CALCULATED DATA	PAGE 217
APPENDIX E	ERROR ANALYSIS AND DATA REPRODUCIBILITY	246
E.1	Errors in Temperature Measurement	246
E.2	Errors in Flow Measurement	248
E.3	Errors in Composition Measurement	249
E.4	Errors in Catalyst Weight and Reactor Pressure	255
E.5	Effect of Measurement Errors on Calculated Rates	256
E.6	Reproducibility of the Data	258
E.7	Summary	263
APPENDIX F	EXAMPLES FROM DATA BOOK	264





## LIST OF TABLES

Table	Page
2.1 Intrinsic Rate Equations	18
2.2 Heats of Adsorption	25
3.1 Catalyst Treatments and Dispersions	40
4.1 Catalyst Activity Following Thermal Treatments	44
4.2 Kinetic Constants	51
4.3 Rate Constants - Aged Catalyst	59
4.4 Arrhenius Constants	61
4.5 Comparison of Catalytic Activity with Pretreatment Conditions	62
5.1 Comparison of Predicted and Measured Fractional Conversions - Low Conversions	83
5.2 Comparison of Predicted and Measured Fractional Conversions - High Conversions	84
5.3 Comparison of Predicted and Measured Fractional Conversions in the IBR	88
5.4 Comparison of Predicted and Measured Fractional Conversions in the IBR	89
5.5 Summary of Integral Bed Results	90
7.1 Results of Dispersion Experiments	121
A.1 Data for Run M 54	155
B.1 Thermocouple Calibrations	187
B.2 High Range Rotameter Calibration	193
B.3 Low Range Rotameter Calibration	196
B.4 Calibration of Beckman G.C. 2	204
B.5 Calibration of Gow-Mac Series 550 Gas Chromatograph	205



Table		Page
B.6	Calibration of Hewlett Packard 5710A Gas Chromatograph	206
C.1	Chromatograph Operating Conditions	208
C.2	Integration Comparisons for High Ethylene Concentrations	214
C.3	Integration Comparisons for Low Ethylene Concentrations	215
D.1	Raw Data - Excess Oxygen Runs DRR	218
D.2	Raw Data - Low Oxygen Runs DRR	219
D.3	Raw Data - Aged Catalyst Runs DRR	221
D.4	Blank Runs - Integral Bed Reactor	222
D.5	Blank Runs - 2 mm Alumina Spheres IBR	223
D.6	Catalyst Pre-treatment IBR	224
D.7	Raw Data - Integral Bed Reactor	22
D.8	Predictions of Isothermal Model of IBR (Low Ethylene Flow Rate , 375 K)	232
D.9	Predictions of Isothermal Model of IBR (High Ethylene Flow Rate , 375 K)	231
D.10	Predictions of Isothermal Model of IBR (Low Ethylene Flow Rate, 440 K)	232
D.11	Predictions of Isothermal Model of IBR (Low Ethylene Flow Rate, 420 K)	233
D.12	Predictions of Isothermal Model of IBR (Low Ethylene Flow Rate, 400 K)	234
D.13	Predictions of Isothermal Model of IBR (Low Ethylene Flow Rate, 380 K)	235
D.14	Measured and Predicted Fractional Conversions in the IBR	236
D.15	Dispersion Experiments - Raw and Calculated Data	242



Table		Page
D.16	Temperature Normalized Rate Constants	245
E.1	Relative Errors in the Fractional Conversion	254
E.2	Reproducibility of Repeated Runs in the DRR	259
E.3	Irreproducibility of Repeated Runs in the IBR	261





## LIST OF FIGURES

Figure		Page
2.1	Adsorption Energetics	24
3.1	Schematic Diagram of Differential Recycle Reactor	29
3.2	Schematic Diagram of Integral Bed Reactor	35
3.3	Thermocouple Locations in Integral Bed Reactor	37
4.1	Activity Changes Following Thermal Treatments of the Catalyst	45
4.2	Rates of Ethylene Oxidation as a Function of the Ratio of Oxygen to Ethylene Concentration in Excess Oxygen	48
4.3	Rates of Ethylene Oxidation as a Function of the Ratio of Oxygen to Ethylene Concentration in Low Oxygen Concentrations	50
4.4	Comparison of Predicted Versus Measured Rates at 375 K for Various Rate Equations	53
4.5	Comparison of Predicted Versus Measured Rates at 472K for Various Rate Equations	54
4.6	Arrhenius Plot for Rate Constants Based on Equation 4.6	55
4.7	Rate Constant as a Function of Temperature (Non-Linearized)	57
4.8	Rates of Ethylene Oxidation as a Function of the Ratio of Oxygen to Ethylene Concentration for the Catalyst Sample Used in the Integral Bed Experiments	60
4.9	Catalyst Bed Temperature as a Function of Time for Adsorption Studies	63
5.1	Results of Blank Runs in IBR ( $C_2H_4$ Feed = 0.135 mole %)	70
5.2	Effect of Inlet Ethylene Concentration on Conversion During Blank Runs at 792 K	70



Figure		Page
5.3	Results for IBR Packed with 2 mm Alumina Spheres	71
5.4	Effect of Inlet Ethylene Concentration on Fractional Conversion for IBR Packed with 2 mm Alumina Spheres	71
5.5	Effect of Thermal Treatments on Catalytic Activity	74
5.6	Predicted Ethylene Conversions for IBR as a Function of Ethylene and Oxygen Feed Rates	75
5.7	Comparison of Measured and Predicted Conversions for the IBR	77
5.8	Comparison of Measured and Predicted Conversions for the IBR (Low Oxygen and Median Ethylene Feed Rates)	79
5.9	Comparison of Measured and Predicted Conversions for the IBR (Excess Oxygen and Median Ethylene Feed Rates)	80
6.1	Typical Temperature Versus Time Behaviour for IBR Runs	95
6.2	Typical Temperature Versus Time Behaviour for IBR Runs in Which the Reaction Front Passed out the Reactor Exit	95
6.3	Temperature Transients in the IBR as a Function of $[O_2]/[C_2H_4]$	97
6.4	Temperature Transients in the IBR	99
6.5	Cyclical Temperature Behaviour in the IBR	100
6.6	Cyclical Temperature and Conversion Behaviour in the DRR (Low Oxygen Concentration)	103
6.7	Cyclical Temperature and Conversion Behaviour in the DRR (High Oxygen Concentration)	104
6.8	Abrupt Temperature Variations in the DRR	106
6.9	Mass and Energy Balances for a CSTR	108



Figure		Page
7.1	Specific Rate as a Function of Dispersion	116
7.2	Effect of Dispersion on the Specific Rate Constant	122
7.3	Temperature Normalized Rate Constants as a Function of Dispersion	127
A.1	Heat and Mass Transfer Correlations in a Fixed Bed	161
A.2	Ratio of External Temperature Gradient to Total Temperature Gradient	170
A.3	Isothermal External Effectiveness Factor	170
A.4	Spherical Isothermal Effectiveness	170
A.5	Comparison of Nonisothermal Effectiveness for a Flat Plate and a Sphere	173
A.6	Effect of $r (=Bi_m/Bi_h)$ on Spherical Nonisothermal Effectiveness Factor	173
B.1	Results of the Thermocouple Calibrations (Extreme Cases)	188
B.2	Calibration Curve for Mid-Range Temperature Controller	190
B.3	Calibration Curve for High-Range Temperature Controller	191
B.4	Calibration Curve for Low-Range Temperature Controller	192
B.5	Calibration Curve for High-Range Rotameter (Matheson #R-2-15-B)	194
B.6	Calibration Curve for the Low-Range Rotameter (Matheson #601)	195
B.7	Calibration Curve for the High-Range Mass Flowmeter (Calibration Gas - $N_2$ )	197
B.8	Calibration Curve for the Low-Range Mass Flowmeter (Calibration Gas - $N_2$ )	197





Figure		Page
B.9	Calibration Curve for the Low-Range Mass Flowmeter (Calibration Gases - 5% C <sub>2</sub> H <sub>4</sub> and 95% N <sub>2</sub> )	199
C.1	Typical Output for 'Air', CO <sub>2</sub> , and C <sub>2</sub> H <sub>4</sub> Analysis Using the Hewlett Packard G.C. and an Electronic Reporting Integrator	210
C.2	Typical Output for N <sub>2</sub> and O <sub>2</sub> Analysis Using the Beckman G.C. and an Electronic Reporting Integrator.	211
C.3	Typical Output for 'Air', CO <sub>2</sub> , and C <sub>2</sub> H <sub>4</sub> Using the Gow-Mac G.C. and a Strip Chart Recorder	212
E.1	Effect of Instabilities on Ethylene Conversion in Subsequent Runs	262



## CHAPTER 1

### INTRODUCTION

#### 1.1 Supported Metal Catalysts

Catalysts may be divided into two groups - homogeneous and heterogeneous. The former type of catalyst is in the same phase as the reactants while the latter type of catalyst is in a different phase than the reactants. Homogeneous catalysts usually contact the reactants in liquid solutions, while the heterogeneous catalysts are most often solid phase catalysts contacting liquid or gas phase reactants. In this work, attention has been focussed on the type of catalysts used by automobile manufacturers in catalytic converters. These catalysts are solid phase metal catalysts used to oxidize carbon monoxide and unburnt hydrocarbons, or to reduce the nitrogen oxides present in automobile exhaust.

These particular heterogeneous catalysts belong to a subgroup, the supported metal catalysts. The catalysts have two components. The active part is the actual catalytic metal or combination of metals, usually from group VIII(b) - Fe, Co, Ni, Ru, Rh, Pd, Ir, and Pt. Small crystallites (less than 10 nm in diameter) of the metal are attached to the surfaces of a support material. Common supports are carbon, alumina ( $\text{Al}_2\text{O}_3$ ) and silica ( $\text{SiO}_2$ ). The supports may appear in a variety of geometric shapes - spheres, cylinders, irregular granules, or honeycomb monoliths made of ceramics or steel alloys (1.1). The metal is dispersed on the support surface by impregnating the porous catalyst support with a solution containing a salt of the desired metal. The entire catalyst is then reduced directly, or is oxidized



to the metal oxide and is then reduced. Particular catalyst preparations vary depending on the application and the actual techniques used in commercial preparations are often not available in the open literature.

Since the rate of a catalytic reaction usually increases as the active surface area of the catalyst increases, it is economically desirable to maximize the ratio of the number of metal atoms at the crystallite surface to the total number of metal atoms in the crystallite. This ratio is referred to as the dispersion. As automotive catalysts are primarily the more expensive noble metal catalysts (Pt, Pd, Ru), the efficient use of the metal is very important. For example, in a platinum crystal, 4 nm in diameter, approximately fifty percent of the precious metal is unused (1.2).

Attempts to produce a finely dispersed metal either by milling the metal or by expanding it into a sponge have been unsuccessful. First, the small particles are readily entrained in the fluid phase resulting in catalyst containment problems. Secondly, at elevated temperatures the small crystallites or the expanded sponges will tend to sinter or agglomerate into larger particles. By placing the small crystallites on a support, the metal particles are anchored inside the reactor and are physically separated, helping to alleviate the two problems just mentioned.

## 1.2 Automotive Catalysts

In the mid 1960's, a growing awareness of the effects of the many forms of environmental pollution forced governments of developed nations to enact pollution control legislation. One particular





pollution source singled out for attention was the emissions from internal combustion engines. Unburnt hydrocarbons, nitrogen oxides and carbon monoxide were found to be the most significant contributors to the photochemical smog which plagued some large industrial cities. In locations such as Los Angeles which were prone to atmospheric inversion conditions, the problem was particularly acute. In response to this concern, the American government passed the Clean Air Act in 1970. This act stringently limited the allowable emission levels of hydrocarbons, carbon monoxide, and nitrogen oxides from automobiles sold in the United States. While the Canadian air quality had not deteriorated to the same extent, Canada's proximity to the U.S.A. and its Auto Pact agreement resulted in Canadian standards being set which were in line with the American standards. The allowable emission levels were set at 0.41 g/mile for hydrocarbons and carbon monoxide and 0.40 g/mile for nitrogen oxides. This presented a two-pronged catalytic problem. The hydrocarbons would have to be oxidized to carbon dioxide and water while the nitrogen oxides would have to be reduced to elemental nitrogen. For a catalyst to be effective, it would have to be both physically and chemically stable. The catalyst would be subject to mechanical degradation caused by the operation of the vehicle. Also, sulphur, lead, phosphorus and bromine in the fuel and in the lubrication oils are potential poisons for the catalyst. In addition, the high temperatures and extreme temperature variations could lead to sintering problems.

This work is an attempt to examine in greater depth some of the parameters that affect the performance of catalysts typical of the automotive catalysts. As very little is known about the kinetics of the



oxidation of hydrocarbons in low concentration at low oxygen levels, some of the many aspects of these catalytic oxidations were studied here. In particular, the catalytic oxidation of ethylene (ethene) in low concentration was examined.

### 1.3 Approach

Rather than attempt to superficially analyse the reaction kinetics of the complex mixture of compounds actually present in the exhaust of internal combustion engines, a detailed investigation of the oxidation of a single component was chosen. In this study, ethylene was the compound selected for a number of reasons. Of all the hydrocarbons present in exhaust fumes, ethylene is present in the highest concentration, about twenty percent of the total hydrocarbon concentration. Also, among the hydrocarbons typically found in automotive exhaust, ethylene is about midway insofar as ease of oxidation is concerned. Finally, the photochemical reactivity of internal olefins is cited as the highest among the other hydrocarbon groups (1.3).

The temperature range studied in detail here, 362 K to 472 K, is considerably below the actual 'warm-running' temperatures encountered in internal combustion engines. Since the oxidation of hydrocarbons to  $\text{CO}_2$  and water at typical operating temperatures (900 K) is no problem (1.3), the greatest concentration of hydrocarbons in the exhaust will occur during startup, when the converter is still cold. In a northern city like Edmonton, Alberta, where the winter temperatures may drop to  $-40^\circ\text{C}$ , a considerable fraction of the cars travelling during rush hours may be operating at sub-optimum temperatures. The ethylene concentrations studied here ( $\leq 2\%$ ) are also intended to simulate startup



conditions rather than the 'warm-running' operation.

The first step in characterizing the performance of these catalysts was the development of a suitable rate equation to model the kinetics of the oxidation. Towards this end, a differential recycle reactor was constructed (described in greater detail in Chapter 3). Since the mass balance equation for this type of reactor is algebraic rather than differential or integral <sup>\*</sup>, the kinetic data could be plotted directly to provide the needed rate equation. The reaction exhibited a very strong inverse order with respect to the hydrocarbon concentration, prompting the postulation of a Langmuir - Hinshelwood type reaction mechanism. The details of these experiments are discussed in Chapter 4.

The second phase of the investigation involved a comparison of the predictions of the kinetic model with the actual conversion performance of an integral bed reactor, somewhat similar in nature to the catalytic converters. In Chapter 3, the integral bed reactor which was constructed for this comparison is described. The rate model developed from the differential bed reactor was used to predict the performance of the integral bed reactor. This comparison is discussed in Chapter 5.

#### 1.4 Reactor Instabilities

The study was not without its problems however. In both the differential recycle reactor and in the integral bed reactor, both cyclical and non-cyclical instabilities were observed. A great

---

\* See Appendix A for the mass and energy balance equations.





deal of attention has been focussed on cyclical reactor instabilities in the last few years, especially in studies of carbon monoxide oxidation. These instabilities have been attributed to a number of phenomena in both experimental and theoretical studies. A brief review of the work in this field is presented in Chapter 2. In Chapter 6, the particular instabilities that were observed in this system are discussed. In Chapter 7, the relationship between catalytic activity and the dispersion of the precious metal on the support is investigated. The reaction of ethylene with oxygen over a 0.5% Pt catalyst was found to be demanding rather than facile. In the final chapter, Chapter 8, the significance of all the experiments is discussed and a possible mechanism for the reaction is presented.





## CHAPTER 2

### SURVEY OF CATALYTIC OXIDATIONS AND REACTOR INSTABILITIES

In this section the historical course of investigations pertinent to this work is outlined, starting with the oxidation of carbon monoxide. In this investigation, no work was done on carbon monoxide oxidation, however there are many similarities between carbon monoxide oxidation and ethylene oxidation. Carbon monoxide oxidation and hydrocarbon oxidation are each discussed with reference to the intrinsic rate functions and reactor instabilities. A few comments on reports of measured and of calculated adsorption data and a brief statement about reactor analysis complete the literature survey.

#### 2.1 Carbon Monoxide Oxidation

The emission control legislation not only limits the amount of hydrocarbons which may be emitted from an automobile engine, but also limits the amount of carbon monoxide. As the kinetics of carbon monoxide oxidation have a number of features in common with ethylene oxidation, a short summary of the efforts to understand carbon monoxide oxidation is appropriate.

The history of catalytic oxidation begins in 1922 with the work of Langmuir using platinum wires (2.1). In what has since become the classic Eley - Rideal mechanism, the reaction was seen as a multi-step process. Dissociative adsorption of oxygen onto the catalyst surface was followed by reaction with gaseous carbon



monoxide to form adsorbed carbon dioxide. However, the carbon monoxide would also compete for sites on the catalyst. Langmuir speculated that the carbon atom would bind to the catalyst surface projecting the oxygen atom outwards. This configuration was not conducive to reaction. Hence, a high concentration of carbon monoxide on the surface would inhibit the reaction.

The catalytic oxidation of carbon monoxide over a variety of supported and pure noble metal catalysts has received considerable attention since Langmuir's initial experiments. While the mechanism of the reaction and the corresponding rate equation have been the subject of some conjecture (2.2 - 2.6), one common attribute among the rate expressions has been the prediction of the possibility of negative order kinetics with respect to the carbon monoxide. This feature has been demonstrated experimentally for supported platinum catalysts by Voltz et al. (2.6) and by Plichta (2.7).

Bonzel and Ku ( 2.8 ) investigated carbon monoxide oxidation on platinum crystals and found that a single mechanism was inadequate to describe the reaction. They saw a shift between a Langmuir - Hinshelwood (L-H) mechanism and an Eley - Rideal (E-R) mechanism resulting in different conversion levels.

Dauchot and Van Cakenberghe ( 2.9 ) , while unable to observe instabilities when they used platinum films and gas chromatography, were able to electronically detect sustained oscillations in the oxidation of carbon monoxide on a platinum wire using resistivity measurements. They attributed this to a very rapid



(0.1 sec.) change in the surface temperature. This surface temperature fluctuation of about  $5^{\circ}\text{C}$  was seen as favouring oxygen adsorption at the high temperatures and carbon monoxide adsorption at low temperatures. With a combined L-H and E-R mechanism, a surface titration effect is achieved which results in the oscillations. Hori and Schmidt (2.10) present experimental data showing that transients in the carbon monoxide oxidation over platinum occur due to a change in the nature of the surface complexes. They further state that these transients will occur only if changes in reaction rates caused by changing surface complexes are slower than the adsorption time constants.

McCarthy et al. (2.11) speculate that if a heterogeneous catalytic reaction exhibits both facile and demanding characteristics (2.12), then there may be more than one rate determining step. They observed sustained oscillations (30 second period) and attributed this to the possibility of two mechanisms existing. The two mechanisms could be due to the reaction exhibiting demanding characteristics at low carbon monoxide concentrations and facile characteristics at high carbon monoxide concentrations and/or to the existence of two forms of adsorbed carbon monoxide: the bridged form and the linear form.

Mathieu (2.13), working with supported alloy catalysts and Hugo and Jakubith, using platinum mesh catalyst (2.14), have each attributed instability in the carbon monoxide oxidation reaction to shifts in the amount of bridged and linear forms of adsorbed carbon monoxide. Plichta (2.7) observed sustained short





period oscillations (less than one minute) in the oxidation of carbon monoxide over platinum wires. Also, he reported unstable transitions from one reaction regime to another, occasionally with multiple peaks in the periodic states.

The work done by Plichta has been summarized by Scheintuch et al. (2.15). They found that the amplitudes of the oscillations were inversely proportional to residence time, temperature, and catalytic activity. They suggest that the following reaction models cannot be used to explain the observed oscillations:

1. Models based on any single rate determining step.
2. Models assuming equilibrium between gaseous and surface phase reactants.
3. Models calling for transformations between linear and bridged forms of carbon monoxide followed by the reaction of bridged carbon monoxide and oxygen.

They stated that the oscillations are best predicted using a model in which the activation energy of one of the kinetic steps is a function of the surface coverage, but concluded that even that model was not without its conceptual difficulties, and was still in need of modifications and refinements.

Some of those findings were confirmed by Beusch et al. (2.16) on a single pellet of a supported platinum catalyst. They also found that the amplitude of oscillations in a carbon monoxide oxidation system decreased with increasing temperatures (180°C to 250°C) while the frequency increased.. At temperatures above 250°C they found no oscillations.

In Section 2.2, the many similarities between the oxidation of carbon monoxide over platinum and the oxidation of ethylene





over platinum will be obvious. The techniques and the principles which were elucidated by those working on carbon monoxide oxidation over the past sixty years can be applied to a certain extent to the understanding of catalytic hydrocarbon oxidation. Since the complete oxidation of ethylene has received very little attention, some parallels should be drawn from similar studies on carbon monoxide. Somewhat distressing, however, is the fact that after sixty years of investigations by many distinguished scientists, the mechanism where by carbon monoxide is oxidized is still a bit of a mystery.

## 2.2 Catalytic Hydrocarbon Oxidation

### 2.2.1 Surface Reactions

The Langmuir - Hinshelwood mechanism and the Eley - Rideal mechanism which were applied to the catalytic oxidation of carbon monoxide are often applied to the the catalytic oxidation of hydrocarbons as well. In the context of emission control studies, supported noble metal catalysts are used for the removal of both pollutants, and it is not surprising that the catalytic oxidation of carbon monoxide and of hydrocarbons are modelled with the same type of equations. In fact, Voltz et al. (2.6) have fitted experimental data for propylene oxidation and for carbon monoxide oxidation to equations of identical form. The theoretical model and the data indicated negative order kinetics. The net negative order



is somewhat contrary to 'conventional wisdom'. Wei (2.17) discussed some of the ramifications of this type of kinetics to reactor and catalyst design problems.

In this work, the oxidation of ethylene over supported platinum catalysts was found to be governed in all cases by negative order kinetics. The L-H and the E-R types of rate equations each can be used to predict rate equations which are non-monotonic. That is, there are usually (2.17) two regimes: a low concentration regime in which the rate is approximately first order, and a higher concentration regime in which the negative order kinetics are observed. In the present work, the low regime was below the experimental limits of detectability in the temperature ranges studied and only the negative order kinetics were observed.

The other area in which there is a similarity between carbon monoxide oxidation and ethylene oxidation is in the appearance of sustained regular and irregular oscillations. Schmitz (2.18), in an extensive 1974 review, surveyed the advances in the theoretical and experimental instabilities in chemically reacting systems. He discussed a variety of mechanisms whereby sustained and damped oscillations could occur in a reaction system, ranging from the classic CSTR thermal instability to a somewhat more subtle instability arising due to a change in the reaction mechanism and/or a change in the nature of the catalyst surface. It is this latter type of instability which is of interest here.

Because the complete oxidation of hydrocarbons in general and ethylene in particular is of scant industrial importance,



the previous studies on this particular system are few indeed. Only in the last few years, with the advent of concern about air quality has the complete catalytic oxidation of ethylene and other hydrocarbons become important.

Some of the earliest work on the oxidation of ethylene was done by Reyerson and Swearingen (2.19). They studied the reaction on a variety of metal catalysts (Ag, Cu, Pt, Pd) supported on silica gels. They studied temperatures from 90°C to 335°C, ethylene concentrations from 19% to 30% , and oxygen concentrations from 16% to 25%. They found little reaction on platinum, copper or or palladium catalysts below 100°C and reported that, for ethylene oxidation on the platinum catalyst, the rate was directly proportional to the oxygen concentration and inversely proportional to the ethylene concentration. They did not however, list any numerical values for the rate constants or any specific rate equations.

Following this in the early 1930's there was a considerable amount of work done on complete and partial oxidation of ethylene over silver catalysts. The interest here was in the production of ethylene oxide rather than the complete oxidation. Among others, Lenher (2.20), Bone et al. (2.21), and Twigg (2.22), studied this reaction over a fair range of experimental conditions. The data presented indicated a variety of rate equations were plausible and led to a correspondingly large number of postulations as to the actual mechanism. The nature of the reaction mechanism remains speculative, commanding the attention of researchers such as Huang et al. (2.23) as recently as 1976. While the oxidation of ethylene over silver catalysts is not particularly similar to the





reaction over platinum, it is significant that the intrinsic rate and the reaction mechanism are still the subjects of conjecture.

Concurrent with the investigations of ethylene oxidation over silver catalysts, Beeck (2.24,2.25) began investigating the hydrogenation of ethylene over evaporated platinum, nickel and palladium films. He found that, at room temperatures, the reaction rate on nickel films was first order in hydrogen and zero order in ethylene concentration. However, the form of his rate function,

$$-r = \frac{k[C_2H_4]^{1.0} [H_2]^{1.0}}{[C_2H_4]^{1.0}} \quad \text{--(2.1)}$$

did allow for negative orders if the powers on the ethylene concentrations were changed slightly. He stated that excess ethylene inhibited the reaction, and speculated that that was due to a dissociative adsorption of the ethylene into two adsorbed hydrogen atoms and an acetylenic residue. The acetylenic residue occupied potential hydrogen adsorption sites, slowing the reaction rate. Beeck felt that this was consistent with an Langmuir - Hinshelwood mechanism.

On the other hand, Twigg, using pellets of alumina supported nickel (2.26) and Jenkins and Rideal, using nickel filaments, (2.27) saw the hydrogenation of ethylene proceeding in the opposite manner. They believed that the ethylene associatively adsorbs, then reacts with gaseous hydrogen. They did however base their conclusions on the same experimental results as did Beeck: first





order reaction with respect to hydrogen concentration and zero order reaction with respect to ethylene concentration. As is often the case, a unique mechanism cannot always be postulated from a particular set of kinetic data!

Wojtowicz et al. (2.28,2.29,2.30) examined the catalytic oxidation of ethylene in aqueous solution. They treated a solution of  $\text{HClO}_4$  with gaseous ethylene, then inserted platinum covered electrodes to produce anodic oxygen. Unlike all of the other catalytic oxidations of ethylene, the adsorbed oxygen on the electrode inhibited the reaction. The reaction would only occur if a 'hole' in the surface layer of adsorbed oxygen was created. This was an unstable situation and resulted in oscillatory behaviour. The oxide layer would be formed on the surface of the electrode, then the ethylene would titrate the oxygen. This cycle would be repeated with a period of less than 15 seconds. They found that these oscillations were primarily due to mass transfer limitations. In a different series of experiments, they found that the oscillations disappeared, ostensibly due to the better mixing characteristics. In the well mixed experiments, they found that increasing the ethylene concentration inhibited the reaction, as it competed for sites on the platinum electrode. Their calculations showed that the surface reaction step was not the rate determining step.

Dmuchovsky et al. (2.31) used an integral bed reactor to study the oxidation of ethylene (2.2% in air) on a variety of supported metal oxide catalysts (Ti,V,Cd,Mn,Fe,W,Mo,Zi, Ni, and Cu) between  $260^\circ\text{C}$  and  $460^\circ\text{C}$  at a total flow rate of 750 standard cubic centimetres per minute(SCCM). They found linear relationships between the



logarithm of the conversion and reciprocal temperature, and calculated apparent activation energies from their figures. This would indicate that the reaction rate was independent of the ethylene and oxygen concentrations, i.e., zero order reaction. As well, tests on uncoated alumina revealed no reaction below 460°C.

Patterson and Kemball (2.4,2.32) studied the catalytic oxidation of olefins ( including ethylene and some methyl-substituted ethylenes) on Pt and Pd films. Specifically, they looked at complete ethylene oxidation on platinum films between 5°C and 100°C. While they found the reaction to be first order in oxygen concentration, they were unable to fit the ethylene dependence to any zero or positive order. Somewhat like Beeck, they attributed this reactant inhibition to adsorbed acetylenic residues, and indeed were able to enhance the inhibition by introducing acetic anhydride into the reaction gases.

Schwartz et al. (2.33) also investigated the complete oxidation of olefins, but on thin Pt and Pd wires. They found negative fractional and negative integral orders with respect to the olefin concentration. While they did not cite a net reaction order for ethylene, they did report orders of -0.25 for propylene ( $C_3H_6$ ) and of -0.2 for butylene ( $C_4H_8$ ), with activation energies in the 10 to 20 kcal/mol range. Voltz et al. (2.6) also looked at the oxidation of olefins, propylene in particular, and also found an inverse dependency of the rate on the olefin concentration. High concentration partial oxidations of ethylene over three alumina supported palladium catalysts were carried out by Omar et al. (2.34). They used high metal content catalysts (greater than 10% by weight) and did not report any negative order kinetics. They also reported



that no reaction occurred below 225°C on the support alone. As well, they noticed an improvement in catalyst activity after high conversion runs at elevated temperatures.

The results of the investigations described above are summarized in Table 2.1.

The subject of catalytic hydrocarbon oxidation has been reviewed by a number of authors. Germain (2.35,2.36) and Margolis (2.37) have published quite extensive surveys. In addition to these references, researchers in the automotive industry have published a number of papers (2.38 -2.42 for example) dealing with hydrocarbon oxidation over a variety of catalysts in relation to chemical reactions in catalytic converters.

### 2.2.2 Adsorption Measurements

Some of the kinetic rate constants in a L-H or E-R type of rate equation can be theoretically equated to combinations of equilibrium constants for adsorbing and desorbing species (2.43). These equilibrium constants are themselves usually functions of the temperature and of the heats of adsorption of the different reactants. For this reason, the heats of adsorption of ethylene, oxygen and of carbon dioxide are of importance in the modelling of a heterogeneous reaction.

Some of the early adsorption measurements of hydrocarbons on various metals were done by Beeck (2.24) in connection with his interest in the catalytic hydrogenation of ethylene. He measured heats of adsorption of ethylene on nickel which ranged from about 58 kcal/mol for clean surfaces to about 10 kcal/mol for





TABLE 2.1 INTRINSIC RATE EQUATIONS

Hydrocarbon	Catalyst	Temperature Range	Hydrocarbon Concentration	Oxygen Conc.	Rate Equation	Ref.
1. ethylene	Pt on silica gel	90°C-335°C	20%-29%	16%-25%	$-r = \frac{k[O_2]}{[C_2H_4]}$	2.19
2. ethylene	Oxides of Ti,V, Cd,Mn,Fe,W,Mo, Zn,Ni,Cu on silica and alumina pellets	262°C-459°C	2.2%	18%	$-r = k[C_2H_4]$	2.31
3. ethylene	Pt films	5°C-100°C	8%	92%	$-r \propto [O_2]^{1/2}$ $-r \propto [C_2H_4]^n$ (n not specified)	2.32
4. ethylene	Pd films	5°C-100°C	8%	92%	$-r=k[O_2]^{1/2}[C_2H_4]^1$	2.32
5. propylene	Pt supported on alumina pellets	205°C-370°C	0.01%-0.08%	3%-10%	$-r= \frac{k[C_3H_6][O_2]}{(1+k[C_3H_6])^2}$	2.6
6. propylene	Pt filaments	77°C-177°C	2%-4%	10%-40%	$-r=k[C_3H_6]^{-.25}[O_2]$ $k = 10^{1.3-22.0/RT}$	2.33
7. ethylene	Pd filaments	75°C-190°C	2%-4%	10%-40%	$-r=k[C_2H_4]^{1.0}[O_2]^0$ $k = 10^{7.04-10.3/RT}$	2.33
8. ethylene	Co <sub>3</sub> O <sub>4</sub> on alumina honeycombs	275°C-450°C	0.08%-0.5%	1%-10%	$-r=k[O_2]^{0.3}[C_2H_4]^{0.7}$ $k = Ae^{-16.0/RT}$	2.63





TABLE 2.1 (continued)

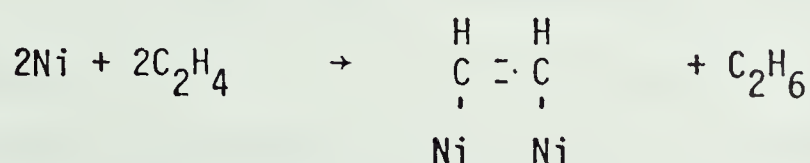
INTRINSIC RATE EQUATIONS

Hydrocarbon	Catalyst	Temperature Range	Hydrocarbon Concentration	Oxygen Conc.	Rate Equation	Ref.
9. ethylene	Silver supported on alumina pellets	280°C	1.5%-5%	excess	$-r = 0.0398[C_2H_4]$	2.23
10. ethylene	Pd supported on alumina and silica pellets (Pd was 10%-15% by weight)	95°C-230°C	16%-37%	63%-84%	$-r=k[C_2H_4]^0[O_2]^1$	2.34
11. ethylene	Pt covered electrodes in HClO <sub>4</sub> sol'n, sat. with C <sub>2</sub> H <sub>4</sub>	20°C-24°C	trace-sat.sol'n	evolved on electrode	rate inversely proportional to conc'n of C <sub>2</sub> H <sub>4</sub> in sol'n	2.28 2.29 2.30



for monolayer coverages. His results were the same at  $-183^{\circ}\text{C}$  and at room temperature. He was able to find evidence that some of the adsorbed ethylene self-hydrogenated to ethane, giving rise to his speculation mentioned earlier that the ethylene adsorbed dissociatively. In a later paper, Beeck (2.44) measured heats of dissociative ethylene adsorption at  $23^{\circ}\text{C}$  on a number of metallic films: Ni, Fe, Rh, W, and Ta. For associative adsorption on nickel, Beeck estimated that the two-site heat of adsorption was around 10 - 15 kcal/mol. His results for oriented and non-oriented nickel films were within 3 % of each other. However, for all metals except Rh, he observed a rapid decrease in heat of adsorption with increasing surface coverage.

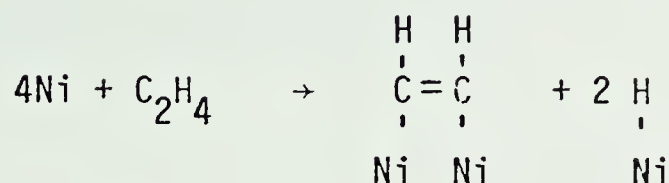
In some cases, calculated heats of adsorption can be used rather than experimentally determined values. However, when the precise nature of the adsorbed species is unknown, caution should be exercised in using the calculated values. Eley (2.45) presents a series of comparisons between reported heats of adsorption and calculated values using the Pauling covalent bond equation (2.46). For oxygen on tungsten, the calculated value is 95.6 kcal/mol and the value observed on tungsten wire is 139 kcal/mol. The calculated value for ethylene on nickel is 36.2 kcal/mol which is significantly lower than the value of 58 kcal/mol reported by Beeck. However, the calculation which Eley proposed was for the associative adsorption,





rather than the reaction proposed by Beeck,

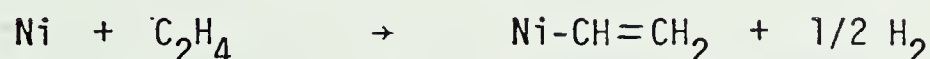
i.e.



which they suggested did not occur. They also cited two other possible reactions,



and

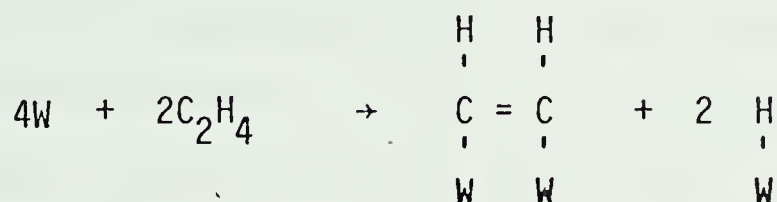


but discarded both of these as the Pauling equation produced an even lower value for the heat of adsorption if either of those two chemical equations are used. So, while Pauling's equation may, for certain cases, reasonably predict actual heats of adsorption, the adsorption mechanism must be known a priori for it to be of use.

Trapnell (2.47) investigated the adsorption of ethylene on tungsten filaments at 0.0°C and found that the uptake was considerably reduced after a gassing-degassing cycle. He attributed this



to irreversible changes in the tungsten surface caused by reaction with the gas and the poisoning of the surface by the auto-hydrogenation reaction, i.e. the desorption of the ethylene into acetylenic residues and hydrogen atoms.



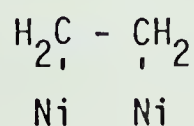
This would require a four site adsorption, one site for each carbon and a site for each hydrogen atom transferred. The four site adsorption was seen as being very rapid. Trapnell (2.47) conjectured that the four site adsorption was followed by a much slower transfer to a two site covering via the self-hydrogenation.

i.e.



The presence of evolved ethane ( $C_2H_6$ ) in the gas phase was presented as evidence for this reaction.

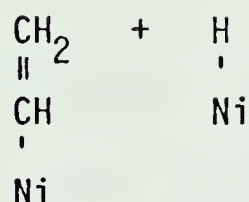
Jenkins and Rideal (2.27) also examined ethylene chemisorption on nickel, concluding that either the associative form,



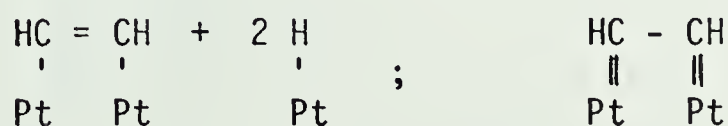




or a dissociative form,



were possible. The measurement of heats of adsorption and adsorption isotherms on supported and pure platinum has presented investigators with many problems. Bond (2.48,2.49) reported that oxygen adsorbed much more readily than ethylene, while Morgan and Somorjai (2.50) reported that, at least for low pressure ( $10^{-5}$  Torr) on the [100] surface of platinum, ethylene chemisorbs appreciably at room temperature while oxygen adsorption is negligible. Morgan and Somorjai also postulated that the adsorbed ethylene may take one of four forms:



Weber et al. (2.51) reported heats of adsorption of oxygen on Pt between 58 kcal/mol and 40 kcal/mol and provided an



empirical equation relating activation energy to the surface coverage,

$$E(n) = 58,000 - 2310 * 10^{-11} (n) \text{ [cal/mol]}$$

where  $n$  = no. of atoms adsorbed per g Pt. Weinberg et al. (2.52) have measured heats of oxygen adsorption on platinum and found values from 53 kcal/mol to 69 kcal/mol. However, they also maintained that the adsorption is strongly dependent on surface impurities. In fact, for oxygen adsorption on carbon contaminated surfaces, they speculated that oxygen adsorption is non-activated. Bonzel and Ku (2.53) felt that oxygen adsorbed in a two step process, the precursor state being molecular adsorption, the final state the chemisorption, as shown in Figure 2.1.

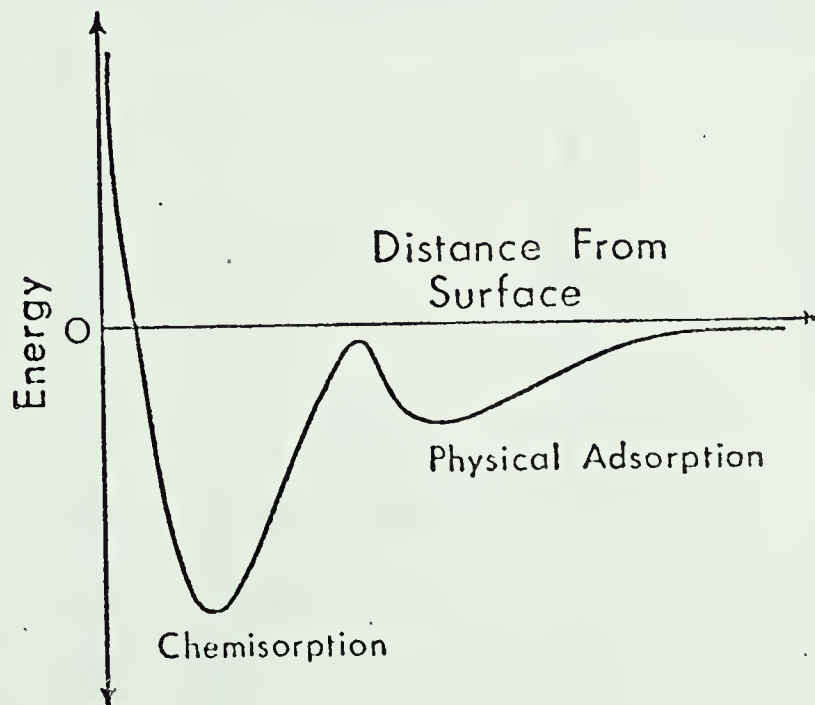


Figure 2.1 : Adsorption energetics.



There are differences of opinion on the adsorption mechanisms and the values of the activation energies and the heats of adsorption. As well, there is considerable evidence (2.54 - 2.56) that the adsorption characteristics of oxygen and ethylene on platinum surfaces is a function of which crystal face is available for adsorption. Further, some researchers (2.57) speculated that oxygen may exist in a variety of adsorbed forms. Some of the more recent studies of adsorbed oxygen on platinum have been discussed by Carrière et al. (2.58) The heats of adsorption of ethylene and of oxygen on various metals is summarized in Table 2.2.

TABLE 2.2  
HEATS OF ADSORPTION

Metal	Temperature (°C)	Oxygen (kcal/mol)	Ethylene (kcal/mol)	Reference
Ni	-183		10 - 55	2.24
Ta	23		138	2.44
W	23		105	2.44
Cr	23		100	2.44
Fe	23		68	2.44
Ni	23		58	2.44
Rh	23		50	2.44
W	20	139		2.45
Pt	- 80	40 - 58		2.51
Pt	22	53 - 69		2.52
Pt (100)	22	~ 0		2.50
Pt	22	40 - 60	10 - 20	2.49





### 2.3 Reactor Analysis

This work does not presume to contribute to the already extensive literature on reactor analysis. A great number of researchers have constructed mathematical models which purport to describe chemical reactors and can, under certain circumstances, predict sustained oscillations in temperature and/or conversion (instabilities). As excellent reviews of the subject have already been written (2.59, 2.60) an additional review here would be, at the best, redundant.

One feature common to many of the papers is that the instability is often attributed to macroscopic phenomena, such as the classical heat generation - heat loss curves associated with stirred tank reactors. In the present work, microscopic effects such as changes in the surface structure of the catalysts can be used as an explanation of the observed instabilities. Since nearly every author has a unique explanation for the particular oscillations he observes, a review of these ideas would perhaps be better left for one's later years.

To determine the reaction rate constants, a differential recycle reactor (described in Chapter 3) was used. This was done in an attempt, with a heterogenous system, to obtain the behaviour of a stirred tank reactor. This particular approach, the use of a recycle reactor, has been used by many others. ( See Yang and Weinstein (2.61) for examples.) Also, other reactor types such as the Notre - Dame spinning basket reactor (2.5) have been used with success. The advantage in using this type of system is that the mass balance equations for an ideal CSTR are algebraic, while the mass balance equations for other reactor types (integral bed, batch,



etc.) are usually differential, thereby necessitating the differentiation of kinetic data.

As a final comment, it should be pointed out that the observation of oscillatory chemical systems has not been narrowly confined to the realm of chemists and chemical engineers. A review, with over three hundred references, of oscillatory phenomena in many fields (chemistry, engineering, medicine, zoology, electrochemistry, and population studies) has been prepared by Nicolis and Portnow (2.62).



## CHAPTER 3

### PROCEDURE AND EQUIPMENT

#### 3.1 Differential Recycle Reactor

##### 3.1.1 Equipment

Figure 3.1 shows a schematic diagram of the differential recycle system used for the kinetic runs. The system can be divided into three sections: gas delivery system, reaction system, and regulation system.

C.P. grade nitrogen, carbon dioxide, ethylene, and oxygen were obtained from local distributors. (The supplier changed during the course of the experiments.) For low oxygen runs, mixtures of ethylene and nitrogen were prepared in high pressure cylinders, then mixed with line air prior to the reactor. The gases used for the high oxygen runs were line air and a specialty gas, nominally 5% ethylene in nitrogen, obtained from Linde. For intermediate oxygen runs, high pressure cylinders of oxygen and nitrogen were prepared as feedstock. The line air was dried by passing it through a cylindrical bed of 4A Molecular Sieve, 30 cm by 706 cm<sup>2</sup>. Occasionally, a run with a high carbon dioxide concentration required the addition of carbon dioxide to one of the high pressure cylinders. The gas flow rates were controlled by Matheson regulators and Whitey needle valves. The flow rates were measured with two Matheson Mass Flow Meters, model 8116-0153, with a flow range of 0 to 500 SCCM (standard cubic centimetres per minute); and model 8116-0112, 0 to 100 SCCM. These mass flow meters were pre-calibrated for a variety of gases, however, the calibrations were rechecked with air, nitrogen and nitrogen and ethylene mixtures. The specifics of these calibrations, and the calibrations for the other regulatory and measurement devices are in Appendix B.



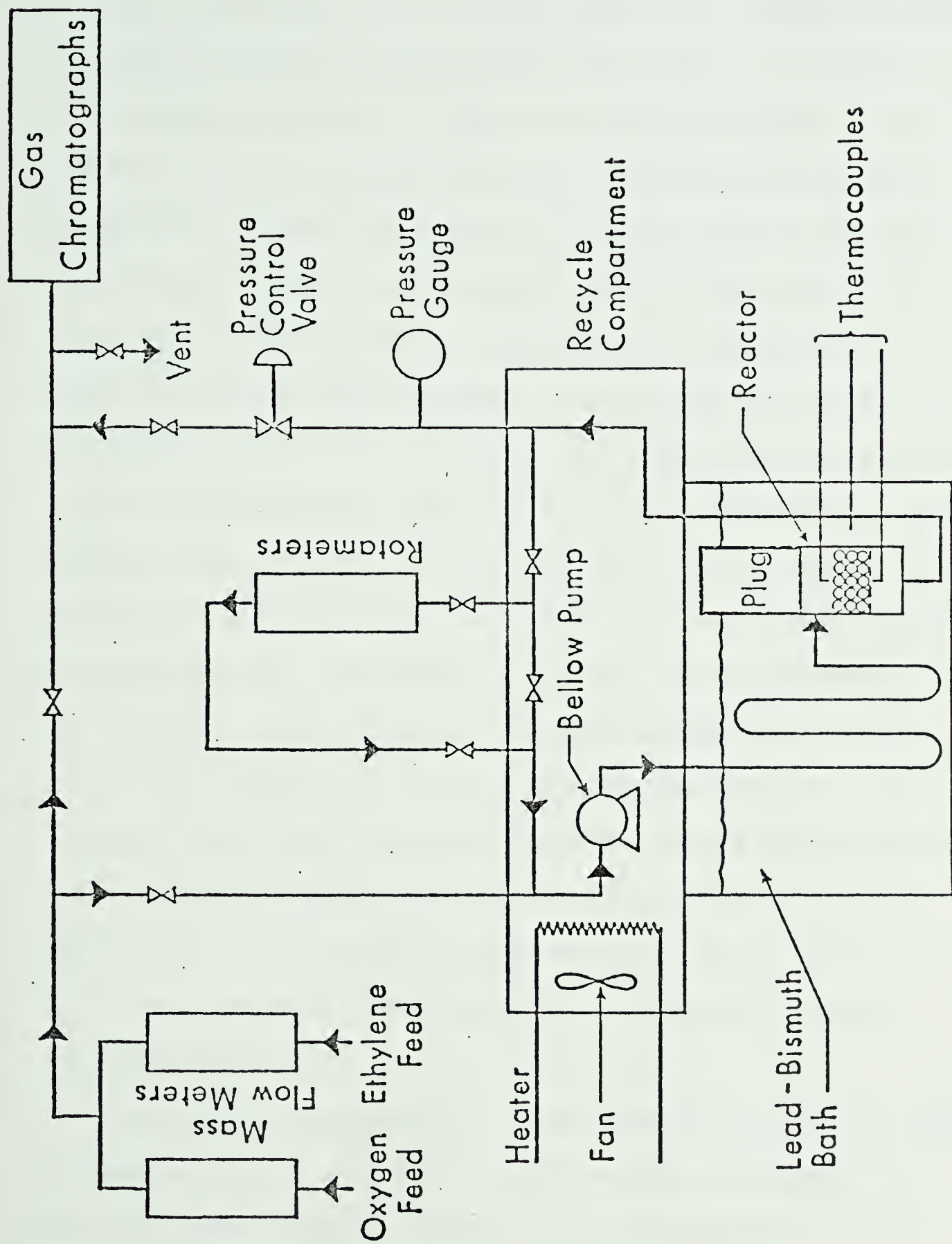


Figure 3.1 : Schematic diagram of differential recycle reactor.





The feed stream could be made to flow either through the reactor, or directly to the gas chromatographs via a bypass. A number of needle valves were placed in the lines and were adjusted so that the pressure drop, and hence the flow rate, through the bypass would be the same as through the reactor. The recirculation was effected by the use of a metallic bellows pump, model MP 301, manufactured by the Metal Bellows Company, and powered by a single phase quarter horsepower induction motor. Since the motor operated only at a single uniform speed, the ratio of the flow through the recycle loop to the exit flow was regulated by a Nupro needle valve. The pressure inside the loop was regulated with a Moore Constant Differential Flow Controller, model 63SU-L with an external variable reference pressure. The reactor was always run at a pressure of  $145 \pm 10$  kPa (  $\sim 7.5$  psig ). The pressure was measured using a J.P. Marsh Bourdon Tube pressure gauge mounted upstream of the flow controller. The flow rate through the recycle loop was measured with a Matheson rotameter, tube size R-2-15-B, mounted outside the hot box. The rotameter loop was isolated from the main recycle loop with Nupro shutoff valves and was used only to spot check the flow rates.

For kinetic determinations, the measurement of isothermal data is preferable if at all possible. This reduces the dimension of the final curve - fitting problem by one and may enable the use of very simple single variable regression formulae. To facilitate the taking of isothermal data, a constant temperature bath for the reactor was constructed. The bath was filled with Cerrobased,



a eutectic mixture of lead (45% by weight) and bismuth (55% by weight) which had a melting point of about 400 K. The bath was heated with a controlled 2500 watt calrod immersion heater. The high thermal conductivity of the lead - bismuth mixture (both in the solid and liquid phase) resulted in essentially constant reactor wall temperatures. The wall temperature never varied by more than 0.5°C. A similar bath was used for kinetic studies by Wanke (3.1) who found that the inclusion of a stirrer in the bath was not necessary to maintain the reactor wall at constant temperature. The lead - bismuth eutectic was contained in a stainless steel cylinder 90 cm long with a diameter of 18 cm. The steel cylinder was further enclosed in an aluminum-clad asbestos container to minimize heat losses from the bath.

The reactor tube was a 3/4 inch, schedule 40 stainless steel pipe, 36 cm long. Approximately five feet of pre-heating coil was wound around the reactor to ensure that the reactants entering the reactor were at the same temperature as the bath. As the molten metal would foul the threads of the reactor fittings, the reactor tube was extended above the level of the bath. A stainless steel plug was placed inside the reactor tube, extending 10 inches down into the reactor tube. A fine screen was mounted 1/2 inch from the bottom of the tube to contain the catalyst. The combination of the plug and the screen reduced the effective volume of the reactor to about 20 cubic centimeters. When the reactor was charged, a layer of glass beads was placed on the screen first. The layer of glass beads was usually 2 to 3 centimetres deep. The layer of glass beads was then followed by



the particular catalyst charge. The bellows pump, the recycle tubing, and the top of the reactor were all contained on top of the bath housing inside an asbestos-insulated sheet metal box. The air in the box was warmed by heat transferred from the molten metal and by a copper coil heater to the same temperature as the bath.

Two iron - Constantan (55% Cu and 45% Ni) thermocouples, one near the middle of the catalyst bed and another near the top of the catalyst bed were used to measure the reaction temperatures. They passed axially down the reactor tube, through the reactor plug.

Gas chromatography was used to analyse the feed and product compositions. A Beckman GC - 2 with a molecular sieve column was used to separate oxygen and nitrogen while a Hewlett - Packard model 5710A gas chromatograph with a Porapak Q column separated nitrogen-oxygen, carbon dioxide, ethylene, and water. The line from the reactor to the chromatographs was heated to prevent condensation of any of the reaction products. The outputs of the chromatographs were recorded and analyzed with a Hewlett - Packard model 3380a electronic reporting integrator. The details of the chromatographic analysis are contained in Appendix C.

The output from the mass flowmeters was continuously monitored on a Hewlett - Packard model 17501A strip chart recorder and the outputs from the thermocouples were recorded on a Watanabe Servocorder strip chart recorder. The control of the eutectic bath heater was accomplished with a Honeywell model MS2 temperature controller. All lines were 1/4 inch seamless 316





stainless steel tubing.

### 3.1.2 Operation

The differential recycle reactor was used for kinetic determinations and for the dispersion versus activity tests. The first kinetic runs were done on a commercial Englehard catalyst. These catalyst pellets were surface-coated  $\gamma$ -alumina cylinders 1/8 inch by 1/8 inch, with a nominal platinum loading of 0.3%. The reactor was charged with 100 pellets (4.73 g) for the initial tests. The activity of the fresh catalyst was determined, The catalyst was then treated in flowing air at 413 K for 16 hours and again at 576 K for 63 hours and the activities were rechecked. This catalyst was then used for the series of kinetic runs.

The flow system allowed for either sequential admittance of the reactants to the reactor or for the complete mixing of all the reactants prior to the reactor. For all the kinetic runs, the reactants were admitted to the reactor in a well mixed flow. Some adsorption studies were also done using this apparatus, and these called for sequential admission of the reactants into the reactor.

For the kinetic runs, the total mass flow rate was kept between 500 and 600 SCCM for the majority of the runs. The total stream would be sent through the bypass for analysis of the feed stream, then switched through the reactor. Analyses were performed on the reactants until steady state was achieved. The time required to reach steady state varied between 20 minutes and 8 hours depending on the instabilities that occurred. Once



steady state was achieved, a number of repeat analyses were performed. The feed composition was occasionally rechecked after the products had been analysed in order to ensure that no change in the feed composition had occurred. While the chemical analyses provided discrete measurements of the reaction progress, a continuous monitoring of the transients was possible via the output of the catalyst bed thermocouples.

Kinetic data were taken at the following temperatures: 362K, 375K, 388K, 400K, 455K, and 472K. Ethylene feed concentrations varied from 0.1% to 3% and the oxygen to ethylene ratio was varied from 0.1 to 200.

The catalyst used during the integral bed runs was also tested in the differential recycle reactor. The reactor was charged with 3.4 g of the aged catalyst and the activity of the catalyst was determined for temperatures between 353 K and 388 K.

## 3.2 Integral Bed Reactor

### 3.2.1 Equipment

A schematic diagram of the integral bed reaction system is shown in Figure 3.2. Again, the system can be divided into three parts, the gas delivery system, the reaction system, and the analysis/regulation system.

The gas delivery system was identical to the system used for the recycle reactor with a few minor exceptions. Two calibrated Matheson rotameters, tube #610 and tube # R-2-15-B were used to measure the flow rates of the reactants into the reactor. The gas flow could be sent to the reactor or directly to the gas



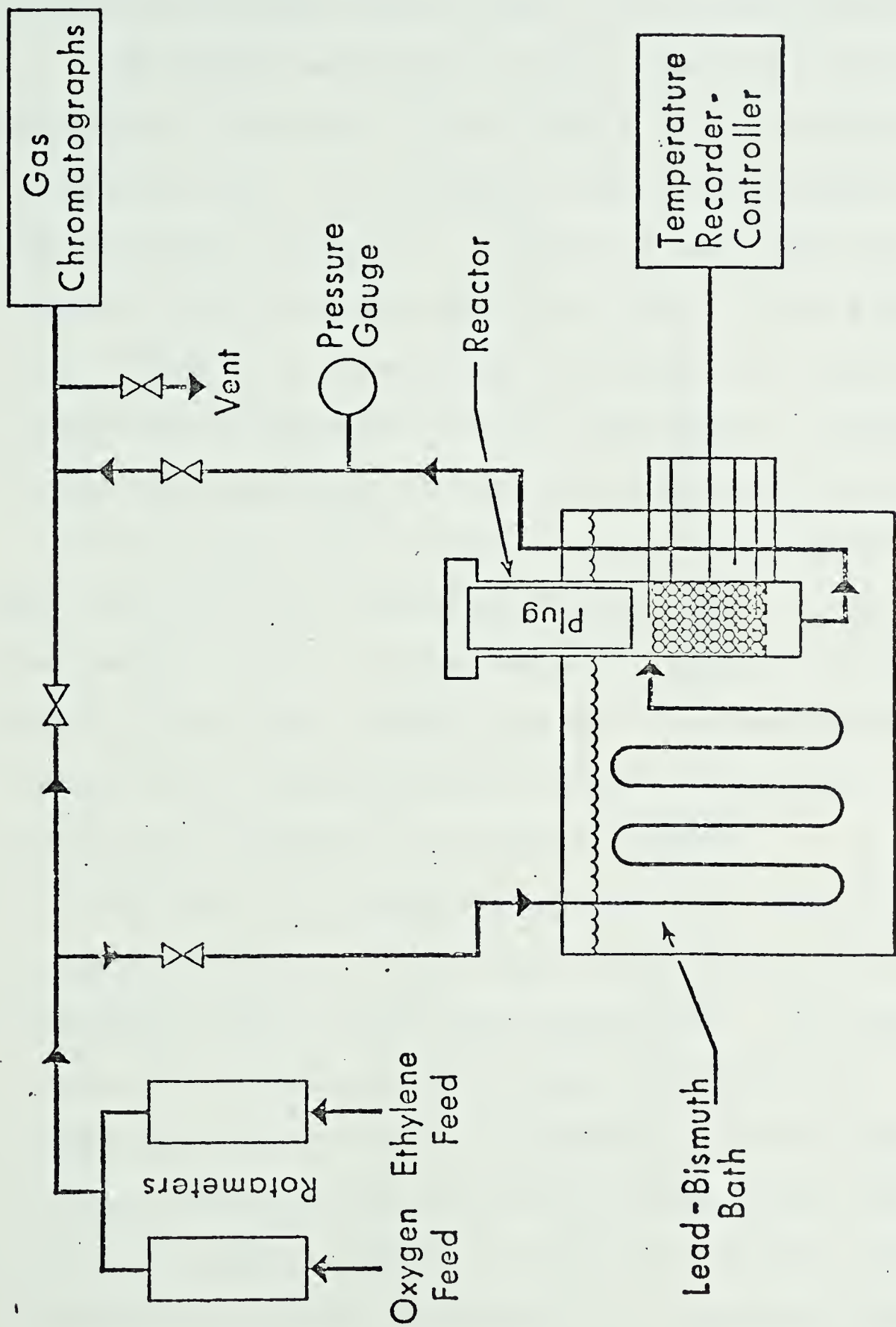


Figure 3.2 : Schematic diagram of integral bed reactor.





chromatographs. Again, the pressure drops in the two loops were equalized with needle valves, so that the flows would be the same.

The integral bed reactor is shown schematically in Figure 3.3. The reactor itself was a 3/4 inch schedule 40 316 stainless steel pipe, 60 cm long. A fine screen was placed at the bottom of the tube to contain the catalyst. A mixture of glass beads and catalyst pellets could be placed in the reactor to form a bed up to 30 cm deep. Six thermocouples were placed in the catalyst bed to monitor the temperature profiles in the reactor. Two thermocouples were imbedded in the outer skin of the reactor tube.

The Cerrobath described previously for the recycle reactor was also used for the integral bed reactor. Since the reaction zone was beneath the level of the molten metal, there was no need to build a hot box above the bath container. The line from the reactor to the chromatographs was insulated and heated to prevent any condensation of the reaction products.

The analysis and regulation instruments were somewhat different. A Honeywell Electronik 16 multi-point recorder was used to record the outputs from the eight reactor thermocouples. The temperature in the bath was controlled with a Foxboro M/62 controller. The Beckman GC-2 mentioned earlier was used to analyse for oxygen and nitrogen and a Gow Mac Series 550 Gas Chromatograph was used to analyse for oxygen- nitrogen, carbon dioxide, ethylene, and water. The output from the two chromatographs was recorded on a Hewlett - Packard model 7100-B strip chart recorder equipped with a Disc Integrator. Also, an on-line gas chromatography analysis package was available on the Chemical Engineering Department's IBM 1800





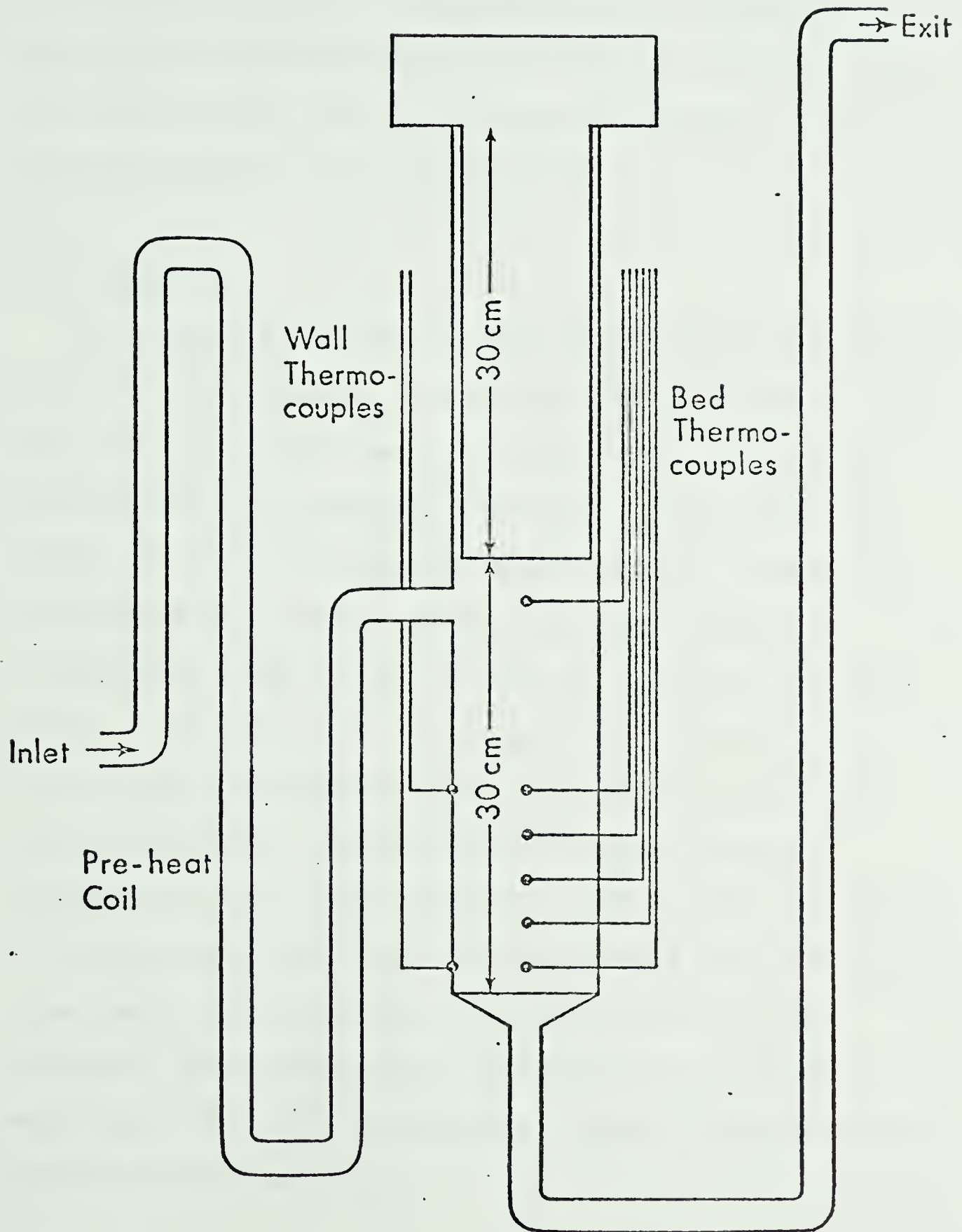


Figure 3.3 : Thermocouple locations in integral bed reactor.



computer. The signals from the chromatographs were analysed using this package of computer programs as a check on the values obtained from the Disc Integrator. Two thermocouples in the bed were continuously recorded on the Watanabe strip chart recorder as well as on the multi-point recorder. Pressure measurements in the reactor were made with a mercury manometer.

### 3.2.2 Operation

The integral bed reactor was operated in much the same fashion as was the recycle reactor. All the reactants were mixed and then fed either to the reactor or to the bypass loop. The transients were observed on the continuous temperature output. The initial catalyst was the 0.3% Pt catalyst described earlier. The catalyst bed contained 13.8 grams of catalyst and seventy - two grams of glass beads. The catalytic activity was checked for the fresh catalyst. The catalyst was then treated in flowing air at 523 K for 60 hours and at 576 K for 12 hours. The activity was rechecked after each treatment. The bulk of the fractional conversion measurements in the reactor were taken at 375 K, 380 K, and 387 K. The ethylene feed concentration was varied from 0.1% to 2 % and the oxygen feed concentration was varied from 1 % to 20 %. Some measurements were taken at 420 K and 440 K as well. Some high temperature (640 K - 766 K) oxidations using only 1/8 inch alumina spheres were also investigated.



### 3.3 Catalyst Activity Comparisons

#### 3.3.1 Procedure

A series of experiments to determine the relationship between catalyst reactivity and platinum dispersion was the final undertaking. A number of catalysts, Englehard 0.5% Pt on 1/8 inch alumina cylinders having dispersions ranging from 0.036 to 0.32 were prepared. The details of the catalyst preparation and the dispersion measurements are in the next section.

In each case, 75 catalyst pellets (about 3.2 grams) were placed in the recycle reactor. The catalyst activity for ethylene oxidation was measured at 385K, 410K, and 425K. The oxygen concentrations were varied from 2 % to 18% and the ethylene concentrations were varied from 0.2% to 2 %. The equipment and techniques used were nearly identical with the kinetic investigations in the recycle reactor described earlier.

#### 3.3.2 Catalyst Preparation and Analysis

The catalyst preparation and analysis was performed by R. Fiedorow. The catalysts were either sintered in flowing oxygen or in flowing hydrogen at a pressure of about 93 kPa. The dispersion measurements were made by introducing hydrogen pulses into a nitrogen carrier gas stream. The hydrogen adsorption uptakes were then used to determine the dispersions. Table 3.1 lists the catalysts, their treatments, and the dispersions. The details of the sintering and the adsorption measurements are explained by Fiedorow and Wanke (3.2).



TABLE 3.1  
CATALYST TREATMENTS AND DISPERSIONS

Catalyst	Treatment			Dispersion
	Atmosphere	Temperature (°C)	Time (hr)	
E-00	-	no treatment	-	0.22
E-29A	O <sub>2</sub>	800	1	0.036
E-26	O <sub>2</sub>	700	1	0.115
E-96	H <sub>2</sub>	800	1	0.120
E-95	H <sub>2</sub>	700	1	0.155
E-27	O <sub>2</sub>	650	1	0.17
E-97	H <sub>2</sub>	500	1	0.22
E-25	O <sub>2</sub>	600	1	0.26
E-24	O <sub>2</sub>	500	1	0.27
E-28	O <sub>2</sub>	550	1	0.31
E23/29	O <sub>2</sub>	550	16	0.32





## CHAPTER 4

### DIFFERENTIAL RECYCLE REACTOR

#### 4.1 Introduction

The recycle reactor was used to obtain kinetic data for the determination of an empirical rate function for the complete oxidation of ethylene to carbon dioxide and water over supported platinum catalysts. Fresh 0.3% Pt/Al<sub>2</sub>O<sub>3</sub> catalysts which had been thermally stabilized and catalyst which had been aged in the integral bed reactor were both used in these tests. It was suspected that the reaction could be modelled using the form of an L-H rate equation and the experiments were performed with this in mind. Three types of experiments were undertaken. Investigations of the oxidation in excess (18%) oxygen and low (1% - 2%) ethylene concentration were conducted first, followed by experiments with near-stoichiometric mixtures of oxygen and ethylene. Experiments with high ethylene concentrations (>5% with sub-stoichiometric oxygen) resulted in no detectable reaction at temperatures up to 472 K due to the inhibition by ethylene.

#### 4.2 Reactor Selection

The number of reactor types used for kinetic determinations is nearly as great as the number of rate equations which have been produced. The type of reactor chosen for this work was dictated by the mass balance equations (see Appendix A) and a few externalities.

The method of analysis chosen, gas chromatography, was fairly slow. Each set of measurements required about eight minutes to complete.



Carbon dioxide, one of the reaction products, had no inhibitory effects on the reaction rate, and hence, the measurement of initial rates was not necessary. Since the reaction was highly exothermic, non-isothermalities and heat transfer limitations would make the use of an integral bed reactor extremely difficult in the determination of kinetic constants. As well, since the rate equation was suspected to be of the form

$$-r = \frac{K_1 K_2 K_3 [O_2]^{n_1} [C_2H_4]^{n_2}}{(1 + K_1 [O_2] + K_2 [C_2H_4])^{n_3}} \quad (4.1)$$

the use of an integral bed reactor for the kinetic determinations was rejected.

Instead, it was decided that a pseudo-stirred tank reactor would be constructed. The choice for the reactor type was narrowed to two - a recycle reactor or a spinning basket reactor similar to the one alluded to in Chapter 2 (2.5). As either reactor type would be acceptable, the decision became one of economics. The recycle reactor described in Chapter 3 was considerably less expensive since some existing pieces of apparatus could be incorporated into the design, and therefore, it was selected.

### 4.3 Blank Runs

The possibility that the reaction could be catalyzed by the metal of the reactor or the alumina support and the possibility of homogeneous gas phase reaction was ascertained in a series of blank



runs. (The experiments were actually done in the integral bed reactor, but the results can be mentioned here. More detail will be offered in Chapter 5.) The first runs were in an empty reactor using a 1.52% ethylene in air mixture as the feed. No reaction occurred up to 593K and the fractional conversion was less than 5% at 792K. In the second series of experiments, a stream of ethylene (up to 1%) in air was passed over a bed of 1/8" alumina spheres. Again, no reaction products were detected up to 593K.

In comparison, Omar et al. (2.34) found no reaction below 498K for ethylene over alumina and Dmuchovsky et al. (2.31) reported that no reaction occurred below 699K. As will be shown in Chapter 5, the reaction kinetics are much different for ethylene oxidation over alumina than for the oxidation over alumina supported platinum. In any case, all of the kinetic runs were below 500K, and the dependence of the kinetics on alumina or reactor metal catalyzed reaction or on homogeneous gas phase reaction is certainly negligible.

#### 4.4 Catalyst Activation

While catalyst manufacturers endeavour to supply catalysts which are physically and chemically stable, most supported metal catalysts are affected in some manner by thermal treatments. The stability of the catalyst used here was studied in two ways. A fresh single catalyst charge (designated A) was subjected to two subsequent thermal treatments in flowing air: first for 15 hours at 478K (B) and then for 13 hours at 568K (C). The activity of this Engelhard 0.3% platinum catalyst was determined for each of the three cases. The first experiment was a test to determine if the activity of the fresh





catalyst would change with time. A 0.64 mole % ethylene-in-air mixture was passed over the catalyst charge (100 pellets; 4.73 g) and the conversion was measured at various times. This run, along with a similar run performed later with the thermally treated catalyst (C) are pictured in Figure 4.1. In each case, the activity remained relatively constant over the 75 hour run time, with the exception of slight initial increases in the activity. The thermal treatment seemed to have caused a permanent increase in the activity of the catalyst.

The activity of the fresh catalyst sample is compared with its activity after the thermal treatments in Table 4.1. Here the negative order dependence of the rate on the ethylene concentration is evident, as well as an increase in activity with increasing treatment severity.

TABLE 4.1  
CATALYST ACTIVITY FOLLOWING THERMAL TREATMENTS

Temp (K)	Inlet Ethylene Conc. (mole %)	Fractional Conversion		
		A	B	C
391	0.64	0.022	0.041	0.088
388	0.65	0.000	0.056	0.065
388	0.37	0.073	0.118	0.283

Even though these treatments are rather moderate, the increase in activity is apparent. This effect was even more pronounced with the catalyst used in the integral bed reactor, although the treatments were more severe. This increase in activity could be explained by



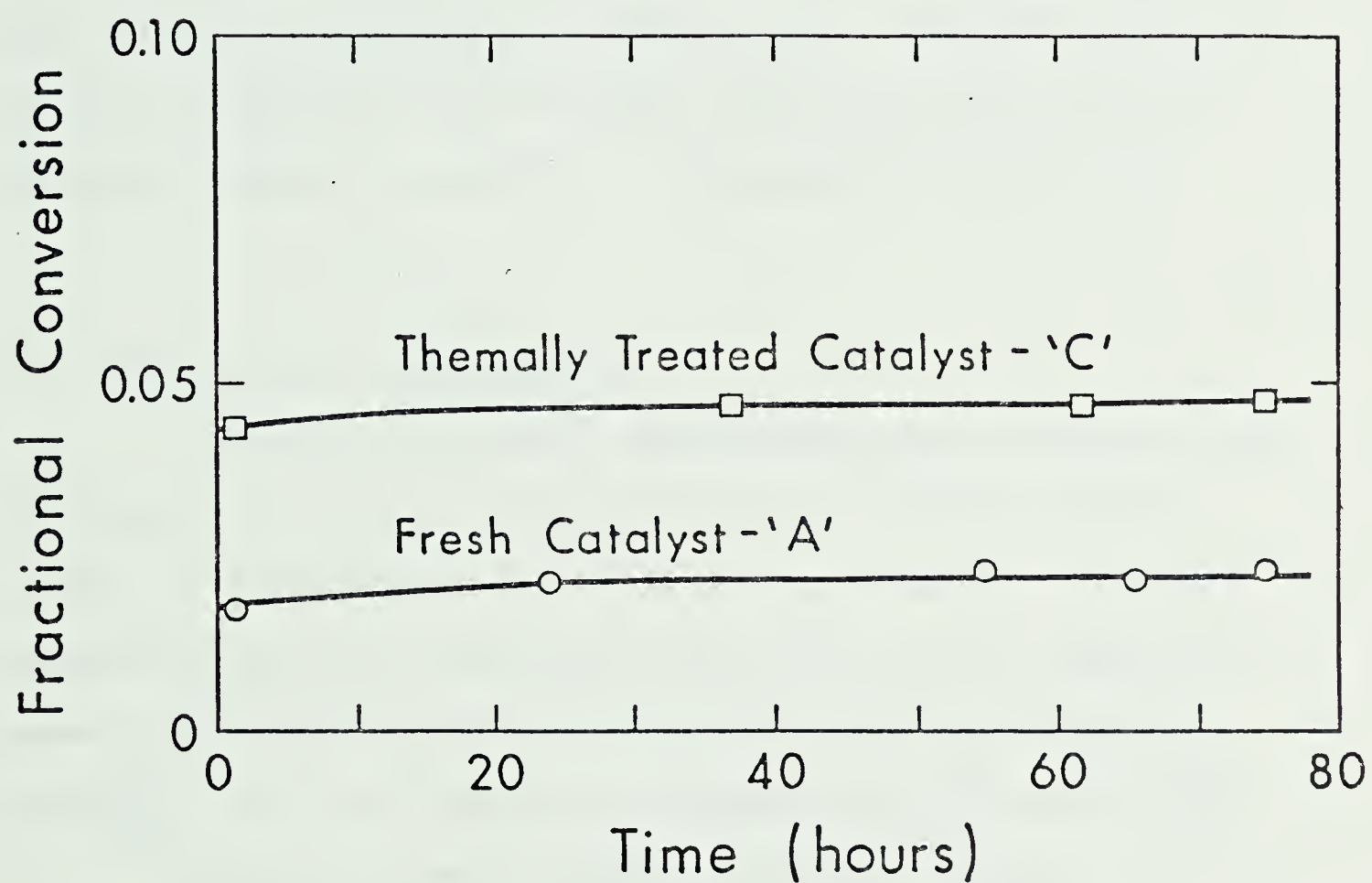


Figure 4.1 : Activity changes following thermal treatment of the catalyst.



postulating that a slight increase in the dispersion of the metal on the support surface occurred. The sintering model for supported metal catalysts proposed by Flynn and Wanke (4.1) does predict this, and experimental evidence for increased dispersion as a result of moderate treatments has been found by Fiedorow and Wanke (3.2). Repeat experiments using the thermally treated catalyst (C), showed that this pre-treatment had partially stabilized the activity of the catalyst, but variations in activity were still observed. The variations in catalytic activity were particularly noticeable immediately after some high temperature unstable runs and complete conversion runs.

#### 4.5 Kinetic Runs - Fresh Catalyst

The bulk of the kinetic determinations were performed on the 0.3% platinum on alumina catalyst which had been heated to 568K in flowing air (designated as "C" in the previous section). Fractional conversion versus exit concentration data were taken for temperatures between 362 and 472K, ethylene concentrations between  $0.048 \frac{\text{mol}}{\text{m}^3}$  and  $0.952 \frac{\text{mol}}{\text{m}^3}$ , and oxygen concentration between  $0.161 \frac{\text{mol}}{\text{m}^3}$  and  $9.29 \frac{\text{mol}}{\text{m}^3}$ .

As was mentioned in Section 4.2, it was suspected that the reaction would have a Langmuir-Hinshelwood type of mechanism, and a rate equation like Equation (4.1). The first series of experiments, conducted in excess oxygen (18%-20%), eliminated the oxygen dependence. If the oxygen concentration does not change appreciably, then Equation (4.1) can be written in the form

$$-r = \frac{k_1 [C_2H_4]^{n_1}}{(1 + K_3 [C_2H_4])^{n_3}} \quad (4.2)$$



After a few runs, the strong inverse nature of the kinetics became apparent, thereby requiring that

$$n_3 > n_1 \quad (4.3)$$

Later, after examining the results of the near-stoichiometric runs, two rate equations were selected for the curve fitting:

$$-r = k_1 \left\{ \frac{[O_2]}{[C_2H_4]} \right\}^{k_2} \quad (4.4)$$

and

$$-r = \frac{k_1 [O_2]}{(1 + k_2 [C_2H_4])} \quad (4.5)$$

also, a special case of (4.4) was also used, i.e.

$$-r = \frac{k[O_2]}{[C_2H_4]} \quad (4.6)$$

A two-dimensional plot can be used to visually evaluate Equations (4.4) and (4.6); however, a depiction of Equation (4.5) is more difficult. The measured rate of reaction versus the ratio of the oxygen concentration to the ethylene concentration for the excess oxygen runs is shown in Figure 4.2. The rates were calculated with the observed fractional conversions as outlined in Appendix A. In turn, the fractional conversions were based on carbon dioxide production or ethylene depletion. This resulted in two values for the measured rate; one based on carbon dioxide, the other on ethylene. The value of the rate used was value based on  $CO_2$  if the conversion was less than 10% and the average of the two values if the conversion was greater than 10% (see Appendix E for justification and elaboration). The lines passing through the





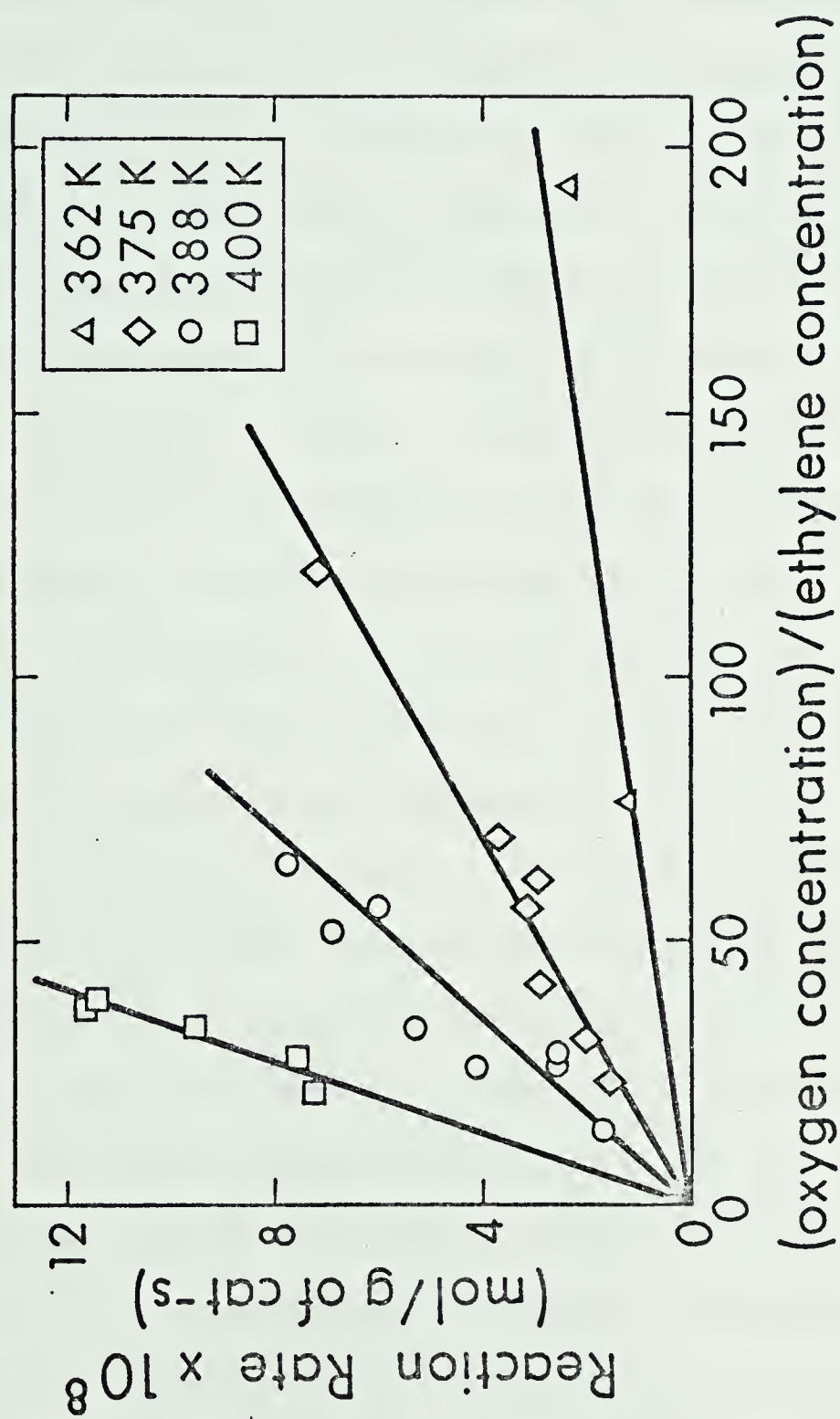


Figure 4.2 : Rates of ethylene oxidation as a function of the ratio of oxygen to ethylene concentration in excess oxygen.



points are least-squares linear fits. The data used to prepare Figure 4.2 are located in Appendix D.

The runs in lower oxygen concentrations were performed in the same manner as were the excess oxygen runs. The rate based on  $\text{CO}_2$  was used if the conversion was less than 10% and the average value was used for conversions above 10%. Only very rarely did the reaction exceed 75% conversion without going to completion (100% conversion). In those very few cases, the rate based on ethylene alone was used for the curve fitting. The data for the low oxygen runs, located in Appendix D, is pictured in Figure 4.3. Again, the measured rate was plotted against the ratio of the exit concentration of oxygen to the exit concentration of the ethylene. The data for both the low and excess oxygen runs were fitted to three equations, (4.4), (4.5) and (4.6) using the Marquardt multi-variable non-linear regression algorithm. The computer program is listed in a separate data book (see Appendix F). The kinetic parameters obtained are summarized in Table 4.2. While the two-parameter equations will, of course, provide generally better fits to the experimental data, the slight added complexity is not always justified, and may in fact be misleading. Equation (4.4) provided only slightly better fits of the data than did Equation (4.6). The variance for that two-parameter equation was generally only a few percent less than the variance for the single parameter equation. The value of the exponent on the concentration ratio in Equation (4.4) varied from 0.709 to 1.4011 without any perceptible pattern. The average value of this parameter was 0.9975, which suggests that the single parameter model, Equation (4.6) can probably be used to model the reaction with little loss of accuracy.



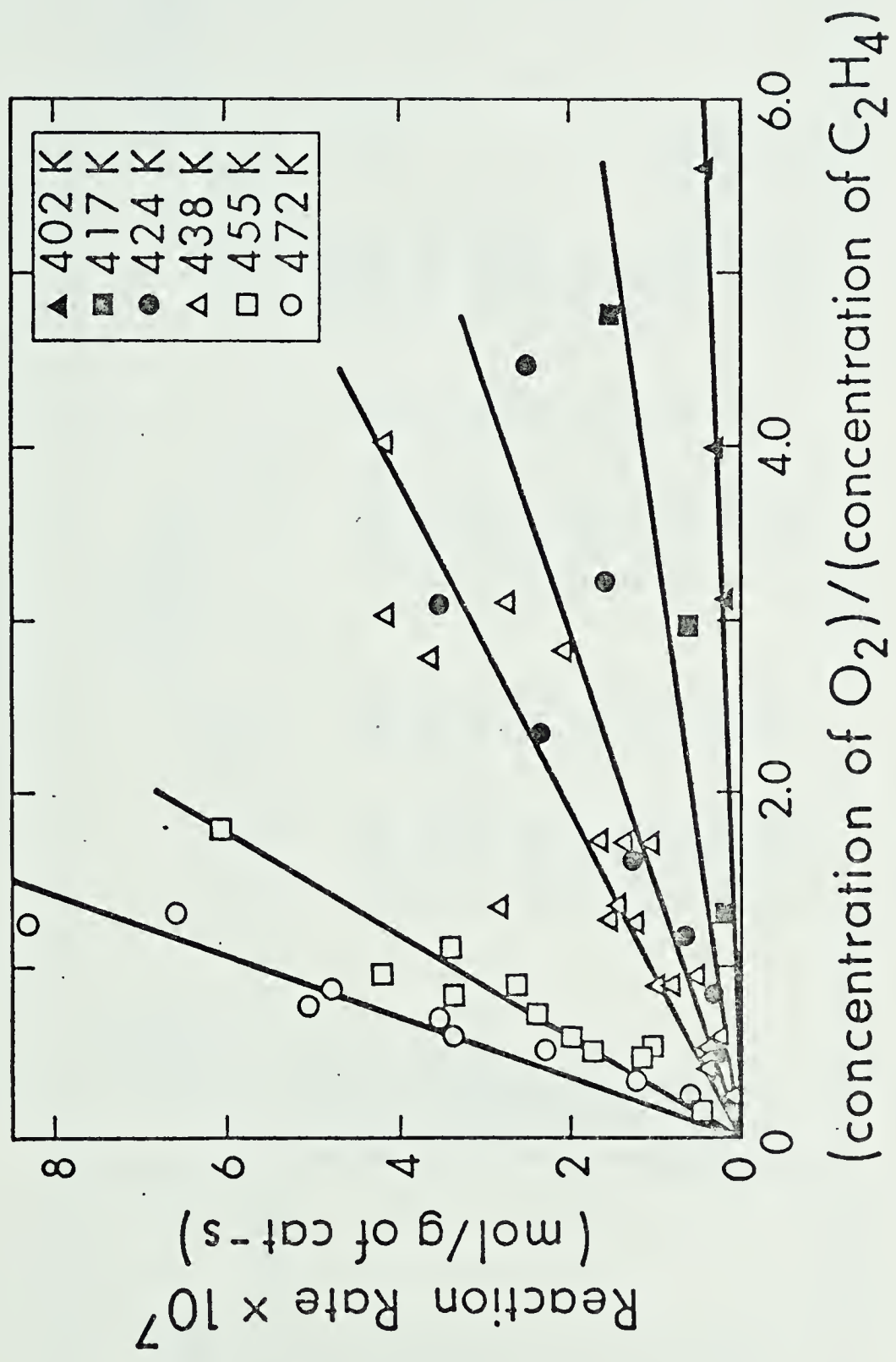


Figure 4.3 : Rates of ethylene oxidation as a function of the ratio of oxygen to ethylene concentration in low oxygen concentrations.



TABLE 4.2

## KINETIC CONSTANTS

Temp (K)	$-r = k \frac{[O_2]}{[C_2H_4]}$	$-r = \frac{k_1 [O_2]}{1 + k_2 [C_2H_4]}$	$-r = k_1 \left\{ \frac{[O_2]}{[C_2H_4]} \right\}^{k_2}$
	$k * 10^8$	$k_1 * 10^8$	$k_2$
362	0.01268	-	0.0126
375	0.05709	$0.1336 * 10^3$	$0.2308 * 10^4$
388	0.11033	$0.46382 * 10^1$	$0.3559 * 10^2$
400	0.28880	$0.17015 * 10^2$	$0.5445 * 10^2$
402	0.7642	$0.3861 * 10^3$	$0.4911 * 10^4$
417	2.930	$0.19311 * 10^4$	$0.6042 * 10^3$
424	6.827	$0.3057 * 10^5$	$0.4273 * 10^4$
438	10.390	$0.9156 * 10^3$	$0.8849 * 10^2$
455	33.53	$0.9501 * 10^2$	$0.1366 * 10^1$
472	55.77	$0.6069 * 10^6$	$0.1464 * 10^5$
			$0.0126$
			$0.4965 * 10^{-1}$
			$0.17316$
			$0.39927$
			$0.4122$
			$4.479$
			$9.553$
			$0.10425 * 10^2$
			$0.3318 * 10^2$
			$0.5598 * 10^2$
			1.000
			1.0313
			0.8847
			0.9087
			1.4011
			0.7583
			0.709
			0.9566
			1.107
			1.218





The other rate equation which was fitted, Equation (4.5) more closely resembled the L-H type of equation. A problem often encountered in the fitting of L-H rate equations also occurred here. The parameters tend to exhibit a correlation, which often prevents the development of a rate constant versus temperature dependence. As can be seen from Table 4.2, the ratio of the two constants in Equation (4.5) is usually close to the corresponding rate constant for the single parameter model, Equation (4.6). However, because of the parameter correlation, the least square minimization can result in parameter values which defy any attempt to cast them into a temperature dependent form.

The value of the predicted rate versus the measured rate has been plotted for the 375K runs and the 472K runs on Figures 4.4 and 4.5 respectively. The values for Equations (4.4), (4.5), and (4.6) with the appropriate constants from Table 4.2 are plotted for those two temperatures. The 45° line represents the case where the predicted value matches the measured value exactly. The difference between the three fits is hardly discernible on Figures 4.4 and 4.5, however Equation (4.5) does seem to be slightly better than the other two on Figure 4.5. The relationship between measured and predicted rates for the other temperatures is not any different than for 375K and 472K.

Because of its simplicity and accuracy, and the failure of the two parameter models to exhibit distinct superiority, the single parameter model, Equation (4.6) was selected as the kinetic equation to model the reaction.

The rate constants obtained from the single parameter fit, Equation (4.6), are shown on an Arrhenius plot as the open circles in Figure 4.6. The solid circles are explained in Section 4.6. The



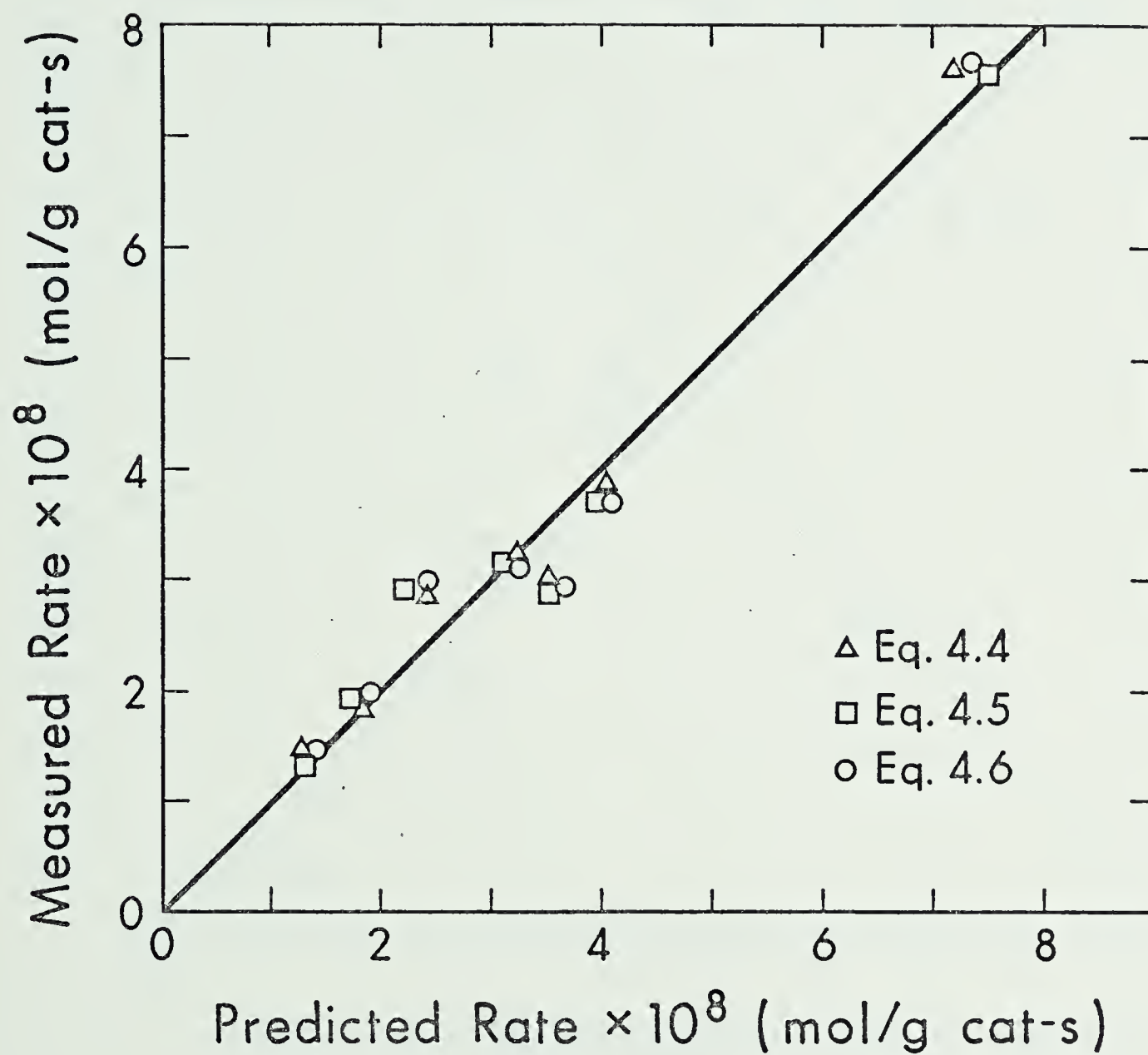


Figure 4.4 : Comparison of predicted versus measured rates at 375 K for various rate equations.



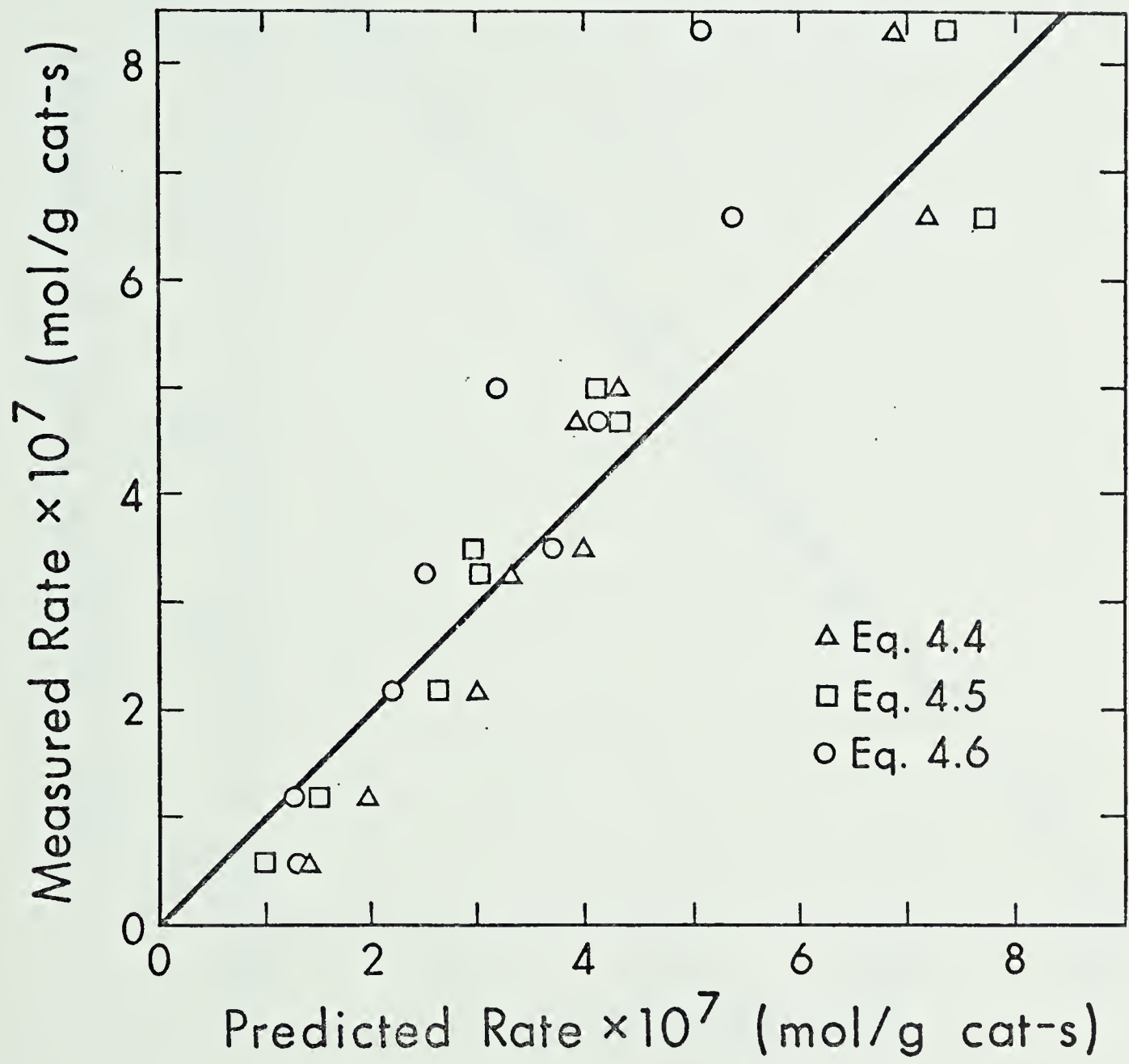


Figure 4.5 : Comparison of predicted versus measured rates at 472K for various rate equations.



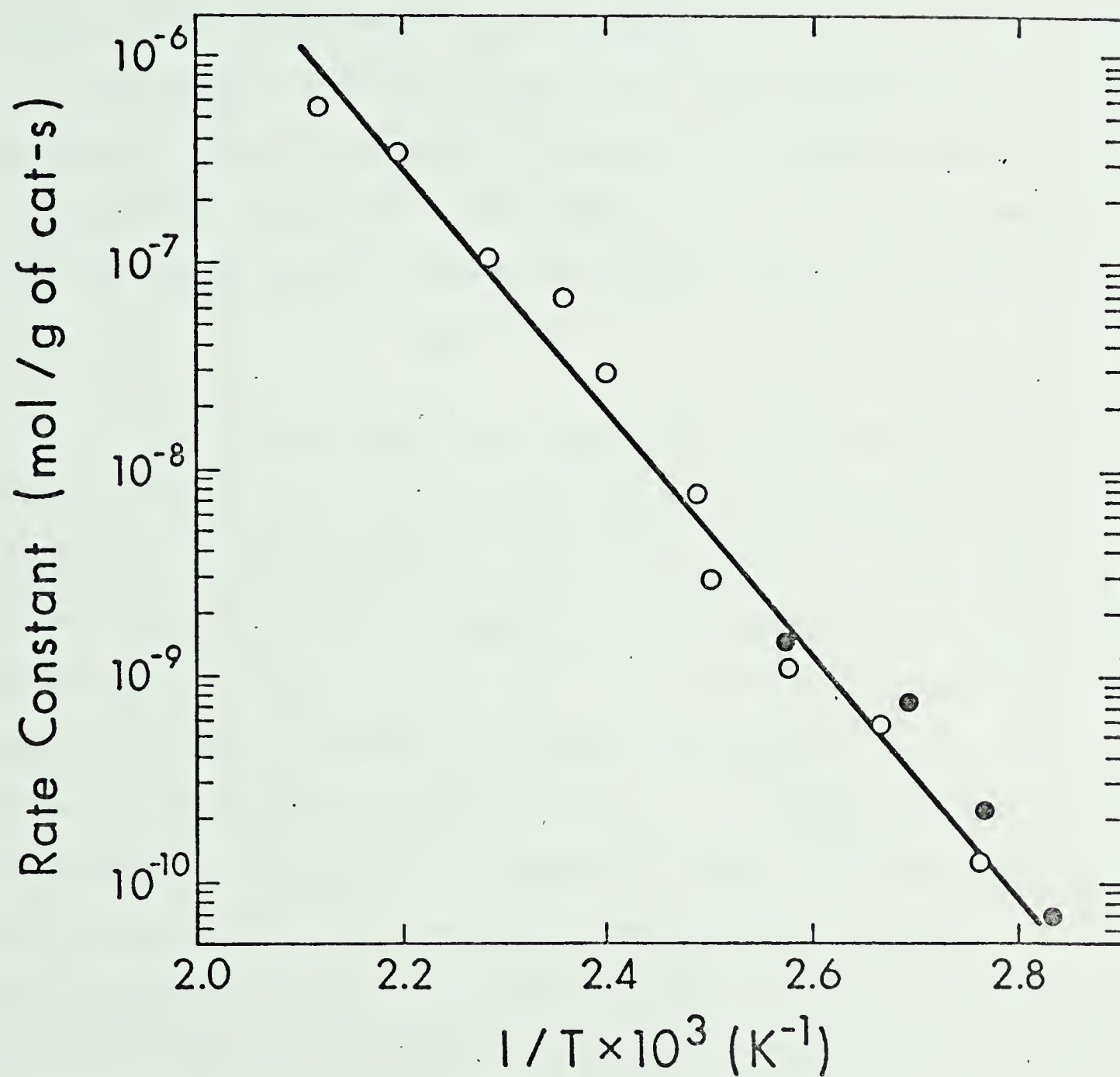


Figure 4.6 : Arrhenius plot for rate constants based on Equation 4.6.





data (open circles) were fitted to the linearized form of the Arrhenius Equation, i.e.,

$$\ln k = \ln A_0 - E/RT \quad (4.7)$$

using a simple linear least squares technique.

The results of this fit, shown as the line in Figure 4.6, yielded an activation energy of 114 kJ/mol (25.5 kcal/mol) and a pre-exponential factor of  $4.12 \times 10^6$  mol/g of cat - s. The rate constant was also plotted against temperature in a non-linearized fashion, i.e.,

$$k = A_0 e^{-E/RT} \quad (4.8)$$

The Marquardt non-linear regression algorithm was again used to curve fit the data to the non-linear form of the Arrhenius equation. The results of this calculation are shown in Figure 4.7. Since there is some numerical correlation between the pre-exponential factor and the activation energy, the non-linear curve fitting program could be made to converge on a number of different pre-exponential factor and activation energy pairs. The values of  $4.12 \times 10^6 \frac{\text{mol}}{\text{gcat-s}}$  for the pre-exponential factor and 116 kJ/mol (27.705 kcal/mol) were obtained by starting the iterative curve fitting program with the results obtained from the linear fit of Equation (4.7) on Figure 4.4. The values for the pre-exponential factor and the activation energy calculated with those initial guesses had the lowest variance of all the pairs obtained however. While the linear and non-linear fits of the rate constants resulted in very similar values for the pre-exponential factor and the activation energy (Figure 4.7), the non-linear fit does show that the emphasis is placed on the low temperature runs, perhaps at the expense



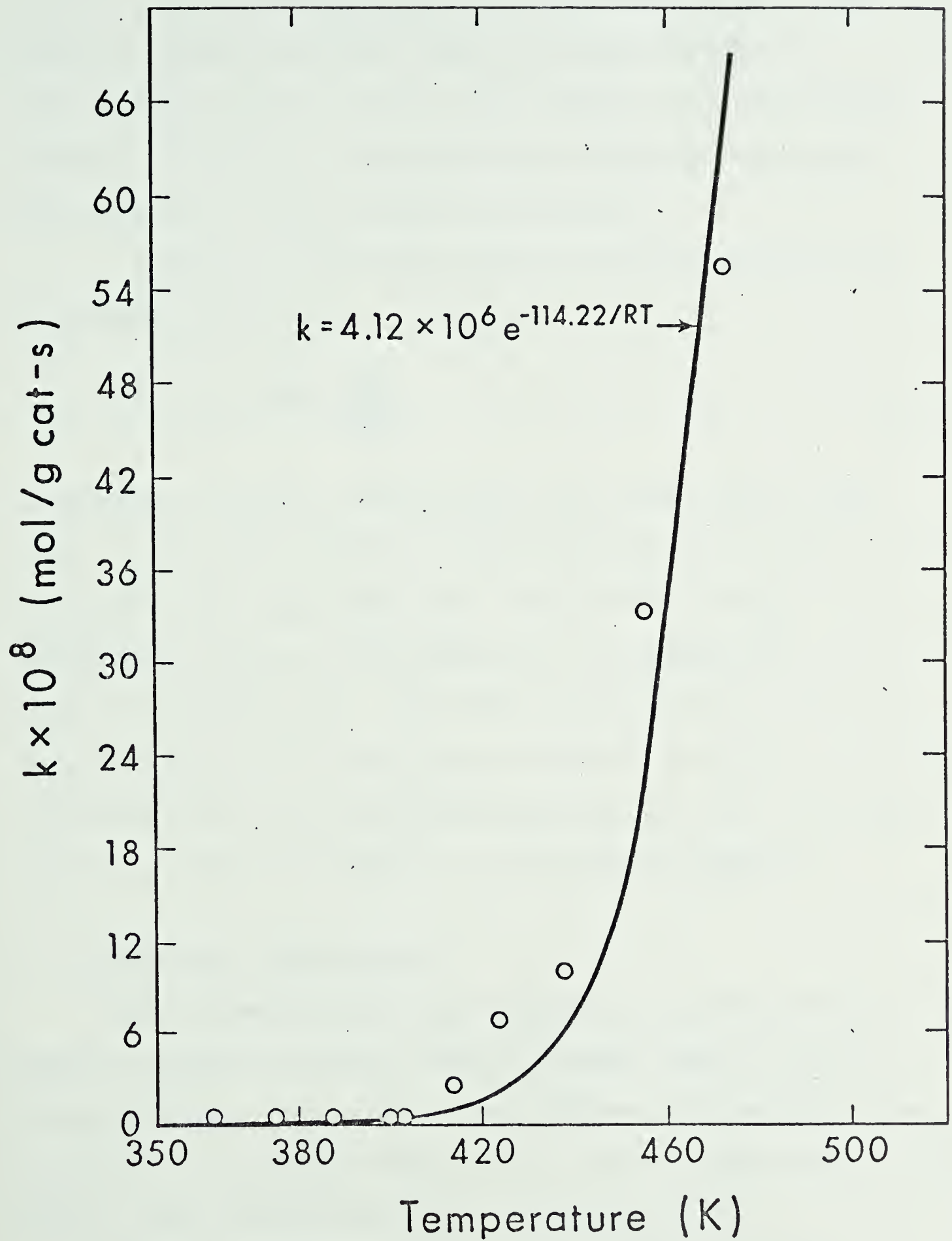


Figure 4.7 : Rate constant as a function of temperature (non - linearized).



of the middle to high temperature values. Since the low temperature runs were usually lower conversion runs, the relative error in the measured fractional conversions used to calculate the rates is probably higher than the relative errors inherent in the high temperature runs. This may have caused some bias in the activation energy and pre-exponential factor obtained from the fits.

Finally, all the kinetic data were fitted simultaneously to the proposed rate equation,

$$-r = A_o e^{-E/RT} \frac{[O_2]}{[C_2H_4]} \quad (4.9)$$

The Marquardt algorithm in multi-variable, non-linear form was again used to estimate the activation energy and pre-exponential factor using the kinetic data at all temperatures. The activation energy determined this way was 114.093 kJ/mol and the pre-exponential factor was  $4.122 \times 10^6$  mol/g cat-s. Both these values agreed very well with the numbers obtained from the linearized form of the Arrhenius equation, and the use of the non-linear fitting algorithm does not, in this case result in a significant difference in the estimated parameters.

#### 4.6 Kinetic Runs - Aged Catalyst

Kinetic experiments were also carried out using the previously described integral bed reactor (IBR) and another sample of the 0.3% Pt/Al<sub>2</sub>O<sub>3</sub> catalyst. The results of these IBR runs are presented in the next chapter. The catalyst sample was used for an extended period, in the IBR, i.e. more than 500 hours under reacting conditions.

Following completion of the IBR runs, a sample of this now "aged" catalyst was tested in the DRR. A charge of 75 pellets



(3.4 g), mixed with glass beads, was placed in the DRR, and a series of kinetic runs were performed on this aged catalyst to determine its activity. The data for these runs are located in Appendix D, Table D.3. Again, the rates of reaction were plotted against the ratio of the exit oxygen concentration to the exit ethylene concentration (see Figure 4.8). Except for the runs at 388K, the investigation of this "aged" catalyst was not as extensive as was the previous work. While only a few points were taken at each temperature, linear least squares fits of the data to Equation 4.6 were performed, and the rate constants were determined. The results of these fits are listed in Table 4.3.

TABLE 4.3  
RATE CONSTANTS - AGED CATALYST

Temperature (K)	$1/T \times 10^3$ (K <sup>-1</sup> )	$k \times 10^{10}$ (mol/g cat-s)
353	2.833	0.7097
361	2.770	2.393
371	2.695	7.449
388	2.577	14.60

The rate constants for the aged catalyst as a function of reciprocal temperature are shown in Figure 4.6 as the solid circles. Results of least squares analyses for determination of activation energies and pre-exponential factors for the fresh catalyst, the aged catalyst, and the combined data are presented in Table 4.4.





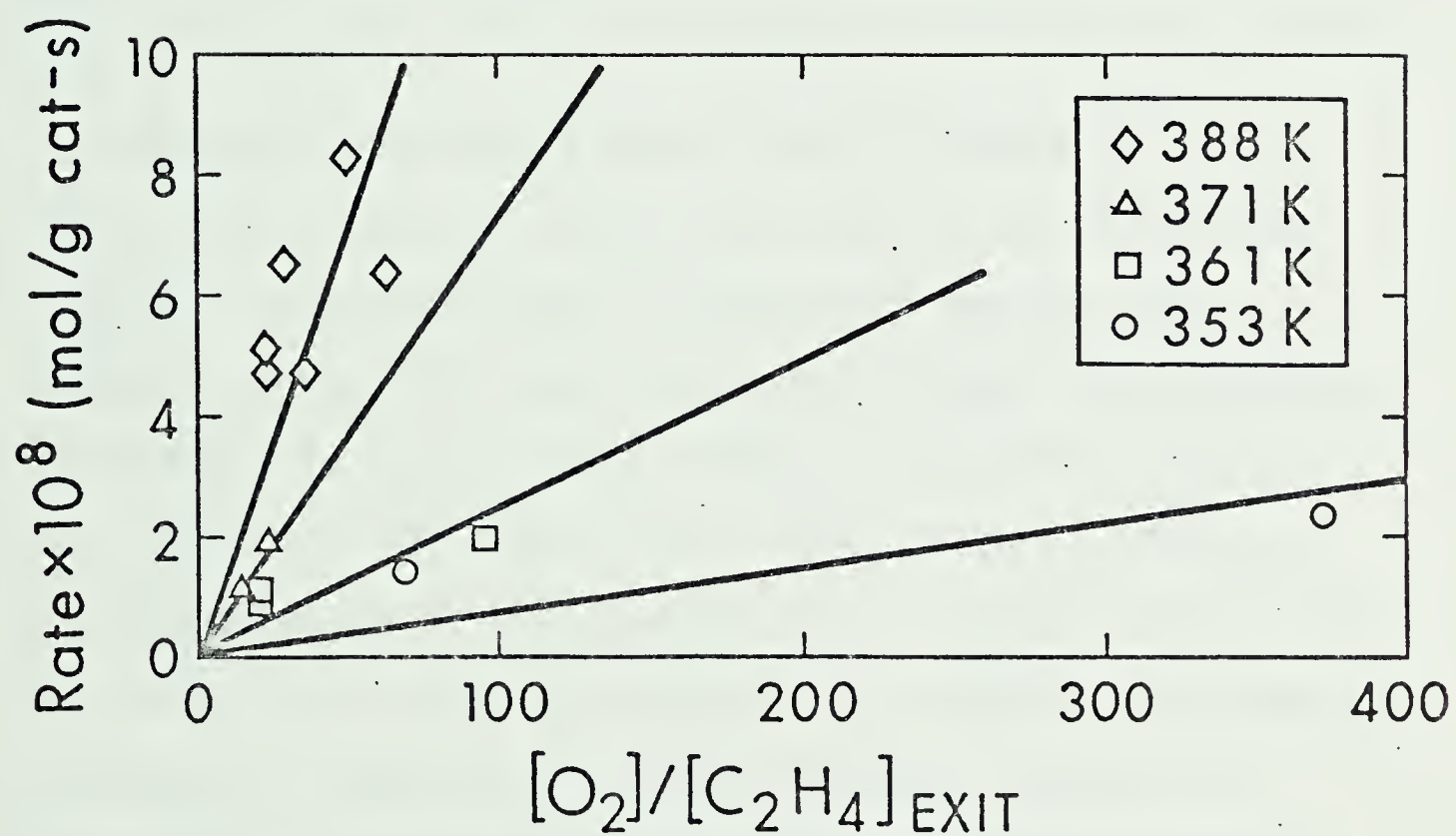


Figure 4.8 : Rates of ethylene oxidation as a function of the ratio of oxygen to ethylene concentration for the catalyst sample used in the integral bed experiments



TABLE 4.4  
ARRHENIUS CONSTANTS

Points Used	Type of Fit	Pre-exponential Factor (mol/g cat-s)	Activation Energy (kJ/mol)
fresh only	linear	$4.116 \times 10^6$	114.22
fresh only	non-linear	$4.122 \times 10^6$	114.093
aged only	linear	$2.028 \times 10^4$	97.71
fresh and aged	linear	$9.342 \times 10^5$	108.95

While the aged catalyst appears to be slightly more active than the fresh catalyst, the difference between the aged and fresh catalysts is within the limits of experimental accuracy. The activation energy of the aged catalyst was only about 14% lower than the value for the fresh catalyst. Except for the rate constant at 388 K, which falls very close to the line in Figure 4.6, the rate constants determined at other temperatures for the aged catalyst were based on only two or three data points. Also, these data were taken at low temperature, and hence low conversion levels. Because of these reasons, the rate equation developed for the fresh catalyst i.e.,

$$-r = 4.12 \times 10^6 e^{-114000/RT} [O_2]/[C_2H_4] \quad (4.9)$$

was adopted as applicable to both the fresh and the aged catalyst. This is the equation that was used to predict fractional conversions in the integral bed reactor.



#### 4.7 Adsorption Studies

All of the kinetic studies were done with reactants which were well mixed prior to their introduction into the reactor. Since the ethylene severely inhibited the reaction, it could be possible that the order in which the reactants were introduced into the reactor could be important. A series of experiments was conducted to investigate this.

For the first experiments, the fractional conversion of ethylene was determined for two cases. Initially, the reactor feed was either an air stream or a 5%  $C_2H_4$  in nitrogen stream which was passed over the catalyst bed for 3 to 4 hours before the other reactants were introduced. The results are summarized in Table 4.5.

TABLE 4.5

COMPARISON OF CATALYTIC ACTIVITY WITH PRETREATMENT CONDITIONS

Run	Temp (K)	Treatment	Inlet Mole %		$\frac{[O_2]}{[C_2H_4]}$	Fractional Conversion
			$C_2H_4$	$O_2$		
N <sub>1</sub>	366	$C_2H_4$ - 4 hrs	0.767	18.16	23.68	0.105
N <sub>2</sub>	366	$O_2$ - 4 hrs	0.724	18.16	25.08	0.114
N <sub>3</sub>	366	$C_2H_4$ - 4 hrs	0.594	18.78	34.21	0.862
N <sub>4</sub>	366	$O_2$ - 4 hrs	0.566	18.92	33.43	0.854
N <sub>5</sub>	370	$C_2H_4$ - 3 hrs	0.756	18.06	23.89	0.263
N <sub>6</sub>	370	$O_2$ - 3 hrs	0.776	18.05	23.68	0.888

The transient temperatures, measured at the centre of the catalyst bed after starting the mixed feed (time = 0), for the above six runs are shown in Figure 4.9. For runs N1 and N2, and N3 and N4, the initial treatment did not affect the steady-state



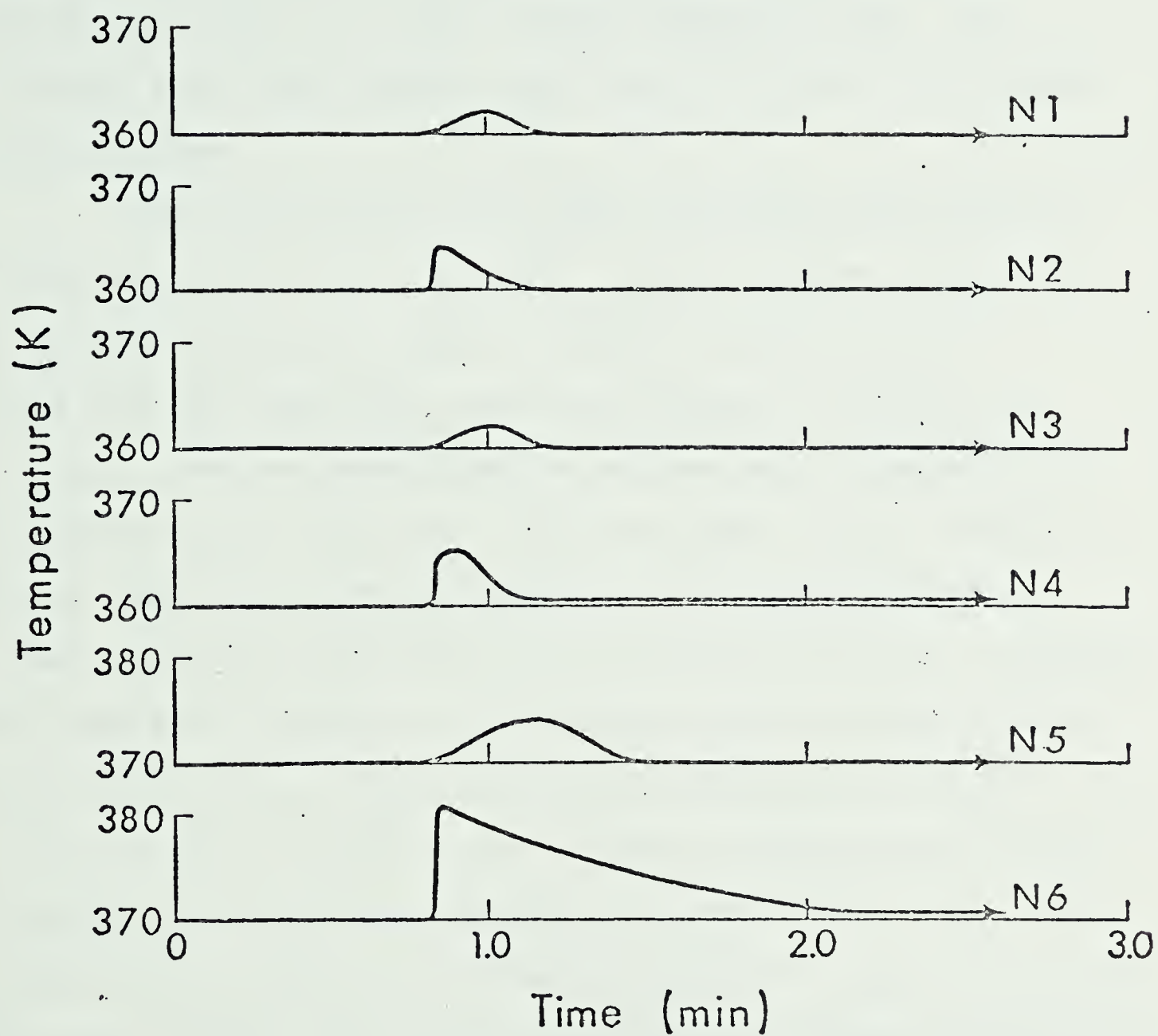


Figure 4.9 : Catalyst bed temperature as a function of time for adsorption studies





conversions. Although the steady-state conversion did not depend on whether the surface was initially covered with  $C_2H_4$  or  $O_2$ , the temperature transient was a function of the initial treatment. The cases where the catalyst was initially covered with oxygen (runs N2 and N4) resulted in a higher transient temperature rise. This indicates that higher transient rates result in the case of the oxygen covered surface.

The initial treatment did affect the steady-state conversion in the other pair of runs (N5 and N6). In this case the steady-state conversion following the oxygen pretreatment was approximately three times the steady-state conversion following the ethylene pretreatment. The feed compositions for both runs were approximately the same and the final steady-state temperatures were also approximately equal. (There was an offset of about 0.75 K for run N6, but this in itself could not be responsible for the threefold increase in conversion.) The temperature transient for run N6 showed a large increase in temperature (10 K) and even though the steady-state temperature returned to the initial value, it is possible that a significant temperature difference existed between the catalyst pellets and the bulk fluid at steady-state. High transient temperature rises had been observed in some of the previous DRR runs, but these runs were not used in the rate function determinations presented earlier in this chapter.

The second type of experiment performed in this series was designed to test whether or not ethylene would displace oxygen from the catalyst surface. A stream of air was passed over the catalyst in the reactor at 366 K for four hours. The reactor was then purged with



nitrogen until analysis of the exit stream showed no oxygen present. Then, a stream containing 5%  $C_2H_4$  in nitrogen was introduced into the reactor. The exit stream was analysed for oxygen, and in one of the analyses following introduction of the  $C_2H_4$ , a small amount ( $\sim 0.5\%$ ) of oxygen was detected. As well, a slight transient temperature rise (1K for about 45s) was noticed. The experiment was repeated with the exit stream being analyzed for carbon dioxide. Again, the small temperature transient was noticed and a small (about 0.01%) amount of carbon dioxide was detected. The ethylene displaced some of the small amount of oxygen left on the surface following the nitrogen purge and reacted with some of it.

The reverse experiment was also conducted. The surface of the catalyst was treated with 5% ethylene in nitrogen for 4 hours then the system was purged with nitrogen until no ethylene appeared in the exit stream. A stream containing 18% oxygen in nitrogen was then introduced. Repeat experiments failed to reveal traces of carbon dioxide or ethylene in the exit stream, and no temperature transients were observed. In this case, either no ethylene was left on the catalyst after the nitrogen purging (somewhat unlikely) or, the oxygen was unable to either react with or displace the ethylene that remained.

From these results, it would appear that ethylene can readily displace oxygen from the platinum surface, while oxygen is completely unable to displace (or react with) the strongly adsorbed ethylene. If the oxygen molecule must be bound to a site on the platinum in order for the reaction to occur, this would account for the strong inhibitory effect that ethylene has on its own catalytic oxidation. The ethylene may displace oxygen from the preferred sites, rendering them



unavailable for reaction. This would suggest that the heat of adsorption of ethylene on the supported platinum crystallites is greater than the heat of adsorption of oxygen. The conclusion that ethylene adsorbs more strongly than oxygen on platinum is contrary to most of the results reported in Chapter 2, Table 2.2. Nevertheless, the observation that ethylene is able to replace adsorbed oxygen and that oxygen is unable to displace adsorbed ethylene definitely indicates that ethylene is adsorbed more strongly than oxygen.

#### 4.8 Conclusions - Differential Recycle Reactor

The main conclusion of the work on the DRR was that the rate equation

$$-r = 4.12 \times 10^6 \exp(-11400/RT) [O_2]/[C_2H_4] \quad (4.10)$$

can be used to describe the oxidation of ethylene in low concentration ( $0.05 - 1.0 \text{ mol/m}^3$ ) over a range of oxygen concentration ( $1 - 8.6 \text{ mol/m}^3$ ) and temperature ( $362 - 372\text{K}$ ). While the data displayed a certain amount of scatter it was believed that this scatter was due to changes in the catalyst activity. Although more complex (more adjustable parameters) rate equations did improve the fits somewhat, it was felt





that the increase in complexity was not warranted, and that Equation (4.10) represented the data adequately.

The adsorption studies confirmed the strong negative order kinetics with respect to ethylene. The conclusion apparent from those experiments was that ethylene adsorbs more strongly than oxygen, on the surface of the catalyst, and a speculation can be made that the surface reaction must be preceded by oxygen adsorption onto the platinum. The precise mechanism cannot be elucidated at this time, and further studies, in apparatus other than that used here, would have to be conducted if one required the step by step mechanism of the reaction. In the same vein, no attempts were made to postulate a mechanism from a statistical analysis of the kinetic data. As Carberry stated (4.2),

"It should now be apparent that no amount of statistical manipulation of kinetic data will yield a mechanism."





## CHAPTER 5

### INTEGRAL BED REACTOR

#### 5.1 Introduction

The development of a rate equation which could model the oxidation of ethylene in low concentration was outlined in Chapter 4. The next step was to determine if this rate equation could be used to predict the fractional conversions obtained in tubular flow reactors. The reactors used as catalytic converters by the automobile industry are designed to minimize the pressure drop through the catalyst bed while still exposing the exhaust fumes to a sufficient amount of catalyst to oxidize the hydrocarbons. This requirement was fulfilled by producing large pancake-like converters with a cross-sectional area from  $1 \text{ ft}^2$  to  $3 \text{ ft}^2$  and a catalyst bed depth of 2-6 inches. The integral bed reactor, described in Chapter 3, had a cross sectional area to bed depth ratio which was a couple orders of magnitude less than the commercial catalytic converters. The object here was not to construct a reactor which resembled a catalytic converter (the purchase of a converter would have been considerably less expensive and less bothersome) but rather to construct a simple bench scale reactor which would mimic some of the features of the converters.

With this reactor, and the simplified mass balance equations outlined in Appendix A, the rate equation developed in the previous chapter could be checked against an independent set of measurements.



## 5.2 Blank Runs

Two types of blank runs were performed in the integral bed reactor. The first series was conducted in an empty reactor to test for homogeneous gas phase reaction between the ethylene and oxygen. A 0.135% ethylene in  $N_2$  mixture and air were mixed and sent through the empty reactor at temperatures from 500K to 792K, the upper limit of the temperature controller. The results are tabulated in Appendix D, Table D4 and are pictured in Figure 5.1. At 792K, where the reaction began to occur, the concentration of ethylene was varied. These results are shown in Figure 5.2. All integral bed runs (using catalyst) were carried out at temperatures below 500K, and hence the contribution of homogeneous reactions to the overall reactions are negligible. The homogeneous reaction does not display the inverse dependence on ethylene concentration. Figure 5.2 indicates that the reaction rate increases with increasing ethylene concentration rather than decreasing. This positive rather than negative order reaction is to be expected for the homogenous reaction. The second series of blank runs was done with alumina cylinders in the reactor. The reactor was charged with 33.4 g of -8 +10 mesh (about 2mm diameter) alumina spheres. The influence of the catalyst support was determined from 500K to 792K at a variety of ethylene concentrations. Figures 5.3 and 5.4 show the results of these experiments. The data are tabulated in Appendix D, Table D5. The values used in Figure 5.3 for temperatures 677K, 698K and 766K were read from Figure 5.4 at the ethylene mole percentage of 0.6086%. An attempt was made for those three



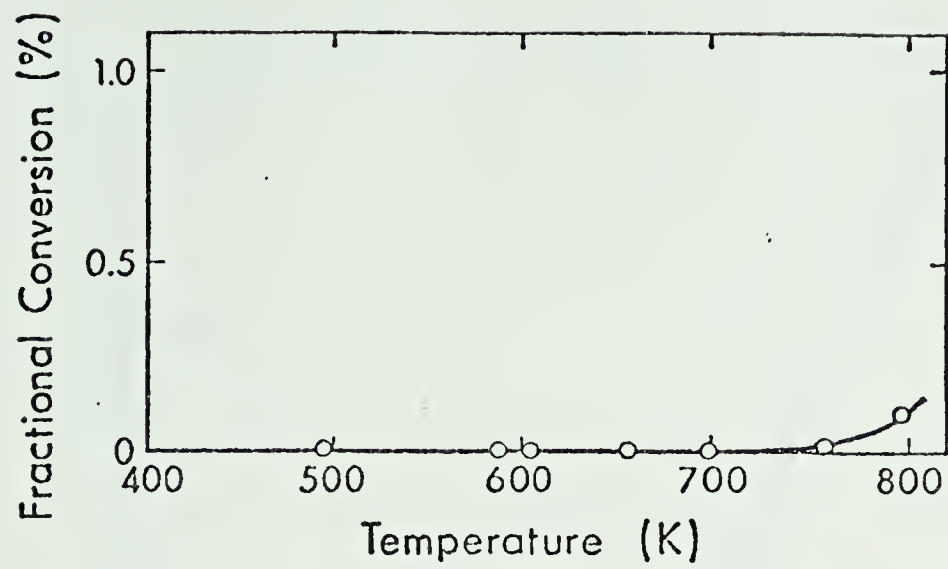


Figure 5.1 : Results of blank runs in IBR  
( $C_2H_4$  feed = 0.135 mole %).

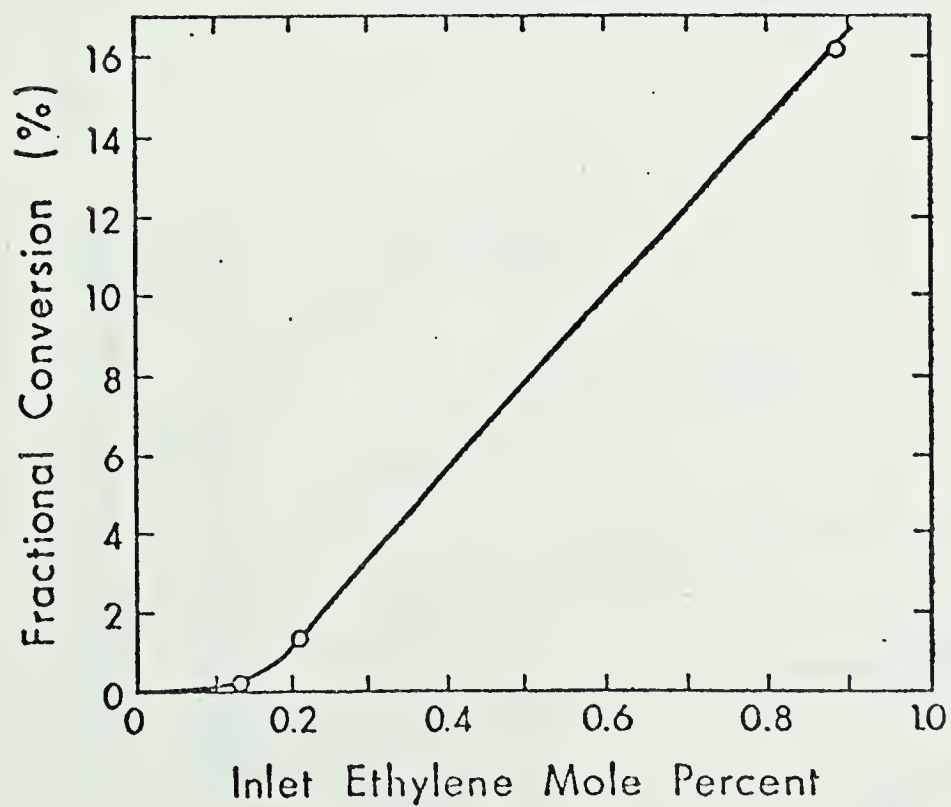


Figure 5.2 : Effect of inlet ethylene concentration  
on conversion during blank runs  
at 792 K.



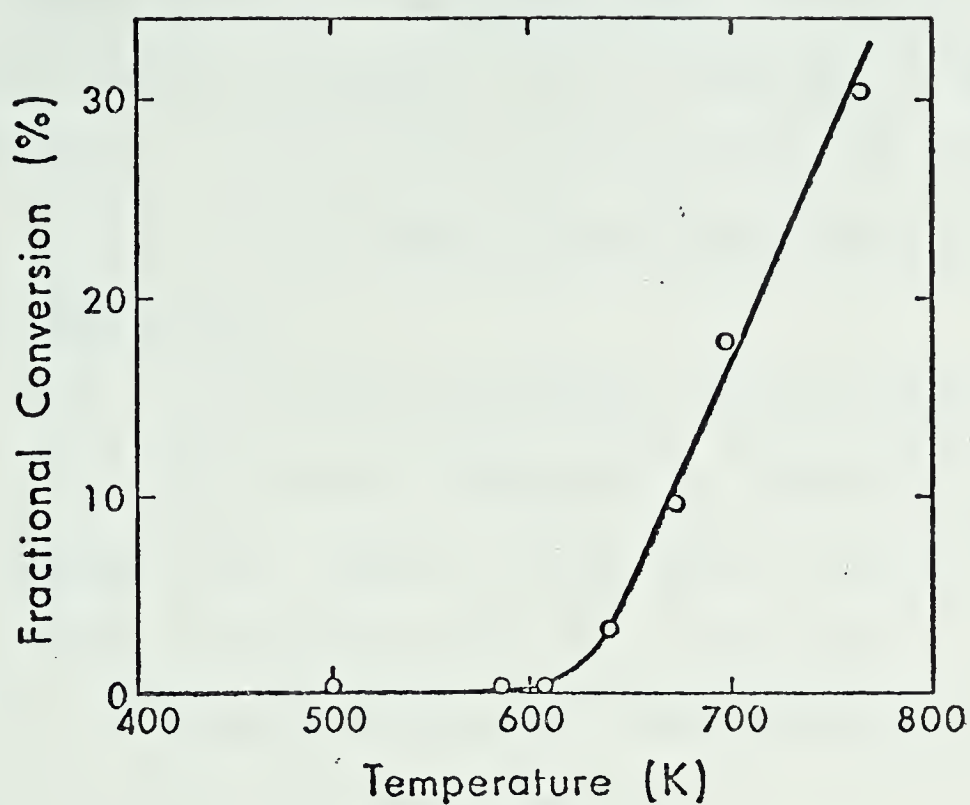


Figure 5.3 : Results for IBR packed with 2 mm  $\text{Al}_2\text{O}_3$  spheres ( $\text{C}_2\text{H}_4$  feed = 0.6086 mole %).

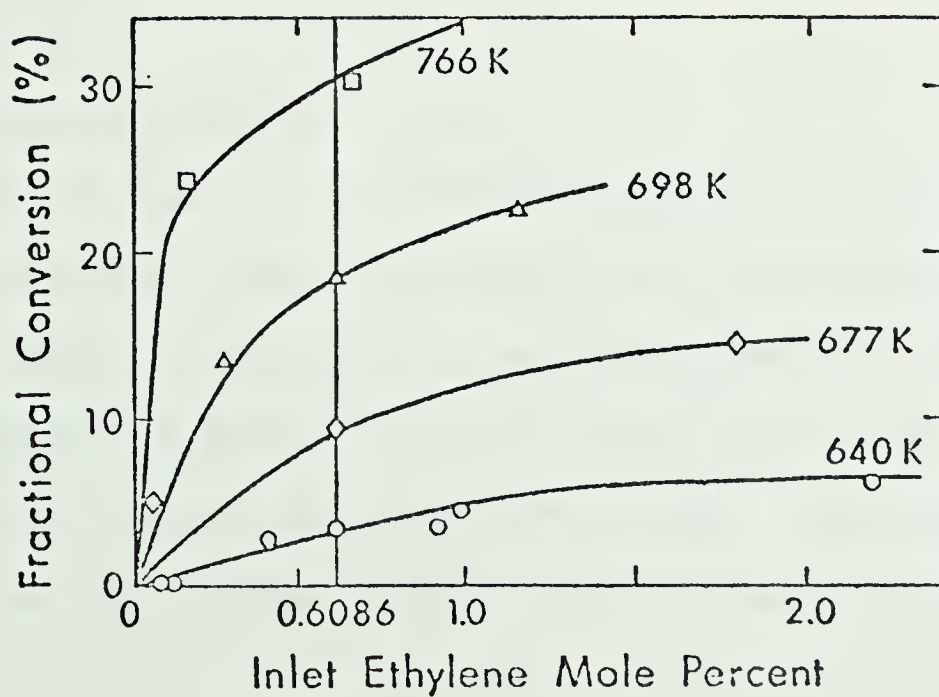


Figure 5.4 : Effect of inlet ethylene concentration on fractional conversion for IBR packed with 2 mm  $\text{Al}_2\text{O}_3$  spheres.





runs to regulate the ethylene flow so that the inlet mole percent would be 0.6086%, but due to the random scatter inherent in the chromatograph and Disc integrator, and the imprecision of the regulating valves the exact mole fraction could not be duplicated. There are values on the 677K, 698K and 766K curves which are fairly close to 0.6086% however.

Again, the negative order kinetics are not apparent here. From Figure 5.4, the oxidation of ethylene over alumina proceeds with some positive order, however it does appear to approach zero order at ethylene concentrations over 2%. From Figure 5.3, it can be seen that for temperatures below 500K, the oxidation of ethylene by the alumina support is certainly negligible.

The majority of the runs in the integral bed reactor were performed with the same 0.3% platinum on alumina catalyst that was used for the DRR runs. A number of different series were conducted in large oxygen excesses (20%), moderate oxygen excesses (7-8%) and at near stoichiometric levels.

### 5.3 Catalyst Pre-Treatment

As was done with the differential recycle catalyst, the catalyst used for the integral bed runs, (0.3% Pt on alumina) was thermally treated. Two thermal treatments were applied. The catalyst was first exposed to 523K in flowing air for 60 hours. The second treatment was at 575K in flowing air for 12 hours. The activity of the catalyst was checked initially and after each pre-treatment.



The results of these tests are shown in Figure 5.5 and are tabulated in Table D6 (Appendix D). In order for this comparison to be meaningful, the fractional conversions must be measured at the same oxygen to ethylene ratio and at the same inlet ethylene flow rate. (See Appendix A.5.2). While an attempt was made to measure fractional conversions at the same oxygen to ethylene ratio, the flow controlling valves a limited precision and exact duplication was impossible. Table D6 shows that the oxygen to ethylene ratio in the feed stream varied from 23.3 to 24.6 for most of these runs. This is undoubtedly the reason for some of the scatter in the data of Figure 5.5. As a result of these pretreatments, the activity of the catalyst increased substantially. The fractional conversions measured after the treatments were up to four times higher than the conversions measured with the fresh catalyst, and the temperature required for complete conversion decreased from 409K to 396K.

#### 5.4 Predictions of the Rate Equation - Isothermal Model

The predictions of the rate equation were first tested on the simplest reactor model, a plug flow, pseudo-homogeneous, isothermal reactor. Under these conditions, the energy balance equation is not needed and the mass balance equation can be solved analytically by integrating the rate equation. (The resulting equation is implicit in the fractional conversion, therefore a root finding technique is required.) The details of this model are outlined in Appendix A.5.2. The resulting expression, equation (A.67),



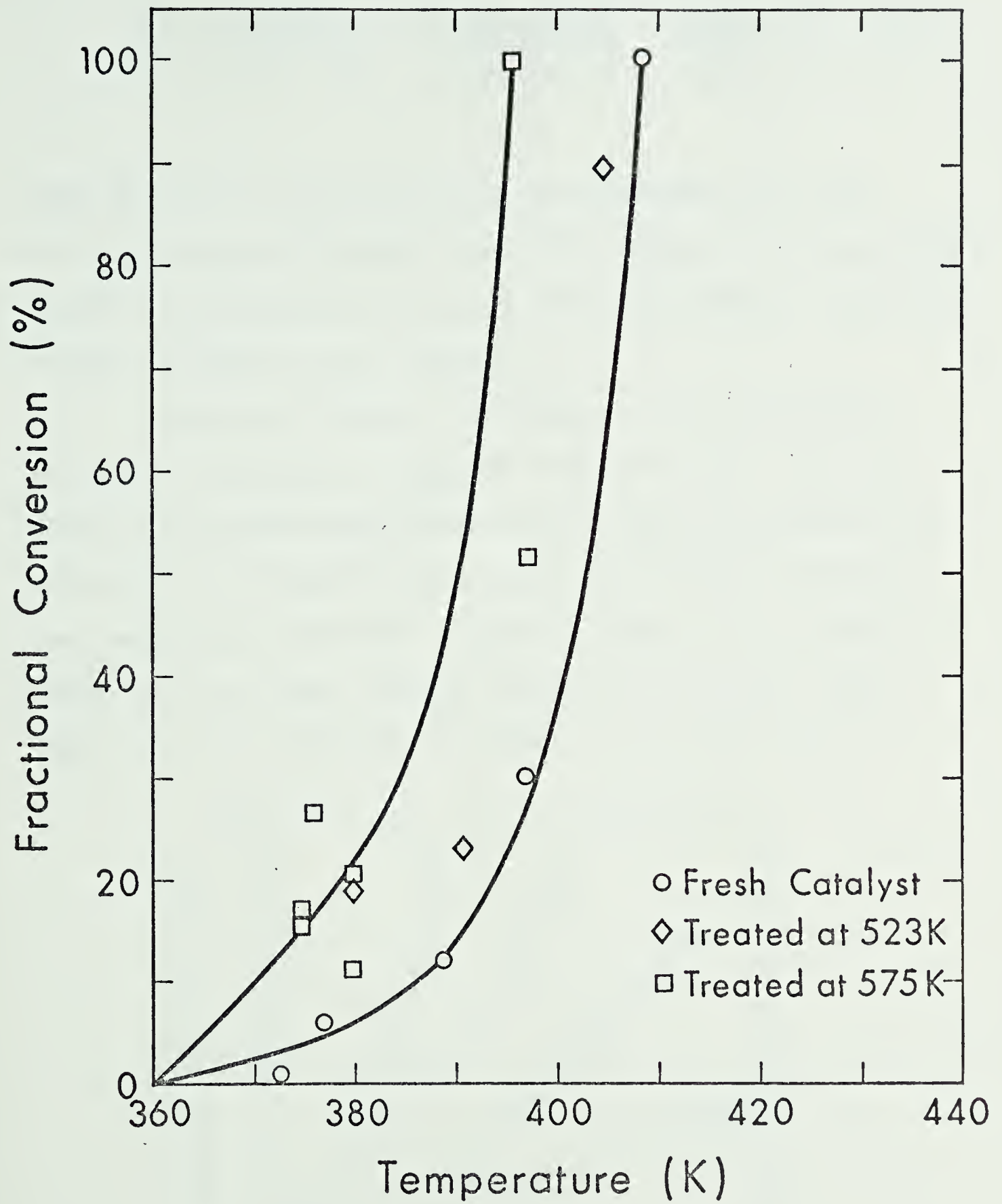


Figure 5.5 : Effect of thermal treatments on catalytic activity.



$$\frac{XE}{3} + \left[ \frac{FO/FE-3}{9} \right] \ln \left[ \frac{FO/FE-3XE}{FO/FE} \right] - \frac{13.8 k}{FE} = 0 \quad (5.1)$$

shows that the fractional conversion is a function of the ratio of the inlet oxygen flow rate to the inlet ethylene flow rate,  $(FO/FE)$  and the inlet ethylene flow rate,  $FE$ . For the isothermal conditions, the rate constant,  $k$ , is a constant.

Since the fractional conversion is a function of both the oxygen to ethylene ratio and the inlet flow rate of ethylene, a plot of fractional conversion versus the oxygen to ethylene ratio will exhibit considerable scatter since no two points will be at the same ethylene flow rate. A family of curves, each at different values of  $FE$ , the inlet ethylene flow rate, will result. Such a family of curves is pictured in Figure 5.6, for a given set of

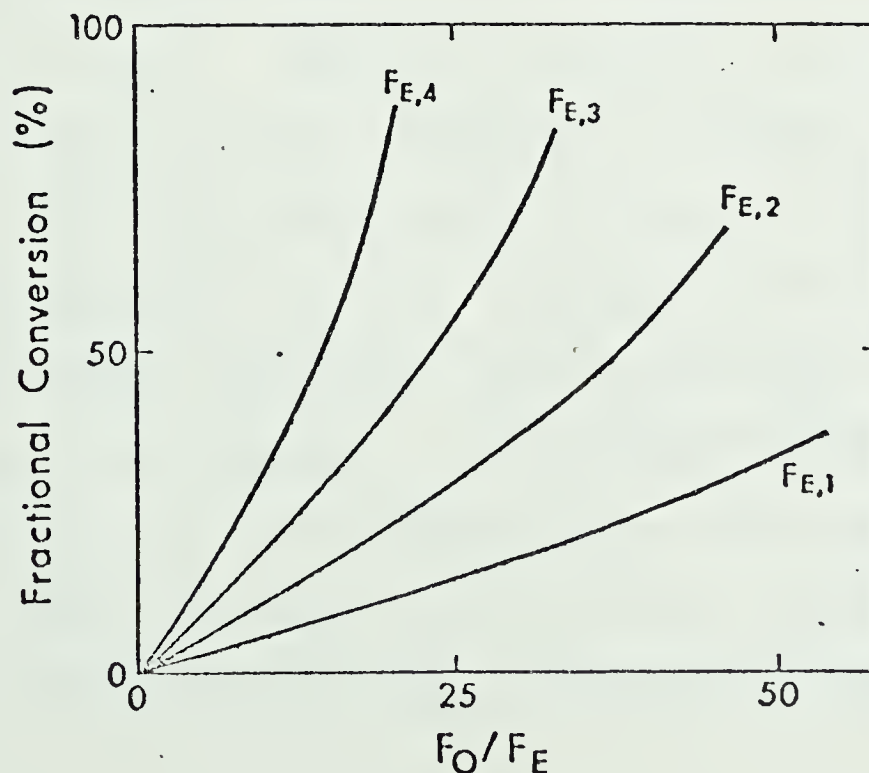


Figure 5.6 : Predicted ethylene conversions for IBR as a function of ethylene and oxygen feed rates.







experiments at the same temperature. A two dimensional representation of the data is thus somewhat awkward, and a tabular comparison of the measured and predicted rates is more appropriate. In Table D7, Appendix D, the raw data for all of the integral bed runs are tabulated. The predictions of the isothermal model, as well as other models, are tabulated in Table D 14. The roots of equation (5.1) are the predicted fractional conversions. They were obtained by evaluating FE, FO and k for each run, then solving equation (5.1) using a Newton's iterative method. (see Appendix F)

The extremes in the ethylene flow rate can be displayed in a two dimensional figure. The data at 375K, were plotted, and the two limiting cases were considered. Two curves, one at the highest ethylene flow rate, and one at the lowest ethylene flow rate were drawn. These curves are shown in Figures 5.7. These data are tabulated in Tables D8 and D9 in Appendix D. Figure 5.7 shows that the two limiting cases enclose most of the measured data points. The curve at  $5.11 \times 10^{-7} \frac{\text{mol}}{\text{s}}$  is at an ethylene flow rate considerably lower than most of the runs. The majority of the runs lie closer to the  $FE = 1.51 \times 10^{-6} \frac{\text{mol}}{\text{s}}$  curve, and for this curve, the predicted value of the fractional conversion is lower than the measured value, especially at higher conversions. Curves at the other temperatures were similar and are not presented. The isothermal reactor model and the rate equation from the DRR, were used, with a value of FE which was roughly the average for the particular temperature series to predict fractional conversions. A comparison of these isothermal



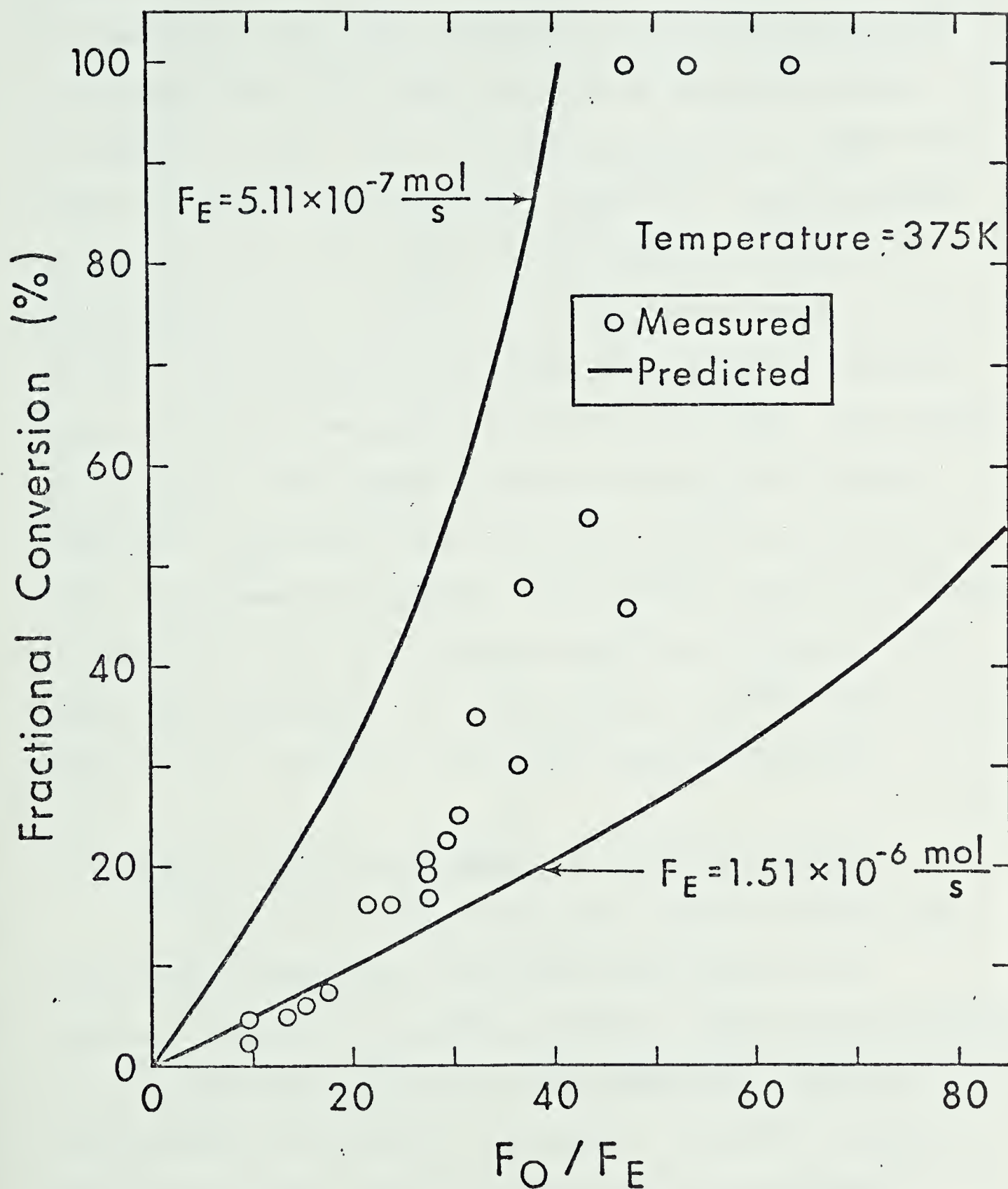


Figure 5.7 : Comparison of measured and predicted conversions for the IBR.



predictions and the measured fractional conversions is shown in Figures 5.8 and 5.9. The predicted data are tabulated in Tables D10 - D13, Appendix D. The simple isothermal model performs fairly well at low conversion levels, where the amount of heat liberated by the reaction is small. This is evident in both the low oxygen runs, Figure 5.8 and the high oxygen runs, Figure 5.9. Even considering that not one line, but a family of lines should be plotted for each temperature, the predictions of the isothermal model are low, and this is not particularly surprising. There were some increases in the reaction gas temperature noticed during the runs, and, because the inside wall heat transfer cannot be infinite, the isothermal assumption is not valid. Also, there will be a finite heat transfer coefficient between the catalyst pellets and the reaction gas, causing the reaction to occur at a temperature that may be higher than the measured gas temperature. For these reasons, a reactor model incorporating a solution of the energy balance was required.

### 5.5 Predictions of the Rate Equation - Non-Isothermal Model

The use of the rate equation developed for the DRR with the isothermal reactor model resulted in predictions of the fractional conversion which were consistently lower than the measured values. A non-isothermal reactor model, described in Appendix A.5.1. was developed to overcome this shortcoming. Initially, a pseudo-homogenous plug flow reactor model was used, with an infinite heat transfer coefficient between the catalyst pellets and the gas phase. A pair of coupled differential equations resulted:





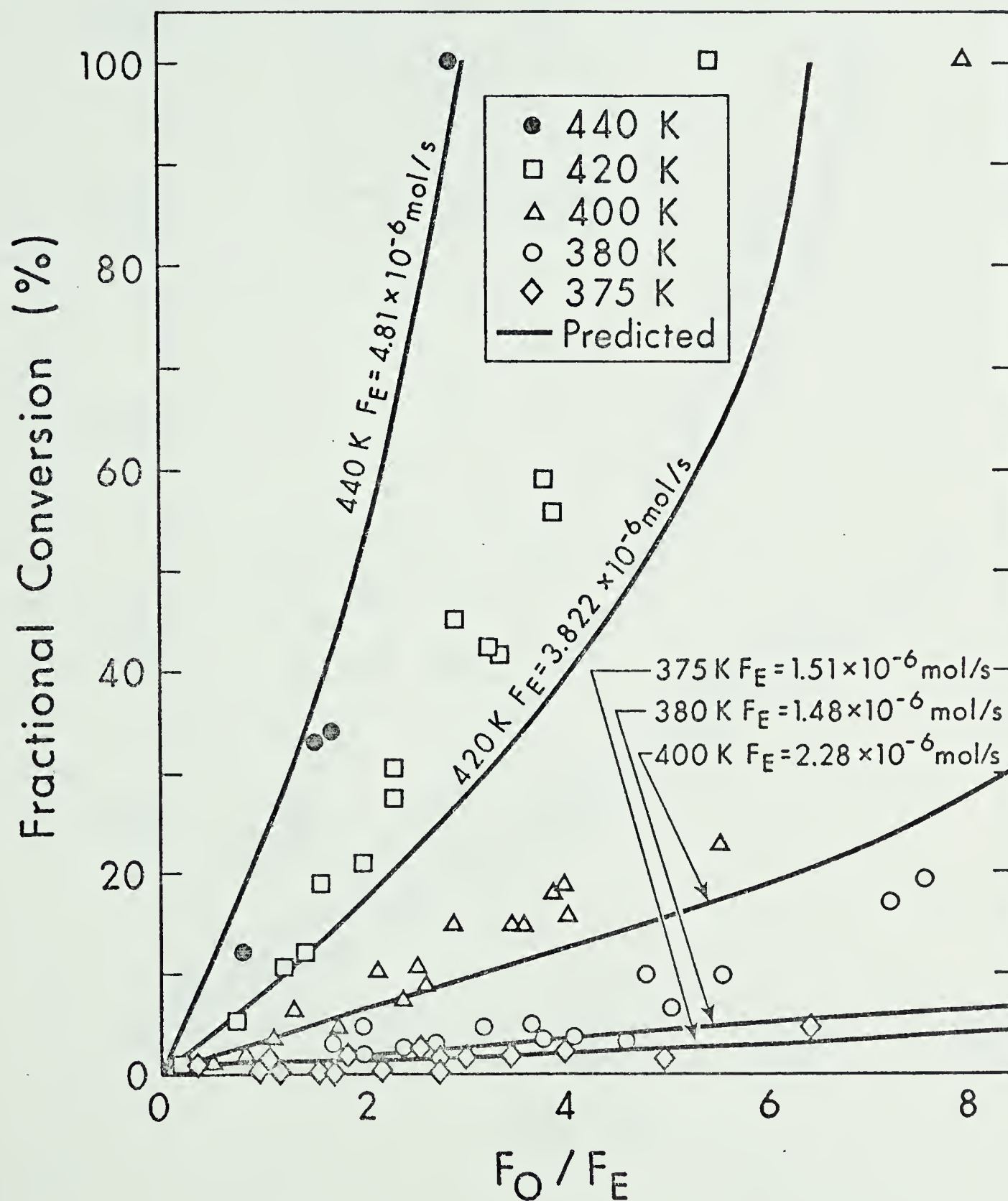


Figure 5.8 : Comparison of measured and predicted conversions for the IBR (low oxygen and median  $C_2H_4$  feed rates).





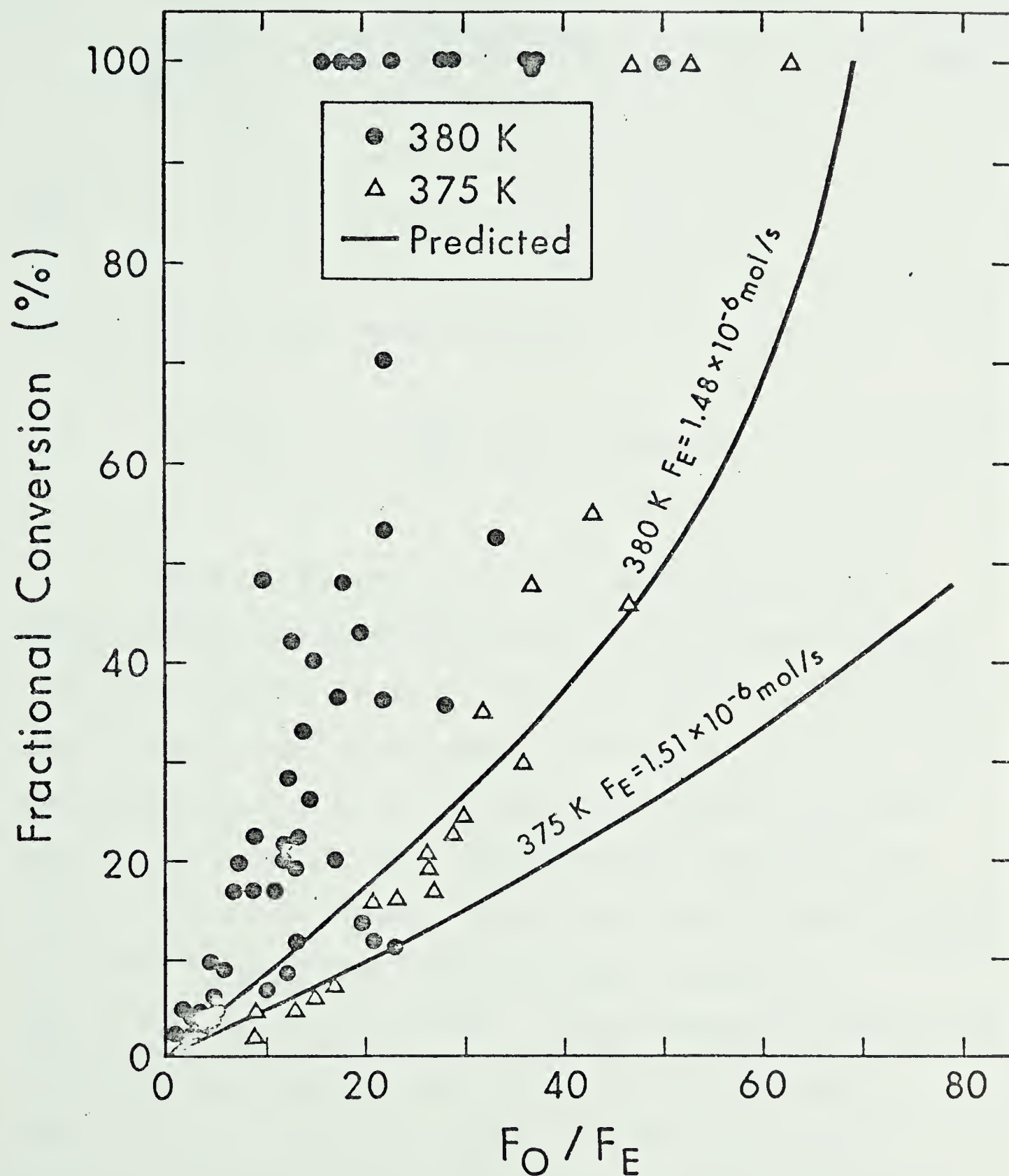


Figure 5.9 : Comparison of measured and predicted conversions for the IBR (excess oxygen and median  $C_2H_4$  feed rates).



(1) the mass balance, equation (A.54)

$$\frac{d}{dW} XE = \frac{A_0 e^{-E/RT} (F_0 - 3FExXE)}{FE^2 (1-XE)} \quad (5.2)$$

and

(2) the energy balance, equation (A.60)

$$\dot{m} C_p \frac{dT}{dW} = - h_W \left( \frac{\Delta A}{\Delta W} \right) (T - T_W) + (-\Delta H_r)(-r) \quad (5.3)$$

These two equations were solved simultaneously using a 4th order Runge-Kutta technique (see Appendix F) to obtain estimates of the exit fractional conversion. Reliable estimates or measurements could be made for most of the parameters in equations (5.2) and (5.3); however, the evaluation of the inside wall heat transfer coefficient posed some difficulties. The correlations used in Appendix A.5 to evaluate the wall coefficient predicted values from  $1.115 \times 10^{-3} \frac{\text{J}}{\text{K-s-cm}^2}$  to  $8.234 \times 10^{-3} \frac{\text{J}}{\text{K-s-cm}^2}$ . The predictions could be made over a range of heat transfer coefficients. As the coefficient increases, the predictions should approach the predictions of the isothermal model discussed in the previous section. As the heat transfer coefficient decreases, the model approaches an adiabatic condition.

In Table D 15, Appendix D, a comparison of the measured fractional conversion (the average value of the ethylene and carbon



dioxide values) with the isothermal and non-isothermal predictions is made. The non-isothermal predictions were made with wall heat transfer coefficients of  $15.0 \times 10^{-3} \frac{\text{J}}{\text{K-s-cm}^2}$ ,  $8.234 \times 10^{-3} \frac{\text{J}}{\text{K-s-cm}^2}$  and  $1.115 \times 10^{-3} \frac{\text{J}}{\text{K-s-cm}^2}$ . The predictions made with the high heat transfer coefficient,  $15.0 \times 10^{-3} \text{ J}/(\text{K-s-cm}^2)$ , were very close to the values obtained with the isothermal model. Table 5.1 illustrates the similarity in the predictions of the isothermal model, the high heat transfer model and the model incorporating the upper bound of the heat transfer correlations.

In all of the runs displayed in Table 5.1, the predictions are slightly below the measured values, and the differences between the isothermal and the two non-isothermal predictions differ by less than 15%. As expected, the lower heat transfer coefficient does predict higher conversions than either the isothermal or the high heat transfer model.

Significant differences are obvious at the higher conversion levels. Table 5.2 is a comparison of the measured and predicted conversions for some of the high conversion runs. Here the predicted values are all considerably less than the measured values. Once again, the predictions of the isothermal and the high heat transfer coefficient models are not too dissimilar. Particularly for Runs I36 and I59, the predictions of the low heat transfer coefficient are much better than for the other two models, however even these predictions are well below the measured values.

For most of the runs in Table D15, the predictions are



TABLE 5.1

COMPARISON OF PREDICTED AND MEASURED FRACTIONAL CONVERSIONS - LOW CONVERSIONS

Run	Temperature (K)	[O <sub>2</sub> ]/[C <sub>2</sub> H <sub>4</sub> ] inlet	measured	Fractional Conversions (%)	
				isothermal model h=15.0x10 <sup>-3</sup>	non-isothermal model h=8.234x10 <sup>-3</sup>
F01	375	9.62	2.69	1.996	2.028
F02	375	14.98	6.33	5.93	6.050
F05	375	17.9358	7.69	7.198	7.360
I56	420	1.4237	12.69	10.32	10.759
H11	380	9.0796	17.04	15.563	15.886
					2.038
					6.101
					7.436
					11.072
					16.023





TABLE 5.2

COMPARISON OF PREDICTED AND MEASURED FRACTIONAL CONVERSIONS - HIGH CONVERSIONS

Run	Temperature (K)	$[O_2]/[C_2H_4]$ inlet	Measured	Fractional Conversions		
				Isothermal	Non-Isothermal $h=15.0 \times 10^{-3}$	Non-Isothermal $h=8.234 \times 10^{-3}$
F15	380	37.1429	100.00	73.42	100.00	100.00
F33	380	22.6902	53.04	19.09	19.85	20.34
H08	380	10.7624	48.98	23.29	23.85	24.13
I36	375	61.8106	100.00	44.10	48.30	52.16
I59	420	3.8796	58.76	31.79	36.46	41.86



lower than the measured values. This trend is most significant at the higher conversion levels. This suggests that the model of the reactor as pseudo-homogeneous may not be valid. If there is a significant heat transfer resistance between the pellets and the bulk gas, the pellets may be at a higher temperature than the bulk gas. This would result in the reaction occurring at a higher temperature, the catalyst pellet temperature, than the bulk gas temperature.

### 5.6 Prediction of the Rate Equation - Non-Homogenous Model

In Appendix A.4.1, the heat transfer limitations for the DRR were considered, and the pellet to bulk phase heat transfer coefficient,  $h_p$  was estimated at  $4.39 \times 10^{-3} \frac{\text{cal}}{\text{K-s-cm}^2}$ . Equation (A.20) was then used to estimate the maximum temperature difference between the bulk gas and the catalyst pellet. The value obtained was

$$(T_p - T_B)_{\text{max, DRR}} \approx 6.3 \text{ K}$$

Equation (A.19)

$$h_p = jH \frac{C_p G}{(\text{Pr})^{2/3}}$$

was used to estimate the heat transfer coefficient. The mass flow rate in the integral bed reactor,  $G$ , is considerably lower than in the recycle reactor, simply because the reaction gases are not recycled. Also, the  $j$  factor, which is correlated to the Reynolds number is dependent on the flow rate. For a mass rate of



$5.71 \times 10^{-3} \frac{\text{g}}{\text{s-cm}^2}$ , the heat transfer coefficient is  $5.3 \times 10^{-3} \frac{\text{J}}{\text{K-s-cm}^2}$

$(1.275 \times 10^{-3} \frac{\text{cal}}{\text{K-s-cm}^2})$  and the difference between the bulk and pellet temperatures (based on reaction rates of  $10 \times 10^{-8} \text{ mol/g cat - s}$ ) would be between 2K and 3K.

For the complete and high conversion runs, which were excluded from the DRR rate equation analysis, the rates are considerably higher. The actual temperature difference between the pellet and the bulk gas could easily exceed 20K during the complete conversion runs. The previous two models assumed that there was no heat transfer resistance between the pellets and the bulk phase, and as a result, they performed relatively poorly in the prediction of complete and high conversion runs. The homogeneous model was thus supplanted by a heterogeneous model in which the pellet temperature could exceed the bulk temperature. Equation (A.21),

$$T_p = T_B + \frac{(-r) (-\Delta H)}{h_p A_m} \quad (5.4)$$

was incorporated into the non-isothermal model to account for the possibility of heat transfer limitations. The mass and energy balance equations, (5.2) and (5.3), were then coupled with (A.21) through the expression for the rate of reaction,

$$(-r) = A_0 e^{-E/RT_p} \quad (5.5)$$



Equations (5.2) to (5.5) were then solved simultaneously using the Runge-Kutta integration. A comparison of the measured conversion, the predictions of the low coefficient model and the predictions of the heterogeneous model with each of the wall coefficients is shown in Table 5.3 for some of the low conversion runs. A slight improvement in the predictions of the heterogeneous model over the homogeneous models is evident for the runs which had been previously predicted below the measured values (e.g. F01, F11, G01, and H03). In the case of the high homogeneous predictions (H12, I55) the homogeneous model performs better than the heterogeneous model. However, for most of the cases, the predictions of the heterogeneous model were still below the measured values. The heterogeneous model with the low wall heat transfer coefficient predicts slightly higher conversions than the heterogeneous model with the high wall transfer coefficient.

In the case of the high conversion runs, the predictions of the heterogeneous model, especially when coupled with the low heat transfer coefficient, often predicts conversions which are higher than the measured conversions. In Table 5.4, some of the predictions of the homogenous and heterogenous models are compared. For runs I51, F08, and F14, the heterogenous model, coupled with the low heat transfer coefficient predicts 100% conversion while the heterogenous model with the high heat transfer coefficient predicts much lower conversions. This is more apparent in runs F16, J07, and I37, where both models using the low wall heat transfer coefficient predict complete conversion, while high wall heat transfer coefficients predict conversions which are lower.





TABLE 5.3

COMPARISON OF PREDICTED AND MEASURED FRACTIONAL CONVERSIONS IN THE IBR

Run	Temperature (K)	Fractional Conversions		
		Measured	Homogeneous Model $h_w=1.115 \times 10^{-3}$	Heterogeneous Model $h_w=8.234 \times 10^{-3}$
				$h_w=1.115 \times 10^{-3}$
F01	375	2.69	2.185	2.065
F11	379	4.25	4.006	3.640
G01	380	3.10	1.447	1.394
H03	380	2.65	1.125	1.102
H12	380	4.99	5.165	4.918
I55	420	5.74	6.470	5.411
				6.821



TABLE 5.4

COMPARISON OF PREDICTED AND MEASURED FRACTIONAL CONVERSIONS IN THE IBR

Run	Temperature (K)	Fractional Conversions		
		Measured	Homogeneous Model $h_w=1.115 \times 10^{-3}$	Heterogeneous Model $h_w=8.234 \times 10^{-3}$ $h_w=1.115 \times 10^{-3}$
F16	380	100.	100.	40.213 100.
F17	380	100.	48.022	23.690 100.00
G07	380	100.	100.00	40.57 100.00
I37	375	100.	100.00	23.398 100.00
I51	400.	23.13	21.208	9.151 100.00
F08	375.	28.78	100.00	32.310 100.00
F14	380	36.18	39.154	22.464 100.00



For the high conversion runs, the predictions of the low heat transfer coefficient heterogenous model are above the measured values, although in general, the predictions of all the models are lower than the measured values.

The presentation of the results of the integral bed reactor is somewhat difficult, and displaying selected excerpts from Table D15 in Tables 5.1 to 5.4 may be misleading. An appreciation of the different models can only be obtained by a close examination of Table D15. The results can be summarized in a quantitative manner though, and this summary is in Table 5.5.

TABLE 5.5  
SUMMARY OF IBR RESULTS

Model	Number of runs for Which the Difference Between the Predicted and Measured Fractional Conversion was		
	Positive	Zero	Negative
Homogeneous-Isothermal	79	5	4
Homogeneous $h_w = 8.234 \times 10^{-3}$	76	6	6
$h_w = 1.115 \times 10^{-3}$	52	13	23
Heterogeneous $h_w = 8.234 \times 10^{-3}$	66	10	12
$h_w = 1.115 \times 10^{-3}$	45	15	28



## 5.7 Conclusions - Integral Bed Reactor

The rate equation developed in the differential recycle reactor was used, in conjunction with different reactor models, to predict fractional conversions in the integral bed reactor. The homogenous isothermal, homogenous non-isothermal, and the heterogenous models all generated more low predictions than high predictions. From the predictions of the two non-isothermal models, it was clear that the selection of a proper wall heat transfer coefficient was perhaps more important than the selection of a heterogenous model over a homogeneous model. The low heat transfer coefficient homogeneous model often predicted the fractional conversions better than the high heat transfer coefficient heterogeneous model.

Since increasing the complexity of the reactor model improves the accuracy of the predictions, the gap between the measured and predicted values could be narrowed by improving the sophistication of the reactor model. In all the models, radial gradients were ignored, and a model incorporating a modification to account for these gradients would generate better predictions. As well, since the reaction exhibits negative order kinetics, backmixing (axial diffusion) would result in higher conversions (5.1). A reactor model incorporating radial and axial diffusion forms would also predict higher conversions. If these additional terms were added to the mass and energy balance equations, a numerical method requiring the solution of a pair of non-linear partial differential equations would be required. While this is





certainly not an insurmountable obstacle, the benefits of that analysis are questionable.

In the DRR studies, a certain amount of scatter in the data was apparent. That scatter was attributable, in part, to changes in the catalyst activity. In fact, runs following periods of instability or high conversions were usually discarded because of their anomalous activity increases. The instabilities and high conversion runs also occurred in the integral bed reactor. However runs following the instabilities and the high conversion runs were not excluded from the analysis. In particular, runs F18 to F34 in Table D15 followed a series of reactor instabilities, and particularly high conversion levels were measured. For these runs, the predictions were all considerably below the measured values. For example, in Run F23, a fractional conversion of 48.75% was measured, and the best prediction, the prediction of the low wall coefficient, heterogenous model, was only 17.79%. The instabilities which occurred prior to Runs R18-34 certainly affected the activity of the catalyst.

Because there was random scatter in the data, and because of the instability in the catalyst activity, it was concluded that the development of a more sophisticated reactor model was not warranted. The predictions obtained with the three models described here were sufficiently close to the measured conversions to provide an independent verification of the validity of the rate equation developed in Chapter 4. Perhaps



more important however was the identification of the sensitivity of the models to the selection of an appropriate heat transfer coefficient at the reactor wall. The rate equation was valid over a wide range of oxygen concentrations ( $1 \text{ mol/m}^3 - 8.6 \text{ mol/m}^3$ ), a range of ethylene concentrations typical of exhaust hydrocarbon concentrations during start-up ( $0.05 - 1.0 \text{ mol/m}^3$ ) and over a temperature range also typical of automobile start up ( $362\text{-}472\text{K}$ ). Also, the analysis showed that despite certain claims that an integral bed reactor is as effective a vehicle for kinetic studies as is a CSTR or pseudo-CSTR (5.2), the presence of heat transfer limitations (and possibly mass transfer limitations as well) will make the determination of kinetic constants from integral bed data little more than exercise in statistical manipulations.



## CHAPTER 6

### REACTION INSTABILITIES

During the course of the investigations of the 0.3 % platinum catalyst, unstable behaviour was often encountered. The increases in activity with initial treatments was one type of instability encountered. The other instabilities were more complex. They were characterized by substantial changes in the apparent activity of the catalyst during a single run. These instabilities, which were manifested in cyclical and non-cyclical fluctuations in fractional conversion and reactor temperature, were observed in both the recycle reactor and the integral bed reactor.

#### 6.1 Instabilities in the Integral Bed Reactor

The temperatures in the catalyst bed of the integral bed reactor were recorded at discrete time intervals at five points in the bed by the multi-point recorder. As well, a continuous trace of the output of two of the bed thermocouples was recorded on a strip chart recorder. The outputs of two thermocouples, one located near the top of the catalyst bed the other one half way down the bed, were continuously recorded. When the feed was introduced into the reactor, a slight temperature rise was noticed. This rise was usually less than 5K and was typically about 1K or 2K. The temperature transient would subside in less than two minutes. Figure 6.1 is a tracing of a bed thermocouple for a typical run.

The non-cyclical instabilities resulted from the passage of the reaction front down the length of the catalyst bed. This is not an uncommon phenomenon. For many positive order systems, this



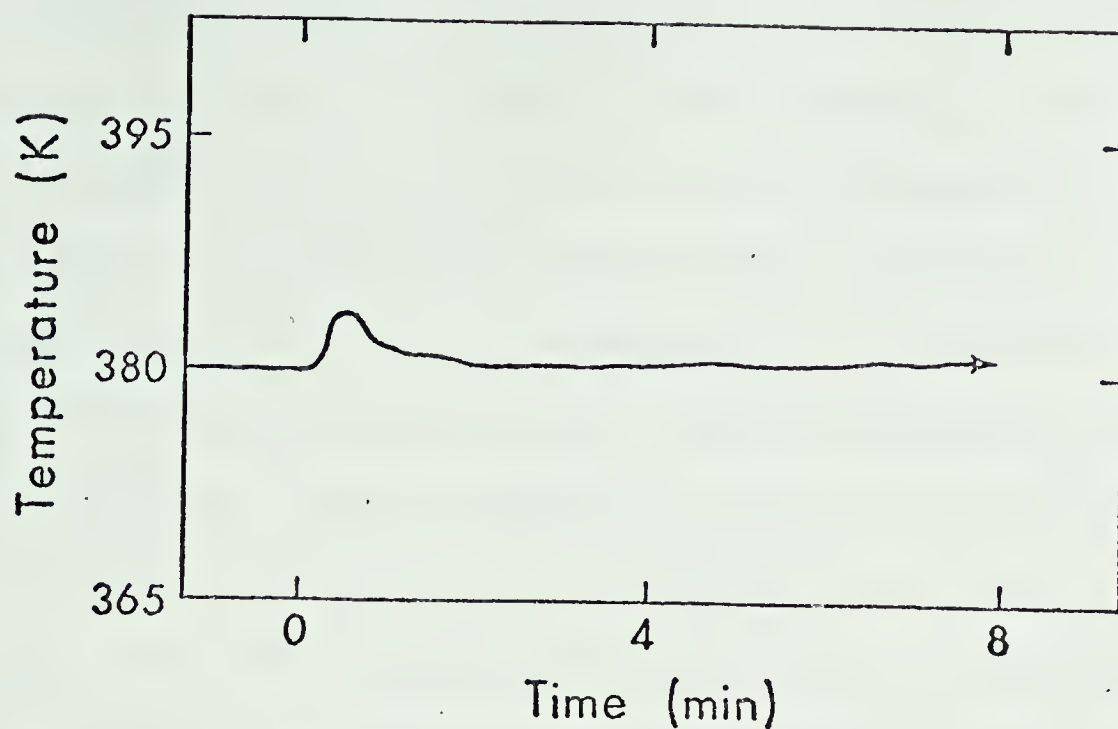


Figure 6.1 : Typical temperature versus time behaviour for IBR runs.

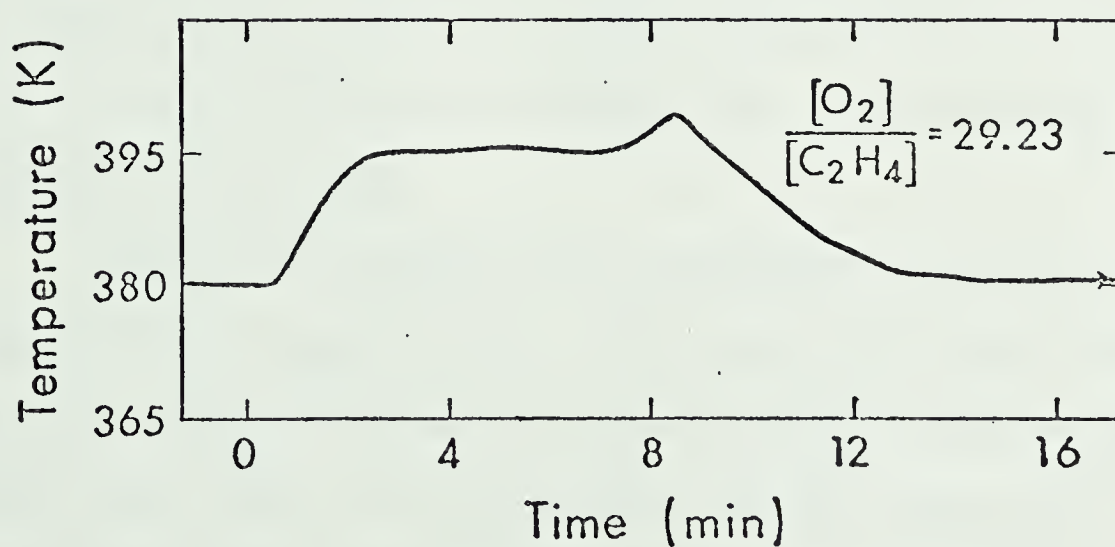


Figure 6.2 : Typical temperature versus time behaviour for IBR runs in which the reaction front passed out the reactor exit.





type of behaviour has been observed and theoretically predicted(6.1). Figure 6.2 is a tracing of the output of the thermocouple half-way down the catalyst bed for one such run. The bath temperature was 380 K and the oxygen to ethylene ratio in the feed was about 30 to one. Within two minutes following the introduction of the reactants into the reactor, the temperature rose to 395K, and remained there for about six minutes. During this time the fractional conversion was measured at 74.4 % . At the eight minute mark, the reaction front moved past the mid point of the reactor, causing a further increase in the temperature to 400K. An analysis of the products revealed that the fractional conversion jumped to 100 % during this transient. Once the reaction front had passed, the temperature of the bed fell to less than a degree above the bath temperature of 380 K. The average fractional conversion once steady state was achieved was 20.15 %. The output of the thermocouple near the top of the bed was nearly identical with Figure 6.1, with the sole exception that the reaction front passed through that point about 90 seconds before it passed through the bed midpoint. The multi-point recording also confirmed that a reaction front did indeed pass down the reactor bed.

Often, the transients were much faster than the one discussed above. Figures 6.3(a), 6.3(b), and 6.3(c) depict three temperature tracings from the half-way thermocouple at  $O_2$  to  $C_2H_4$  ratios of 25.28, 43.11, and 53.19 respectively. In these cases, the reaction front passed through half the length of the bed about four minutes after the feed had been introduced into the reactor. As can be seen from Figure 6.3, increasing the oxygen concentration relative to the ethylene at constant bath temperature tended to reduce the severity of the



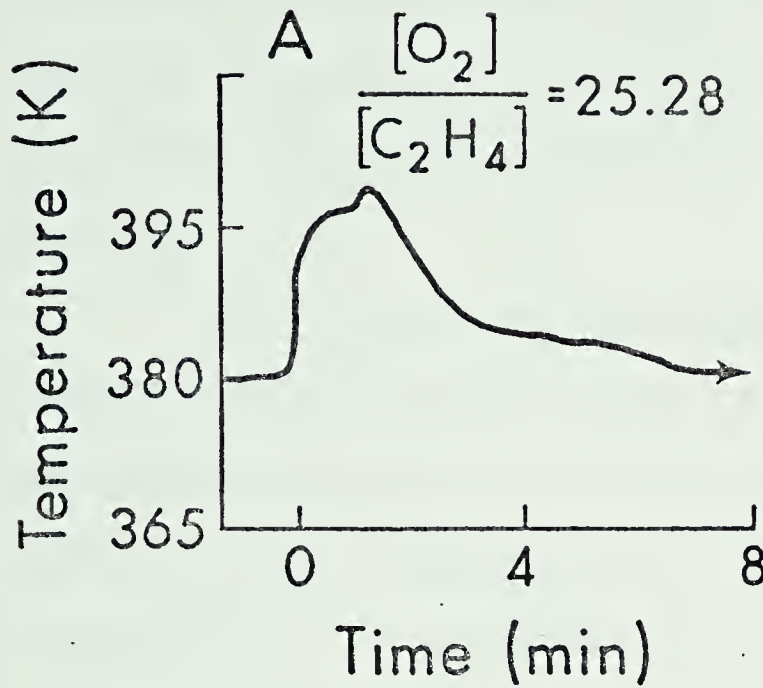


Figure 6.3(a)

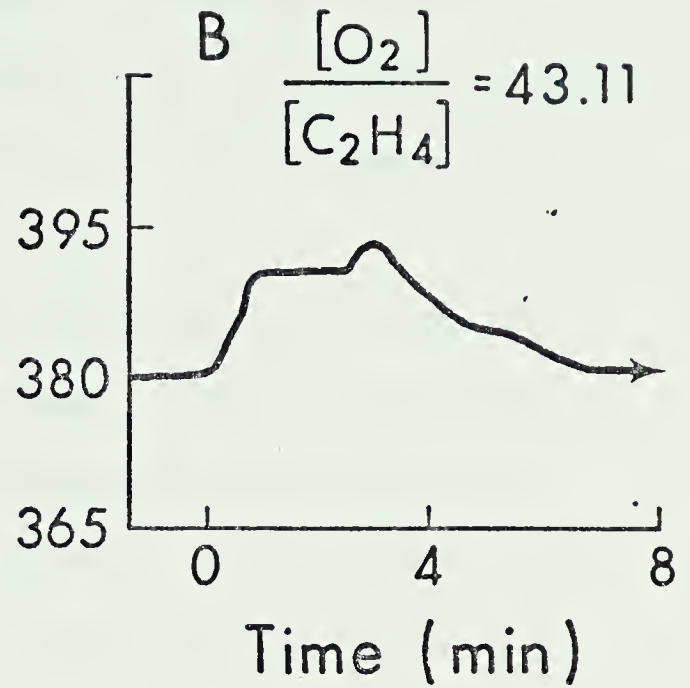


Figure 6.3(b)

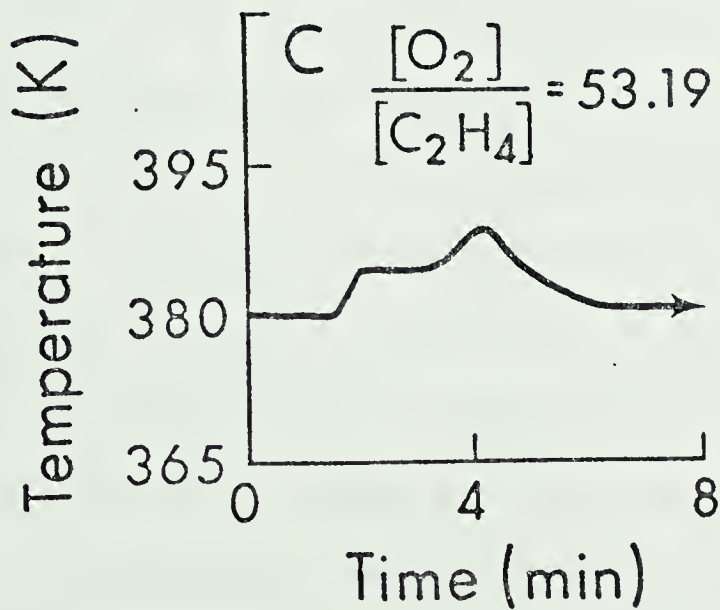


Figure 6.3(c)

Figure 6.3 : Temperature transients in the IBR as a function of  $[O_2]/[C_2H_4]$ .



transient wave. After these instabilities occurred, the fractional conversion was often inordinately high for the run immediately following, and also for a few subsequent runs. This is responsible for some of the scatter in the DRR and IBR data. For the kinetic fitting of the DRR data, the unstable run and the run following the instability were usually discarded.

The non-cyclical instabilities occasionally appeared as a doublet, with two distinct temperature peaks. Tracings of two such temperature histories of the mid-bed thermocouple are depicted in Figure 6.4. Again, the passage of a reaction front was evident from a comparison of the two thermocouples. During the high temperature transient, the fractional conversion was 100 %. After the transient had subsided, the steady state values for the fractional conversion were 58.6 % for the run pictured in 6.4(a) and 56.0 % for the run pictured in 6.4(b).

As well as the non-cyclical transients which were observed, a number of runs also exhibited instabilities which were periodic in nature. These runs often produced a series of doublet peaks similar to those just described. A series of these peaks from a tracing of the mid-bed thermocouple are shown in Figure 6.5. For this run, the ratio of the inlet oxygen to inlet ethylene concentrations was 3.1. After an initial temperature rise of about 8 K, a series of doublet peaks appeared on the temperature tracing. The period of the oscillation varied from five minutes to eight minutes and the maximum amplitude was about 5 K. The oscillations continued in the fashion depicted for six hours, until the run was terminated. The fractional conversion during the trough periods was about 62 % while the conversions



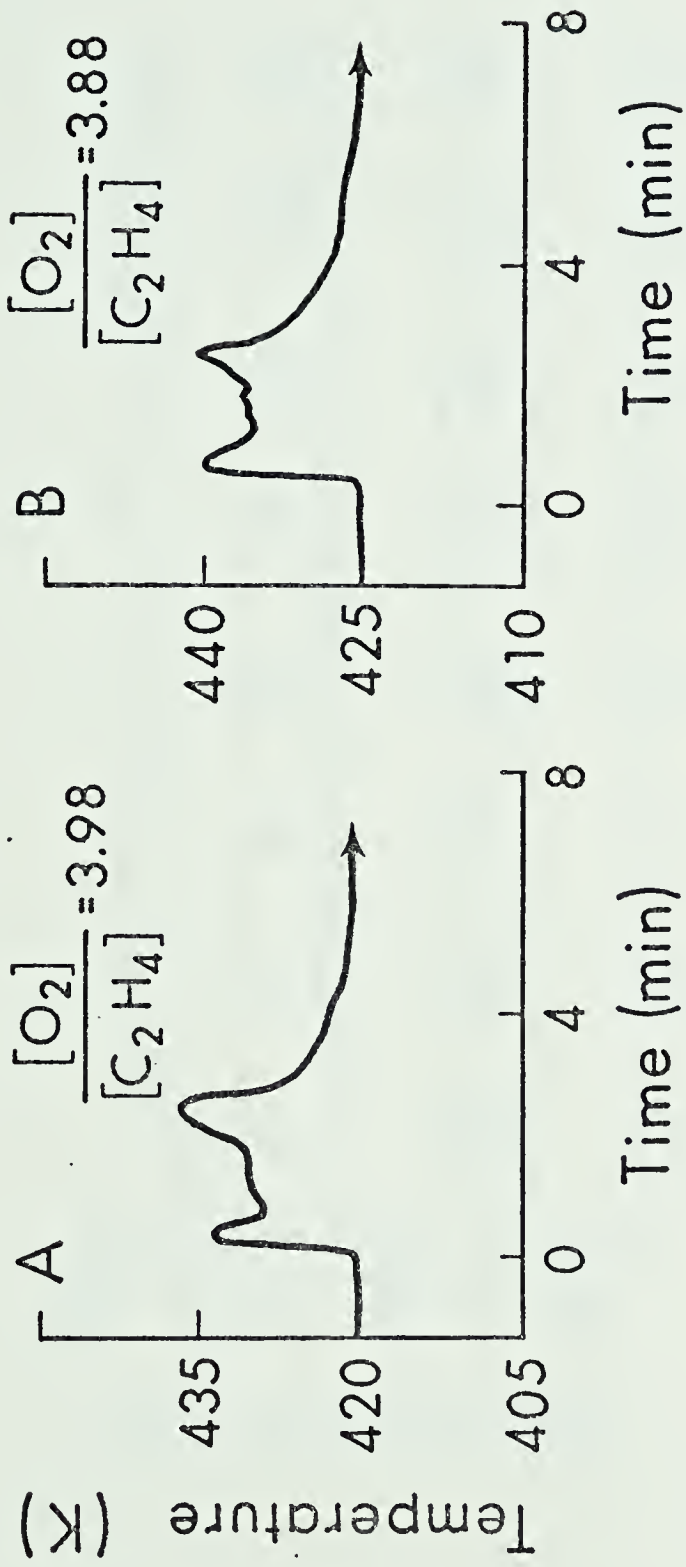


Figure 6.4(a)

Figure 6.4(b)

Figure 6.4 : Temperature transients in the IBR





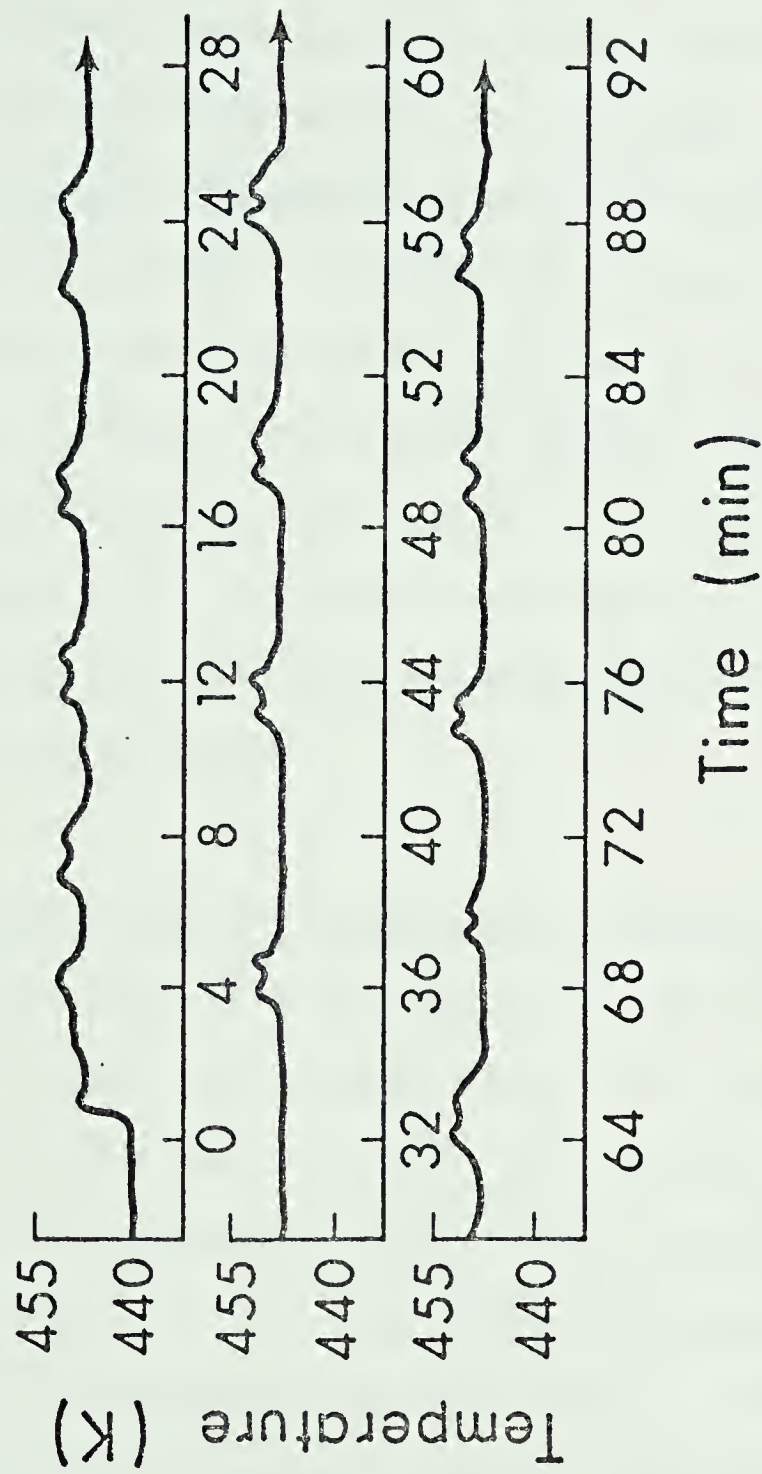


Figure 6.5 : Cyclical temperature behaviour in the IBR.



during the peaks was 100 %. Slight induced changes in the inlet ethylene concentration ( $0.1 \text{ mol/m}^3$ ) did not affect the period or the amplitude of the oscillations. Cyclical oscillations of this type occurred only at bath temperatures above 420 K, while no instabilities of any kind were noticed below 380 K. In all cases, the passage of the reaction was marked by complete conversion of the ethylene. The oscillations were observed in runs with both slight and large excesses of oxygen, but were never observed during runs in which the oxygen supply was near or below stoichiometric amounts. (Inhibitory effects of the ethylene during those runs would result in very low conversions, usually less than 5 %). The oscillations were unaffected by small changes in the feed concentration or the bath temperature once a series of fluctuations was established.

## 6.2 Instabilities in the Differential Recycle Reactor

The non-cyclical instabilities observed in the integral bed reactor did not appear during the DRR runs. Since the length of the catalyst bed was much less in the DRR, the passage of a reaction front through the catalyst bed would not be noticed. The continuous recordings of the output of the thermocouple in the bed and at the top of the bed were nearly identical for all the runs. The catalyst bed, as is the intent in a differential reactor, remained at a uniform temperature (and probably reaction rate) at any instant. For a number of runs periodic undamped oscillations in the bed temperature and the final fractional conversion were observed.



The catalyst which had been aged in the integral bed reactor and then placed in the recycle reactor exhibited oscillations with fairly well defined amplitudes and periods. Figure 6.6 and Figure 6.7 show the tracings of the bed thermocouple and the corresponding fractional conversions measured at the reactor exit. The equipment was designed primarily to produce steady state-data, and the compositional analyses were performed with a gas chromatograph. Continuous monitoring of the fractional conversion was impossible, and hence substantial portions of the fractional conversion versus time curves in Figures 6.6 and 6.7 are inferred from the temperature tracing rather than being actually measured.

The run pictured in Figure 6.6 was at a bath temperature of 371K and a ratio of inlet oxygen to inlet ethylene concentrations of 21.87. The period of the oscillations varied somewhat from 3.5 to 4 minutes while the amplitude of the temperature oscillation was only about 2K. This produced a fluctuation in the fractional conversion from 0.5% to 3.5%. The oscillations in the run pictured in Figure 6.7 were more pronounced. For this run the bath temperature was 388K and the ratio of inlet oxygen to inlet ethylene was 54.69. Under these conditions, oscillations with a period between 5.5 and 6 minutes and a temperature amplitude of 4-6K were produced. The corresponding range of fractional conversions measured was 31.7% to 100%. The runs pictured in Figure 6.6 and 6.7 continued undamped until they were terminated at three and six hours, respectively.

It is interesting to note that the temperature trace in Figure 6.7 falls below the value of the bath temperature in the "trough" section of the oscillations. This may suggest that the pre-heating



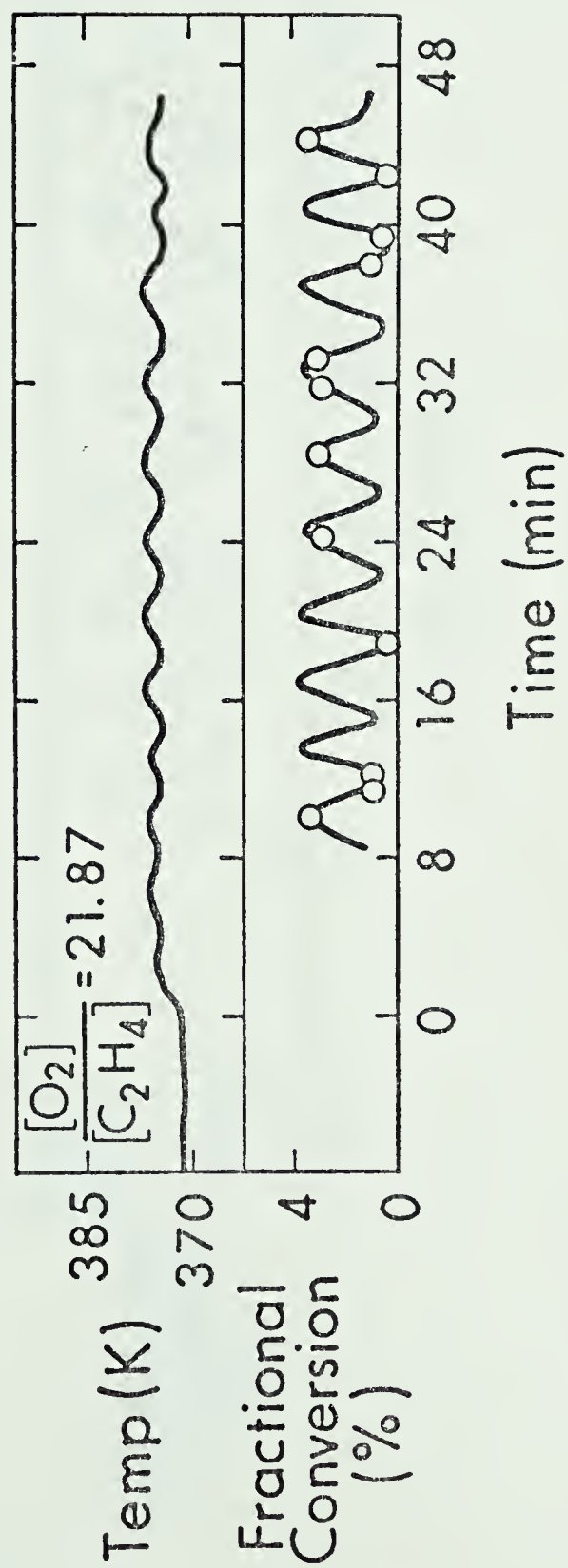


Figure 6.6 : Cyclical temperature and conversion behaviour in the DRR (low oxygen concentration).





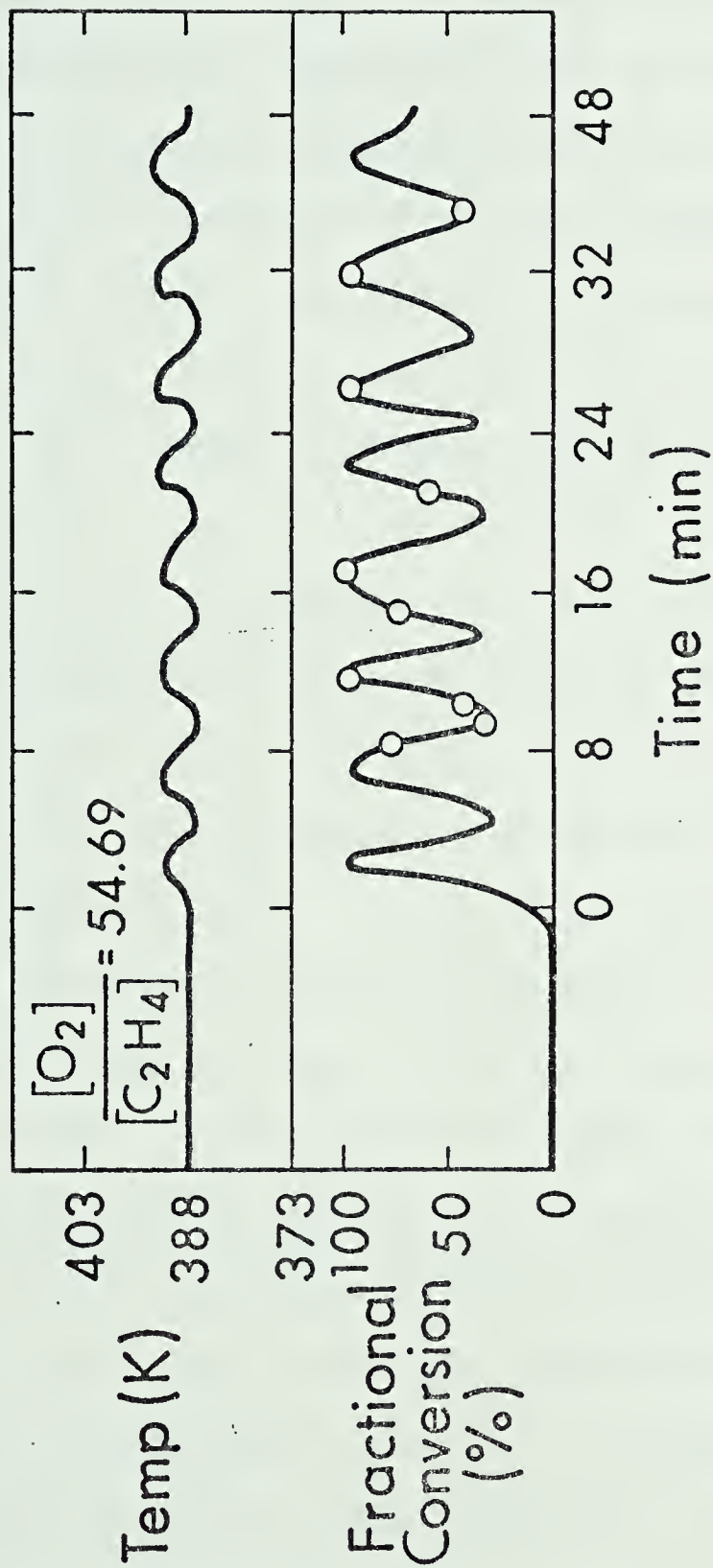


Figure 6.7 : Cyclical temperature and conversion behaviour in the DRR (high oxygen concentration).



coil was too short and that the recycle compartment was not sufficiently insulated. This was the only run (M54) in which this phenomenon was observed. During steady operation, the exothermicity of the reaction prevented the gases from cooling below the bath temperature. To prevent the reaction gases from cooling below the bath temperature, the power supplied to the recycle compartment heater was increased for all the subsequent runs and the cooling never reoccurred.

Cyclical instabilities were also observed in the DRR with the fresh 0.3% Pt catalyst. Occasionally, the instabilities were cyclical, but not periodic. In these cases, the temperature and fractional conversion would abruptly jump from a low conversion level to a high conversion level. Such a run is pictured in Figure 6.8. Here, the periods of high or low conversion lasted from a few hours to over a day. A careful examination of the outputs from the mass flow meters revealed no appreciable fluctuations in the inlet flow rates over the duration of the run, and the output of the bath thermocouple was also steady throughout the run. The low conversion levels resulted in fractional conversions from 15% to 30% while the high conversion periods were characterized by complete oxidation of the ethylene. As was the case for the IBR instabilities, small induced fluctuations in the inlet flow rates and the bath temperature did not affect oscillations.

If this oscillatory behaviour of the ethylene oxidation system were to be studied more extensively, modifications to the equipment used here would certainly have to be made. The continuous monitoring of not only the temperature of the catalyst bed, but also of the exit concentrations would be necessary to study the transients in detail.



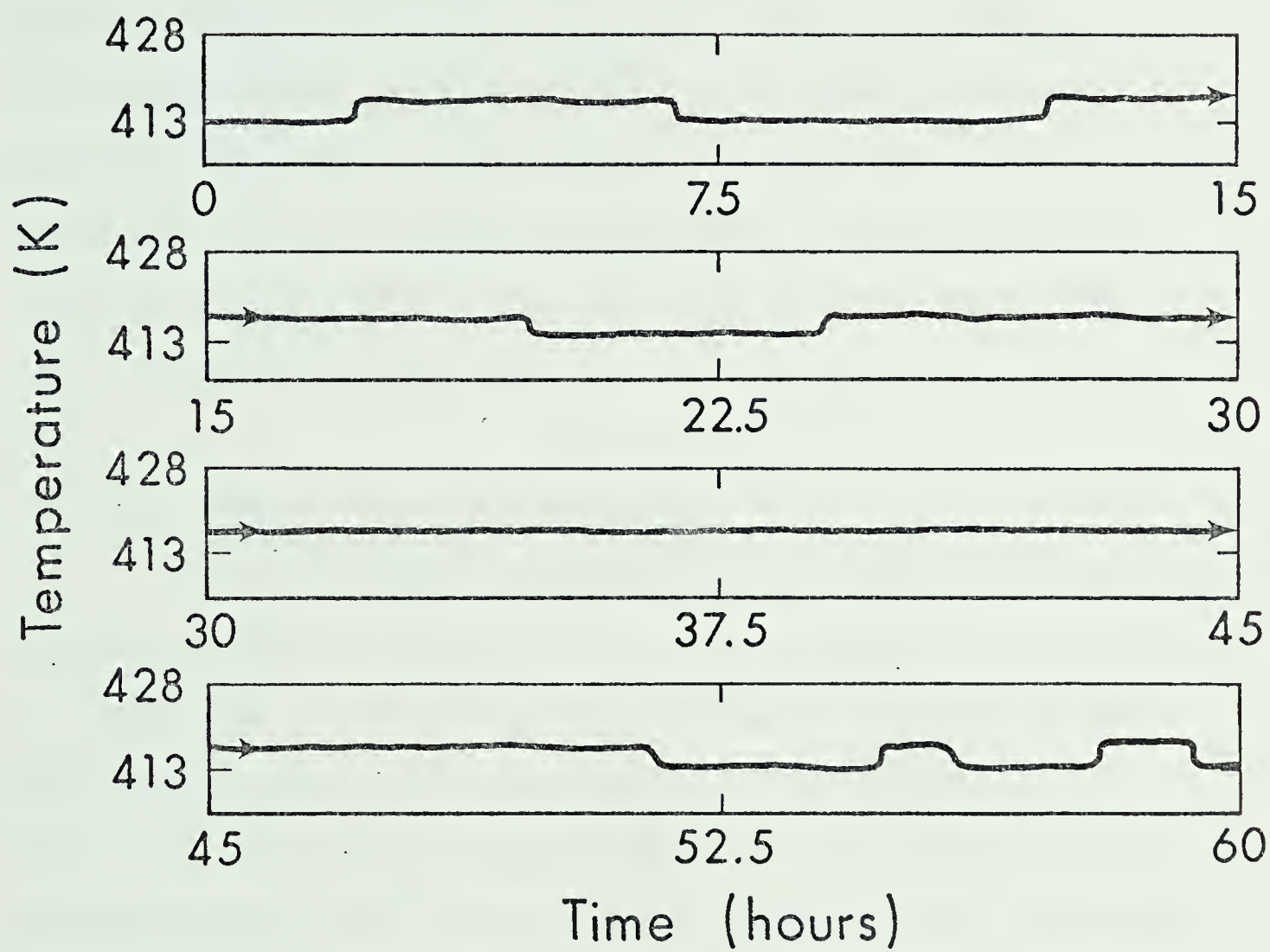


Figure 6.8 : Abrupt temperature variations in the DRR.



### 6.3 Physical Models

While the reactor instabilities could not be studied extensively with the equipment used for this work, and while they were primarily a hindrance to the development of a rate equation, speculations as to their origin can certainly be offered. As was mentioned in Chapter 2, many authors have studied oscillations in the CO oxidation system, and have offered a corresponding number of hypotheses explaining why they occurred. A definitive statement as to the origin of the oscillations in this system, ethylene oxidation, cannot be presented at this time, but a few of the more promising explanations will be mentioned.

#### 6.3.1 Macroscopic CSTR Instability

One of the better documented (6.2,6.3) causes for instability in adiabatic CSTR's and pseudo-CSTR's (such as the DRR) arises because of multiple intersections between the mass and energy balances (see Appendix A). This is often depicted in a figure similar to Figure 6.9. The upper and lower intersection points, A and C, are stable operating conditions while the intersection at B is metastable. This type of instability is frequently manifested in abrupt jumps from one stable state to another, in a manner very similar to that pictured in Figure 6.8. There are reasons to believe that the instabilities observed during the course of this work were not due to this classical CSTR instability however. First, the classical CSTR instability does not occur spontaneously, but rather results from a disturbance in the operating conditions (change of concentration, flow rate, temperature, etc., in the feed). As was mentioned, no measurable







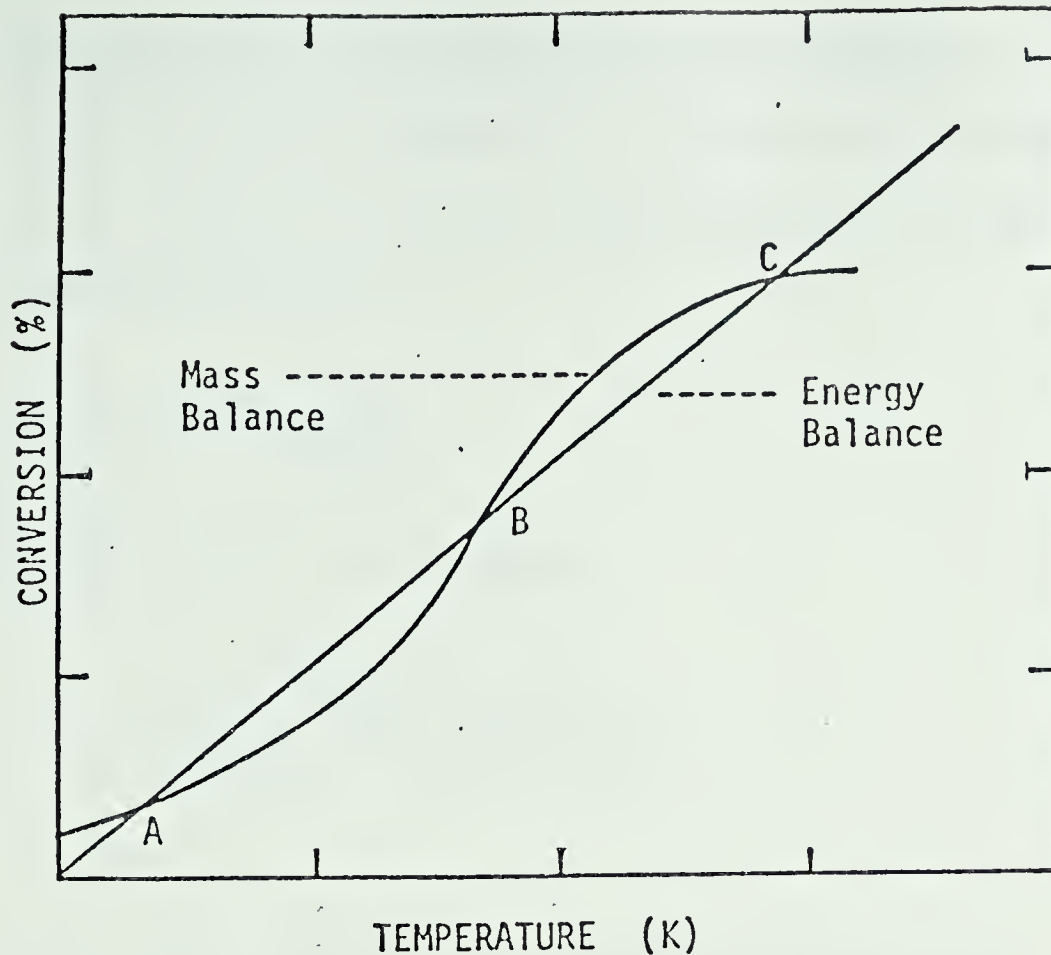


Figure 6.9 : Mass and energy balances for a CSTR.

changes in any of the feed parameters were noticed. While absence of evidence is not evidence of absence, it seems unlikely that the shifts in conversion levels was precipitated by shifts in one of the feed conditions. Second, small induced changes in the flow rates (less than 10%) and in the bath temperature (less than 3K) did not cause any changes in the pattern of oscillations observed in either the DRR or the IBR.

So, while the abrupt jumps from one steady state to another pictured in Figure 6.8 may resemble the classical CSTR instabilities, it is believed that the instabilities do not arise from any macroscopic effects, but rather are due to some other microscopic effects.



### 6.3.2 Instabilities Due to the Nature of the Rate Equation

One of the simplest explanations for the oscillations can be presented from a consideration of the rate equation. The final empirical equation selected was

$$-r = A_0 e^{-E/RT} \frac{[O_2]}{[C_2H_4]} \quad (6.1)$$

which was a limiting form of the equation

$$-r = \frac{A_0 e^{-E/RT} [O_2]^{n1} [C_2H_4]^{n2}}{(1 + k_1 [O_2]^{n3} + k_2 [C_2H_4]^{n4})^{n5}} \quad (6.2)$$

While no positive order behaviour with respect to ethylene was observed during this study, there must certainly be a concentration range (less than 0.01%) of ethylene in which zero or positive order kinetics do exist. If the DRR was non-isothermal, then, as the reactants entered the reactor, the high exothermicity of the reaction would cause an increase in the reactor temperature and in the reaction rate. The increased rate would cause a drop in the ethylene concentration which would further result in a yet higher rate followed by increasing temperatures and rates and decreasing ethylene concentrations. Once the complete (or very near complete) conversion level is reached, the reaction order with respect to the ethylene concentration becomes positive, and further reaction, in the incomplete conversion case, decreases the rate. Once the rate begins to decrease, the ethylene concentration increases, and the inhibitory effect of the increased ethylene concentration causes a further decrease in the rate and the temperature. This phenomenon could conceivably continue until the



reactant gases were at the original state, at which time the cycle could begin again. Under isothermal conditions, the cycling would not occur.

This model, while not without appeal due to its simplicity, does suffer from a few shortcomings. First, it is only speculation that the positive order kinetics exists for this system. Since it is certain that no positive order kinetics were apparent at ethylene concentrations below 0.1%, it is somewhat difficult to postulate a shift from positive to the negative order kinetics at concentrations below this level. Especially at oxygen concentrations around 20%. The continuation of the cycle once the reactant gases had returned to the initial state would require that the reaction rate increases. For these reasons, a model incorporating only the rate equation as an explanation for the instabilities is unsuitable, and a model which postulates more subtle surface phenomena is required.

### 6.3.3 Multiple Types of Adsorbed Oxygen

The possibility that two different forms of the reacting species may exist on the catalyst surface, and thereby result in multiple steady states has been discussed by McCarthy et al. (2.11) and by Hugo and Jakubith (2.14). They both speculated, that for carbon monoxide oxidation, two forms of adsorbed CO may exist ( $\text{CO}_A$  and  $\text{CO}_B$  or bridged and linear) and that one of the forms displays considerably more activity for oxidation than the other. In this work, it is not known whether the reaction proceeds via an L-H mechanism (reaction between adsorbed oxygen and adsorbed ethylene) or via an E-R mechanism (reaction between one adsorbed species and one gaseous species). From the adsorption studies however, it seems evident that the oxygen, at least, must be adsorbed





in order for the reaction to occur. If, as Kikuchi et al. (6.4) suspect, oxygen adsorbed on platinum can exist in more than one form on the metal surface, then a difference in reactivity between the two forms could result in the observed instabilities if there is a shift from one non-reactive form to a reactive form. This possibility, while very promising, is also very difficult to verify. Typically, the nature of adsorbed species is inferred from analyses of IR spectra. Unfortunately, oxygen adsorbed on Pt/Al<sub>2</sub>O<sub>3</sub> cannot be detected by IR since the adsorbed oxygen bands are masked by the Al<sub>2</sub>O<sub>3</sub> bands. Because of this, different oxygen species can be observed only indirectly. Sheintuch et al. (2.15) believe that the CO oxidation/oscillation models which ascribe multiplicities to transformations between bridged and linear forms of adsorbed carbon monoxide should not be used. They discarded this model on the basis that their predictions with the model would oscillate only for "unreasonably" high values of certain parameters. As well, they felt that the model had no applicability to other reactions which exhibited oscillatory behaviour. This does not imply that a model incorporating an equilibrium transition between a reactive and non-reactive adsorbed oxygen specie as a rate determining step is untenable. However, they showed very little enthusiasm for this kind of postulation.

#### 6.3.4 Instabilities Due to Periodic Burn-Off

The possibility that a burn-off of adsorbed carbon monoxide may occur periodically was considered by Beusch et al. (2.16) as an explanation for the observed oscillations in carbon monoxide oxidation. A similar type of explanation could also be proffered in this case. In

the deactivation phase of this model, the surface of the catalyst (or the active sites only) become covered with ethylene. As the surface coverage of ethylene increases, the concentration of adsorbed oxygen, and the reaction rate decrease. Once the surface is covered to a high degree with adsorbed ethylene, the reaction is at its lowest rate. If the oxygen rich gas phase can then begin to oxidize the ethylene at a localized "hole" in the ethylene coverage, the proximity of the many adsorbed ethylene molecules to each other could cause a chain reaction in which the surface coverage of ethylene is burned off. A similar phenomenon can occasionally occur in the catalytic converters. Prolonged driving at unsteady state (rush hours for example) can result in the converter pellets becoming coated with carbon. An engine misfire can initiate the combustion of this adsorbed carbon, and the resulting temperature rise may have catastrophic effects on the catalyst, the converter, and even the entire automobile.

This model is attractive; however, there is little basis for the speculation that a chain reaction burn-off occurs. Since no experimental verification could be made with the equipment used here, the veracity of this explanation could not be tested.

#### 6.3.5 Instabilities Arising from Changes in the Catalyst Surface

The final model to explain the oscillations is based on the possibility that changes to the platinum surface occur during the course of the oscillation. In the next chapter, the effect of the metal dispersion on the apparent catalytic activity is examined. It was found that the specific activity of a supported platinum catalyst increases as the dispersion decreases, so that any changes in the metal dispersion which







occur during the course of a run will be reflected in changes in the measured fractional conversion. The oscillations could arise from a cycle of sintering and redispersal of the platinum crystallites. Flynn and Wanke (4.1) and Fiedorow and Wanke (3.2) support the contention that atomic migration model for the sintering of supported metal catalysts will predict the redispersal of sintered crystallites. A cycle could involve the progressive sintering of the metal surface as the reaction rate increased until the decrease in the rate due to loss of metal area matched the rate increases due to lower ethylene concentrations. This would be followed by a period of further sintering during which time the rate would decrease, causing a decrease in the temperature of the surface. If the temperature is then lowered, the redispersion of the catalyst could begin to occur, resulting in a return to the higher rates and temperatures. In this manner cyclical behaviour would be detected in the measured catalyst temperature and exit fractional conversions.

The changes in the catalyst surface need not be particularly severe. The adsorption studies cited in Chapter 2 indicated that the heats of adsorption were strong functions of the platinum surface for both oxygen and ethylene. A change in the distribution of active sites on the catalyst, rather than a redistribution of the actual crystallites would probably be sufficient to account for the observed instabilities.

Some of the experimental observations indicate that a change in the platinum surface may well be the reason for the occurrence of oscillations in this system, since it was frequently noted that the activity of the catalyst following an instability run was inordinately high.



Some temporary changes in the catalyst must have taken place during the run in which the instabilities occurred. These temporary changes were then responsible for the subsequent increases in activity. It is of course difficult to determine which is the cause and which the effect. The cyclical instabilities in the DRR can certainly be viewed as resulting from changes in the supported metal. The apparent activity increases following a single high conversion run or long term transient (Figure 6.4) may well have been caused by increases in metal dispersion which were themselves caused by the higher pellet temperatures. In the latter case, the instability caused the change in the catalyst rather than vice versa.

The dispersion studies outlined in the next Chapter also indicated that thermal treatment of the catalyst in oxygen atmospheres may result in changes in the dispersion and hence in the activity. Some of the oxygen-treated catalyst samples had activities which were lower than catalyst samples of the same dispersion which had been treated in hydrogen. While an explanation for this would also have to be speculative, the observation is enough to give some support to the postulation that changes in the catalyst are responsible for the non-cyclical instabilities and perhaps cyclical ones also. Since many of the runs were conducted in excess oxygen (up to 20%), the surface of the catalyst was regularly exposed to conditions similar to those used to prepare the samples discussed in Chapter 7. This could result in both permanent and temporary changes in the catalyst surface.



#### 6.4 Summary

Non-cyclical oscillations and cyclical oscillations of regular and irregular periods were observed in both the integral bed reactor and the differential recycle reactor. These oscillations occurred in both the bed temperature and the measured fractional conversion. The amplitudes of the oscillations ranged up to 80% for the fractional conversions and up to 6K for the temperatures. The instabilities caused temporary increases in the activity of the catalyst. A number of explanations for the oscillations can be presented, but none merits wholehearted support. A model based on periodic changes in the surface morphology of individual platinum crystals seems promising, but extensive experimentation would be required before any model could be adopted.





## CHAPTER 7

### THE EFFECT OF PLATINUM DISPERSION ON ACTIVITY

#### 7.1 INTRODUCTION

In Chapter 1, the importance of a fine dispersal of the active metal on the support was mentioned. As the dispersion increases (smaller crystallites), the surface area per unit mass of the precious metal increases. For many catalytic reactions, the rate of reaction is directly proportional to the surface area of the catalyst and hence directly proportional to the dispersion. However, for many other catalytic reactions, the activity is not only a function of the metal area, but also of the structure of the catalyst surface. Boudart (7.1) referred to the former structure insensitive reactions as facile reactions and to the latter structure sensitive reactions as demanding reactions.

This characterization does not specify the nature of the structure sensitivity, and a demanding reaction may exhibit increased or diminished activity compared with a facile reaction. In Figure 7.1, (7.2) a number of demanding reactions and a facile reaction (Curve 1) are pictured. The facile reaction is a horizontal line on a specific rate versus dispersion plot.

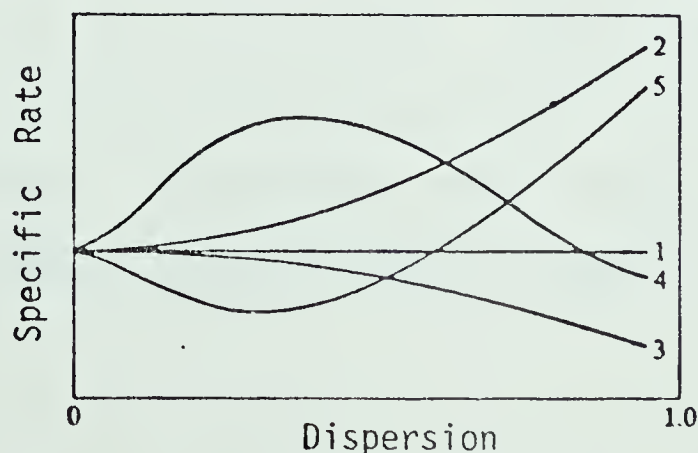


Figure 7.1 : Specific rate as a function of dispersion (Ref. 7.2)



Huang and Carberry (7.3) reported that the oxidation of hydrocarbons over supported platinum catalysts was demanding. It was decided that an examination of the structure sensitivity/insensitivity of a series of surface coated supported platinum catalysts might prove interesting. A number of 0.5% Pt/  $\text{Al}_2\text{O}_3$  catalysts with dispersions ranging from 0.036 to 0.32 were available and they were used to determine if the oxidation of ethylene over supported platinum is demanding or facile.

The catalysts with different dispersions were obtained by thermally treating (sintering) 0.5% Pt/ $\text{Al}_2\text{O}_3$  (Engelhard) catalyst samples. Some of the samples were sintered in an oxygen atmosphere, and some in a hydrogen atmosphere, but in all cases the samples were reduced in hydrogen at 500°C for one hour following the sintering. The catalyst treatments and the measurements of the dispersions were done by Dr. R. Fiedorow. The details of the treatments and dispersion determinations have been previously described by Fiedorow and Wanke (3.2). A summary of the thermal treatments and the dispersions of the catalysts used were outlined in Chapter 3 (Table 3.1).

Fractional conversions as a function of ethylene and oxygen concentrations were measured at 385 K, 410 K, and 425 K for the catalyst samples using the recycle reactor. For all experiments, 75 catalyst pellets (3.0 to 3.5g) and an equal volume of Pyrex beads were placed into the reactor. The procedure used for these dispersion runs was the same as that described in Chapter 4 for the



kinetic runs.

## 7.2 RESULTS

A number of experimental difficulties were encountered during the studies on the sintered catalysts. Variations in catalytic activity and instabilities similar to those previously described occurred. Fluctuations in the recycle ratio, large transient temperature gradients, and difficulties in obtaining steady state all hindered the investigation. In consequence, many of the experimental points had to be discarded from the analysis.

The recycle ratio decreased during the study from the 20:1 value of previous runs to between 10 and 12 to one. Replacement of the inline filter, cleaning of the tubing, and checking of all valves and fittings failed to rectify the problem. The recycle ratio was restored to its original level by switching to a new metal bellows in the recycle pump. Experiences of other members of the Chemical Engineering Department confirmed that the metal bellows was a particularly vulnerable piece of the apparatus.

The catalyst used for these studies had a 0.5% platinum loading compared with a 0.3% loading on the catalyst used for the previous work. Since the reaction rate will generally increase with the metal loading, it was feared that the reaction rates at temperatures comparable to the ones previously studied (362 K - 472 K) might be too high. This indeed was a problem. High temperature differences, up to 40°C between the bath and the catalyst bed as well as within the catalyst bed, occurred for runs at high





oxygen concentration ( $\sim 18$  mole %). For these runs, heat transfer limitations, internal, external and at the reactor wall would mask the intrinsic reaction rates.

For several of the experiments, exceptionally long time periods (4 to 8 hours) were required to achieve steady-state product concentrations. Except for unstable runs, steady state was always achieved in less than 30 minutes for the other DRR and the IBR runs. This long period to achieve steady-state was probably due to a restructuring of the platinum crystallites. The catalyst samples were all reduced in hydrogen, and were not treated in air after the dispersion determinations. Since these changes were slow compared with the time required to perform the chromatographic analysis, it is certainly possible that changes in activity occurred even after the product compositions appeared to be steady.

The experimental results for the sintered catalysts are presented in Appendix D, Table D15. The results for runs which were unreliable, i.e., runs during which instabilities occurred, runs following an unstable run, runs in which large temperature gradients were observed, and 100% conversion runs are not included in Table D15. All of the runs are listed in the Separate Data Book. The rate for most of the experiments where the average conversion was less than 10% was, as before, calculated from the carbon dioxide formation. Exceptions to this were runs Q1, R6, S3, T4, T13 and T14 where the rate of  $\text{CO}_2$  formation was, for unknown reasons, very low or zero. In these cases, the conversion based on ethylene depletion was used for the rate calculation. At conversion levels above 10%, the average conversion was used to calculate the





rate.

The rate data in Table D15 were fitted to the same equation used

$$-r = \frac{k [O_2]}{[C_2H_4]} \quad -(7.1)$$

at each temperature and for each catalyst sample using the Marquardt algorithm. The rate constants were then normalized with respect to the dispersion, i.e.

$$k' = \frac{k}{\text{DISPERSION}} \quad -(7.2)$$

The values of  $k$  and  $k'$  are tabulated in Table 7.1 for the various catalysts and a plot of  $k'$  versus dispersion for the sintered catalysts is shown in Figure 7.2.

Rates were also measured for an unsintered 0.5% Pt/Al<sub>2</sub>O<sub>3</sub> catalyst (E-000, Table 3.1; Series 0, Table 7.1) assuming that the dispersion of that catalyst was 0.22, i.e. equal to the dispersion of the catalyst treated only in hydrogen at 500°C (E-97, Table 3.1; Series U in Table 7.1). The normalized rate constants,  $k'$ , for the untreated catalyst were approximately twice the value of the corresponding normalized rate constants for catalysts E-97. For example, at 385 K, the normalized rate constant for sample E-000 was  $15.58 \times 10^{-8}$  compared with  $6.145 \times 10^{-8}$  mol/g cat-s for catalyst E-97.

### 7.3 Discussion of Results

Although the previously discussed uncertainties may cast some doubt on the accuracy of the results presented above, the



Table 7.1  
Results of Dispersion Experiments

Series	Dispersion	Rate Constants $\times 10^8$ (mol/g cat-s)					
		385 K		410 K		425 K	
		k	k'	k	k'	k	k'
O	(0.22)	3.427	15.58	5.705	25.93	-	-
P	0.036	-	-	1.750	48.62	2.568	71.33
Q	0.115	-	-	2.365	20.56	5.143	44.72
R	0.12	1.179	9.823	3.021	25.18	5.009	43.55
S	0.155	0.4438	2.863	2.068	13.34	5.842	37.69
T	0.17	-	-	1.815	10.68	2.782	16.36
U	0.22	1.3521	6.145	3.545	16.11	5.913	26.88
V	0.26	0.4765	1.833	2.261	8.694	-	-
W	0.32	0.5187	1.621	2.461	7.691	4.889	15.28

$$k' = \frac{k}{\text{dispersion}}$$

Series R,S,U, Sintered in H<sub>2</sub>

Series P,Q,T,V,W Sintered in O<sub>2</sub>

Series O Unsintered



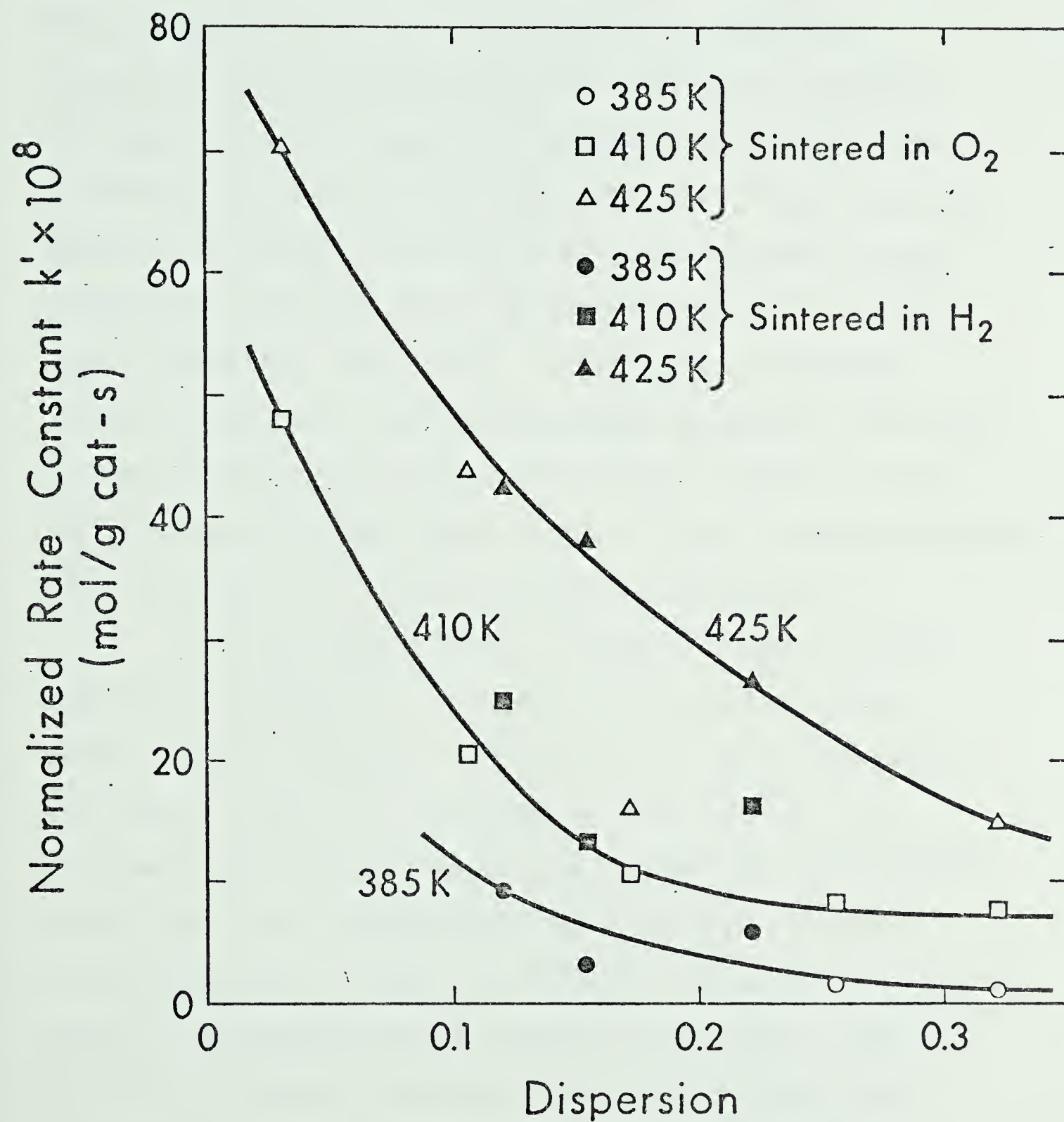


Figure 7.2 : Effect of dispersion on the specific rate constant.



plot of normalized rate constants,  $k'$ , versus dispersion do show a definite trend. The normalized rate constant, and hence the rate per unit of platinum surface, decreases with increasing dispersion. This decrease in the specific rate with decreasing platinum crystallite size (increasing dispersion corresponds to decreases in average crystallite size) is in agreement with reported effects of platinum crystallite size on oxygen adsorption. Dalla Betta and Boudart (7.4) and Wilson and Hall (7.5) found that small platinum crystallites adsorb less oxygen per surface platinum atom than do large crystallites. The results of the adsorption experiments reported in Section 4.7 indicate that oxygen adsorption is the rate determining step in the oxidation of ethylene. If this is in fact the case, then the trends shown in Figure 7.2 are in agreement with the effects of crystallite size on the oxygen adsorption capacity.

While the general trend of decreasing specific activity with increasing dispersion does agree with reported adsorption versus dispersion behaviour, it is difficult to accept the shape of the curves in Figure 7.2 in the light of other findings. For platinum dispersions less than 0.1, i.e. crystallites with diameters greater than 10 nm the specific activity should be independent of the dispersion. At dispersions below 0.1, the average coordination number of surface platinum atoms becomes independent of crystallite size (7.6, 7.7) and the readiness of the catalyst samples with dispersions of 0.036, 0.115, and 0.120 to adsorb oxygen should be approximately the same. This behaviour is not displayed in Figure 7.2.





The normalized rate constants at a dispersion of 0.036 are nearly twice the normalized rate constants at a dispersion of 0.115. The normalized rate constants do not become constant at low values of the dispersion. This may be due to several factors.

When determining the structural sensitivity of supported metal catalyst, the metal crystallite size should be used as the independent variable. Although the dispersion is related to the average crystallite size, it does not reflect the distribution of crystallite size. Ideally, a catalyst having a narrow crystallite size distribution should be used for these studies. Unfortunately in most supported metal catalysts, the metal is present in crystallites of various sizes. This crystallite size distribution may be broad, and for sintered catalysts may even be bimodal (7.8). Broad and/or bimodal crystallite size distributions will tend to obscure structural sensitivity (7.9). Also, the catalyst samples may have differed in aspects other than the dispersion. The pore size distributions were never measured, and the sintering temperatures, up to 1073K, may have caused changes in the pore size distribution of the alumina support. In extreme cases, the internal mass transfer limitations which were pronounced negligible for the DRR kinetic runs could be significant. If mass transfer limitations are coupled with the strong negative order kinetics, it is uncertain exactly what the measured global rate represents. Hence, using dispersion as the independent variable in testing for structural sensitivity will only result in qualitative findings.



Furthermore, the reported dispersions were determined by the dynamic pulse method, and this method tends to underestimate the platinum dispersion. Hydrogen adsorption uptake from which the dispersion is calculated are lower for the dynamic pulse method than for the static method (7.10). Therefore, the dispersion of the catalysts having a reported dispersion of 0.115 and 0.12 may be sufficiently high so that the majority of the crystallites in these catalysts are small enough to display structural sensitivity.

As a further test on the consistency of the data, an attempt was made to collapse all the results pictured in Figure 7.2 into a single line. The data for each series was analyzed, and an activation energy was determined for each series. A temperature normalized rate constant,  $k''$ , was calculated for each catalyst sample,

$$k''_{ij} = \frac{k_{ij}}{e^{-\bar{E}/RT_i}} \quad -(7.3)$$

where

$k''_{ij}$  = temperature normalized rate constant at the  
ith temperature for the jth catalyst

$k_{ij}$  = rate constant at ith temperature for the jth catalyst

$\bar{E}$  = average apparent activation energy for all the  
sintered catalysts



The average activation energy obtained from fitting the rate constants to an Arrhenius expression using the Marquardt algorithm was 54.745 kJ/mol. A plot of the temperature normalized rate constant,  $k''$  versus dispersion is shown in Figure 7.3; the data is tabulated in Appendix D, Table D16. If the reaction were facile, the points in Figure 7.3 would all fall on a single straight line through the origin, the slope of which would be the proportionality constant between dispersion and catalyst activity. The data pictured in Figure 7.3 are too scattered to support a contention that the reaction is facile, however neither do they lend themselves to a single concise correlation between reaction rate and dispersion.

The average activation energy obtained from the 0.5% Pt/Al<sub>2</sub>O<sub>3</sub> catalyst (54.745 kJ/mol) was only half the value of the activation energy determined for the 0.3% Pt/Al<sub>2</sub>O<sub>3</sub> catalyst (114.2 kJ/mol). Also, although there are some exceptions, the apparent activation energies listed in Table D16 increase as the dispersion increases from 26.752 kJ/mol to 86.794 kJ/mol. Part of the reason for the differences in the activation energies must lie in the fact that some of the rate constants used in the estimation are based on very few points. Because of experimental difficulties, many points had to be discarded. In some cases (Series V, 425 K in Table 7.1) all of the data at a particular temperature were discarded. For Series V, O, P, and Q, the activation energy was calculated from only two temperature - rate constant pairs. In this light, it is not surprising that temperature normalization



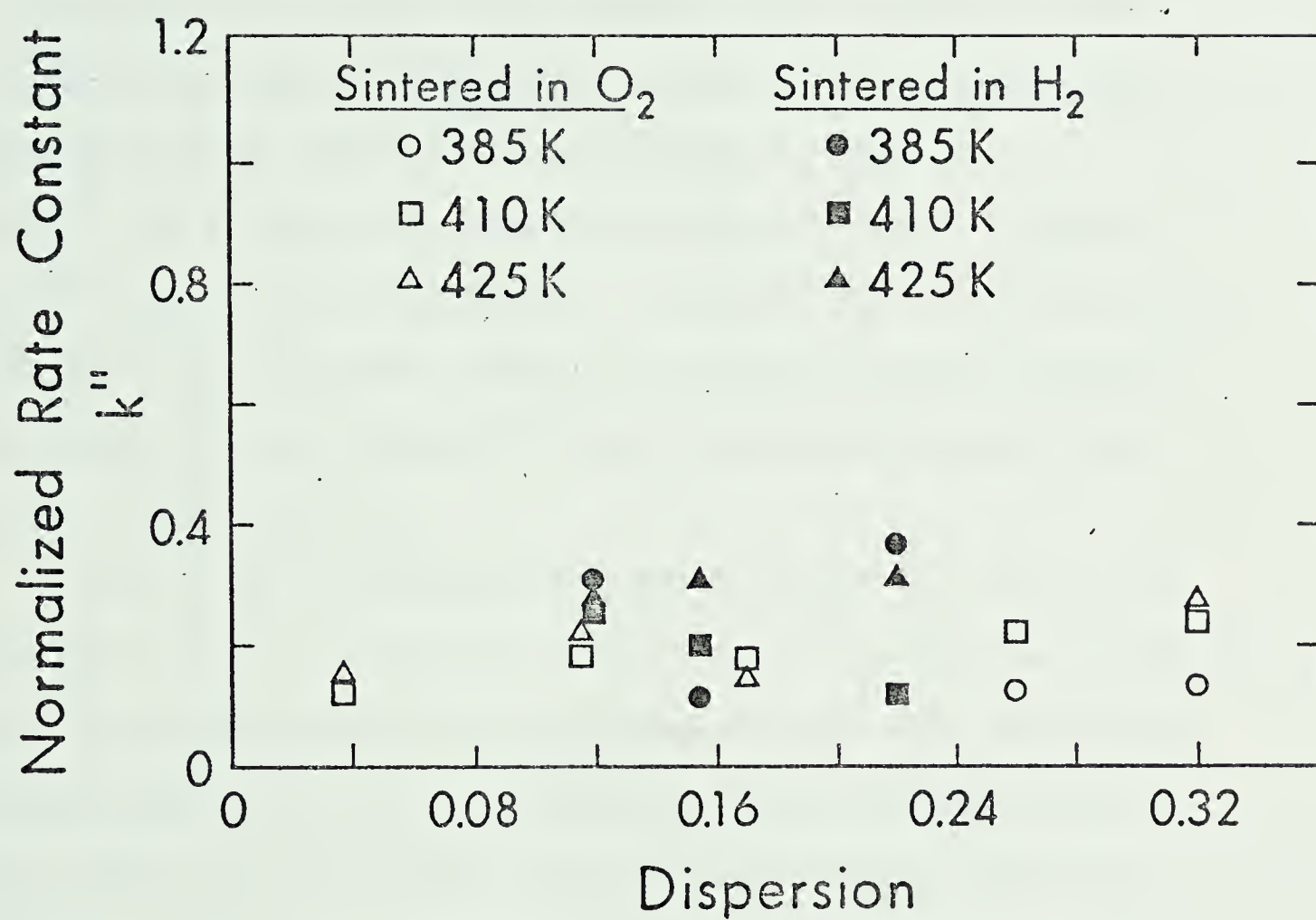


Figure 7.3 : Temperature normalized rate constants as a function of dispersion.





using a single activation energy failed to produce a single line in Figure 7.3.

Finally, the possibility that the sintering atmosphere had a bearing on the results cannot be discounted. Carberry (7.11) cites a study by Taylor et. al. (7.12) on supported nickel catalysts in which a catalyst sintered in air (oxidizing atmosphere) produced a reaction less demanding than a reaction over a catalyst reduced in hydrogen (reducing atmosphere). As some of the catalyst samples were sintered in oxygen, and some in hydrogen, there may be some differences between the catalysts sintered in oxygen and the ones sintered in hydrogen. In Figure 7.2, on the 410 K curve, the dispersion normalized rates for the hydrogen sintered catalysts at dispersions of 0.120 and 0.22 seem relatively higher than the oxygen sintered catalysts.

One of the postulations forwarded in Chapter 6 to explain the instabilities and oscillations in this reaction included the possibility that the platinum crystallites supported on the alumina surface may change during a run. It is unlikely, even during the high conversion runs, that the pellet temperatures would approach the temperatures (550°C - 800°C) encountered during the sintering treatments of the catalysts. Because of this, it is improbable that any "large" scale changes in the dispersion as a result of inter-crystallite movement of the platinum occurred. The experimental results and difficulties can be attributed to changes in the platinum crystallites however. As was mentioned in Chapter 2, the heats of adsorption of



oxygen on platinum are markedly influenced by the surface of the platinum. If "small" scale changes occur on the surfaces of the crystallites, (referred to as the surface roughening effect), the oxygen adsorption could be affected. This surface roughening is an intra-particle change, and is sometimes viewed as either the spreading of the particles along the surface of the support or the creation of "steps" on the surface of the crystallite. In either event, an increase in the measured dispersion results. During the dispersion runs, it was noticed that very long times were occasionally required for steady-state in the product composition, and this was attributed to a restructuring of the platinum crystallites. It is possible that changes in the surface structure of the crystallites, which occur slowly at moderate temperatures, could proceed much faster at the higher temperatures encountered during the complete conversion instability runs.

#### 7.4 CONCLUSIONS

From the dispersion series of experiments, it can be concluded that the catalytic oxidation of ethylene over the 0.5% Pt/Al<sub>2</sub>O<sub>3</sub> catalysts is not a facile reaction. Experimental difficulties, and uncertainties in the catalyst structure may have significantly affected the measurements, but there is a definite trend indicating that the rate per surface area of platinum decreases as the platinum area increases. These findings were in agreement with the oxygen adsorption behaviour observed by Dalla Betta and Boudart (7.4) and



Wilson and Hall (7.5). While the results do not confirm any instability model, the postulation that the instabilities arise due to changes in the platinum surface and dispersion is not discredited.



## CHAPTER 8

### SOME COMMENTS ON THE CATALYTIC OXIDATION OF ETHYLENE

In the previous chapters, various aspects of the oxidation of ethylene over  $\text{Pt}/\text{Al}_2\text{O}_3$  surface coated catalysts were discussed. In Chapter 4, the kinetics of the reaction in low and excess oxygen were studied. A global rate equation was determined from the kinetic measurements. The global equation is shown in Appendix A to be a true measure of the intrinsic chemical reaction rate. In Chapter 6, instabilities and oscillations in the reaction were described and in Chapter 7, the demanding nature of the reaction was investigated. Despite the comment made before that manipulation of kinetic data will not yield a mechanism, the author is compelled to speculate on the mechanism. Hopefully, these speculations will lend some cohesiveness to the aspects of the reaction discussed in the previous four chapters.

#### 8.1 Possible Mechanisms for Ethylene Oxidation

In Chapter 4, some adsorption studies with ethylene and oxygen were performed on the 0.3% Pt catalyst. From these experiments, it was determined that ethylene will displace oxygen from the catalyst surface and that the reverse process, oxygen displacing ethylene, does not occur. This indicates that the ethylene is more strongly bound to the surface, and hence has a higher heat of adsorption than does oxygen. These findings contradict some of the published findings mentioned in Chapter 2, Table 2.2. The adsorption experiments were done at high temperatures (366 K - 370 K) in a flow system. Similar experiments



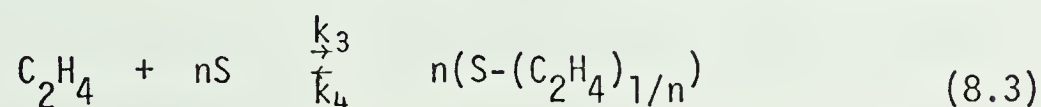
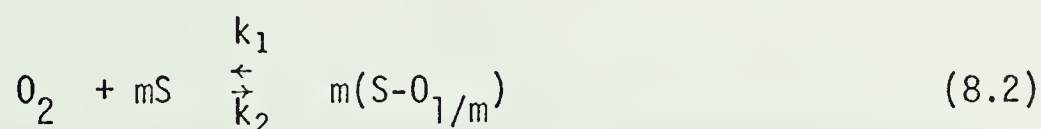


on the competitive adsorption of ethylene and oxygen on the 0.3% Pt/Al<sub>2</sub>O<sub>3</sub> catalyst were also performed by Hasegawa (8.1). His studies were done in a static system at lower temperatures. At conditions under which the reaction between oxygen and ethylene did not occur, he also found that ethylene displaced oxygen from the catalyst surface while oxygen never displaced ethylene.

There are a number of plausible mechanisms which can be shown, in some limiting form, to result in a rate equation identical to the empirical rate equation developed in Chapter 4, i.e.,

$$-r = \frac{k [O_2]}{[C_2H_4]} \quad (8.1)$$

Equations for oxygen and ethylene adsorption on platinum surface sites, S, can be written as



where  $m$  = the number of sites for oxygen adsorption

$n$  = the number of sites for ethylene adsorption

As well, there may be many different surface reactions, the number of which is limited by imagination only. If the adsorption follows Langmuir isotherms, then a variety of mechanisms and attendant assumptions



will result in the required equation. Three possible mechanisms will be mentioned here.

In the first mechanism, the surface reaction between adsorbed ethylene or adsorbed ethylene fragments and adsorbed oxygen is the rate controlling step.. If,

$$1 + K_{O_2} [O_2] \ll K_{C_2H_4} [C_2H_4]$$

where

$$K_{O_2} = k_1/k_2$$

$$K_{C_2H_4} = k_3/k_4$$

then the resulting rate equation will have the same form as Equation (8.1). However, in order for this to occur, both the ethylene and the oxygen must be non-dissociatively adsorbed onto a single site, i.e.,

$$m = n = 1$$

While this mechanism does result in the desired equation, the adsorption of oxygen onto a single site is unlikely, and this mechanism is not favoured.

The second mechanism also requires that the surface reaction be the rate controlling step. In this case however, the ethylene and oxygen must both be dissociatively adsorbed on two sites. Then, if,

$$1 + (K_{O_2} [O_2])^{1/2} \ll (K_{C_2H_4} [C_2H_4])^{1/2}$$



an equation of the form of Equation (8.1) is obtained. In this case,

$$m = n = 2 .$$

The third possible mechanism requires that the rate of oxygen adsorption be rate controlling. In this case, the oxygen and the ethylene must each dissociatively adsorb onto two sites. If this occurs, and if

$$(K_{C_2H_4} [C_2H_4])^{1/2} \gg 1$$

then Equation (8.1) is again obtained. This final mechanism is the most reasonable of the three mechanisms. Oxygen adsorption on platinum is an activated process, so that there is an energy barrier. Since the adsorption studies indicated that ethylene displaces oxygen from the surface, the speculation that the concentration of oxygen covered sites is very low is reasonable.

The three mechanisms presented here are, by no means, the only three mechanisms and sets of assumptions which could result in Equation (8.1). The purpose of the discussion here is simply to show that there is at least one plausible mechanism which would result in the observed rate function. It should be noted that the requirement that

$$1 + (K_{O_2} [O_2])^{1/2} \ll (K_{C_2H_4} [C_2H_4])^{1/2}$$

is common to both the first and second mechanisms and is implied



in the third mechanism. Hence, a kinetic study could not be used to differentiate between the three mechanisms. Adsorption and adsorption / reaction studies coupled with techniques that allow the determination of surface species are necessary to elucidate the mechanism.

## 8.2 Variations in Catalytic Activity

Speculating on the mechanism for the reaction is somewhat unrewarding, but speculating on the reasons for the observed variations in catalytic activity is more promising. In Appendix E, the reproducibility of the data is discussed, and it was shown that inaccuracies in the measurements were not likely sources for the observed irreproducibilities. An explanation which can be regarded favourably is that the variations in catalytic activity were caused by changes in the surfaces of the crystallites, sometimes called surface roughening. The nature of the platinum surface can be very important. In a recent article, Flytzani-Stephanopoulos et al. (8.2) state:

"It is clear, however, that morphology changes may be as important as surface chemical composition and total surface area in determining the behaviour of catalysts."

This surface roughening is usually a function of the temperature and partial pressures of the reacting gases. Flytzani-Stephanopoulos et al. also found evidence that the surface morphology of single platinum spheres (  $\leq 0.06$  cm diameter) changed during the reaction of carbon monoxide and oxygen over the platinum spheres.

Changes in surface morphology during the course of the





reaction is a handy scapegoat on which to hang the irreproducibilities in the kinetic data. The long time periods required for attaining steady state for some of the sintered catalysts do seem to indicate that some surface restructuring was occurring.

In Chapter 7, results of specific rates as a function of metal dispersion were presented. This study was an attempt to determine whether the oxidation of ethylene on platinum was facile or demanding. The use of catalyst with varying dispersions for the determination of whether a reaction is facile or demanding rests on the premise that the surface morphology (types of surface sites) is a function of crystallite size (i.e. dispersion). But, if the surface morphology of the largest crystals in supported metals (0.06cm Pt crystals are larger than any supported crystallites) is governed by the reaction conditions, (8.2) then the determination of structure sensitivity by comparing normalized rates as a function of dispersion is not a valid procedure.

In Chapter 6, it was postulated that changes in surface morphology may also be the cause of the instabilities observed in both the DRR and the IBR. This idea was also recently expressed by Krylov (8.3) who studied hydrocarbon oxidation on cobalt-containing spinels. In explaining oscillations in the reaction, he said:

"One explanation of these phenomena is the slow generation of some structure on the surface, which then undergoes rapid transformation into an active structure which allows rapid catalytic reaction and a new period of transformation.".

The idea that oscillations in the oxidation of ethylene over platinum can result from changes in surface morphology of the individual



platinum crystallites is not without support.

In this Chapter, some of the features common to the results presented in the four previous chapters were discussed. A simple mechanism based on oxygen adsorption being the rate determining step was presented as the possible mechanism of the reaction. The role of surface morphology changes in the data reproducibility, the dispersion studies and the instability studies was discussed. It was shown that using dispersion as the criteria for examining the structure sensitivity of a reaction may not be valid for situations where the surface changes during the reaction. While the equipment limitations prevent the pursuit of some of the speculations discussed here, the speculations provide a base from which to recommend further investigations in the final chapter.



## CHAPTER 9

### CONCLUSIONS AND RECOMMENDATIONS

#### 9.1 Conclusions

1. It is concluded that changes in the platinum crystallites (changes such as restructuring, surface roughening, or crystallite spreading) occurred during the oxidation of ethylene over supported platinum catalysts. This conclusion is supported by the following observations:

(i) Thermal pretreatments in air resulted in changes in catalytic activity.

(ii) Long time periods were required to attain steady state for some catalysts that had not been thermally pretreated.

and (iii) Increases in catalytic activity occurred after some complete conversion runs and after some runs in which high transient temperatures occurred.

It is believed that changes in the platinum surface were responsible for the large variation in catalytic activity and the oscillatory behaviour.

2. Although the catalytic activity of the catalysts varied, the empirically determined rate function, i.e.,

$$-r = k[O_2]/[C_2H_4]$$

is believed to reflect the correct functional dependence of the rate of ethylene oxidation on ethylene and oxygen concentrations



over supported platinum catalysts. The temperature dependence of the rate constant was adequately described by the relation

$$k = 4.12 \times 10^6 \exp(-114200/RT) \text{ (mol/s-g cat).}$$

3. Based on the empirical rate function and the adsorption measurements, it is concluded that the most likely mechanism for ethylene oxidation involves dissociative adsorption of ethylene and oxygen with the adsorption of oxygen being the rate controlling step.

4. The adsorption measurements support the contention that ethylene adsorbed more strongly (higher heat of adsorption) than oxygen on the supported platinum catalyst.

5. The specific rate (rate per unit of platinum area) was found to be a function of dispersion, i.e., higher dispersions resulted in lower specific activity.

6. The results of the integral bed reactor studies (experimental and modelling) clearly showed that for an integral bed reactor with constant wall temperatures and a highly exothermic reaction, reliable analysis of data is not possible in the absence of accurate values of the wall heat transfer coefficient.

## 9.2 Recommendations

1. Kinetic studies with the aim of determining a more accurate intrinsic rate function should be abandoned

2. Detailed studies of the effects of pretreatment





on the catalytic activity should be carried out.

3. The range of conditions at which cyclical instabilities occur should be determined. This would require a method for continuous analysis of the product stream.

4. Adsorption and adsorption/reaction studies in a static apparatus should be carried out to elucidate the reaction mechanism. If possible, these studies should be coupled with in situ infra red measurements of adsorbed species.

5. Direct observations of platinum crystallites under reaction conditions would be very valuable in determining the nature of the changes occurring in the Pt crystallites. Controlled atmosphere electron microscopy (CAEM) studies could be used to carry out these studies.



## NOMENCLATURE

### N.1 Latin Letters

Symbol	Meaning	Units
$A, a$	Surface area, cross sectional area	$\text{cm}^2$
$A_i$	Area under gas chromatograph peak	
$a_i$	Stoichiometric coefficient	
$A_0$	Pre-exponential factor	$\text{mol/s-g cat}$
$Bi$	Biot number	
$C$	Concentration	$\text{mol/m}^3$
$C_p$	Specific heat	$\text{cal/g-K}$
$D$	Molecular diffusivity	$\text{cm}^2/\text{s}$
$D^*$	Effective diffusivity in catalyst pellets	$\text{cm}^2/\text{s}$
$d$	Diameter of reactor, pellets	$\text{cm}$
$Da$	Damköhler number	
$E$	Activation energy	$\text{kJ/mol}$
$\bar{E}$	Average activation energy for sintered catalysts	$\text{kJ/mol}$
$E_c$	Carbon mass balance error	%
$F$	Molar flow rate	$\text{mol/s}$
$G$	Mass flow rate per unit cross sectional area	$\text{mol/s-cm}^2$
$h$	External heat transfer coefficient	$\text{J/K-s-cm}^2$
$h_p$	Pellet heat transfer coefficient	$\text{J/K-s-cm}^2$
$h_w$	Inside reactor wall heat transfer coefficient	$\text{J/k-s-cm}^2$



Symbol	Meaning	Units
$\Delta H_r$	Heat of reaction	J/mol
$j_D$	j factor for mass transfer	
$j_H$	j factor for heat transfer	
$K$	Thermal conductivity of bulk gas	J-cm/K-s-cm <sup>2</sup>
$k$	Kinetic rate constant	mol/s-g cat
$K_1, K_2$	Adsorption rate constants in Equation (8.2)	
$K_3, K_4$	Adsorption rate constants in Equation (8.3)	
$k'$	Dispersion normalized rate constant	mol/s-g cat
$k''$	Temperature normalized rate constant	mol/s-g cat
$k_m$	External mass transfer coefficient	cm/s
$K_{O_2}$	Oxygen adsorption equilibrium constant	
$K_{C_2H_4}$	Ethylene adsorption equilibrium constant	
$K^*$	Effective thermal conductivity in catalyst pellets	J-cm/K-s-cm <sup>2</sup>
$L$	Reactor length	cm
$Le$	Lewis number	
$M$	Molecular weight	g/mol
$m$	Number of sites for oxygen adsorption	
$\dot{m}$	Mass flow rate	g/s
$n$	Exponent in Langmuir-Hinshelwood rate equation	
$n$	Number of sites for ethylene adsorption	



Symbol	Meaning	Units
P	Reactor pressure	kPa
Pr	Prandtl number	
R	Reactor tube radius	cm
-r	Rate of ethylene disappearance	mol/s-g cat
$r_p$	Pore radius in catalyst pellets	cm
Re	Reynolds number	
RF	Response factor for G.C. analysis	
S	Catalyst surface sites	
T	Temperature	K
t	Time	s,min
W	Catalyst mass	g
x	Mole fraction, mole percent	
	Distance in axial direction	cm
X	Fractional conversion	
Y,y	Mole fraction, mole percent	

## N.2 Subscripts

Symbol	Meaning
A	Axial
B	Bulk flow
$C_2H_4$	Based on ethylene
$CO_2$	Based on carbon dioxide





Symbol	Meaning
H	Heat transfer related
i	Component i, Inlet
j	Component j
K	For Knudsen diffusion case
m	Mass transfer related
O <sub>2</sub>	Based on Oxygen
P	Product
p	Pellet
R	Radial
T	Total
w	At the reactor wall

### N.3 Greek Letters

Symbol	Meaning	Units
$\gamma$	Catalyst bed void fraction	
$\Delta$	Difference operator	
$\epsilon$	Void fraction of the catalyst pellets	
$\lambda$	Mean free path	cm
$\mu$	Viscosity	g/cm-s
$\rho$	Density	g/cm <sup>3</sup>
$\sigma$	Constriction factor	
$\tau$	Tortuosity factor	
$\phi$	Thiele parameter	



#### N.4 Abbreviations

E-R	Eley - Rideal
DRR	Differential recycle reactor
IBR	Integral bed reactor
L-H	Langmuir - Hinshelwood
SCCM	Standard cubic centimeters per minute



## REFERENCES

- 1.1 Dulieu, C.A., Evans, W.D.J., Laraby, R.J., Verral, A.M., Wilkins, A.J.J., and Povey, J.H., Paper 77029 presented at the IAECE meeting, Detroit, Michigan, March 1977.
- 1.2 Flynn, P.C., Ph.D. Thesis, The University of Alberta, 1974.
- 1.3 Wei, J., Advan. Catal. 24, 57 (1975).
- 2.1 Langmuir, I., Trans. Farad. Soc. 17, 621 (1922).
- 2.2 Heyne, H. and Tompkins, F.C., Proc. Roy. Soc. A 292, 460 (1966).
- 2.3 Tretyakov, I.I., Sklyarov, A.V., and Shub, B.R., Kinetics and Catalysis 11, 133 (1970).
- 2.4 Patterson, W.R. and Kemball, C., J. Catal. 2, 465 (1963).
- 2.5 Tajbl, D.G., Simons, J.B., and Carberry, J.J., IEC Fund. 5 (2) 171 (1966).
- 2.6 Voltz, S.E., Morgan, C.R., Liederman, D., and Jacob, S.M., IEC Prod. Res. & Dev. 12, 294 (1973)
- 2.7 Plichta, R., Ph.D. Thesis, The University of Illinois, 1976.
- 2.8 Bonzel, H.P. and Ku, R., Surface Sci. 33, 91 (1972).
- 2.9 Dauchot, J.P. and Van Cakenberghe, J., Nature Phys. Sci. 246, (Nov.26), 61 (1973).
- 2.10 Hori, G.K. and Schmidt, L.D., J. Catal. 38, 335 (1975).
- 2.11 McCarthy, E., Zahradnik, J., Kuczynski, G.C., and Carberry, J.J., J. Catal. 39, 29 (1975).
- 2.12 Boudart, M., Aldag, A.W., Benson, J.E., Dougharty, N.A., and Harkins, C.G., J. Catal. 6, 92 (1966).
- 2.13 Mathieu, M.V., private communication.
- 2.14 Hugo, P. and Jakubith, M., Chem. Ing.-Tech. 44, 383 (1972).
- 2.15 Sheintuch, M.S., Plichta, R., and Schmitz, R.A., Paper 109b presented at the 69th AIChE meeting, Chicago, Ill. (1976).



- 2.16 Beusch, H., Fieguth, P., and Wilke, E., "Advances in Chemistry Series 109", 615 (1970).
- 2.17 Wei, J., "Chemical Reaction Engineering Reviews", (H.M. Hulburt, ed.). Adv. Chem. Series 148, p. 1, Washington, 1975.
- 2.18 Schmitz, R.A., *ibid.*, p. 156.
- 2.19 Reyerson, L.H. and Swearingen, L.E., J. Amer. Chem. Soc. 50, 2872 (1928).
- 2.20 Lenher, S., J. Amer. Chem. Soc. 53, 3737 (1931).
- 2.21 Bone, W.A., Haffner, A.E., and Rance, H.F., Proc. Roy. Soc. A 143, 16 (1934).
- 2.22 Twigg, G.H., Proc. Roy
- 2.23 Huang, T., Martinez, E., Carberry, J.J., and Varma, A., Paper 91f presented at the 69th AIChE meeting, Chicago, Ill., (1976).
- 2.24 Beeck, O., Rev. Mod. Phys. 17, 61 (1945).
- 2.25 Beeck, O., Smith, A.E. and Wheeler, A., Proc. Roy. Soc. A 177, 62 (1940).
- 2.26 Twigg, G.H., Discuss. Farad. Soc. 8, 152 (1950).
- 2.27 Jenkins, G.I. and Rideal, E., J. Chem. Soc. 2490 (1955).
- 2.28 Wojtowicz, J. and Conway, B.E., J. Chem. Phys. 52, 1407 (1970).
- 2.29 Wojtowicz, J., Marincic, N., and Conway, B.E., J. Chem. Phys. 48, 4333 (1968).
- 2.30 Wojtowicz, J., Gilroy, D., and Conway, B.E., Electrochim. Acta. 14, 1119 (1969).
- 2.31 Dmuchovsky, B., Freerks, M.C., and Zienty, F.B., J. Catal. 4, 577 (1965).





- 2.32 Kemball, C. and Patterson, W.R., Proc. Roy. Soc. A270, 219 (1962).
- 2.33 Schwartz, A, Holbrook, L.L., and Wise, H., J. Catal. 21, 199 (1971).
- 2.34 Omar, A., Djega-Mariadassou, G., Bozon-Verduraz, F., and Pannetier, G., Soc. Chim. de France, Bull. Ser. 5, 2740 (1974).
- 2.35 Germain, J.E., "Catalytic Conversion of Hydrocarbons", p 231, Academic Press, London, 1969.
- 2.36 Germain, J.E., Intra-Sci. Chem. Rep. 6, 3, 101 (1972).
- 2.37 Margolis, L. Ya., Advan. Catal. 14, 429 (1963).
- 2.38 Klimisch, R.L., and Schlatter, J.C., General Motors Research, GMR-1268 PCP-2 (1972).
- 2.39 Schlatter, J.C., Klimisch, R.L., and Taylor, K.C., Science 179, 798 (1973).
- 3.40 Hansel, J.C., Aykan, K. and Cohn, J.G., SAE paper 740247, IAECE meeting, Detroit, Michigan, 1974.
- 2.41 Haslett, R.A., *ibid.*, paper 740246.
- 2.42 Sakai, Y., Nakagawa, Y., Tange, S., and Maruyama, R., SAE paper 770297 IAECE meeting, Detroit, Michigan, 1977.
- 2.43 Laidler, K.J., "Chemical Kinetics", p 274, McGraw Hill, N.Y. , 1965.
- 2.44 Beeck, O., Discuss. Farad. Soc. 8, 118 (1950).
- 2.45 Eley, D.D., Discuss. Farad. Soc. 8, 34 (1950).
- 2.46 Pauling, L.P., "The Nature of the Chemical Bond", Chap. 3, Cornell University Press, N.Y., 1939.
- 2.47 Trapnell, B.M.W., Trans. Farad. Soc. 48, 160 (1952).
- 2.48 Bond, G.C., "Heterogeneous Catalysis: Principles and Applications", p. 21, Clarendon Press, Oxford, 1974.
- 2.49 Bond, G.C., "Catalysis by Metals", Chap. 4, Academic Press, N.Y., 1962.
- 2.50 Morgan, A.E. and Somorjai, G.A., Surface Sci. 12, 405 (1968).



- 2.51 Weber, B., Fusy, J., and Cassuto, A., J. Chim. Phys. 66, 708 (1969).
- 2.52 Weinberg, W.H., Lambert, R.M., Comrie, C.M., and Linnett, J.W., Surface Sci. 30, 299 (1972).
- 2.53 Bonzel, H.P., and Ku, R., Surface Sci. 40, 85 (1973).
- 2.54 Nieuwenhuys, B.E., Hagen, D.I., Rovida, G., and Somorjai, G.A., Surface Sci. 59, 155 (1976).
- 2.55 Lang, B., Joyner, R.W., and Somorjai, G.A., Surface Sci. 30, 454 (1972).
- 2.56 Pearce, H.A., and Sheppard, N., Surface Sci. 59, 205 (1976).
- 2.57 Hagen, T.S., and Handel, K.D., "Proc. Int. Symp. Chem. React. Eng. 3rd", p 395, Evanston, Ill., 1974.
- 2.58 Carrière, B., Lègare, P., and Maire, G., J. Chim. Phys. 71 17 (1974).
- 2.59 Hlaváček, V., and Votruba, J., "Proc. Int. Symp. Chem React. Eng. 3rd", p 545, Evanston, Ill., 1974.
- 2.60 Perlmutter, D.D., "Stability of Chemical Reactors", p 545, Prentice Hall, Englewood Cliffs, N.J., 1972.
- 2.61 Yang, T.-C., and Weinstein, H., Advances in Chemistry Series 133, 53 (1974).
- 2.62 Nicolis, G. and Portnow, J., Chem. Rev. 73, 365 (1973).
- 2.63 Yao, Y.-F.Y., J. Catal. 33, 108 (1974).
- 3.1 Wanke, S.E., M.Sc. Thesis, The University of Alberta, 1966.
- 3.2 Fiedorow, R.M.J. and Wanke, S.E., J. Catal. 43, 34 (1976)..
- 4.1 Flynn, P.C. and Wanke, S.E., J. Catal. 34, 390 (1974).
- 4.2 Carberry, J.J., "Chemical and Catalytic Reaction Engineering", p 410, McGraw Hill, N.Y., 1976.



- 5.1 *Ibid.*, p. 125.
- 5.2 Boag, I.F., Bacon, D.W., and Downie, J., *Can. J. Chem. Eng.* 54, 107 (1976).
- 6.1 Liu, S.-L., Amundson, N.R., *IEC Fund.* 1, 200 (1962).
- 6.2 Smith, J.M., "Chemical Engineering Kinetics", p 232, McGraw Hill, N.Y., 1970.
- 6.3 Denbigh, K.G., *Chem Eng. Sci.* 8, 125 (1958).
- 6.4 Kikuchi, E., Flynn, P.C., and Wanke, S.E., *J. Catal.* 34, 132 (1974).
- 7.1 Boudart, M.,
- 7.2 Carberry, J.J., "Chemical and Catalytic Reaction Engineering", p 424, McGraw Hill, N.Y., 1976.
- 7.3 Huang, T. and Carberry, J.J., Paper 109a, presented at the 69th AIChE meeting, Chicago, Ill., November, 1976.
- 7.4 Dalla Betta, R.A., and Boudart, M., "Proc. Int. Congr. Catal. 5th", 2, pp 96 -1392 (1972).
- 7.5 Wilson, G.R. and Hall, W.K., *J. Catal.* 17, 190 (1970).
- 7.6 Van Hardeveld, R. and Hartog, F., *Surface Sci.* 15, 189 (1969).
- 7.7 Boudart, M., "Proc. Int. Congr. Catal. 6th", 1, p 1 (1976).
- 7.8 McVicker, G.B., Garten, R.L., and Baker, R.T.K., Preprints - 5th Canadian Symposium on Catalysis, Calgary, Alberta, 346, 1977.
- 7.9 Luss, D., *J. Catal.* 23, 119 (1971).
- 7.10 Flynn, P.C. and Wanke, S.E., *Can. J. Chem. Eng.* 53, 636 (1975).
- 7.11 Carberry, J.J., "Chemical and Catalytic Reaction Engineering", p 432, McGraw Hill, N.Y., 1976.
- 7.12 Taylor, W.F., Yates, D.J.C., and Sinfelt, J.H., *J. Catal.* 4, 374 (1965).



- 8.1 Hasegawa, E., Private communication.
- 8.2 Flytzani-Stephanopoulos, M., Wong, S., and Schmidt, L.D.,  
J. Catal. 49, 51 (1977).
- 8.3 Krylov, O.V., "Proc. Int. Congr. Catal. 6th", p 766, London, 1976.
  
- A.1 Carberry, J.J., "Chemical and Catalytic Reaction Engineering",  
p 96, McGraw Hill, N.Y., 1976.
- A.2 Smith, J.M., "Chemical Engineering Kinetics", 2nd ed., p 365,  
McGraw Hill, N.Y., 1970.
- A.3 "The Chemical Engineers Handbook", 4th ed., Perry, J.H., editor,  
p 3-197 , 1963.
- A.4 *Ibid.*, p. 6-46.
- A.5 *Ibid.*, p. 14-19.
- A.6 *Ibid.*, p. 3-197.
- A.7 *Ibid.*, p. 3-206.
- A.8 Keller, R., "Basic Tables in Chemistry", p 52, McGraw Hill,  
N.Y., 1967.
- A.9 Carberry, J.J., "Chemical and Catalytic Reaction Engineering",  
p 232, McGraw Hill, N.Y., 1976.
- A.10 Smith, J.M. "Chemical Engineering Kinetics", 2nd ed., pp 513-  
522, McGraw Hill, N.Y., 1970.
- A.11 Petersen, E.E., "Chemical Reaction Analysis", pp 115 - 126,  
Prentice Hall, N.J., 1965.
- A.12 Carberry, J.J., "Chemical and Catalytic Reaction Engineering",  
p 462, McGraw Hill, N.Y., 1976.





- A.13 Vanderveen, J.W., Luss, D., and Amundson, N.R., AIChEJ 14, 4, 636 (1968).
- A.14 Deans, H.A. and Lapidus, L., AIChEJ 6, 656 (1960).
- A.15 Hlavacek, V., Ind. Eng. Chem. 62, (7), 8 (1970).
- A.16 Yagi, S. and Kunii, D., AIChEJ 6, 97 (1960).
- A.17 Smith, J.M., "Chemical Engineering Kinetics", 2nd ed., p 510, McGraw Hill, N.Y., 1970.
- B.1 Dietz, W.A., J. of Gas Chromatography 5, 68 (1967).
- C.1 Schech, R.L.H., M.Sc. Thesis, The University of Alberta 1977.



## Appendix A

### Mass Balance Equations and Sample Calculations

#### A.1 Component Balances for a Differential Recycle Reactor

The component balance equations for an ideal differential recycle reactor (DRR) and an ideal continuous stirred tank reactor (CSTR) are the same. Carberry (A.1) states that for recycle ratios above about 10:1 that a recycle reactor behaves like an ideal CSTR. Since the recycle ratio used in the present study was about 20:1, the assumption that this reactor behaves like a CSTR should be valid.

A DRR (or a CSTR) is considered ideal if the fluid composition and temperature are independent of position in the reaction zone and if the properties of the exit stream are the same as the properties of the fluid inside the reactor. In an ideal DRR, the steady state component balance for a stoichiometrical simple reaction is

$$r = \frac{r_i}{a_i} = \frac{F_{i,in}}{-a_i W} X_i \quad (A.1)$$

where  $F_{i,in}$  = feed rate of reactant i [mol/s]

$X_i$  = fractional conversion

or

$$X_i = \frac{F_{i,in} - F_{i,out}}{F_{i,in}} \quad (A.2)$$

$W$  = mass of catalyst in the reactor [g]

$r$  = normalized reaction rate [mol/g of catalyst-s]

$r_i$  = rate of reaction for component i [mol/g of catalyst-s]

$a_i$  = stoichiometric coefficient of component i

( $< 0$  for reactants;  $> 0$  for products)

Alternatively, the fractional conversion can be expressed in terms of



product flow rates by substituting

$$(F_{i,in} - F_{i,out}) = (F_{p,in} - F_{p,out}) \frac{a_i}{a_p}$$

where  $F_p$  is the molar flow rate of a product compound.

For the complete oxidation of ethylene, i.e.



the total molar flow rate is constant. Therefore the mole fraction for each component in the feed and in the product streams is proportional to its molar flow rate. In this work the fractional conversions of ethylene were calculated from feed and product analyses based on ethylene and carbon dioxide mole fractions. (This also provided a quick approximate check of the overall mass balance.) The fractional conversion based on the ethylene mole fractions,  $X_1$  is given by

$$X_1 = \frac{\bar{y}_{C_2H_4,in} - \bar{y}_{C_2H_4,out}}{\bar{y}_{C_2H_4,in}} \quad (A.5)$$

and the fractional conversion of ethylene based on the carbon dioxide mole fractions,  $X_2$ , is

$$X_2 = \frac{\bar{y}_{CO_2,out} - \bar{y}_{CO_2,in}}{2\bar{y}_{C_2H_4,in}} \quad (A.6)$$

where the  $y_i$ 's are the average mole fractions of component  $i$  (here  $C_2H_4$  and  $CO_2$ ). The averages were obtained from a number (3 to 10) of repeat analyses of the feed and product streams at steady state. The molar feed rate of ethylene was calculated from the known total feed rate  $F_T$  (in standard cubic centimeters per minute - SCCM), the feed composition, and the assumption of ideal gas behaviour, i.e.



$$F_{C_2H_4, in} = \frac{F_T \bar{y}_{C_2H_4, in}}{22414 * 60} \left[ \frac{mol}{s} \right] \quad (A.7)$$

The normalized rates of reaction were then computed using Equation (A.1).

The concentrations at which the reaction occurred are required for fitting the rate equation. They were computed from the product analyses using the ideal gas law, i.e.,

$$C_i = \frac{P_T \bar{y}_{i, out}}{RT} \quad (A.8)$$

where  $C_i$  is the concentration of the  $i$ th component  $[mol/cm^3]$  and

$P_T$  is the pressure in the reactor  $[kPa]$

## A.2 Sample Calculation for DRR

The results of Run M54 will be used for the sample calculation.

The particulars of the run are given in Table A.1.

Table A.1

Data for Run M54

---

$T$ = Temperature	472 K
$P_T$ = Pressure in reactor	145 kPa
$W$ = Weight of catalyst	4.73 g
Flow rate of stream A ( $N_2 + C_2H_4$ )	= 500 sccm
Flow rate of stream B ( $N_2 + O_2$ )	= 108 sccm
$F_T$ = Total feed rate (A + B)	= 608 sccm
$\bar{y}_{C_2H_4, in}$	= 0.017737
$\bar{y}_{C_2H_4, out}$	= 0.008825
$\bar{y}_{CO_2, in}$	= 0.000
$\bar{y}_{CO_2, out}$	= 0.017232
$\bar{y}_{O_2, out}$	= 0.011070

---





### Calculations

From Equation (A.5)

$$x_1 = \frac{0.017737 - 0.008825}{0.017737} = 0.50245$$

From Equation (A.6)

$$x_2 = \frac{0.017232 - 0.000}{2 * 0.017737} = 0.48576$$

From Equation (A.7)

$$F_{C_2H_4, in} = \frac{608 * 0.017737}{22414 * 60} = 8.016 * 10^{-6} \left[ \frac{mol}{s} \right]$$

So, from (A.1), the normalized rate based on ethylene depletion is

$$r_1 = \frac{8.016 * 10^{-6} * 0.50245}{-(-1) * 4.73} = 8.52 * 10^{-7} \left[ \frac{mol}{gcat-s} \right]$$

and based on carbon dioxide production

$$r_2 = \frac{8.016 * 10^{-6} * 0.48576}{-(-1) * 4.73} = 8.23 * 10^{-7} \left[ \frac{mol}{gcat-s} \right]$$

The concentrations at the reacting conditions from Equation (A.8) are

$$C_{C_2H_4} = \frac{145 * 10^3 * 0.008825 * 10^{-6}}{8.31434 * 472} = 3.26 * 10^{-7} \left[ \frac{mol}{cm^3} \right]$$

Similarly,

$$C_{O_2} = 4.08 * 10^{-7} [mol/cm^3]$$

### A.3 Carbon Balance

An overall carbon balance on the reactor inlet and exit was determined as a check on the consistency of the data. The total number of gram-atoms of carbon in the feed stream was calculated from the total feed rate, the mole fractions and the ideal gas law, i.e.



$$G_{C,in} = \frac{(b_1 \bar{y}_{C_2H_4,in} + b_2 \bar{y}_{CO_2,in}) * F_T}{22414} \left[ \frac{\text{g-atoms}}{\text{min}} \right] \quad (\text{A.9})$$

Similarly, the number of gram atoms of carbon in the exit stream is

$$G_{C,out} = \frac{(b_1 \bar{y}_{C_2H_4,out} + b_2 \bar{y}_{CO_2,out}) * F_T}{22414} \left[ \frac{\text{g-atoms}}{\text{min}} \right] \quad (\text{A.10})$$

where  $b_1$  = number of gram atoms of carbon per mole of ethylene - (2)

$b_2$  = number of gram atoms of carbon per mole of carbon dioxide - (1)

The mass balance error was then expressed as a percent of the inlet value, i.e.

$$E_C = \frac{G_{C,in} - G_{C,out}}{G_{C,in}} * 100\%$$

For Run M54,

$$G_{C,in} = \frac{(2 * 0.017737 + 0.000) * 608}{22414} = 9.623 * 10^{-4} \frac{\text{g-atom}}{\text{s}}$$

$$G_{C,out} = \frac{(2 * 0.008825 + 0.017232) * 608}{22414} = 9.462 * 10^{-4} \frac{\text{g-atom}}{\text{s}}$$

and

$$E_C = \frac{9.623 * 10^{-4} - 9.462 * 10^{-4}}{9.623 * 10^{-4}} * 100\% = 1.66\%$$

The rate and carbon balance equations were calculated with the computer program KARIN located in the Data Book (see Appendix E).

#### A.4 Mass and Energy Transfer Limitations

In order to develop an intrinsic rate equation, the measured global rates must faithfully represent the rates of reaction on the



catalyst surface, and not the rates of mass and energy transfer to or from the catalyst. That is, in order to use the DRR rate data, it is essential that the reaction rates are unaffected by external and internal mass and energy transfer.

#### A.4.1 External Transfer Limitations

The external transfer limitations can be checked by calculating the heat and mass transfer coefficients between the bulk phase and the individual pellets in the reactor. The Chilton-Colburn "j factor" analogy as described by Smith (A.2) can be used to determine the two transfer coefficients.

The j factors are defined as

$$j_D = \frac{k_m \rho}{G} \left( \frac{\mu}{\rho D} \right)^{2/3}$$

or (A.11)

$$j_D = \frac{k_m \rho}{G} (S_C)^{2/3}$$

and

$$j_H = \frac{h}{C_p G} \left( \frac{C_p \mu}{K} \right)^{2/3}$$

or (A.12)

$$j_H = \frac{h}{C_p G} (P_r)^{2/3}$$

where  $k_m$  = external mass transfer coefficient  $\left[ \frac{\text{cm}}{\text{s}} \right]$

$\rho$  = density of bulk gas  $\left[ \frac{\text{g}}{\text{cm}^3} \right]$

$G$  = superficial gas velocity based on the cross-sectional area  
 $\left[ \frac{\text{g}}{\text{s-cm}^2} \right]$



$\mu$  = viscosity of the bulk gas  $[\frac{g}{cm-s}]$

$D$  = molecular diffusivity of the reacting species (ethylene)  
 $[\frac{cm^2}{s}]$

$h$  = external heat transfer coefficient  $[\frac{cal}{K-s-cm^2}]$

$C_p$  = heat capacity of the bulk gas  $[\frac{cal}{g-K}]$

$K$  = thermal conductivity of the bulk gas  $[\frac{cal}{K-cm-s-cm^2}]$

The  $j$  factors are functions of the Reynolds number,  $\frac{d_p G}{\mu}$ , (A.2). The pellet diameter,  $d_p$ , used is the diameter of a sphere having the same external area as the pellet. For  $1/8" \times 1/8"$  cylindrical pellets, the external area is

$$A_p = 2\pi R^2 + 2\pi RL \quad (A.13)$$

$$A_p = 2\pi (\frac{1}{16} \text{ in})^2 + 2\pi (\frac{1}{16} \text{ in})(\frac{1}{8} \text{ in}) = 0.074 \text{ in}^2$$

$$A_p = 0.48 \text{ cm}^2$$

A sphere with the same area has a radius of

$$R_s = (\frac{0.48 \text{ cm}^2}{4\pi})^{1/2} = 0.195 \text{ cm}$$

so

$$d_p = 0.39 \text{ cm}$$

If the gas is assumed to be entirely nitrogen, then at  $100^\circ\text{C}$ , the viscosity,  $\mu$ , is 0.021 cp or  $2.1 \times 10^{-4} \frac{g}{cm-s}$ , (A.3).

The mass velocity based on the cross-sectional area is

$$G = \frac{\dot{m}}{A} \quad (A.14)$$

The overall flow rate,  $F_T$ , was around 550 SCCM for most of the





runs. The recycle ratio was about 20:1, however a conservative estimate of 15:1 will be used here. The mass recycle rate,  $\dot{m}$ , on which the Reynolds number is based, is

$$\dot{m} = 550 \text{ SCCM} * \frac{15}{1} * \frac{1 \text{ gmol}}{22414 \text{ SCC}} * \frac{30 \text{ g}}{\text{gmole}} * \frac{1 \text{ min}}{60 \text{ s}}$$

$$\dot{m} = 1.84 * 10^{-1} \frac{\text{g}}{\text{s}}$$

For schedule 40 stainless steel 3/4 inch pipe, the cross-sectional area is 2.148 cm<sup>2</sup> (A.4). So,

$$G = \frac{1.84 * 10^{-1} \text{ g/s}}{2.148 \text{ cm}^2} = 8.57 * 10^{-2} \frac{\text{g}}{\text{s-cm}^2}$$

and the average Reynolds number is

$$R_e = \frac{0.39 \text{ cm} * 8.57 * 10^{-2} \frac{\text{g}}{\text{s-cm}^2}}{2.1 * 10^{-4} \frac{\text{g}}{\text{cm-s}}} = 159$$

Then, from the j factor correlation, Figure A.1,

$$j_H = 0.161$$

$$j_D = 0.108$$

From Equation (A.11)

$$k_m = \frac{j_D G}{\rho} \left( \frac{\mu}{\rho D^*} \right)^{-2/3} \quad (\text{A.15})$$

Assuming that the gas is ideal, and using a typical temperature and pressure,

$$\rho = \frac{m}{V} = \frac{\rho M}{RT} = \frac{1.5 \text{ atm} * 30 \text{ g/gmole}}{82.057 \frac{\text{cm}^3\text{-atm}}{\text{gmole K}} * 373\text{K}}$$



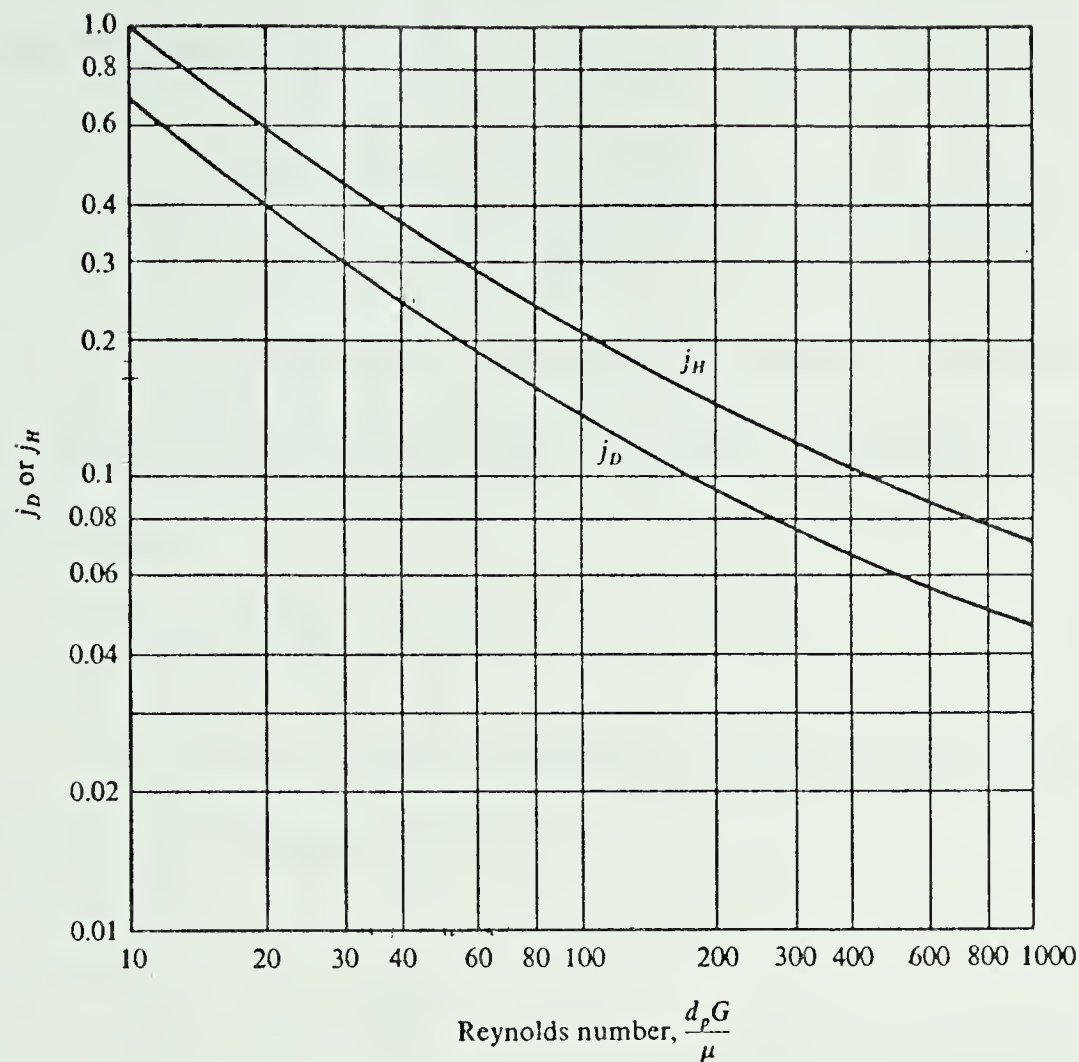


Figure A.1 : Heat and mass transfer correlations in fixed beds (Ref. A.2).

$$\rho = 1.470 \times 10^{-3} \frac{\text{g}}{\text{cm}^3}$$

The molecular diffusivity of ethylene in air can be estimated using the method of Hirschfelder, Bird, and Spotz as outlined in the Chemical Engineers' Handbook (A.5). Using this method, the molecular diffusivity,  $D$ , is  $0.1893 \frac{\text{cm}^2}{\text{s}}$ . So, the Schmidt number is

$$S_C = \frac{\mu}{\rho D} = \frac{2.1 \times 10^{-4} \frac{\text{g}}{\text{cm-s}}}{1.470 \times 10^{-3} \frac{\text{g}}{\text{cm}^3} * 0.1893 \frac{\text{cm}^2}{\text{s}}} = 0.755$$

and

$$(S_C)^{-2/3} = 1.206$$



So, substituting into (A.15)

$$k_m = \frac{0.108 * 8.57 * 10^{-2} \frac{\text{g}}{\text{s-cm}^2}}{1.47 * 10^{-3} \frac{\text{g}}{\text{cm}^3}} * 1.206 = 7.59 \frac{\text{cm}}{\text{s}}$$

If the reaction is diffusion controlled, then the measured global rates will be rates of mass transfer rather than rates of reaction, i.e.

$$r = k_m A_p (C_B - C_p) \quad (\text{A.16})$$

The concentration difference between the bulk phase and the surface of the catalyst will be

$$(C_B - C_p) = \frac{r}{k_m A_p} \quad (\text{A.17})$$

The maximum concentration difference will occur at the maximum rates. The rate\* calculated for Run M54 in Section A.2 was one of the higher rates and that value is used here.

$$(C_B - C_p) = \frac{8.52 * 10^{-7} \frac{\text{gmoles}}{\text{sec g cat}} * \frac{4.73 \text{ g cat}}{100 \text{ pellets}}}{7.59 \frac{\text{cm}}{\text{s}} * 0.48 \text{ cm}^2}$$

$$(C_B - C_p) = 1.10 * 10^{-8} \frac{\text{gmoles}}{\text{cm}^3}$$

If the worst case is considered, the lowest ethylene mole fraction was about 0.005, the lowest pressure about 1 atm, and the highest temperature was about 200°C. Then, using Equation (A.8)

---

\* The value of the rate used here is the value based on the ethylene conversion, which is slightly higher than the value based on CO<sub>2</sub> production. The value of the rate appearing in Table D2 and the value used for the curve fitting, was the average reaction rate. Since this is a "worst-case" analysis, the higher rate was chosen here.



$$C_{C_2H_4, \text{worst case}} = 1.29 * 10^{-7} \frac{\text{gmol}}{\text{cm}^3} \quad (\text{A.18})$$

Comparing this with the estimation of the concentration difference of  $1.10 * 10^{-8} \frac{\text{mol}}{\text{cm}^3}$ , the bulk concentration is only about 8.5% higher than the surface concentration. Note, however, that this represents the worst case, the highest rate coupled with the lowest ethylene concentration at the highest temperature. Under conditions more typical of the kinetic runs, the difference was usually less than 5% which is close to the uncertainty in the concentration measurements.

For example, more typical ethylene concentrations are about 1%, the temperature are generally below 400K and the rates are about  $2 * 10^{-7} \text{ mol/s-g-cat}$ . Using these values, the bulk concentration from (A.8) is  $3.05 * 10^{-7} \text{ mol/cm}^3$  and the concentration difference from (A.17)  $5.50 * 10^{-9} \text{ mol/cm}^3$ . Here the difference between the bulk concentration and the pellet concentration is only 1.8%. For the majority of the runs in the differential recycle reactor, the reaction is in the kinetically limited region. However, at particularly high temperatures and low ethylene concentrations, diffusional limitations may well be present.

The external heat transfer limitations may be determined by estimating the heat transfer coefficient from Equation (A.12), i.e.,

$$h = \frac{j_H C_p G}{(P_r)^{2/3}} \quad (\text{A.19})$$

For air at 100°C, the heat capacity is  $0.25 \frac{\text{cal}}{\text{gK}}$  (A.7) and the thermal conductivity is  $0.757 * 10^{-4} \frac{\text{cal}}{\text{K cm s cm}^2}$  (A.8). The heat of combustion of ethylene at 100°C is  $331.6 \frac{\text{kcal}}{\text{mol}}$  (A.8).





So,

$$(P_r)^{2/3} = \left( \frac{C_p \mu}{k} \right)^{2/3} = \left[ \frac{0.25 \frac{\text{cal}}{\text{g-K}} * 2.1 * 10^{-4} \frac{\text{g}}{\text{cm}^2}}{0.757 * 10^{-4} \frac{\text{cal}}{\text{K-s-cm}}} \right]^{2/3}$$

$$= (0.6935)^{2/3} = 0.784$$

and

$$h = \frac{0.161 * 0.25 \frac{\text{cal}}{\text{g-K}} * 8.57 * 10^{-2} \frac{\text{g}}{\text{s-cm}^2}}{0.784} = 4.39 * 10^{-3} \frac{\text{cal}}{\text{K-s-cm}^2}$$

At steady state, the rate of heat produced via the exothermic reaction must be equal to the heat removed from the pellet via conduction, convection, and radiation. As a 'worst-case' analysis, it may be assumed that the heat is removed by convection alone. (This is fairly close to the actual case in fact.) Then, the maximum temperature difference can be calculated using the previously determined values of the rate of reaction and the heat transfer coefficient, i.e.

$$r(-\Delta H) = h A_m (T_p - T_B) \quad (\text{A.20})$$

or

$$T_p - T_B = \frac{-r(-\Delta H)}{h A_m} \quad (\text{A.21})$$

So,

$$T_p - T_B = \frac{8.52 * 10^{-7} \frac{\text{mol}}{\text{s-g cat}} * \frac{4.73 \text{ g cat}}{100 \text{ pellets}} * 331.6 * 10^3 \frac{\text{cal}}{\text{mol}}}{4.39 * 10^{-3} \frac{\text{cal}}{\text{K-s-cm}^2} * 0.48 \frac{\text{cm}^2}{\text{pellet}}}$$



or

$$T_p - T_B = 6.3K$$

The method used here is also used by Smith with the j factor analogy. His expression for the temperature difference

$$T_p - T_B = (C_B - C_p) \frac{(\Delta H)}{C_p \rho} (Le)^{2/3} \frac{j_D}{j_H}$$

should result in the same prediction. (Note however that Smith advises that the assumption of a unity Lewis number is acceptable.)

$$T_p - T_B = \frac{1.1 * 10^{-8} \frac{\text{mol}}{\text{cm}} * 331.6 * 10^3 \frac{\text{cal}}{\text{mol}}}{0.25 \frac{\text{cal}}{\text{g-K}} * 1.47 * 10^{-3} \frac{\text{g}}{\text{cm}^3}} \left( \frac{0.6935}{0.755} \right)^{2/3} * \frac{0.108}{0.161}$$

which of course results in

$$T_p - T_B = 6.3K$$

As these calculations are for 'worst-case' conditions, the actual temperature difference in most runs is undoubtedly less than these estimates. Since the reaction rates are more typically  $2 * 10^{-7} \frac{\text{mol}}{\text{s-g-cat}}$ , the temperature difference between the bulk gas and the pellet surface will likely be around 1.6K at the most. In any case, the temperature measured by the thermocouples (which may be in the bulk gas, the thermal gradient between the bulk and the surface, or actually touching the pellet surface) is probably a good indication of the temperature of the catalyst surface, the temperature at which the reaction is occurring.



### A.4.2 Internal Transfer Limitations

Given a calculated or measured external temperature gradient, Carberry (A.9) presents a method for estimating the internal temperature gradient. The calculation requires the Biot numbers for mass transfer,

$$Bi_m = \frac{k_m L}{D^*} \quad (A.22.1)$$

and the Biot number for heat transfer

$$Bi_H = \frac{hL}{K^*} \quad (A.22.2)$$

Combining (A.22.1) and (A.22.2)

$$\frac{Bi_m}{Bi_H} = \frac{k_m}{h} \frac{K^*}{D^*} \quad (A.23)$$

where  $L$  = characteristic length<sup>1</sup> of catalyst pellet [cm]

$D^*$  = effective diffusivity in the catalyst pellet [ $\frac{cm^2}{s}$ ]

$K^*$  = effective thermal conductivity of the catalyst pellet

$$\left[ \frac{\frac{cal}{K-cm}}{-s-cm^2} \right]$$

Smith (A.10) has calculated the effective thermal conductivity of alumina at about  $4 \times 10^{-4} \frac{cal}{K-s-cm}$ .

The effective diffusivity can be calculated using the method described by Peterson (A.11). He states that

$$D^* = \epsilon_p \left( \frac{\sigma}{\tau} \right) D \quad (A.24)$$

<sup>1</sup> This is often taken as the ratio of pellet volume to pellet surface area ( $V_p/A_p$ ). In this case, it is the thickness of the platinum coating, about 0.3 mm.



where  $\epsilon$  = porosity (void fraction) of the catalyst pellet

$\sigma$  = constriction factor

$\tau$  = tortuosity factor

$D$  = diffusivity  $\frac{\text{cm}^2}{\text{s}}$

The diffusivity may be either the molecular diffusivity or the Knudsen diffusivity.

The pore size distribution of the catalyst was measured using the nitrogen adsorption-condensation method and the average pore radius was found to be 5 nm. In the mixture of ethylene, oxygen, nitrogen, carbon dioxide and water at 145 kPa, and 100°C, the mean free path,  $\lambda$ , for the molecules will be between 50 nm and 80 nm. Therefore, at least,

$$\frac{\lambda}{2r_p} \geq 5 \quad (\text{A.25})$$

so that the diffusion is in the Knudsen flow region and the Knudsen diffusivity will be required for Equation (A.24).

The Knudsen diffusivity can be calculated using Equation (A.24).

$$D_K = \frac{8}{3} \frac{\epsilon_p}{S \rho_p} \sqrt{\frac{2RT}{\pi M}} \quad (\text{A.26})$$

where  $\epsilon_p$  = the porosity of the pellet (0.47)

$S$  = total (internal and external) surface area of the catalyst pellets per unit mass ( $100 * 10^4 \frac{\text{cm}^2}{\text{g}}$ )

$\rho_p$  = apparent density of the pellets ( $1.88 \frac{\text{g}}{\text{cm}^3}$ )

$M$  = molecular weight of the diffusing molecule ( $\frac{30 \text{ g}}{\text{mole}}$ )

The porosity was determined from the pore size distribution, the surface area from a BET measurement and the apparent density from a measured weighing. Since both the oxygen ( $M=32$ ) and ethylene ( $M=28$ )





must reach the active sites, an average molecular weight was chosen for this calculation. So, at 400K,

$$D_K = \frac{8 * 0.47}{3 * 100 * 10^4 \frac{\text{cm}^2}{\text{g}} * 1.88 \frac{\text{g}}{\text{cm}^3}} \sqrt{\frac{2 * 8.314 * \frac{\text{kg-m}^2}{\text{s}^2 \text{ gmole-K}} 400\text{K} * \frac{10^3 \text{g}}{1 \text{kg}}}{3.1416 * 30 \frac{\text{g}}{\text{gmole}}}}$$

$$D_K = 1.771 * 10^{-2} \frac{\text{cm}^2}{\text{s}}$$

Petersen (A.11) cites values of  $\tau/\sigma$  from 1.5 to 10. An intermediate value,

$$\frac{\tau}{\sigma} = 5.0$$

will be used to estimate the effective diffusivity. Substituting into Equation (A.23) yields

$$D^* = 0.47 \left(\frac{1}{5}\right) 1.771 * 10^{-2} \frac{\text{cm}^2}{\text{s}}$$

$$D^* = 1.665 * 10^{-3} \frac{\text{cm}^2}{\text{s}}$$

So,

$$\frac{K^*}{D^*} = \frac{4 * 10^{-4} \frac{\text{cal}}{\text{K-s-cm}}}{1.665 * 10^{-3} \frac{\text{cm}^2}{\text{s}}} = 2.402 * 10^{-1} \frac{\text{cal}}{\text{K-cm}^3} \quad (\text{A.27})$$

From the previous section,

$$k_m = 7.59 \frac{\text{cm}}{\text{s}}$$

$$h = 4.4 * 10^{-3} \frac{\text{cal}}{\text{K-s-cm}^2}$$

So,

$$\frac{k_m}{h} = \frac{7.59}{4.4 * 10^{-3}} \frac{\text{cm}^3}{\text{cal}} = 1.73 * 10^{13} \frac{\text{cm}^3}{\text{cal}} \quad (\text{A.28})$$



Substituting (A.27) and (A.28) into (A.23)

$$\frac{Bi_m}{Bi_H} = 1.73 \times 10^{13} \frac{\text{cm}^3\text{-K}}{\text{cal}} 2.402 \times 10^{-1} \frac{\text{cal}}{\text{cm}^3\text{-K}}$$

$$\frac{Bi_m}{Bi_H} = 415.5 \quad (\text{A.29})$$

The Damköhler number,  $Da$ , and the external effectiveness factor  $\bar{\eta}$  are related by

$$\bar{\eta} Da = \frac{r_g}{k_m a C_{C_2H_4, \text{bulk}}} \quad (\text{A.30})$$

Using the values from Section A.2

$$\bar{\eta} Da = \frac{8.5 \times 10^{-7} \frac{\text{mol}}{\text{g cat-s}}}{3.2 \frac{\text{cm}}{\text{s}} * \frac{0.48 \text{ cm}^2}{\text{pellet}} * \frac{100 \text{ pellets}}{4.73 \text{ g-cat}} * 3 * 10^{-7} \frac{\text{moles}}{\text{cm}^3}}$$

$$\bar{\eta} Da = 0.087 \quad (\text{A.31})$$

Then, with (A.29) and (A.31), from Figure A. 2

$$\frac{\Delta T_{\text{external}}}{\Delta T_{\text{total}}} \% = 97\%$$

If the worst case analysis used earlier is adopted, and

$$\Delta T_{\text{external}} = 6.7^\circ\text{C}$$

then

$$\Delta T_{\text{internal}} = 0.2\text{K}$$

Since this was a worst case analysis, the internal temperature



gradient will no doubt be less than this, and, for the majority of the runs, the pellets will be nearly isothermal.

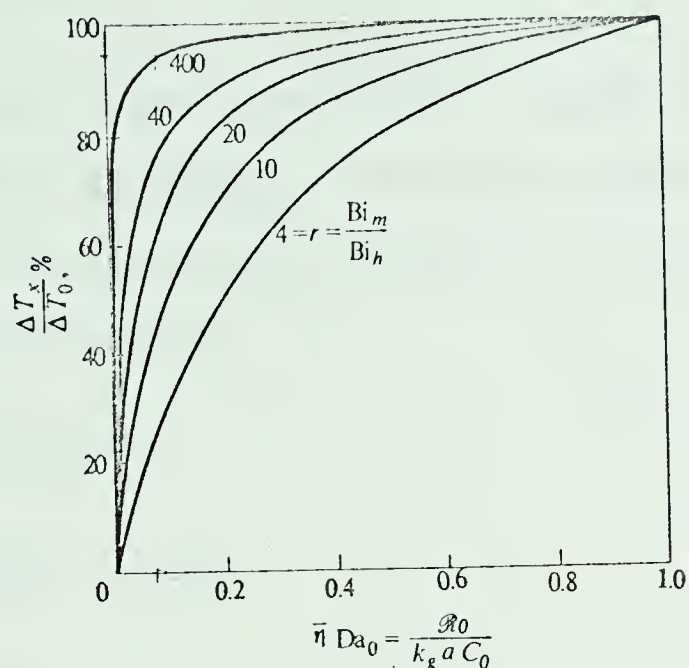


Figure A.2: Ratio of external temperature gradient to total temperature gradient (from Ref. A.1)

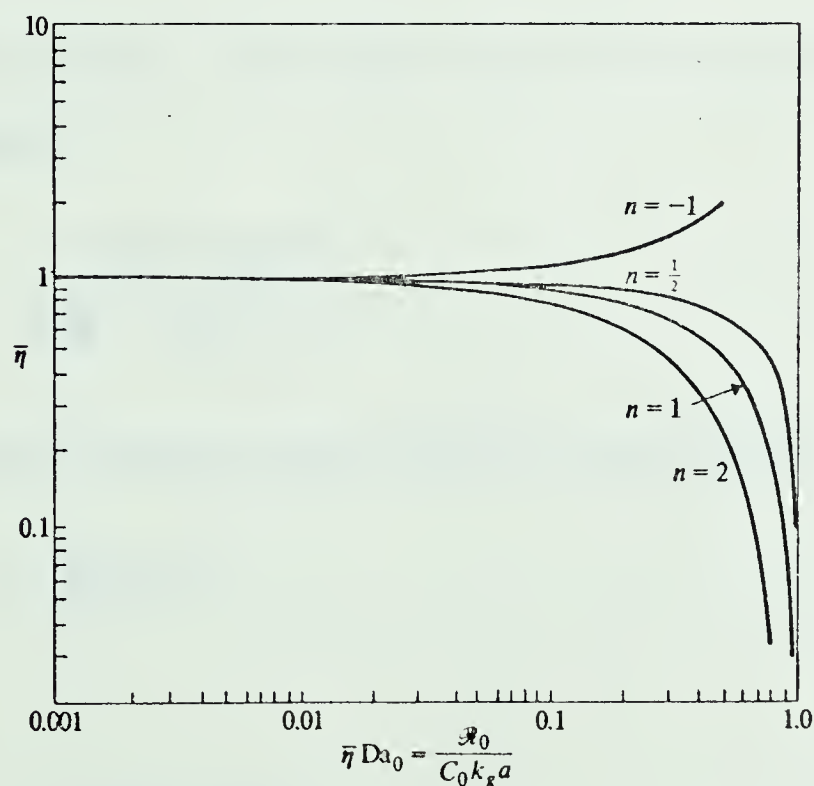


Figure A.3: Isothermal external effectiveness factor (from Ref. A.1)

Carberry also uses the Damköhler number to evaluate external mass transfer limitations. If the reaction can be modelled with a power



law rate expression,

$$-r = k[C_2H_4]^n \quad (A.32)$$

and if the external temperature gradient is small, then Figure A.3 can be used to estimate an external effectiveness factor. At high oxygen concentrations, the oxidation of ethylene can be represented fairly well with the rate equation

$$-r = k[C_2H_4]^{-1} \quad (A.33)$$

with  $n = -1$  and  $\bar{\eta}Da = 0.087$ ,

$$\bar{\eta} = 1.01$$

which indicates that the external mass transfer limitations are indeed negligible.

The internal effectiveness factor can be estimated using the Thiele parameter,

$$\phi = L \sqrt{\frac{k[C_2H_4]_{bulk}^{n-1}}{D^*}} \quad (A.34)$$

If the reaction can be modelled using (A.32), then

$$k = -r[C_2H_4]^{-n} \quad (A.35)$$

and

$$\phi = L \sqrt{\frac{-r[C_2H_4]^{-1}}{D^*}} \quad (A.36)$$

i.e., independent of the reaction order. Since the catalyst used here





was surface coated only, the characteristic length is not the pellet radius (or  $V_p/A_p$  for non spheres) but is rather the thickness of the coated layer. This thickness was measured for a number of pellets, and the values ranged from 0.2 mm to 0.4 mm. With an average value of 0.3 mm and the previously used "worst-case" conditions,

$$\phi = 3.0 * 10^{-2} \text{ cm} \sqrt{\frac{8.52 * 10^{-7} \frac{\text{gmol}}{\text{s-g cat}} * \frac{4.73 \text{ g cat}}{7.5 \text{ cm}^3 \text{ of reactor}}}{1.29 * 10^{-7} \frac{\text{gmol}}{\text{cm}^3 \text{ of reactor}} * 1.665 * 10^{-3} \frac{\text{cm}^2}{\text{s}}}}$$

$$\phi = 1.5005 \quad (A.37)$$

Carberry (A.12) has plotted internal effectiveness factors for L-H mechanisms and for carbon monoxide oxidations (at conditions quite similar to this work) against the Thiele parameter. These plots are shown in Figures A.4, A.5 and A.6. In all cases, the effectiveness factor is very close to one, regardless of the geometry or parameters. Hence, the internal mass transfer limitations are negligible as well.

To summarize, in this section the internal and external, mass and energy, limitations have each been estimated (sometimes in more than one way) and found to be small. With this, the measured global rates can be equated to the intrinsic kinetic rates. As well, the assumptions needed to simplify the integral bed mass balance equation (see Appendix A.5) will rest heavily on the calculations done in this section.



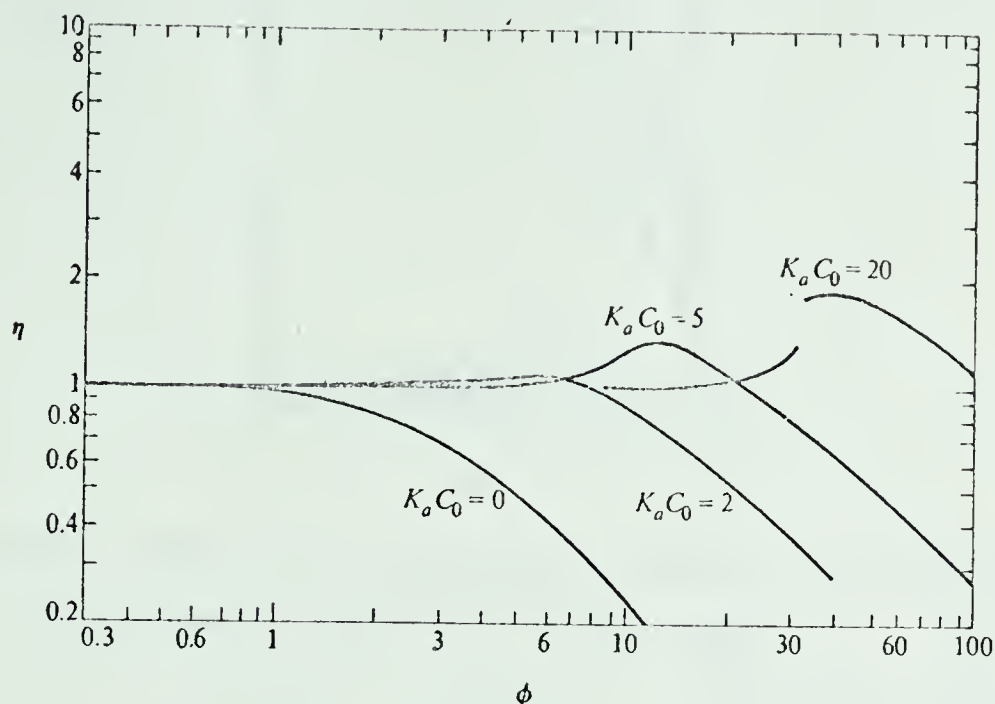


Figure A.4 : Spherical isothermal effectiveness;  $Bi_m = \infty$ ,  $r = kC/(1 + K_a C_0 C)^2$ , LHHW kinetics. [T.G. Smith, J. Zahradnik, and J.J. Carberry, Chem. Eng. Sci., 30: 763 (1975).]

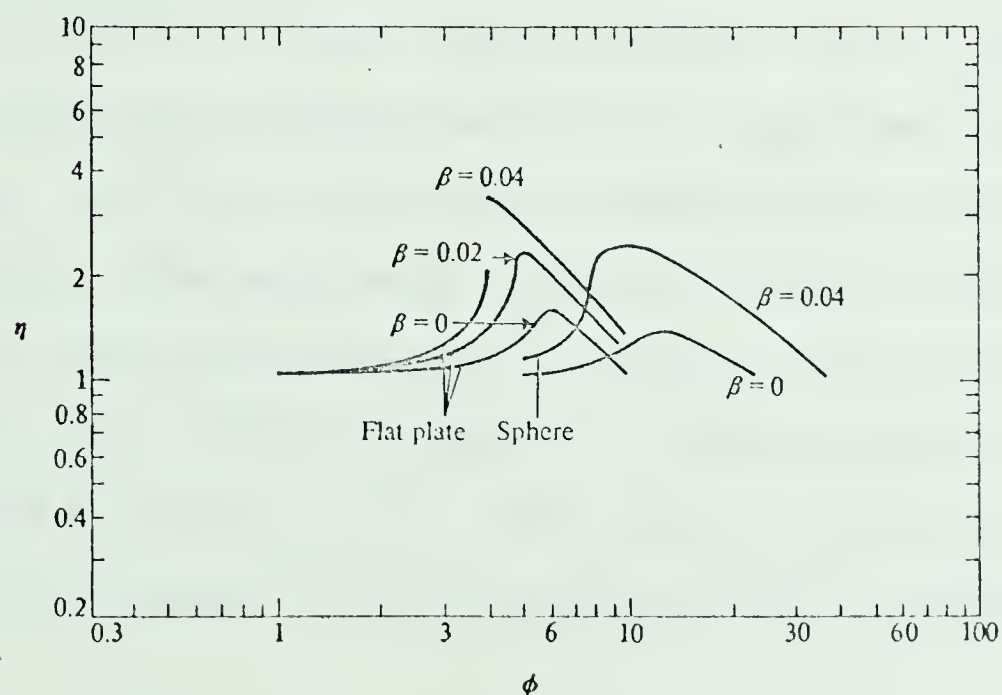


Figure A.5 : Comparison of nonisothermal effectiveness for a flat plate and a sphere;  $Bi_{h,m} = 200$ ,  $\epsilon = 30$ , LHHW kinetics. [T.G. Smith, J. Zahradnik, and J.J. Carberry, Chem. Eng. Sci., 30: 763 (1975).]



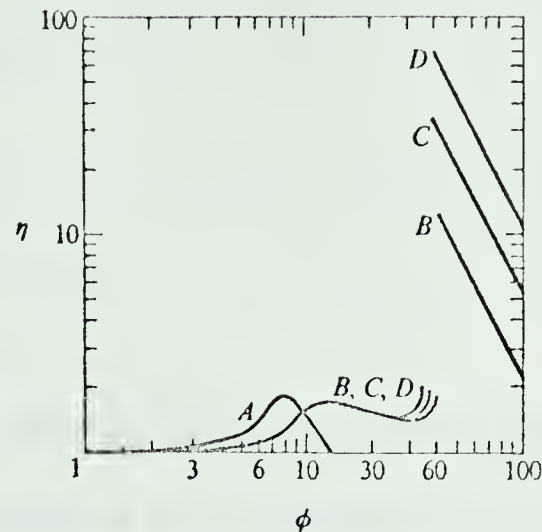


Figure A.6 : (a) Effect of  $r (=Bi_m/Bi_h)$  on spherical nonisothermal effectiveness factor;  $\beta = 0.005$ ,  $K_a C_0 = 5$ ,  $\epsilon = 30$ . Curve A:  $r = 1$ ,  $Bi_m = 2$ , curve B:  $r = 100$ ,  $Bi_m = 200$ ; curve C:  $r = 250$ ,  $Bi_m = 500$ , curve D:  $r = 500$ ,  $Bi_m = 1000$ . (from Ref. A.1)<sup>m</sup>

## A.5 Integral Bed Reactor

### A.5.1 Non-Isothermal Case

In order that the rate equation developed from the DRR data be tested, a mathematical model of the integral bed reactor must be developed. This will require a mass balance equation and an energy balance equation. The modelling of integral bed reactors has provided an outlet for many mathematically inclined authors (A.13,A.14) to display their talents, and a review of the models of fixed bed reactors has recently been presented by Hlaváček (A.15). The particular form of the balance equations do vary somewhat, and the presentation here is certainly not unique.

The mass balance equation, for a single reacting component can be written as,

$$\begin{aligned}
 -\frac{\partial}{\partial x} G_A C_B + \frac{1}{R} \frac{\partial}{\partial R} G_R C_B + \rho_G D_A^* \frac{\partial^2 C_B}{\partial x^2} + \frac{1}{R} \frac{\partial}{\partial R} R(D_R^* \frac{\partial}{\partial R} C_B) \\
 + A_V k_g(C_P - C_B) = \frac{\partial}{\partial t} \rho_G \gamma C_B
 \end{aligned}
 \tag{A.38}$$



where the subscripts are

A - axial

R - radial

B - bulk flow

P - pellet

and the symbols are defined in the List of Symbols. This unsteady state equation incorporates both axial and radial diffusion terms. The reaction rate is incorporated into a mass transfer between the bulk phase and pellet phase term.

The use of Equation (A.38) can be facilitated by certain simplifications appropriate to the integral bed system used here. If only steady state measurements are taken, the final terms is zero, i.e.,

$$\frac{\partial}{\partial t} \rho_G \gamma C_B = 0 \quad (\text{A.39})$$

For a fully developed turbulent flow pattern, which can reasonably be expected to exist at steady state, the radial and axial diffusion terms will be negligible. This is particularly true for small diameter tubes at high space velocities, i.e.

$$\frac{1}{R} \frac{\partial}{\partial R} R G_R C_B \sim 0 \quad (\text{A.40})$$

and

$$\frac{1}{R} \frac{\partial}{\partial R} R (D_R^* \frac{\partial}{\partial R} C_B) \sim 0 \quad (\text{A.41})$$

Further, if the space velocities are sufficiently high, the effect of axial diffusion is also small.





$$\rho_G D_A \frac{\partial^2 C_B}{\partial x^2} \sim 0 \quad (\text{A.42})$$

Substituting (A.39) to (A.42) into (A.38), the following simplified equation is obtained

$$A_V k_g (C_P - C_B) = \frac{d}{dx} G_A C_B \quad (\text{A.43})$$

The next step is to assume that the reactor, rather than being a true heterogeneous system of catalyst pellets and bulk fluid phase, can be represented by a pseudo-homogeneous reactor. Under this assumption, the rate of disappearance of the component of interest can be written simply as the overall or global rate of reaction per unit reactor volume. Then, Equation (A.43) becomes

$$-r = \frac{d}{dx} G_A C_B \quad (\text{A.44})$$

In order for this final assumption to be valid, it must be shown that the reaction is entirely in the kinetically controlled region. In Section A.4, it was shown, at least for the DRR, that the internal and external heat and mass transfer limitations were small. As the operating conditions for the integral bed reactor are quite similar to those of the DRR, this assumption should be valid.

The IBR was used to measure fractional conversions,  $X$ . Equation (A.44) has units of  $\text{mol}/\text{cm}^3\text{-s}$  and the rate equation developed from the DRR data was expressed in  $\text{mol}/\text{g cat-s}$ . Equation (A.44) can be expressed in terms of fractional conversion and  $\text{mol}/\text{g cat-s}$ . The rate equation developed in Chapter 4 was in the form



$$-r = A_0 e^{E/RT} \frac{[O_2]}{[C_2H_4]} \quad (A.45)$$

In terms of the fractional conversion of ethylene,

$$[C_2H_4] = \frac{F_{C_2H_4}}{F_T} C_T \quad (A.46)$$

$$F_{C_2H_4} = F_{C_2H_4,0}(1 - X_{C_2H_4}) \quad (A.47)$$

or

$$[C_2H_4] = \frac{F_{C_2H_4,0}(1 - X_{C_2H_4}) C_T}{F_T} \quad (A.48)$$

$$[O_2] = \frac{F_{O_2}}{F_T} C_T$$

$$F_{O_2} = F_{O_2,0} - 3(F_{C_2H_4,0} - F_{C_2H_4}) \quad (A.49)$$

(since three molecules of oxygen react for each molecule of ethylene which reacts). Substituting (A.47) into (A.49)

$$F_{O_2} = F_{O_2,0} - 3F_{C_2H_4,0} X_{C_2H_4} \quad (A.50)$$

So

$$[O_2] = \frac{F_{O_2,0} - 3F_{C_2H_4,0} X_{C_2H_4}}{F_T} C_T \quad (A.51)$$

Then,

$$\frac{[O_2]}{[C_2H_4]} = \frac{F_{O_2,0} - 3F_{C_2H_4,0} X_{C_2H_4}}{F_{C_2H_4,0}(1 - X_{C_2H_4})} \quad (A.52)$$

Then, (A.44) becomes



$$-r = \frac{d}{dw} F_{C_2H_4,0} X_{C_2H_4} \quad (A.53)$$

or

$$\frac{d}{dw} X_{C_2H_4} = \frac{A_0 e^{-E/RT} (F_{O_2,0} - 3F_{C_2H_4,0} X_{C_2H_4})}{F_{C_2H_4,0} [F_{C_2H_4,0} (1 - X_{C_2H_4})]} \quad (A.54)$$

This equation, (A.45), was the equation actually used as the mass balance equation.

A quick inspection of Equation (A.44) reveals why the integral bed reactor is unsuitable for determining rate equations. In integrated form, Equation (A.44) becomes

$$\frac{1}{F_{C_2H_4,0}} \int_{x=0}^{x=L} dx = \int_{X_{C_2H_4}=0}^{X_{C_2H_4}=X_F} \frac{d X_{C_2H_4}}{r} \quad (A.55)$$

To evaluate the kinetic constants, the form of the rate equation must first be guessed, then integrated in the mass balance equation. While this approach is certainly not impossible (a number of authors have in fact used this approach), it is a rather difficult method, especially if one suspects the rate equation to have an L-H form:

$$-r = \frac{k_1 k_2 k_3 [O_1]^{n_1} [C_2H_4]^{n_2}}{(1 + K_2 [O_2] + K_3 [C_2H_4])^{n_3}} \quad (A.56)$$

The energy balance equation was obtained incorporating many of the same assumptions used to derive the mass balance equations. The simplified equation takes the form



$$-in C_p \frac{dT}{dW} = -u\left(\frac{\Delta A}{\Delta W}\right)(T - T_{bath}) + (-\Delta H_r)(-r) \quad (A.57)$$

where  $\left(\frac{\Delta A}{\Delta W}\right)$  = the heat transfer area along the reactor wall per gram of catalyst.

$u$  = the overall heat transfer coefficient between the reaction fluid and the constant temperature bath.

The overall heat transfer coefficient can be treated as a series of resistances.

$$\frac{1}{u} = \frac{1}{h_w} + \frac{\Delta x}{k_T} + \frac{1}{h_o} \quad (A.58)$$

where  $h_w$  = the film heat transfer coefficient inside the reactor

$k_T$  = thermal conductivity of the reactor wall

$\Delta x$  = thickness of the reactor wall

$h_o$  = film heat transfer coefficient outside the reactor.

Since the reactor wall was stainless steel and the bath fluid was molten lead and bismuth, only the inside film transfer coefficient would contribute significantly to the thermal resistance, i.e.

$$u \sim h_w \quad (A.59)$$

So, (A.57) becomes

$$-in C_p \frac{dT}{dW} = -h_w\left(\frac{\Delta A}{\Delta W}\right)(T - T_{wall}) + (-\Delta H_r)(-r) \quad (A.60)$$

Equation (A.60) was the final form of the energy balance used to model the reactor.

Equations (A.60) and (A.54) were simultaneously integrated using a 4th order Runge-Kutta technique. The computer coding of the integration was from the IBM Scientific Subroutine Program library





(SSP), subroutine RKGS. The entire program used for this integration is in the Data Book (see Appendix E). The numerical values of the parameters used are as follows:

$$\begin{aligned}
 W_{\min} &= 0.0 \text{ g} \\
 W_{\max} &= 13.85 \text{ g} \\
 A_0 &= 4.12 * 10^6 \text{ mol/g cat/s} \\
 E &= 114.22 \text{ kJ/mol} \\
 X_{\min} &= 0.0\% \\
 X_{\max} &= 100\% \\
 \dot{m} &= \text{read in for each run} \\
 C_p &= 1.05 \frac{\text{J}}{\text{g-k}} \\
 T_w &= \text{read in for each run} \\
 \left(\frac{\Delta A}{\Delta W}\right) &= 7.2 \frac{\text{cm}^2}{\text{g-cat}} \\
 (-\Delta H_r) &= 1.411095 * 10^6 \frac{\text{J}}{\text{mol}}
 \end{aligned}$$

The initial flow rates of oxygen and of ethylene were calculated from the initial mole fractions of the two components and the total molar flow rates which were read in for each run from (A.46)

$$F_{C_2H_4,0} = \frac{[C_2H_4]_0 F_T}{C_T} \quad (A.61)$$

$$F_{C_2H_4,0} = \frac{[x_{C_2H_4,0} C_T] F_T}{C_T}$$

$$F_{C_2H_4,0} = x_{C_2H_4,0} F_T \quad (A.62)$$

Similarly,



$$F_{O_2,0} = x_{O_2,0} F_T \quad (A.63)$$

The heat transfer coefficient on the inside of the tube can be estimated in a number of ways. Yagi and Kunii (A.16) cite a correlation equation developed for packed annular beds which they claim is also valid for cylindrical beds if the proper values for certain parameters are used. Their equation is

$$h_w \frac{dp}{k} = h_w^o \frac{dp}{k} + \alpha_w P_r R_e \quad (A.64)$$

The Reynolds number and the Prandtl number were calculated earlier,

$$R_e = 159$$

$$P_r = 0.6935$$

The Reynolds number was based on the pellet diameter of 0.39 cm. However, the pellets were mixed with glass beads having a diameter of 0.2 cm. These smaller pellets would tend to fill the voids along the wall of the tube. The appropriate value for the Reynolds number along the reactor wall should be based on the diameter of the glass beads, or at least a diameter somewhere between that of the beads and the catalyst pellets. As well, the Reynolds number was based on the recycle rate, and for the integral bed reactor, the reaction mixture passes through the catalyst bed only once. So, for the IBR, the pellet Reynolds number along the reactor wall will range from  $(R_e)_1 = 10.60$  for the catalyst pellets to  $(R_e)_2 = 5.43$  for the glass beads.



The range of values for the ratio of the tube diameter to the diameter of the packing can also be calculated.

$$\left(\frac{d_p}{d_T}\right)_1 = \frac{0.39 \text{ cm}}{2.09 \text{ cm}} = 0.187 \quad \text{for the pellets}$$

$$\left(\frac{d_p}{d_T}\right)_2 = \frac{0.2 \text{ cm}}{2.09 \text{ cm}} = 0.096 \quad \text{for the glass beads}$$

For cylindrical beds with

$$(1) \quad 0.833 < \frac{d_p}{d_T} < 0.167$$

and

$$(2) \quad 0.431 \text{ cm} < d_p < 0.635 \text{ cm}$$

Yagi and Kunii recommend that

$$h_w^\circ \frac{D_p}{k} = 5$$

and for all cylindrical beds they use

$$\alpha_w = 0.054$$

So

$$\begin{aligned} \left(\frac{h_w d_p}{k}\right)_1 &= 5 + 0.054 * 0.6935 * 10.60 \\ &= 5.47 \end{aligned}$$

and

$$\begin{aligned} \left(\frac{h_w d_p}{k}\right)_2 &= 5 + 0.054 * 0.6935 * 5.43 \\ &= 5.20 \end{aligned}$$



Then

$$(h_w)_1 = \frac{5.47 * 3.167 * 10^{-4} \frac{J}{K-s-cm}}{0.39 \text{ cm}} = 4.442 * 10^{-3} \frac{J}{K-s-cm^2}$$

and

$$(h_w)_2 = \frac{5.20 * 3.167 * 10^{-4} \frac{J}{K-s-cm}}{0.2 \text{ cm}} = 8.234 * 10^{-3} \frac{J}{K-s-cm^2}$$

Hence, using the Yagi and Kunii correlation, the inside heat transfer coefficient could vary from  $4.442 * 10^{-3} \frac{J}{K-s-cm^2}$  up to  $8.234 * 10^{-3} \frac{J}{K-s-cm^2}$ .

Smith (A.17) also cites a correlation for the calculation of inside heat transfer coefficients. He recommends the use of Equation (A.65) for the estimation of the wall coefficient.

$$\frac{h_w d}{k} = 3.50(R_e)^{0.7} e^{-4.6 dp/dT} \quad (A.65)$$

Again, a range of values can be obtained depending on the diameter of the packing.

$$\begin{aligned} \left(\frac{h_w d}{k}\right)_1 &= 3.50(10.60)^{0.7} e^{-4.6 * 0.187} \\ &= 7.73 \end{aligned}$$

and

$$\begin{aligned} \left(\frac{h_w d}{k}\right)_2 &= 3.50(5.43)^{0.7} e^{-4.6 * 0.096} \\ &= 7.36 \end{aligned}$$

So





$$(h_w)_1 = \frac{7.773 * 3.167 * 10^{-4} \frac{J}{K-s-cm}}{2.09 \text{ cm}} = 1.171 * 10^{-3} \frac{J}{K-s-cm^2}$$

$$(h_w)_2 = \frac{7.36 * 3.167 * 10^{-4} \frac{J}{K-s-cm}}{2.09 \text{ cm}} = 1.115 * 10^{-3} \frac{J}{K-s-cm^2}$$

Here the range in the heat transfer coefficient is from

$1.171 * 10^{-3} \frac{J}{K-s-cm^2}$  to  $1.115 * 10^{-3} \frac{J}{K-s-cm^2}$ . Hence, the heat transfer coefficient used for the calculation can vary considerably, and depending on the correlation used, the heat transfer coefficient could vary from  $1.115 * 10^{-3} \frac{J}{K-s-cm^2}$  up to  $8.234 * 10^{-3} \frac{J}{K-s-cm^2}$ , almost an order of magnitude.

As the heat transfer coefficient decreases, the reactor approaches adiabatic operation, i.e. no heat is lost from the reactor. As the heat transfer coefficient increases, the reactor approaches isothermal operation, i.e. all the heat generated by the reaction leaves the reactor immediately. This latter limiting case simplifies the calculation considerably, as the energy balance equation is no longer necessary in the reactor model. This case is detailed in Section A.5.2.

#### A.5.2 Isothermal Case

The bismuth-lead bath was constructed so that the reactor would operate at isothermal conditions. Because the reaction was highly exothermic, and there were finite heat transfer resistances between the reaction gases and the bath, some small temperature rises were indeed noticed. This was the reason for the non-isothermal calculation outlined in the previous section. If, however, the reactor



were isothermal, then the mass balance equation could be solved analytically. At constant temperature, Equation (A.54) becomes

$$\frac{dX}{dW} = \frac{k(F_0 - 3F_E X)}{F_E[F_E(1 - X)]} \quad (\text{A.66})$$

or

$$\frac{k}{F_E} dW = \frac{F_E(1 - X)}{(F_0 - 3F_E X)} dX$$

$$\int_{w=0}^{w=13.8} \frac{k}{F_E} = \int_{X=0}^{X=X_E} \frac{F_E(1 - X)}{(F_0 - 3F_E X)} dX$$

$$13.8 \frac{k}{F_E} = \frac{X_E}{3} + \left[ \frac{F_0/F_E - 3}{9} \right] \ln \left[ \frac{F_0/F_E - 3X_E}{F_0/F_E} \right]$$

or

$$f(X_E) = \frac{X_E}{3} + \left[ \frac{F_0/F_E - 3}{9} \right] \ln \left[ \frac{F_0/F_E - 3X_E}{F_0/F_E} \right] - 13.8 \frac{k}{F_E} \quad (\text{A.67})$$

Equation (A.67) can be solved for a root of the equation, i.e.

$X_E$  such that

$$f(X_E) = 0 \quad (\text{A.68})$$

using a variety of techniques. The one used here was a simple Newton's Method.

$$x_{i+1} = x_i - \frac{f(x)}{f'(x)} \quad (\text{A.69})$$

The derivative of  $f(X_E)$  is

$$f'(X_E) = \frac{1}{3} - \frac{3F_0/F_E}{F_0/F_E - 3X_E} \quad (\text{A.70})$$



Equations (A.67) and (A.70) were used in the program ROOTS (Appendix E) to generate isothermal predictions of the integral bed runs. As can be seen from Equation (A.67), the fractional conversion is a function of both the ratio of oxygen to ethylene in the feed stream ( $F_0/F_E$ ) and of the inlet ethylene flow rate  $F_E$ . This presents certain problems in displaying the data since it is difficult to adjust the values in precisely the same manner for each run.



APPENDIX B  
EQUIPMENT CALIBRATION

In this Appendix, the calibrations for the instruments used in the experimental studies are presented. Calibrations for the thermocouples, temperature controllers, rotameters, mass flow meters and the gas chromatographs are discussed.

B.1 THERMOCOUPLES

The thermocouples used to measure temperatures in the IBR and DRR were calibrated in the Chemical Engineering Department Instrument shop by D. Sutherland. They were compared against a standardized Pt-10% Rh vs. Pt thermocouple over a range of temperatures. The results of the calibration are shown in TABLE B.1.

TABLE B.1  
THERMOCOUPLE CALIBRATIONS  
Measured Temperatures (°C)

Standard	Iron vs. Constantan Thermocouples									
Thermocouple	A	B	C	D	E	F	G	H	I	J
20.53	20.70	20.64	20.73	20.73	20.65	20.71	20.77	20.75	20.70	20.68
171.41	171.85	171.83	171.90	171.89	172.01	172.01	171.89	171.80	171.82	171.88
293.50	293.80	293.72	293.77	293.85	294.00	294.10	293.95	293.82	293.79	293.86
416.23	417.94	417.76	417.94	417.98	418.26	418.20	418.04	417.58	417.62	417.81
586.74	590.10	589.90	589.91	590.07	590.33	590.10	589.92	589.27	589.66	589.91

The curves for thermocouples E and H, which are the worst and best respectively, are plotted in Figure B.1. Thermocouples A to H were used in the IBR, I and J in the DRR.





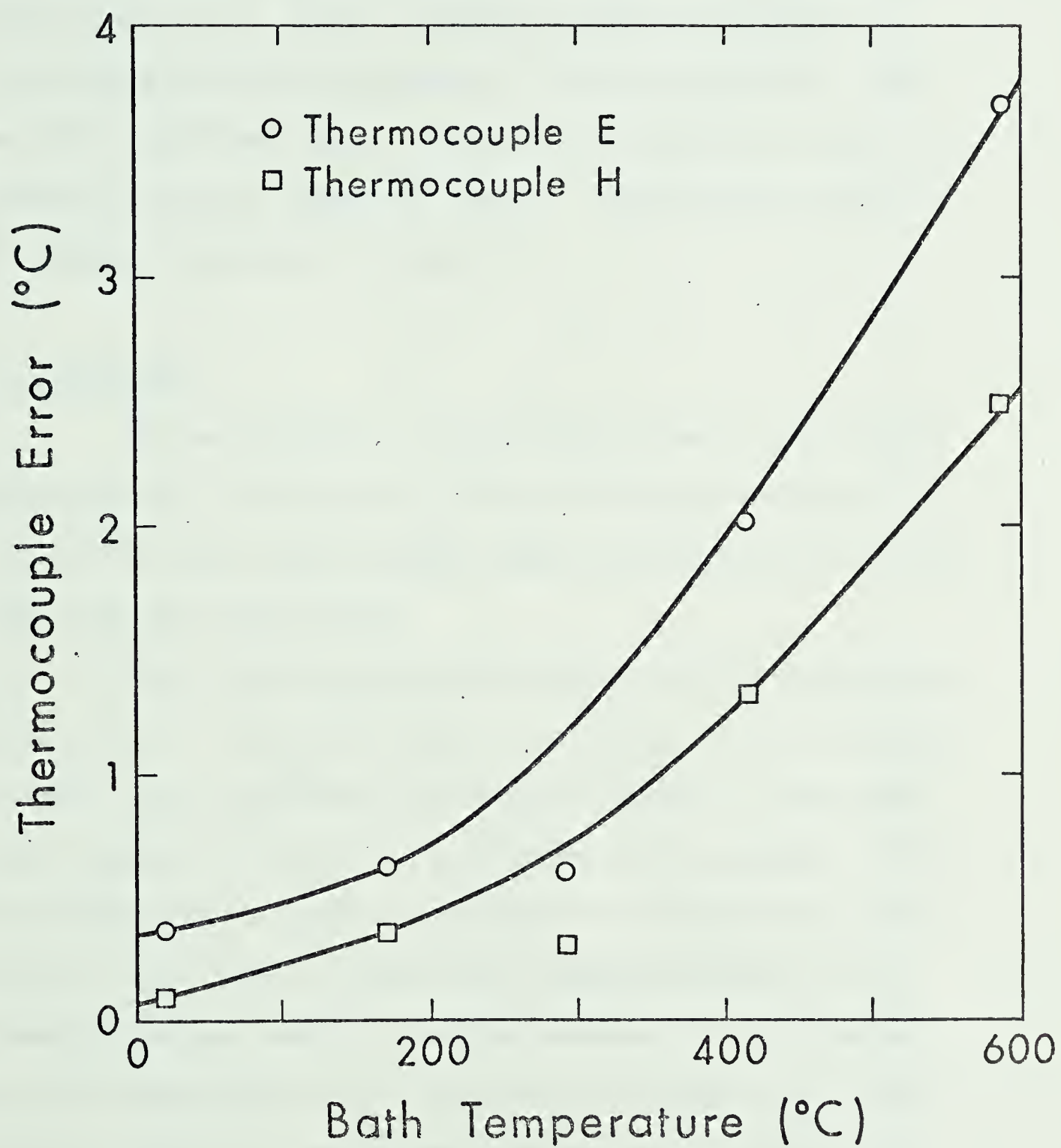


Figure B.1 : Results of the thermocouple calibrations (extreme cases).



## B.2 TEMPERATURE CONTROLLERS

The temperature of the lead-bismuth bath was controlled with a Honeywell MS2 temperature controller during the DRR runs and with a Foxboro M/62 controller for the IBR runs. The Foxboro controller could be set for a variety of temperature ranges, by installing different range spanners. Two spanners, 100°C - 300°C and 200°C - 500°C were used. The calibration curves for these two spanners is shown in Figures B2 and B3. The calibration curve for the Honeywell controller is Figure B4.

## B.3 ROTAMETERS

The two rotameters used to monitor flows in the integral bed system were calibrated with air at 27.65 inches of mercury and 70°F for the high range flow meter (tube #R-2-15-B) and for the low range flow meter (tube #601).

The calibrations were performed at fairly high pressures, 28 psig for the high range rotameter and 50 psig for the low range rotameter. While the reactor pressure was always well below this (near atmospheric in fact) the positioning of the rotameter valves downstream of the rotameters necessitated the calibration at high pressures. The supply cylinders were connected directly to the rotameters through regulators and the pressures in the rotameters were thus independent of the flow rates and dependent only on the regulator pressures. Particularly in the case of the low range rotameter, the needle valve used to regulate the flow provided a relatively large pressure drop, and hence the rotameters were calibrated at the pressures mentioned.



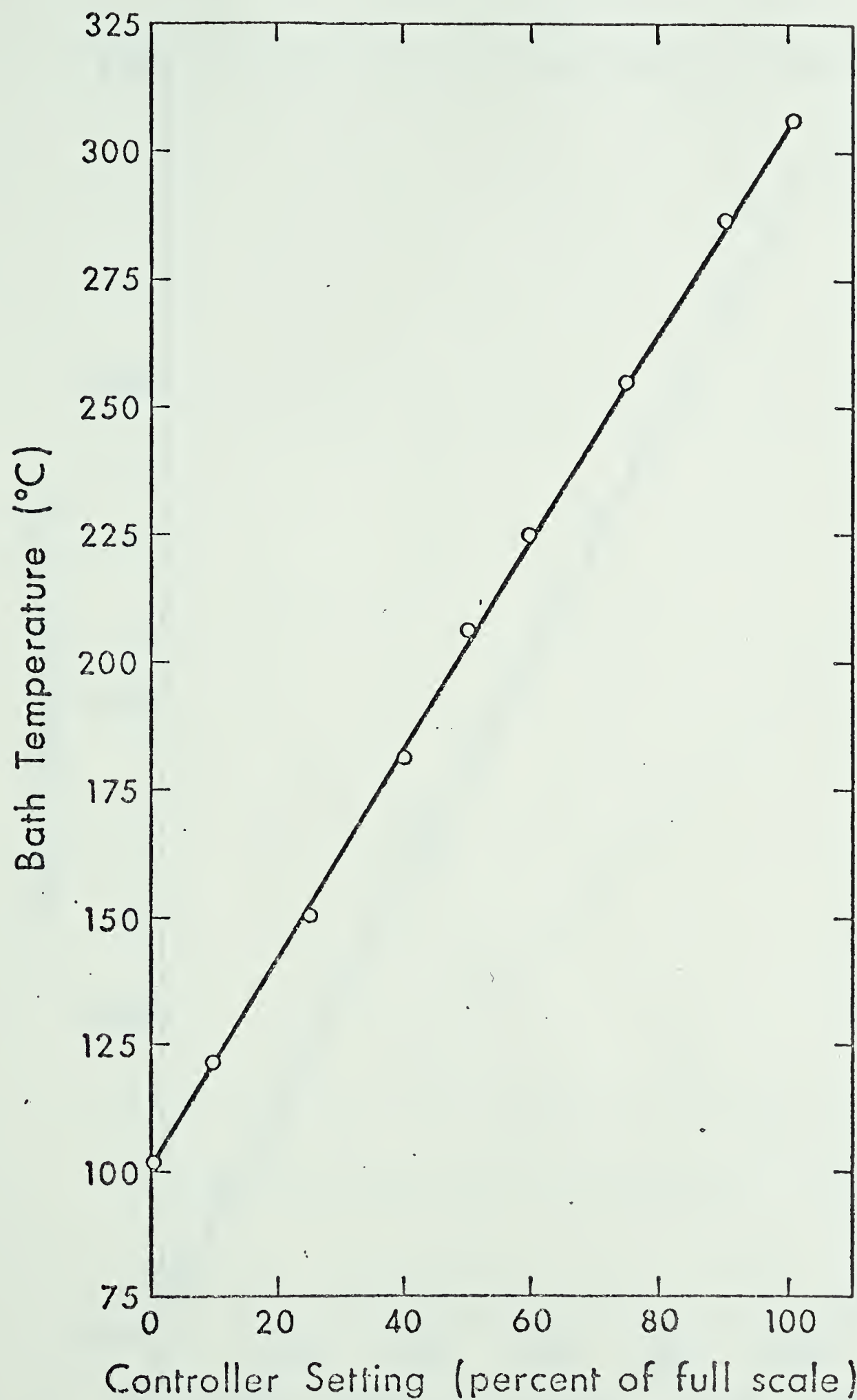


Figure B.2 : Calibration curve for mid-range temperature controller.



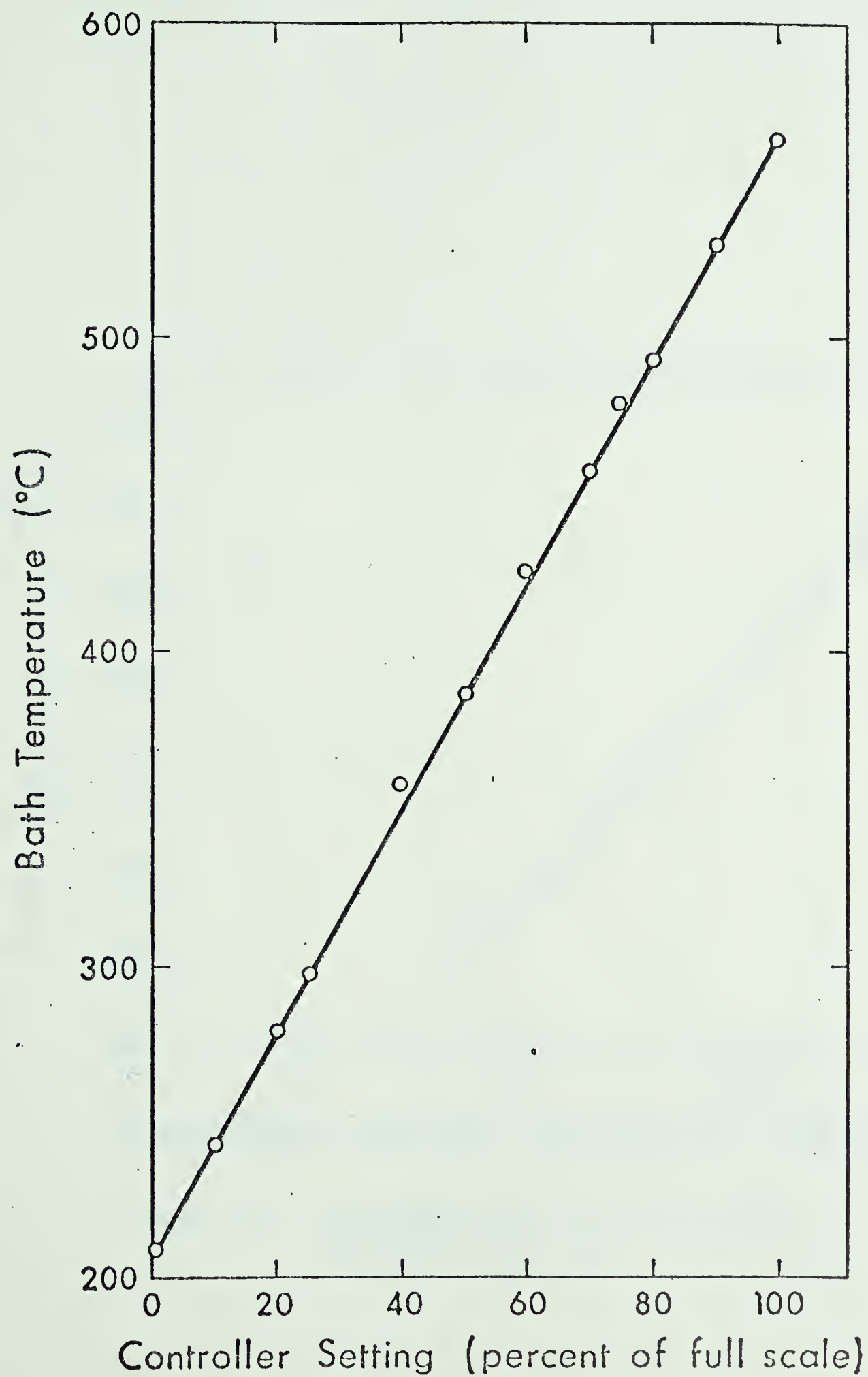


Figure B.3 : Calibration curve for the high range temperature controller





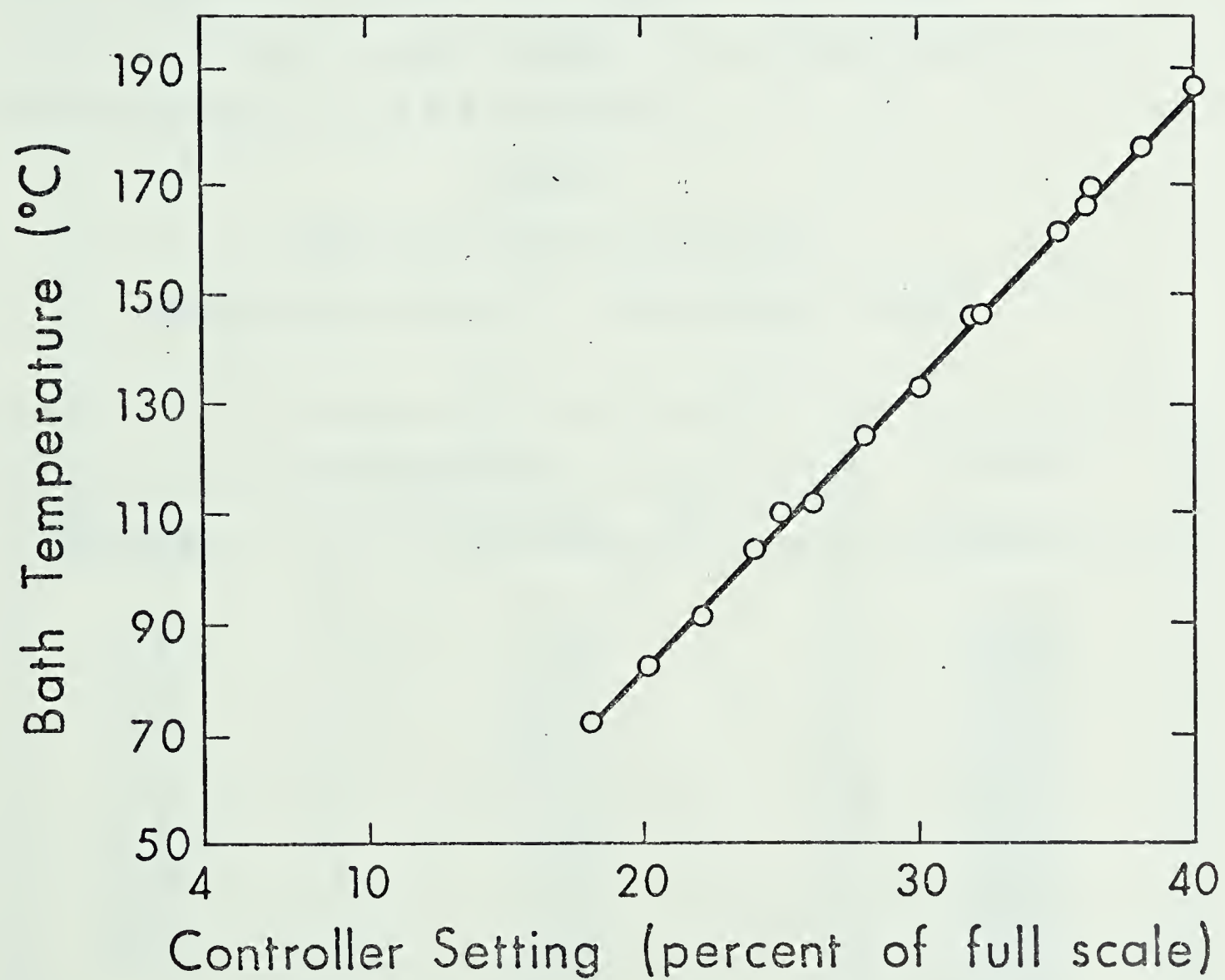


Figure B.4 : Calibration curve for the low range temperature controller.



The actual calibrations were done using a five cubic foot, American Meter Company, Meter Prover. The volume of air that passed through the rotameters was collected in the copper displacement tank and the volume was read from a scale on the tank. The prover compensated for buoyancy changes and changes in the water level as the tank rose. The volume was measured at laboratory temperature and pressure and the time was measured with a stop watch. The calibration data is tabulated on Table B.2 for the high range rotameter and in Table B.3 for the low range rotameter. The calibration curves are shown on Figures B.5 and B.6 respectively.

TABLE B.2

## HIGH RANGE ROTAMETER CALIBRATION

MATHESON TUBE #R-2-15-B      TUBE PRESSURE - 28 psig

ROTAMETER READING		FLOW RATE
GLASS BALL	STEEL BALL	(L/min.)
1.0	0.5	0.3090
2.0	1.0	0.8098
3.0	1.5	1.2883
4.0	2.0	1.7211
5.0	2.5	2.0973
6.0	2.95	2.4971
7.0	3.4	2.8538
9.0	4.25	3.4895
11.0	5.05	4.0876
13.0	5.8	4.1516
15.0	6.45	4.5487
	8.0	5.3969
	10.0	6.4144
	12.0	7.4104
	14.0	8.1892
	15.0	8.6360



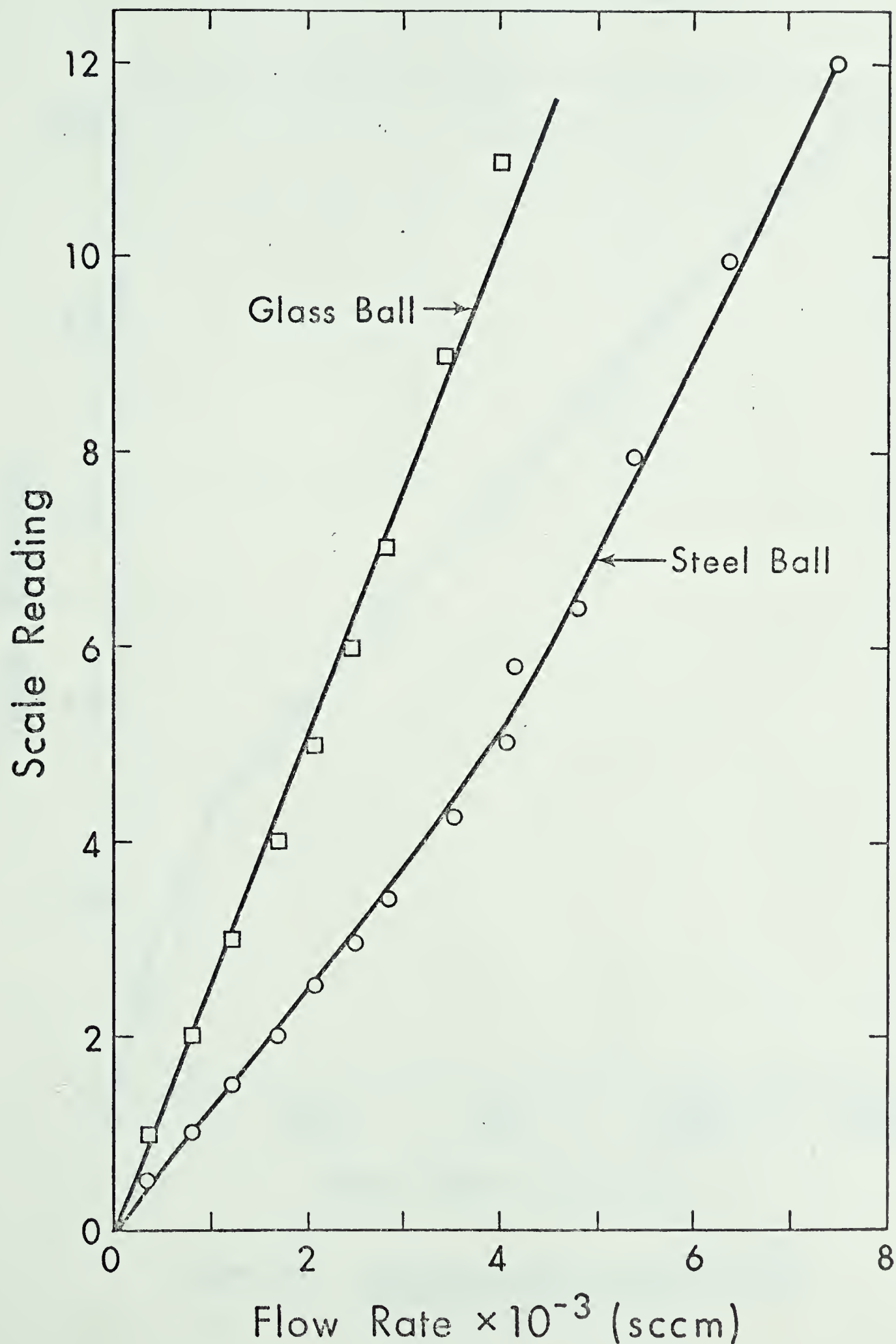


Figure B.5 : Calibration curve for the high range rotameter (Matheson #R-2-15-B).



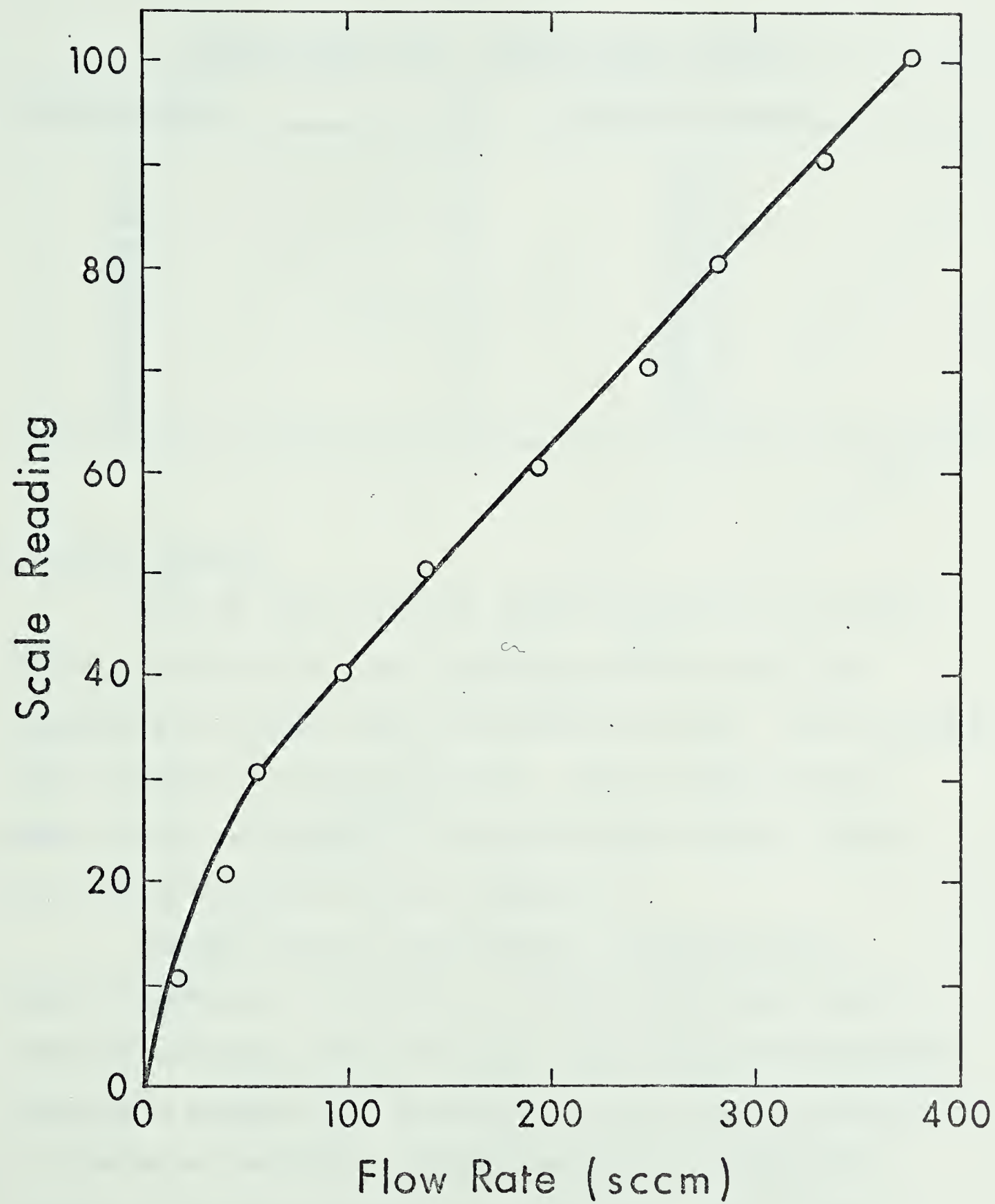


Figure B.6 : Calibration curve for the low range rotameter (Matheson #601).





TABLE B.3

## LOW RANGE ROTAMETER CALIBRATION

MATHESON TUBE # 601	TUBE PRESSURE 50 PSIG
ROTAMETER READING	FLOW RATE (cc/min)
10	13.5
20	35.3
30	52.2
40	95.5
50	136.4
60	192.3
70	245.9
80	283.0
90	333.3
100	375.0

B.4 MASS FLOWMETER

The high range flow meter, model 8116-0153, was calibrated with dry air and the low range flow meter, model 8116-0112, was calibrated with nitrogen, each from 10 psig to 30 psig. The calibration curves are shown in Figures B.7 and B.8. The low range mass flow meter was also calibrated with a 5% ethylene 95% nitrogen mixture. This calibration curve is shown in Figure B.9.

The low range mass flow meter was calibrated using a bubble flow meter and a stop watch. The measurements were taken at laboratory conditions, 21°C and 95 kPa. The results plotted have been converted to standard cubic centimeters (at zero degrees Centigrade and 1.0 atmospheres) per minute. The high range mass flow meter was calibrated with a wet test meter and a stop watch. The wet test meter was standardized by the Department of Chemical Engineering Instrumentation Shop. Again, the measurements were taken at ambient conditions, i.e., 21°C and 95 kPa. In both cases, the



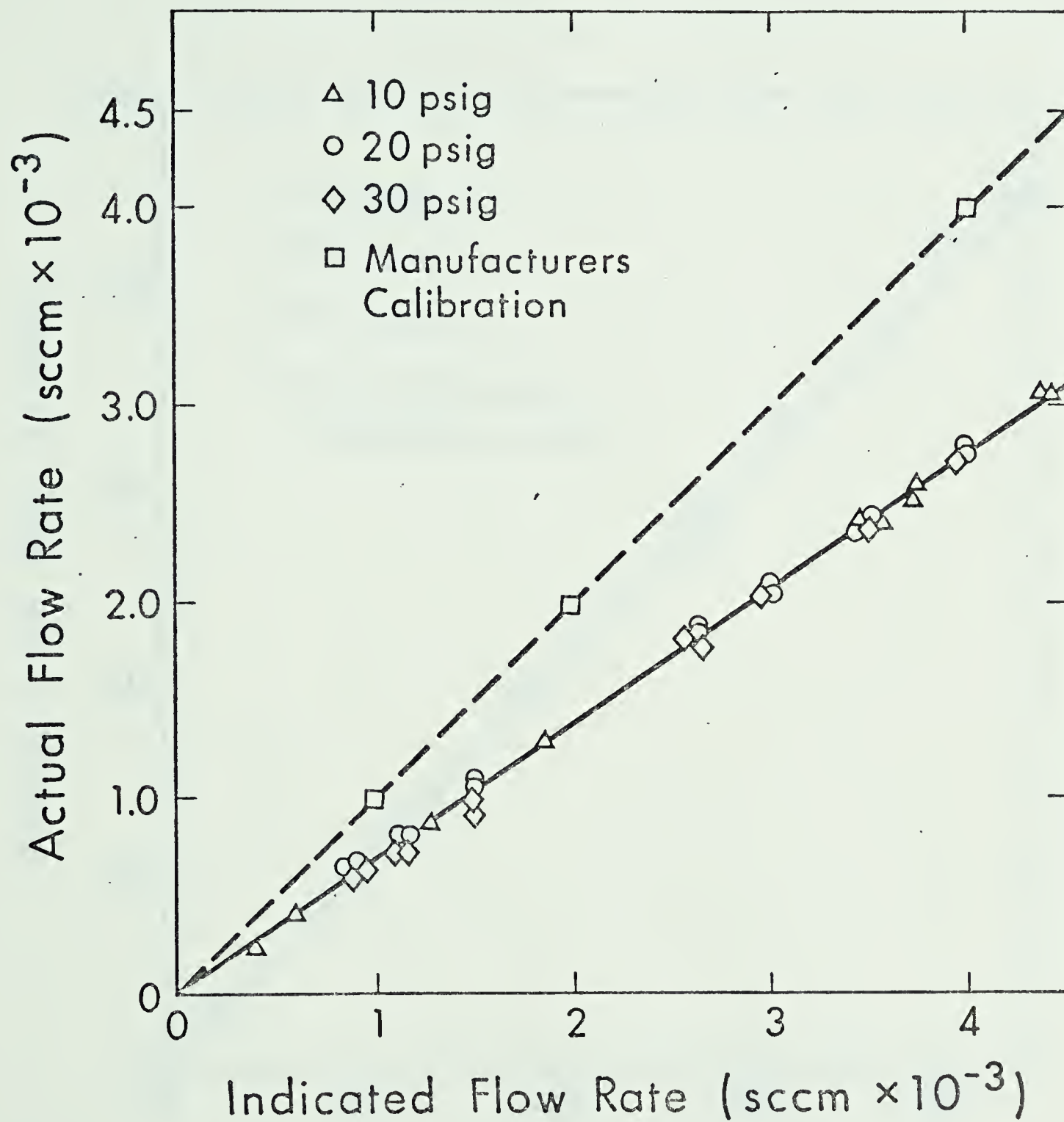


Figure B.7 : Calibration curve for the high range mass flowmeter (calibration gas -  $N_2$ ).



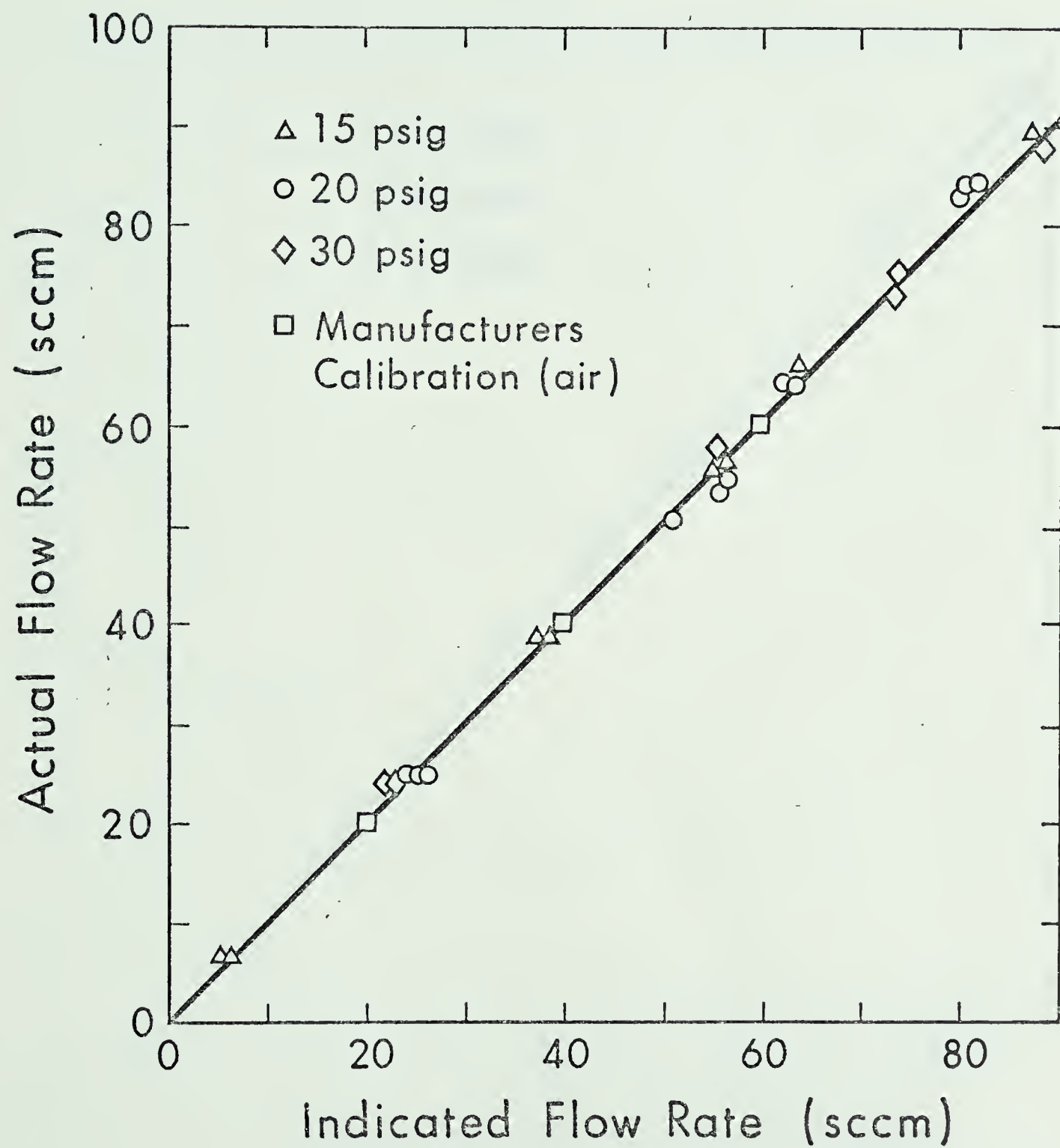


Figure B.8 : Calibration curve for the low range mass flowmeter (calibration gas -  $N_2$ ).



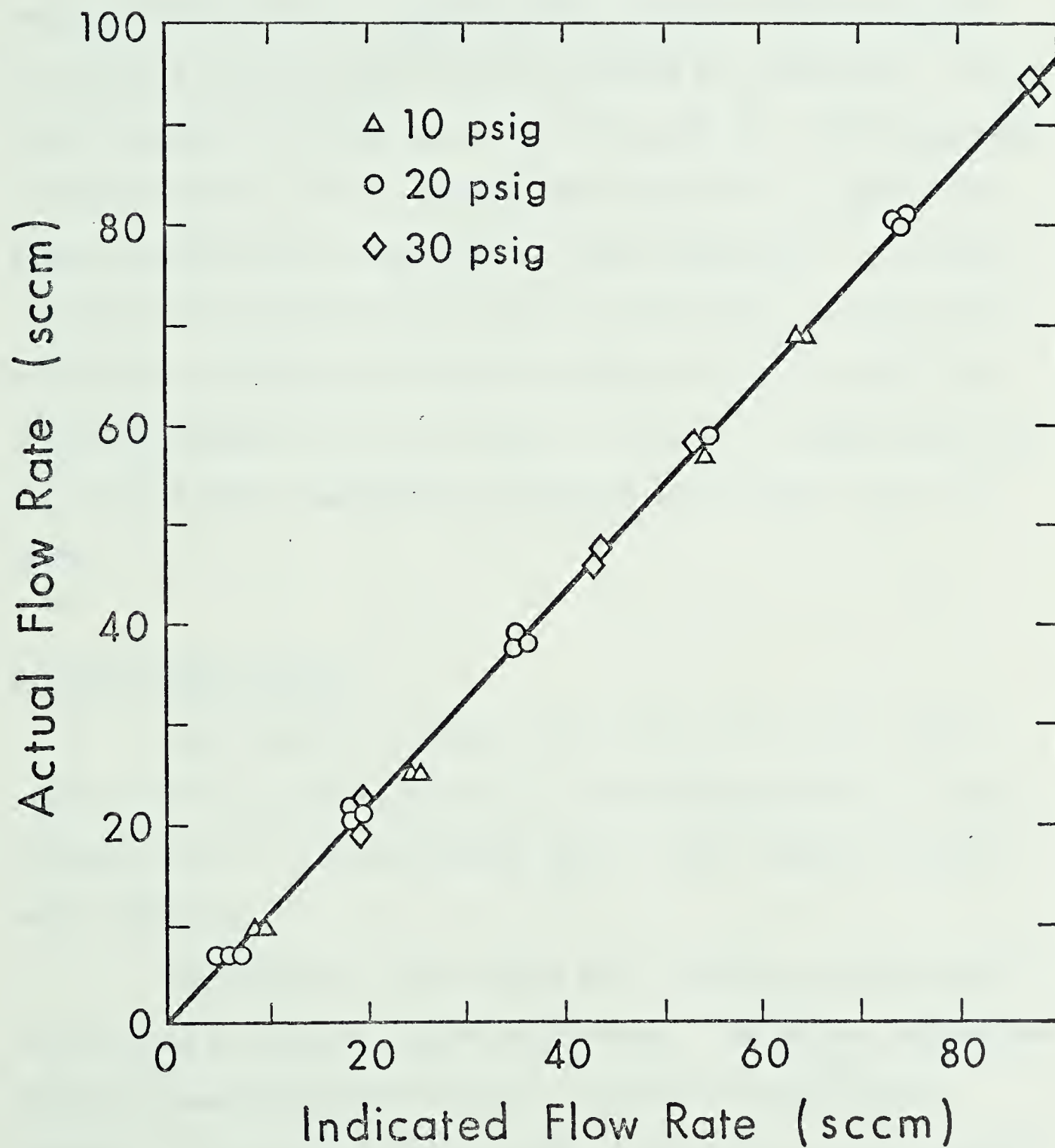


Figure B.9 : Calibration curve for the low range mass flowmeter (calibration gases - 5%  $C_2H_4$  and 95%  $N_2$ ).





regulating valves were located downstream of the mass flow meters so that the pressures in the meters would not be functions of the flow rates.

However, once the calibrations had established that the indicated flow rates were not pressure dependent, the installation of valves in the flow system could be altered for convenience. The line pressure to both flow meters was set at 30 psig. This presented a slight problem since the pressure drop across the low range flow meter was higher than across the high range flow meter. To prevent a reverse flow through the low range mass flow meter, a needle valve was installed downstream of the low range meter and upstream of the connection between the low and high flow lines. The regulating valve for the high range flow meter was upstream of the high range flow meter.

## B.5 GAS CHROMATOGRAPHS

Gas chromatography was used to analyze the feed to the reactors and the reaction products. Three chromatographs were used: a Beckman G.C. -2, a Gow Mac series 550 G.C. and a Hewlett Packard model 5710A G.C.

The Beckman G.C. was fitted with a molecular sieve column and was used to separate oxygen and nitrogen. The Gow Mac and Hewlett Packard Chromatographs used PoraPak Q columns and were used to separate air, carbon dioxide and water. The Gow Mac G.C. was used in conjunction with the integral bed reactor while the Hewlett Packard G.C. was used with the recycle reactor. The Beckman G.C. was used in both cases. The details of the operation and the specifics of the columns



are in Appendix C. Only the calibration data are presented in this section.

The chromatographs were calibrated for nitrogen and oxygen in the case of the Beckman G.C. and for air, carbon dioxide and ethylene for the other two. Water was not used in the calibration as there were certain problems specific to water analysis which are discussed at greater length in Appendix C. The samples used as standards for the calibrations were prepared in a number of different ways. Samples of oxygen in nitrogen, carbon dioxide in nitrogen, ethylene in nitrogen and carbon dioxide and ethylene in nitrogen were prepared using two techniques. The first method was volumetric. A 100 ml mercury filled buret equipped with two-way valves at each end was used to first measure gas volumes and then to compress the mixed gases into sample bombs. The second method was gravimetric. Gases were admitted into weighed sample bombs and the weight changes were measured using an electronic balance. The gravimetric method was somewhat less reliable. It required the subtraction of two relatively large and nearly equal numbers in order to determine the weight percents of the components and was hence inherently inaccurate. The sample bombs were four small (about 100 c.c. volume) aluminum cylinders equipped with needle valves and fittings. The total weight of the sample bombs, valves and fittings was about 160 g. The calibrations for ethylene were also checked against a standardized ethylene-nitrogen sample obtained from Linde Gases.

The actual calibration was done with the nitrogen as an arbitrary reference component. This meant that the response factor for nitrogen was set to unity.



The response factors were calculated in the following manner. Consider a gas mixture containing  $n$  components. The mole fraction of the  $i$  th component,  $x_i$ , is given by the relation

$$x_i = \frac{A_i R_i}{\sum_{i=1}^n A_i R_i} \quad (B.1)$$

where  $A_i$  is the area under the peak of the  $i$  th component and  $R_i$  is the response factor appropriate to the  $i$  th component. Here the term response factor is used to describe the  $R_i$  values defined in Equation (B.1). (Some authors refer to  $1/R_i$  as the response factor.) Similarly, for the reference component, here nitrogen,

$$x_N = \frac{A_N R_N}{\sum_{i=1}^n A_i R_i} \quad (B.2)$$

But, by definition  $R_N=1$ , so, dividing Equation (B.1) by (B.2)

$$R_i = \frac{x_i}{x_N} \frac{A_N}{A_i} \quad (B.3)$$

Equation B.3 was used to calculate the response factors for oxygen, ethylene, and carbon dioxide. The mole fractions  $x_i$  and  $x_N$  were obtained either from the mass fraction or the volume fraction of the prepared samples.

The calibrations for  $O_2$  and  $N_2$  mixtures using the Beckman-G.C. appear in Table B.4. The average response factor was 0.996,





but 1.0 was the value actually used. Dietz (B.1) reports a value of 1.05 for the  $O_2$  vs.  $N_2$  response factor.

The calibrations for the Gow-Mac G.C. with a PoraPak Q column are displayed in Table B5. The  $CO_2$  response factor was 0.8670 and the ethylene response factor was 0.8716, however, 0.87 was used in each case.

The last gas chromatograph calibrated was the Hewlett-Packard model 5710A, with a PoraPak Q column. The average response factor for ethylene was 0.8593, however 0.86 was the value actually used in the subsequent analysis. The average response factor for carbon dioxide was 0.8616, and as the calibration data exhibited very little scatter, 0.8616 was the value used in the analysis. The calibrations are in Table B6.





TABLE B.4  
 CALIBRATION OF BECKMAN G.C. 2  
 CALIBRATION GASES  $O_2 + N_2$

Mole % $O_2$	Preparation G=gravimetric V=volumetric	Response Factor	
		$N_2$	$O_2$
0.82	G	1.0	1.15
0.84	G		1.08
1.01	G		1.06
1.20	G		1.06
2.98	V		1.0
3.06	V		0.98
3.50	V		0.99
3.47	V		1.02
6.00	V		0.95
6.00	V		0.96
6.48	V		1.09
6.53	V		0.96
9.90	G		0.85
10.11	G		1.09
10.00	G		0.98
10.63	G		1.04
11.10	V		0.95
11.46	V		0.97
11.52	V		0.95
12.44	V		0.94
12.00	G		1.12
12.46	G		1.24
12.59	G		1.15
12.35	G		1.17
17.81	V		1.00
17.98	V		0.99
18.0	V		1.02
18.4	V		1.07
21.9	AIR		1.11
AVERAGE RESPONSE FACTORS		1.0	0.996
VALUES REPORTED BY DIETZ		1.0	1.05



TABLE B.5

## CALIBRATION OF GOW-MAC SERIES 550 GAS CHROMATOGRAPH

CALIBRATION GASES  $\text{CO}_2, \text{C}_2\text{H}_4, \text{N}_2$ 

Mole % $\text{CO}_2$	Mole % $\text{C}_2\text{H}_4$	Preparation G=Gravimetric V=Volumetric	Response Factors		
			$\text{N}_2$	$\text{CO}_2$	$\text{C}_2\text{H}_4$
2.01		G	1.0	0.8783	
3.82		V		0.8680	
7.56		G		0.8563	
8.43		V		0.8665	
8.49		G		0.8734	
13.35		V		0.8697	
14.04		G		0.8571	
	1.01	G	1.0		0.8431
	1.03	V			0.8722
	1.55	V			0.8629
	2.63	V			0.8691
	3.08	G			0.8622
	4.37	V			0.8837
	4.42	G			0.8970
	5.36	G			0.8651
	5.98	V			0.8892
AVERAGE RESPONSE FACTORS			1.0	0.8670	0.8716
VALUES REPORTED BY DIETZ			1.0	0.875	0.875



TABLE B.6

## CALIBRATION OF HEWLETT PACKARD 5710A GAS CHROMATOGRAPH

CALIBRATION GASES  $\text{CO}_2, \text{C}_2\text{H}_4, \text{N}_2$ 

Mole % $\text{CO}_2$	Mole % $\text{C}_2\text{H}_4$	Preparation G=Gravimetric V=Volumetric	Response Factors		
			$\text{N}_2$	$\text{CO}_2$	$\text{C}_2\text{H}_4$
	1.0	G	1.0		0.8444
	3.75	G			0.8586
	7.78	G			0.8604
	9.98	G			0.8961
	13.62	G			0.8437
	16.09	G			0.8808
	2.03	V	1.0		0.8445
	5.00	V			0.8669
	5.03	V			0.8411
	7.48	V			0.8530
	7.52	V			0.8632
	9.55	V			0.8692
	10.27	V			0.8697
	10.60	V			0.8590
	12.31	V			0.8582
	5.24	Linde Sample			0.8773
7.04	5.99	V	1.0	0.8560	0.8431
8.06	6.21	V		0.8616	0.8420
8.95	6.98	V		0.8573	0.8443
4.31	14.03	V		0.8650	0.8718
5.58		V	1.0	0.8622	
8.77		V		0.8620	
9.51		V		0.8626	
11.33		V		0.8619	
13.97		V		0.8604	
8.02		G		0.8571	
AVERAGE RESPONSE FACTOR			1.0	0.8616	0.8593
VALUES REPORTED BY DIETZ			1.0	0.875	0.875



## APPENDIX C

### GAS CHROMATOGRAPHY ANALYSIS

All of the analyses of the reactants and products were done by gas chromatography. The principles involved in the analysis of gases using chromatography are well established now and a discussion of the fundamentals will not be presented. Three gas chromatographs were used in this study: a Gow Mac series 550, a Beckman G.C.2, and a Hewlett Packard model 5710-A. A Hewlett Packard model 7100-B strip chart recorder equipped with a Disc integrator was used to integrate the signals from the Gow Mac G.C. and also, during the integral bed tests, from the Beckman G.C. A Hewlett Packard model 3380A electronic reporting integrator analysed the signals from the Hewlett Packard G.C. and from the Beckman G.C. As well, during the integral bed runs, an on-line G.C. analysis program supported on the Department's I.B.M. 1800 computer was used to confirm the integrations performed via the Disc integrator.

#### C.1 Chromatographic Operating Conditions

The details of the operation of the three chromatographs is summarized in Table C.1. The columns for the separations were recommended by J.P. Moser. The actual operating conditions are the end result of a number of trial and error iterations, converging to a set of conditions which resulted in distinct and reproducible separations of the reaction gases.





TABLE C.1  
CHROMATOGRAPH OPERATING CONDITIONS

G.C.	COLUMN			SAMPLE VALVE		CARRIER GAS		DETECTOR		
	Length	O.D.	Packing	Temp.	Volume	Temp.	Gas	Flowrate	Current	Temp.
Gow Mac Series 550	5 ft. S.S. tube (316 seamless)	1/4"	PoraPak Q	70°C	2 Loops 1/2 c.c. each	220°C	He	1.2 cc/s @ 21°C 94 kPa	150 ma	220°C
Beckman GC-2	3 ft. s.s. tube (316 seamless)	1/4"	molecular sieve 5A	21°C (Room Temp.)	2 Loops 1/2 c.c. each	21°C (Room Temp)	He	2.4cc/s @ 21°C 94 kPa	150 ma	100°C
Hewlett Packard 5710A	2 columns 5 ft. s.s. tube 316 seamless	1/4"	PoraPak Q	70°C	2 Loops 1/2 c.c. each	200°C	He	1.05 cc/s @ 21°C 94 kPa	150 ma	200°C



## C.2 Signal Analysis

In all cases, the analyses were performed on a normalized basis. The mole fractions of the  $i$ th component in an  $n$ -component mixture was determined using equation (C.1)

$$x_i = \frac{A_i R_i}{\sum_{i=1}^n A_i R_i} \quad (C.1)$$

$A_i$  represents the area under the peak of the  $i$ th component and  $R_i$  is the response factor of the  $i$ th component. Nitrogen was selected (arbitrarily) as the reference component ( $R_i = 1.0$ ) and the remaining response factors were determined as described previously in Appendix B, section 5. Sample outputs from the three chromatographs are pictured in Figures C.1, C.2, and C.3.



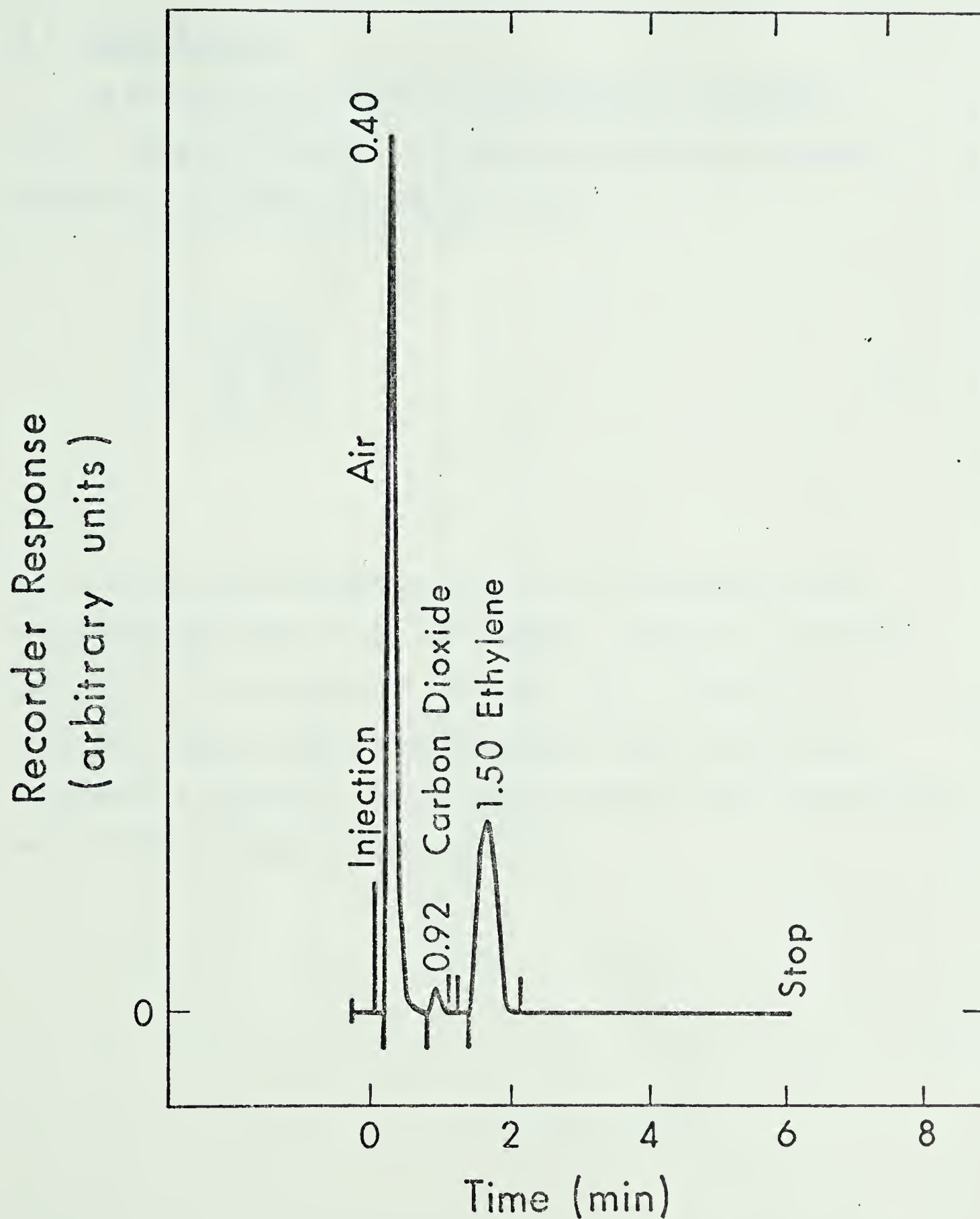


Figure C.1 : Typical output for 'air',  $\text{CO}_2$ , and  $\text{C}_2\text{H}_4$  analysis using the Hewlett Packard G.C. and an electronic reporting integrator.



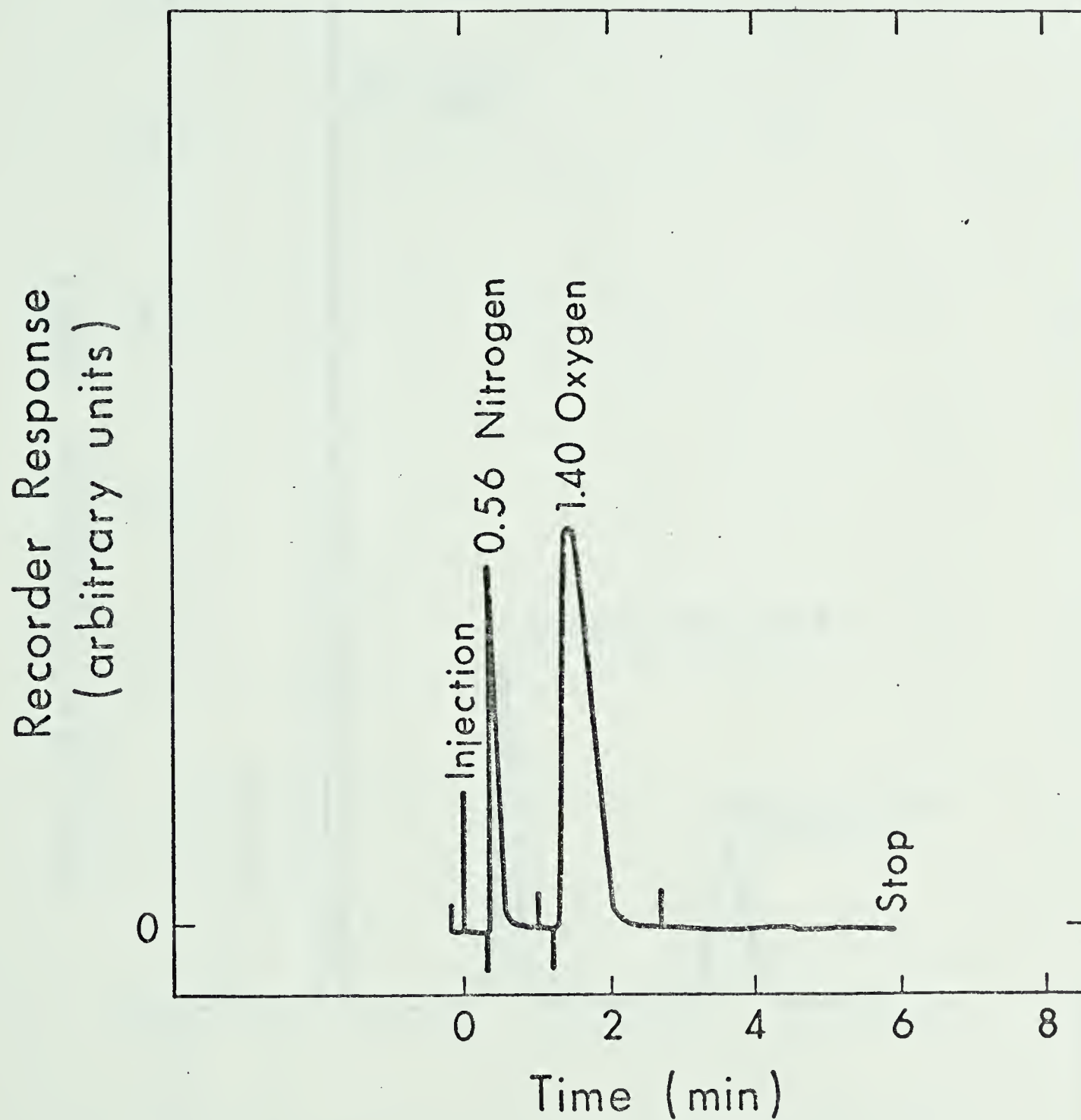


Figure C.2 : Typical output for  $N_2$  and  $O_2$  analysis using the Beckman G.C. and an electronic reporting integrator.





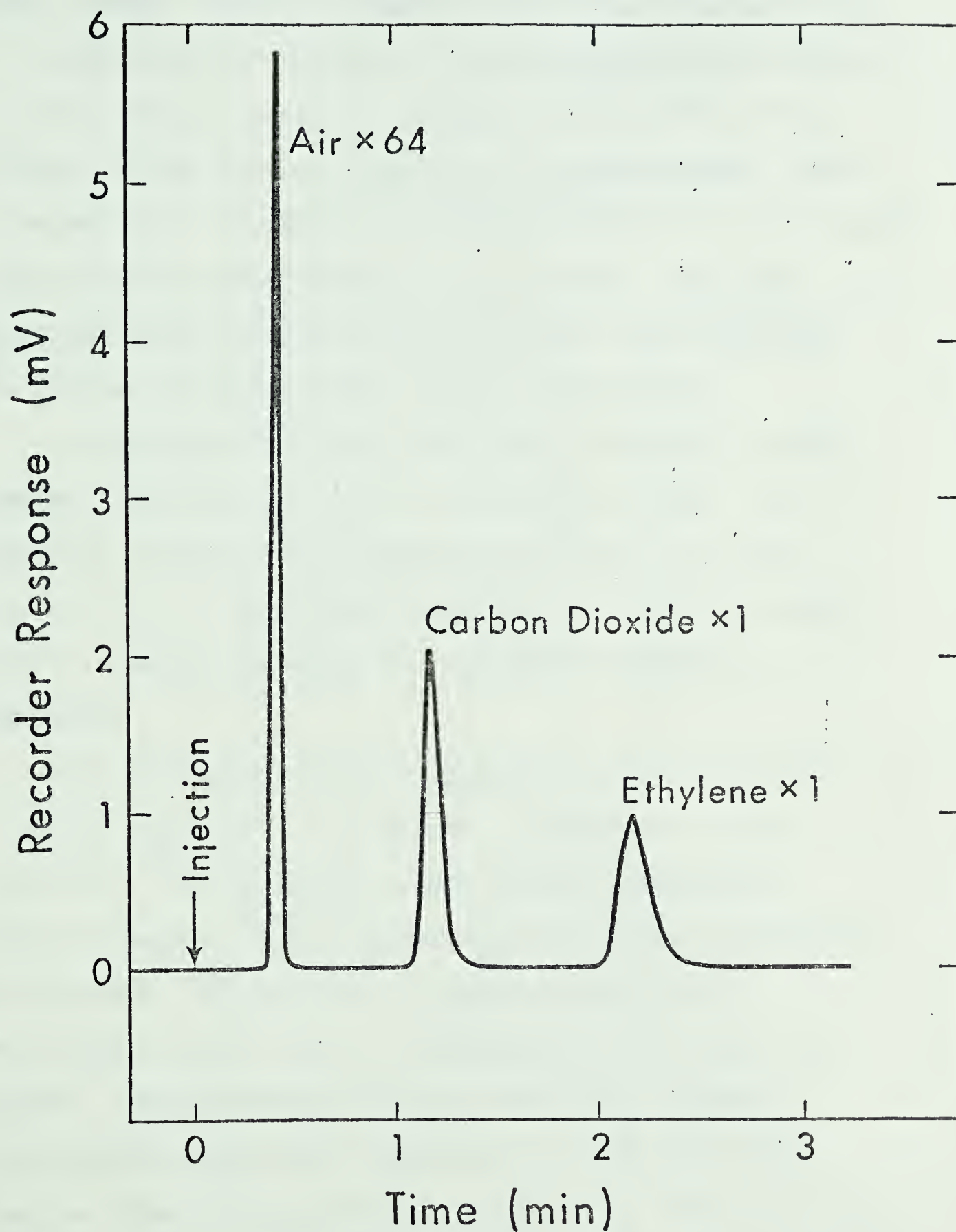


Figure C.3 : Typical output for 'air,  $\text{CO}_2$ , and  $\text{C}_2\text{H}_4$  using the Gow-Mac G.C. and a strip chart recorder.



The output depicted in Figure C.1 was recorded on the strip chart recorder; output in Figures C.2 and C.3 was recorded on the H.P. 3380A reporting integrator. The numbers printed above the peaks are the retention times of the compounds and the vertical lines delineate the area which is integrated. The chromatographic signal is automatically attenuated on a logarithmic scale to fit the recorder paper so that no manual attenuation was required. Also, the integrator output was on heat sensitive paper, thus eliminating the ink flow problems so common to many older recorders.

A comparison of the three methods (Disc integrator, on-line computer, and electronic reporting integrator) was made. The results of a test with high ethylene concentrations are given in Table C.2. The sample bomb composition was determined volumetrically. The Hewlett Packard G.C. was used to separate the components.

All three methods provided reasonably accurate measurements of the gas composition. The electronic recorder was the most consistent. A second series at lower ethylene concentration showed the weakness of the computer based system for the detection of small peaks. The on-line G.C. package required that an analog signal be sent from the chromatograph to the computer for analysis. The transmission distance (four floors) resulted in some extraneous peaks being reported due to random noise along the line. More serious problems arose due to the limitations of the analog to digital converter (ADC) however. The ADC had a sensitivity of 0.03 mv, and small signals would often be lost in the ADC noise. This problem was also encountered by Schech (C.1) who studied



TABLE C.2

## INTEGRATION COMPARISONS FOR HIGH ETHYLENE CONCENTRATIONS

Nominal Composition    48.07 % N<sub>2</sub>  
                              35.71 % C<sub>2</sub>H<sub>4</sub>  
                              16.22 % CO<sub>2</sub>

REPORTED COMPOSITIONS (%)

DISC INTEGRATOR		COMPUTER		ELECTRONIC INTEGRATOR	
CO <sub>2</sub>	C <sub>2</sub> H <sub>4</sub>	CO <sub>2</sub>	C <sub>2</sub> H <sub>4</sub>	CO <sub>2</sub>	C <sub>2</sub> H <sub>4</sub>
17.6	35.0	16.0	35.5	16.34	35.94
15.1	37.1	16.4	35.2	16.30	36.00
16.1	36.2	16.3	35.3	16.28	35.29
14.2	33.4	15.9	35.2	16.29	35.57
14.7	33.9	15.9	35.5	16.25	35.76
16.9	35.6	15.8	36.1	16.31	34.98
17.3	36.3	16.0	35.7	16.12	35.61
17.3	36.7	15.6	35.1	16.18	35.68
15.8	35.0	15.1	35.0	16.22	35.90
15.4	35.1	16.9	35.0	16.20	35.62
16.6	34.9	16.8	35.7	16.43	35.75
AVE. 16.1	35.3	16.6	35.3	16.27	35.64



the problem more thoroughly. His solution was to amplify the signal considerably prior to transmission from the chromatograph to the computer. Other possible solutions would have been to digitize the signal prior to transmission or to install a micro computer based analysis system adjacent to the chromatograph. The second alternative was the one selected. i.e. the H.P. 3380A reporting integrator was used to analyse the signals from the chromatographs. The results of the low ethylene concentration tests are shown in Table C.3.

TABLE C.3

## INTEGRATION COMPARISONS FOR LOW ETHYLENE CONCENTRATIONS

Nominal Composition: 0.40 % ethylene

99.60 % nitrogen

## Reported Compositions of Ethylene (%)

Computer		Electronic Integrator	
	0.10		0.35
	0.00		0.44
	0.00		0.46
	0.00		0.39
	0.4		0.30
	0.2		0.29
	0.00		0.38
Average	0.10		0.37







In all cases, water, which was eluted last, was not analysed. While exclusion of the water area in equation (1) will result in some error for each component, the error is quite small. For the run pictured in Figure C.2, the nitrogen peak area was 114070 (arbitrary units), the carbon dioxide area was 168, and the ethylene area was 2719. The water area would have been about 150. The percentage error in the term in the denominator of equation (C.1) is only 0.13% if the water is excluded from the total area calculation. This is considerably lower than the error inherent in the calibrations. Even for high conversion runs, the fact that only very dilute mixtures of ethylene and/or oxygen are used will render negligible the error incurred by excluding the water peak.

The water peak itself was somewhat troublesome. Each loop of the Gow Mac G.C. would give rise to a water peak which differed by up to 100% from the other loop. The water also tended to tail badly, which lengthened the analysis time considerably. While the H.P.5710 G.C. did have a temperature-programmable column oven, which could be used to sharpen the water peak, this feature was not used. The time required to cool the oven back to 70°C after heating was longer than the time required to completely elute the water. As the three analysis devices, Disc integrator, H.P. 3380A, and I.B.M. 1800 could each handle only one input at a time, the signal from the G.C. separating air, CO<sub>2</sub>, C<sub>2</sub>H<sub>4</sub> and H<sub>2</sub>O could be truncated after the C<sub>2</sub>H<sub>4</sub> peak. Then, the signal from the Beckman G.C.2 could be analysed while the tailing water peak was eluted. This procedure shortened the time required for each analysis from ten minutes to about five minutes.



APPENDIX D  
MEASURED AND CALCULATED DATA

In this Appendix, the measurements made in the integral bed reactor (IBR) and the differential recycle reactor (DRR) are tabulated. As well, some calculations of predicted fractional conversions in the integral bed reactor are tabulated here. The raw chromatographic data and the computer programs used for many of the calculations in this work are too lengthy to include here. The raw data and computer programs are contained in a separate volume available upon request from the Chemical Engineering Department, The University of Alberta.



TABLE D1

RAW DATA - EXCESS OXYGEN RUNS  
DIFFERENTIAL RECYCLE REACTOR

RUN	TEMP	ETH	OXY	O/E	RATE*10**3
	(K)	(MOL/CU. M)			(MOL/G CAT-S)
L27	362.0	0.1118	8.6319	195.74	1.247
L28	362.0	0.0444	8.6409	77.21	2.355
L19	375.0	0.1190	8.3240	69.9496	3.6800
L20	375.0	0.1960	8.3130	42.4133	2.9500
L22	375.0	0.1330	8.3260	62.6015	2.9300
L23	375.0	0.1480	8.3230	56.2365	3.1200
L24	375.0	0.2580	8.3050	32.1899	1.9700
L25	375.0	0.3470	8.2900	25.8905	1.4800
L26	375.0	0.0650	8.3280	128.1231	7.6100
L08	388.0	0.2790	8.0210	26.7491	2.5900
L11	388.0	0.2980	8.0150	26.8960	4.0800
L12	388.0	0.2320	8.0260	34.5948	5.3000
L13	388.0	0.1530	8.0360	52.5229	6.9000
L14	388.0	0.1220	8.0370	65.8770	7.7400
L16	388.0	0.1420	8.0390	56.6127	6.0400
L17	388.0	0.2970	8.0170	26.9933	2.5200
L18	388.0	0.5030	7.9820	15.8688	1.6400
L37	400.0	0.2000	7.9410	39.7050	11.4000
L39	400.0	0.2030	7.9420	39.1231	11.6000
L40	400.0	0.2300	7.8930	34.3174	9.5400
L42	400.0	0.2750	7.7870	28.3164	7.5700
L44	400.0	0.3360	7.4330	22.1220	7.3300





TABLE D2

RAW DATA - LOW OXYGEN RUNS  
DIFFERENTIAL RECYCLE REACTOR

RUN	TEMP	ETH	OXY	O/E	RATE*10**8
	(K)	(MOL/CU. M)			(MOL/G CAT-S)
M03	402.0	0.4920	1.5420	3.1341	1.7700
M04	402.0	0.4220	2.3660	5.6006	4.5300
M05	402.0	0.4650	1.8520	3.9828	3.1900
M06	417.0	0.5280	0.7000	1.3258	2.0700
M07	417.0	0.4540	1.3260	2.9207	6.7800
M08	417.0	0.3880	1.8400	4.7423	15.5000
M09	424.0	0.3560	1.5910	4.4691	24.8000
M10	424.0	0.4060	1.3090	3.2241	15.7000
M57	424.0	0.8230	0.4340	0.5273	2.4200
M58	424.0	0.7130	0.6270	0.8794	3.1700
M59	424.0	0.6930	0.8340	1.2055	6.8400
M60	424.0	0.6410	1.0500	1.6381	12.5000
M61	424.0	0.5600	1.3230	2.3625	23.5000
M62	424.0	0.5010	1.5500	3.0938	35.4000
M11	438.0	0.3560	0.9910	2.7857	20.5000
M12	438.0	0.2610	1.0510	4.0208	41.5000
M13	438.0	0.4380	0.7440	1.6986	10.7000
M14	438.0	0.4100	0.7080	1.7208	13.6000
M15	438.0	0.4650	0.4420	0.9505	5.3700
M16	438.0	0.5000	0.2770	0.5540	2.3300
M17	438.0	0.4670	0.2500	0.5353	3.8100
M18	438.0	0.2380	0.7200	3.0252	41.6000
M19	438.0	0.3280	1.0160	3.0976	27.1000
M21	438.0	0.7270	1.2750	1.7558	16.5000
M22	438.0	0.7870	0.9910	1.2592	12.0000
M23	438.0	0.8380	0.7440	0.8878	8.5400
M24	438.0	0.9040	0.3980	0.4403	3.5100
M30	438.0	0.4069	0.5524	1.3571	14.5000
M31	438.0	0.2910	0.8060	2.7698	36.1000
M32	438.0	0.8040	1.0190	1.2674	15.5000
M33	438.0	0.8100	0.7180	0.8804	9.4000
M34	438.0	0.9070	0.4500	0.4901	3.9700
M35	438.0	0.9520	0.2550	0.2679	0.6900
M36	438.0	0.7350	0.9980	1.3578	28.0000





TABLE D2 (CONT.)

RAW DATA - LOW OXYGEN RUNS

RUN	TEMP	ETH	OXY	O/E	RATE*10**8
	(K)	(MOL/CU. M)			(MOL/G CAT-S)
M37	455.0	0.6680	0.6510	0.9746	42.0000
M38	455.0	0.7610	0.6860	0.9014	25.9000
M39	455.0	0.8800	0.4310	0.4898	11.3000
M40	455.0	0.9350	0.1610	0.1722	4.9900
M41	455.0	0.8410	0.4320	0.5157	17.1000
M42	455.0	0.7230	0.6120	0.8465	33.7000
M43	455.0	0.8080	0.5100	0.6312	19.9000
M44	455.0	0.6370	0.4730	0.7425	23.9000
M45	455.0	0.7050	0.3910	0.5546	10.4000
M46	455.0	0.5390	0.5990	1.1113	34.1000
M47	455.0	0.4040	0.7160	1.7723	60.9000
M48	472.0	0.3790	0.4960	1.3087	66.0000
M49	472.0	0.7190	0.1830	0.2545	5.6700
M50	472.0	0.6840	0.2330	0.3406	12.1000
M51	472.0	0.6200	0.3320	0.5355	22.4000
M52	472.0	0.4820	0.4280	0.8880	47.7000
M53	472.0	0.5600	0.3380	0.6036	33.4000
M54	472.0	0.3260	0.4080	1.2515	83.8000
M55	472.0	0.4730	0.3720	0.7805	50.6000
M56	472.0	0.5490	0.3930	0.7158	35.2000



TABLE D3

RAW DATA - AGED CATALYST  
DIFFERENTIAL RECYCLE REACTOR

RUN	TEMP (K)	EXIT CONCENTRATIONS (MOL/CU. M)		(OX)/(ETH)	RATE*10**7 (MOL/G CAT-S)
		ETHENE	OXYGEN		
K10	353.	0.1374	9.393	69.73	0.1601
K11	353.	0.0264	9.815	371.78	0.2222
K04	361.	0.3630	8.347	22.99	0.1170
K12	361.	0.3635	8.346	22.96	0.0990
K13	361.	0.0965	9.323	96.61	0.2076
K06	371.	0.3653	8.101	22.18	0.1877
K09	371.	0.3998	7.921	19.81	0.1197
K15	388.	0.3433	7.620	22.20	0.4955
K20	388.	0.1344	8.365	62.21	0.6422
K21	388.	0.2285	8.043	35.21	0.6530
K22	388.	0.2983	7.826	26.23	0.5115
K23	388.	0.3447	7.630	22.13	0.5159
K25	388.	0.1476	8.285	55.98	0.8488
K26	388.	0.0466	8.180	175.93	2.569



TABLE D4

## BLANK RUNS - INTEGRAL BED REACTOR

RUN	TEMP (K)	INLET MOLE PERCENTS		FRACTIONAL CONVERSIONS (%)
		ETH	OXY	
B01	494.	0.135	20.	0.0
B02	587.	0.135	20.	0.0
B03	604.	0.135	20.	0.0
B04	658	0.135	20.	0.0
B05	693.	0.135	20.	0.0
B06	755.	0.135	20.	0.0
B07	792.	0.135	20.	0.1
B08	792.	0.2046	20.	1.36
B09	792.	0.8792	20.	16.24



TABLE D5  
BLANK RUNS - INTEGRAL BED REACTOR  
2. MM ALUMINA SPHERES

RUN	TEMP (K)	INLET MOLE PERCENTS		FRACTIONAL CONVERSIONS (%)
		ETHENE	OXYGEN	
C0.1	500.	0.6086	20.	0.000
C0.2	586.	0.6086	20.	0.000
C0.3	603.	0.6086	20.	0.000
C0.4	640.	0.6086	20.	3.03
C1	640.	0.0723	20.	0.1
C2	640.	0.4040	20.	2.74
C3	640.	0.9565	20.	3.63
C9	640.	0.1012	20.	0.1
C10	640.	0.9788	20.	4.73
C11	640.	2.215	20.	6.07
C5	677.	0.0512	20.	5.38
C6	677.	0.6374	20.	9.84
C12	677.	1.838	20.	14.85
C4	698.	0.621	20.	18.23
C13	698.	1.156	20.	22.80
C14	698.	0.2814	20.	13.98
C7	766.	0.6225	20.	30.06
C8	766.	0.1719	20.	24.70





TABLE D6

CATALYST PRE-TREATMENT  
INTEGRAL BED REACTOR

TREATMENT	RUN	TEMPERATURE (K)	(OX/ETH) INLET	FRACTIONAL CONVERSION (%)
NONE	E2	373.	23.26	0.08
(FRESH CATALYST)	E4	409.	23.55	100.00
	E5	377.	23.77	6.08
	E6	389.	24.20	11.97
	E7	397.	23.69	30.31
523K FOR 60 HOURS (IN FLOWING AIR)	E9	380.	24.60	20.02
	E10	391.	24.26	22.90
	E11	405.	25.39	89.83
575K FOR 12 HOURS (IN FLOWING AIR)	E12	376.	39.45	27.30
	E13	396.	41.86	100.00
	E14	398.	23.55	52.54
	E15	375.	23.97	17.89
	E26	380.	23.04	10.98
	E29	380.	24.53	20.22
	F07	375.	23.19	16.53



TABLE D7  
RAW DATA - INTEGRAL BED REACTOR

RUN	TEMP	FLOW	INLET MOLE PERCENT		CONVERSION (%)	
	(K)		ETHENE	OXYGEN	ETHENE	CO2
E02	373.	500.	0.8599	20.	5.84	0.08
E03	398.	500.	0.8025	20.	1.82	3.55
E04	409.	484.	0.8493	20.	100.00	101.00
E05	377.	476.	0.8413	20.	6.36	6.08
E06	389.	473.	0.8264	20.	11.78	12.16
E07	397.	484.	0.8441	20.	33.02	27.60
E09	380.	479.	0.8129	20.	18.22	21.81
E10	391.	474.	0.8243	20.	22.87	22.92
E11	405.	474.	0.7877	20.	87.52	92.14
E12	376.	950.	0.5070	20.	29.63	24.97
E13	396.	1000.	0.4778	20.	100.00	103.16
E14	398.	547.	0.8493	20.	56.65	48.43
E15	375.	536.	0.8343	20.	21.26	14.52
E16	375.	513.	0.6865	20.	21.52	26.38
E17	375.	478.	0.3574	20.	100.00	105.8
E18	375.	534.	0.7378	20.	19.33	15.91
E19	375.	520.	0.5497	20.	30.42	31.26
E20	375.	507.	0.4587	20.	54.47	55.84
E21	387.	416.	0.9119	20.	25.51	23.14
E22	387.	448.	0.7683	20.	47.60	46.85
E23	387.	433.	0.6636	20.	100.00	99.62
E24	398.	472.	0.9584	20.	100.00	98.94
E25	398.	500.	0.4957	20.	100.00	102.46
E26	380.	700.	0.8680	20.	10.15	11.80
E27	380.	449.	1.009	20.	12.24	14.21
E28	380.	455.	0.9213	20.	12.89	10.66
E29	380.	435.	0.8155	20.	19.61	20.83
E30	380.	426.	0.7147	20.	38.29	33.38
E31	380.	420.	0.5967	20.	54.71	50.44
E32	380.	401.	0.3924	20.	100.00	111.38
E33	375.	592.	0.7247	20.	18.46	23.00
E34	375.	572.	0.6086	20.	36.16	33.87
E35	375.	563.	0.4178	20.	100.00	103.14
E36	375.	571.	0.5296	20.	50.32	46.80
E37	375.	591.	0.6614	20.	27.42	23.34



TABLE D7 (CONT.)  
RAW DATA - INTEGRAL BED REACTOR

RUN	TEMP	FLOW	INLET MOLE PERCENT		CONVERSION	
	(K)		ETHENE	OXYGEN	ETHENE	CO2
F01	375.	598.	0.763	7.34	2.63	2.74
F02	375.	563.	0.432	6.47	6.80	5.86
F03	375.	574.	0.791	7.35	7.04	2.85
F04	375.	553.	0.554	7.69	6.06	4.18
F05	375.	554.	0.436	7.82	7.31	8.08
F06	375.	540.	0.373	8.07	18.34	15.28
F07	375.	513.	0.360	8.35	18.84	14.21
F08	375.	503.	0.251	8.26	33.11	24.45
F09	375.	493.	0.135	8.58	86.79	112.15
F10	375.	509.	0.178	8.47	43.08	50.79
F11	379.	578.	0.722	7.46	9.58	4.25
F12	379.	525.	0.613	7.55	10.20	7.18
F13	380.	555.	0.557	7.74	9.82	13.42
F14	380.	541.	0.356	8.10	36.21	36.15
F15	380.	514.	0.231	8.58	100.00	121.27
F16	380.	522.	0.295	8.30	100.00	128.34
F17	380.	529.	0.361	8.49	100.00	122.45
F18	380.	529.	0.426	8.35	100.00	110.97
F19	380.	559.	0.517	8.35	100.00	107.85
F20	380.	584.	0.684	8.35	21.81	19.50
F21	380.	571.	0.649	8.35	19.62	19.15
F22	380.	564.	0.468	8.35	8.93	32.97
F23	380.	551.	0.463	8.35	50.55	46.95
F24	380.	524.	0.305	8.35	100.00	97.44
F25	380.	502.	0.939	8.35	35.70	12.21
F26	380.	584.	0.719	8.35	15.57	18.62
F27	380.	568.	0.672	8.35	21.00	21.90
F28	380.	562.	0.625	8.35	22.88	24.31
F29	380.	554.	0.568	8.35	33.29	33.43
F30	380.	546.	0.572	8.35	24.90	26.49
F31	380.	549.	0.470	8.35	38.11	35.32
F32	380.	543.	0.422	8.35	45.41	41.12
F33	380.	537.	0.368	8.35	52.74	53.33
F34	380.	538.	0.376	8.35	78.83	62.43





TABLE D7 (CONT.)  
 RAW DATA - INTEGRAL BED REACTOR

RUN	TEMP	FLOW	INLET MOLE PERCENT		CONVERSION	
	(K)		ETHENE	OXYGEN	ETHENE	CO2
G01	380.	840.	0.6212	2.8795	1.94	4.26
G02	380.	586.	0.7407	3.0431	3.25	4.04
G03	380.	575.	0.5912	3.0028	5.95	7.52
G04	380.	557.	0.5087	2.8614	9.86	9.65
G05	380.	540.	0.4167	3.0581	16.18	18.33
G06	380.	519.	0.2612	3.4033	42.57	42.65
G07	380.	520.	0.1805	3.3434	100.00	93.94
G08	380.	529.	0.2859	3.3606	29.10	28.84
H01	380.	585.	0.8399	1.4586	2.69	2.36
H02	380.	560.	0.7584	1.4462	7.41	2.38
H03	380.	570.	0.6136	1.5254	2.04	3.25
H04	380.	551.	0.5035	1.6535	4.38	4.40
H05	380.	541.	0.4343	1.5925	3.02	6.50
H06	380.	519.	0.3470	1.6828	9.22	10.14
H07	380.	518.	0.2189	1.6471	15.79	23.42
H08	380.	509.	0.1515	1.6305	55.11	42.84
H09	380.	500.	0.0488	1.8128	100.00	117.95
H10	380.	495.	0.0482	1.7795	100.00	124.35
H11	380.	498.	0.1885	1.7115	16.04	18.03
H12	380.	523.	0.3199	1.6604	2.96	7.03
H13	380.	533.	0.4840	1.2654	1.85	3.76
H14	380.	509.	0.1133	1.8047	40.22	41.36
H15	390.	563.	0.6392	1.5387	9.11	4.67
H16	390.	535.	0.4335	1.6412	16.32	10.37





TABLE D7 (CONT.)  
 RAW DATA - INTEGRAL BED REACTOR

RUN	TEMP	FLOW	INLET MOLE PERCENT		CONVERSION	
	(K)		ETHENE	OXYGEN	ETHENE	CO2
I01	375.	575.	1.6227	4.3742	1.49	1.34
I02	375.	568.	1.6765	3.6742	0.98	0.91
I03	375.	549.	1.7269	2.8656	1.11	0.62
I04	375.	524.	1.8183	1.6886	1.24	0.18
I05	380.	690.	1.5082	5.8005	3.64	3.44
I06	380.	495.	1.6275	4.3625	3.22	1.90
I07	380.	570.	1.6847	3.2597	1.01	1.28
I08	390.	690.	1.4975	5.9245	8.48	7.92
I09	390.	584.	1.6060	4.3121	4.49	4.22
I11	375.	578.	1.2456	4.3833	1.65	1.83
I12	375.	545.	1.3147	3.1699	1.61	1.12
I13	400.	589.	1.2346	4.4271	15.05	15.60
I14	400.	557.	1.3155	3.2234	7.62	7.99
I15	400.	538.	1.3703	2.3988	5.28	4.77
I16	400.	523.	1.3970	1.5981	4.06	3.43
I17	400.	516.	1.4405	0.8472	1.19	1.23
I18	400.	573.	1.2890	3.4299	11.09	10.60
I19	400.	700.	1.2230	4.8907	19.91	18.76
I20	400.	577.	1.2993	3.3720	9.80	9.31
I21	420.	586.	1.2489	4.3403	42.83	41.88
I22	420.	560.	1.3065	3.1308	27.38	26.32
I23	420.	528.	1.3847	1.7090	11.17	10.66
I24	420.	581.	1.0552	4.1982	56.84	55.07
I25	420.	688.	0.8072	9.2426	100.00	100.33
I26	375.	501.	1.2409	0.4497	0.72	0.04
I27	375.	503.	1.1985	1.2182	0.20	0.04
I28	375.	531.	1.1681	1.8158	0.74	0.53
I29	375.	550.	1.1586	2.2415	1.85	0.67
I30	375.	495.	1.1063	3.0806	0.24	1.18
I31	375.	577.	1.0682	3.7723	0.95	2.28
I32	375.	545.	1.0486	4.2466	2.25	2.08
I33	375.	650.	0.9645	6.2202	5.58	4.18



TABLE D7 (CONT.)  
RAW DATA - INTEGRAL BED REACTOR

RUN	TEMP	FLOW	INLET MOLE PERCENT		CONVERSION	
	(K)		ETHENE	OXYGEN	ETHENE	CO2
I34	375.	720.	0.8870	7.5768	4.24	6.03
I35	375.	640.	0.7070	17.9185	100.00	96.83
I36	375.	531.	0.3152	19.4827	100.00	95.47
I37	375.	547.	0.4347	19.0351	100.00	99.68
I38	375.	568.	0.6320	18.4550	95.41	88.64
I39	375.	582.	0.7291	17.8521	34.03	30.40
I40	375.	576.	0.6242	18.2709	100.00	94.60
I41	375.	603.	0.8440	17.4754	21.12	18.43
I42	375.	500.	0.7072	17.9391	30.32	28.59
I43	375.	576.	1.1083	3.3907	2.23	1.11
I44	375.	795.	1.0070	5.0565	0.85	1.46
I45	400.	585.	1.065	4.209	19.31	16.96
I46	400.	575.	1.0756	3.8017	15.43	15.88
I47	400.	563.	1.1165	3.2512	16.18	14.30
I48	400.	590.	1.1467	2.5024	11.37	9.47
I49	400.	526.	1.1863	1.6157	7.41	6.76
I50	400.	511.	1.2109	0.9909	2.31	1.81
I51	400.	690.	0.9847	5.5578	23.13	23.12
I52	400.	580.	1.0646	4.1892	16.54	15.89
I53	400.	590.	0.8776	7.18667	100.00	102.97
I54	420.	545.	1.2400	0.2590	0.30	1.02
I55	420.	515.	1.2207	0.8866	7.04	4.45
I56	420.	534.	1.1529	1.6414	12.11	13.26
I56	420.	531.	1.1651	1.8603	19.77	18.34
I57	420.	546.	1.1025	2.5439	30.43	30.69
I58	420.	561.	1.080	3.1857	45.16	44.64
I59	420.	584.	1.0400	4.0348	59.87	57.65
I60	420.	695.	0.9980	5.5144	100.00	98.74
I61	420.	578.	1.0890	3.6404	43.68	40.85
I62	420.	544.	1.1503	2.2727	21.90	20.05
I63	440.	521.	1.2246	1.0079	13.76	11.88
I64	440.	542.	1.1653	1.9911	34.93	32.96
I65	440.	571.	1.0972	3.3984	100.00	97.33
I66	440.	530.	1.1622	1.9552	34.35	33.11



TABLE D8  
PREDICTIONS OF ISOTHERMAL MODEL -INTEGRAL BED REACTOR  
LOW ETHYLENE FLOW RATE

TEMPERATURE = 375.K  
ETHYLENE FLOW RATE = 5.110E-07 MOL/S  
RATE CONSTANT = 5.065E-10 MOL/G CAT-S  
TOTAL FLOW RATE = 509. SCCM

MOLE FRACTIONS (%)		(OXY/ETH)	FRACTIONAL CONVERSION	FUNCTION VALUE
ETHENE	OXYGEN			
0.135	1.600	11.852	0.174	-1.535E-09
0.135	1.800	13.333	0.198	-4.066E-08
0.135	2.000	14.815	0.223	-1.184E-09
0.135	2.200	16.296	0.249	-2.426E-10
0.135	2.400	17.778	0.276	3.936E-08
0.135	2.600	19.259	0.304	-1.708E-09
0.135	2.800	20.741	0.333	-1.620E-09
0.135	3.000	22.222	0.363	6.510E-08
0.135	3.200	23.704	0.395	-5.160E-08
0.135	3.400	25.185	0.428	-1.412E-09
0.135	3.600	26.667	0.464	-2.296E-08
0.135	3.800	28.148	0.502	-2.546E-08
0.135	4.000	29.630	0.543	3.930E-09
0.135	4.200	31.111	0.588	5.161E-08
0.135	4.400	32.592	0.639	1.250E-08
0.135	4.600	34.074	0.697	4.029E-12
0.135	4.800	35.555	0.771	-3.122E-10
0.135	5.000	37.037	0.883	6.545E-08

COMPLETE CONVERSION AT O2/ETH = 37.778





TABLE D9  
PREDICTIONS OF ISOTHERMAL MODEL - INTEGRAL BED REACTOR  
HIGH ETHYLENE FLOW RATE

TEMPERATURE = 375.K  
ETHYLENE FLOW RATE = 1.514E-06 MOL/S  
RATE CONSTANT = 5.065E-10 MOL/G CAT-S  
TOTAL FLOW RATE = 509. SCCM

MOLE FRACTIONS (%)		(OXY/ETH)	FRACTIONAL	FUNCTION
ETHENE	OXYGEN		CONVERSION	VALUE
0.400	1.500	3.750	0.017	-8.227E-10
0.400	3.500	8.750	0.041	2.722E-09
0.400	5.500	13.750	0.065	1.477E-10
0.400	7.500	18.750	0.090	-6.633E-11
0.400	9.500	23.750	0.116	-1.092E-09
0.400	11.500	28.750	0.142	-5.604E-11
0.400	13.500	33.750	0.169	1.516E-09
0.400	15.500	38.750	0.197	-5.889E-10
0.400	17.500	43.750	0.226	-1.570E-10
0.400	19.500	48.750	0.256	-4.011E-08
0.400	21.500	53.750	0.288	-4.811E-10
0.400	23.500	58.750	0.321	-2.205E-10
0.400	25.500	63.750	0.355	-1.993E-08
0.400	27.500	68.750	0.392	-2.875E-11
0.400	29.500	73.750	0.430	4.412E-08
0.400	31.500	78.750	0.472	8.437E-08
0.400	33.500	83.750	0.517	-4.005E-08
0.400	35.500	88.750	0.567	-2.484E-11
0.400	37.500	93.750	0.624	6.213E-09
0.400	39.500	98.750	0.690	7.253E-08
0.400	41.500	103.750	0.775	-1.304E-10
0.400	43.500	108.750	0.929	-3.311E-08

COMPLETE CONVERSION AT O2/ETH = 109.021





TABLE D10  
PREDICTIONS OF ISOTHERMAL MODEL - INTEGRAL BED REACTOR  
LOW ETHYLENE FLOW RATE

TEMPERATURE = 440.K  
ETHYLENE FLOW RATE = 5.180E-06 MOL/S  
RATE CONSTANT = 1.135E-07 MOL/G CAT-S  
TOTAL FLOW RATE = 571. SCCM

MOLE FRACTIONS (%)		(OXY/ETH)	FRACTIONAL CONVERSION	FUNCTION VALUE
ETHENE	OXYGEN			
1.220	0.600	0.492	0.101	-5.290E-08
1.220	0.700	0.574	0.119	-3.456E-08
1.220	0.800	0.656	0.137	-4.713E-08
1.220	0.900	0.738	0.155	-1.389E-07
1.220	1.000	0.820	0.174	-8.311E-08
1.220	1.100	0.902	0.192	-8.205E-08
1.220	1.200	0.984	0.211	-1.413E-07
1.220	1.300	1.066	0.231	-6.998E-08
1.220	1.400	1.148	0.250	-1.058E-07
1.220	1.500	1.230	0.270	-6.468E-08
1.220	1.600	1.311	0.291	-9.624E-09
1.220	1.700	1.393	0.312	-7.293E-09
1.220	1.800	1.475	0.333	-7.276E-09
1.220	1.900	1.557	0.355	-2.018E-07
1.220	2.000	1.639	0.377	-2.811E-08
1.220	2.100	1.721	0.399	-3.592E-08
1.220	2.200	1.803	0.423	-1.642E-07
1.220	2.300	1.885	0.446	-2.932E-08
1.220	2.400	1.967	0.471	-3.919E-08
1.220	2.500	2.049	0.496	1.758E-07
1.220	2.600	2.131	0.522	1.011E-07
1.220	2.700	2.213	0.549	6.030E-08
1.220	2.800	2.295	0.577	-1.561E-08
1.220	2.900	2.377	0.606	-3.695E-08
1.220	3.000	2.459	0.637	-1.094E-08
1.220	3.100	2.541	0.669	-7.905E-08
1.220	3.200	2.623	0.702	2.428E-08
1.220	3.300	2.705	0.739	-1.630E-08
1.220	3.400	2.787	0.778	-4.973E-08
1.220	3.500	2.869	0.821	-6.087E-09
1.220	3.600	2.951	0.871	1.753E-08
1.220	3.700	3.033	0.935	2.650E-08

COMPLETE CONVERSION AT O2/ETH = 3.115



TABLE D11  
PREDICTIONS OF ISOTHERMAL MODEL - INTEGRAL BED REACTOR  
LOW ETHYLENE FLOW RATE

TEMPERATURE = 420.K  
ETHYLENE FLOW RATE = 3.822E-06 MOL/S  
RATE CONSTANT = 2.566E-08 MOL/G CAT-S  
TOTAL FLOW RATE = 515. SCCM

MOLE FRACTIONS (%)		(OXY/ETH)	FRACTIONAL	FUNCTION
ETHENE	OXYGEN		CONVERSION	VALUE
0.998	0.900	0.902	0.076	-1.608E-08
0.998	1.200	1.202	0.102	-1.184E-09
0.998	1.500	1.503	0.129	-6.578E-09
0.998	1.800	1.804	0.157	-2.016E-08
0.998	2.100	2.104	0.186	-2.213E-08
0.998	2.400	2.405	0.216	1.382E-09
0.998	2.700	2.705	0.247	1.387E-08
0.998	3.000	3.006	0.279	1.061E-08
0.998	3.300	3.307	0.312	-4.288E-10
0.998	3.600	3.607	0.347	-1.283E-08
0.998	3.900	3.908	0.383	-4.198E-09
0.998	4.200	4.208	0.422	-1.470E-08
0.998	4.500	4.509	0.463	-1.980E-08
0.998	4.800	4.810	0.508	-2.468E-08
0.998	5.100	5.110	0.556	-1.413E-08
0.998	5.400	5.411	0.609	2.933E-08
0.998	5.700	5.711	0.670	-3.523E-08
0.998	6.000	6.012	0.743	1.122E-11
0.998	6.300	6.313	0.844	-3.991E-09

COMPLETE CONVERSION AT O2/ETH = 6.613



TABLE D12  
PREDICTIONS OF ISOTHERMAL MODEL - INTEGRAL BED REACTOR  
LOW ETHYLENE FLOW RATE

TEMPERATURE = 400.K  
ETHYLENE FLOW RATE = 2.280E-06 MOL/S  
RATE CONSTANT = 5.000E-09 MOL/G CAT-S  
TOTAL FLOW RATE = 511. SCCM

MOLE FRACTIONS (%)		(OXY/ETH)	FRACTIONAL CONVERSION	FUNCTION VALUE
ETHENE	OXYGEN			
0.600	1.100	1.833	0.054	-1.056E-09
0.600	1.600	2.667	0.080	-2.257E-08
0.600	2.100	3.500	0.107	-1.804E-08
0.600	2.600	4.333	0.134	-4.254E-09
0.600	3.100	5.167	0.162	-8.469E-09
0.600	3.600	6.000	0.191	-2.268E-08
0.600	4.100	6.833	0.222	-3.134E-09
0.600	4.600	7.667	0.253	-4.448E-09
0.600	5.100	8.500	0.286	3.889E-08
0.600	5.600	9.333	0.320	-4.608E-10
0.600	6.100	10.167	0.356	3.393E-08
0.600	6.600	11.000	0.394	-2.578E-08
0.600	7.100	11.833	0.434	1.272E-08
0.600	7.600	12.667	0.478	1.253E-08
0.600	8.100	13.500	0.525	-3.881E-08
0.600	8.600	14.333	0.577	-6.534E-09
0.600	9.100	15.167	0.637	1.922E-09
0.600	9.600	16.000	0.708	4.900E-09
0.600	10.100	16.833	0.802	-2.772E-08
0.600	10.600	17.667	1.037	-2.562E-04
0.600	11.100	18.500	0.742	-3.725E-03

COMPLETE CONVERSION AT O2/ETH = 19.333





TABLE D13  
PREDICTIONS OF ISOTHERMAL MODEL - INTEGRAL BED REACTOR  
LOW ETHYLENE FLOW RATE

TEMPERATURE = 380.K  
ETHYLENE FLOW RATE = 1.484E-06 MOL/S  
RATE CONSTANT = 8.202E-10 MOL/G CAT-S  
TOTAL FLOW RATE = 509. SCCM

MOLE FRACTIONS (%)		(OXY/ETH)	FRACTIONAL CONVERSION	FUNCTION VALUE
ETHENE	OXYGEN			
0.392	1.600	4.082	0.031	-2.679E-09
0.392	2.600	6.633	0.051	-2.459E-09
0.392	3.600	9.184	0.072	-5.591E-10
0.392	4.600	11.735	0.093	-1.899E-09
0.392	5.600	14.286	0.114	-1.774E-09
0.392	6.600	16.837	0.136	-1.788E-10
0.392	7.600	19.388	0.159	-2.994E-09
0.392	8.600	21.939	0.182	-2.510E-09
0.392	9.600	24.490	0.206	-4.124E-08
0.392	10.600	27.041	0.230	1.829E-08
0.392	11.600	29.592	0.256	3.965E-08
0.392	12.600	32.143	0.282	-1.122E-09
0.392	13.600	34.694	0.309	-3.979E-08
0.392	14.600	37.245	0.337	2.668E-08
0.392	15.600	39.796	0.367	-8.848E-08
0.392	16.600	42.347	0.398	5.062E-10
0.392	17.600	44.898	0.431	-5.829E-11
0.392	18.600	47.449	0.466	-4.573E-08
0.392	19.600	50.000	0.503	5.250E-08
0.392	20.600	52.551	0.543	-2.995E-11
0.392	21.600	55.102	0.587	6.503E-08
0.392	22.600	57.653	0.636	-4.588E-08
0.392	23.600	60.204	0.693	-7.225E-08
0.392	24.600	62.755	0.762	-3.292E-08
0.392	25.600	65.306	0.864	-1.326E-08
0.392	26.600	67.857	0.934	-1.800E-03

COMPLETE CONVERSION AT O2/ETH = 70.408





TABLE D14

MEASURED AND PREDICTED FRACTIONAL CONVERSIONS  
INTEGRAL BED REACTOR

RUN	TEMP	FRACTIONAL CONVERSIONS					
		MEA- SURED	ISO- THERMAL	HOMOGENOUS (HW*10**3)	NONISOTHERMAL HOMOGENOUS (HW*10**3)	HETEROGENOUS (HW*10**3)	
				15.0	8.234	1.115	8.234 1.115
F01	375.	2.69	1.996	2.028	2.038	2.185	2.065 2.217
F02	375.	6.33	5.930	6.050	6.101	6.886	6.232 7.078
F03	375.	4.94	1.937	1.967	1.977	2.115	2.002 2.145
F04	375.	5.12	4.333	4.417	4.451	4.964	4.537 5.086
F05	375.	7.69	7.198	7.360	7.436	8.669	7.633 8.993
F06	375.	16.81	10.585	10.859	11.001	13.512	11.376 14.257
F07	375.	16.52	12.493	12.839	13.024	16.475	13.514 17.578
F08	375.	28.78	28.172	29.356	30.122	100.000	32.310 100.000
F09	375.	99.47	100.000	100.000	100.000	100.000	100.000 100.000
F10	375.	46.93	82.000	100.000	100.000	100.000	100.000 100.000
F11	379.	4.25	3.469	3.538	3.566	4.006	3.640 4.113
F12	379.	8.69	5.407	5.527	5.582	6.479	5.726 6.710
F13	380.	7.18	7.039	7.217	7.309	8.900	7.548 9.362
F14	380.	36.18	19.697	20.489	21.006	39.154	22.464 100.000
F15	380.	100.00	73.420	100.000	100.000	100.000	100.000 100.000
F16	380.	100.00	32.705	34.552	35.904	100.000	40.213 100.000
F17	380.	100.00	20.638	21.501	22.069	48.022	23.690 100.000
F18	380.	100.00	14.094	14.570	14.863	21.639	15.655 25.153
F19	380.	100.00	8.828	9.077	9.215	11.814	9.583 12.678
F20	380.	20.65	4.737	4.846	4.898	5.752	5.035 5.981
F21	380.	19.38	5.398	5.526	5.590	6.651	5.756 6.943
F22	380.	20.95	10.779	11.111	11.304	15.210	11.820 16.715



TABLE D14 (CONT.)  
MEASURED AND PREDICTED FRACTIONAL CONVERSIONS  
INTEGRAL BED REACTOR

RUN	TEMP	FRACTIONAL CONVERSIONS					
		MEA- SURED	ISO- THERMAL	NONISOTHERMAL			
				HOMOGENEOUS (HW*10**3)	HETEROGENEOUS (HW*10**3)		
				15.0	8.234	1.115	8.234 1.115
F23	380.	48.75	11.300	11.653	11.859	16.107	12.410 17.790
F24	380.	100.00	30.239	31.851	33.009	100.000	36.592 100.000
F25	380.	23.96	2.900	2.955	2.977	3.325	3.035 3.406
F26	380.	17.10	4.278	4.374	4.418	5.134	4.534 5.322
F27	380.	21.45	5.053	5.171	5.227	6.170	5.376 6.425
F28	380.	23.60	5.927	6.073	6.145	7.389	6.337 7.739
F29	380.	33.36	7.327	7.520	7.621	9.436	7.889 9.984
F30	380.	25.70	7.331	7.523	7.623	9.425	7.890 9.966
F31	380.	36.71	10.989	11.328	11.524	15.519	12.049 17.056
F32	380.	43.26	13.986	14.461	14.755	21.551	15.549 25.141
F33	380.	53.04	19.086	19.846	20.343	37.184	21.734 100.000
F34	380.	70.63	18.161	18.865	19.322	33.342	20.591 100.000
G01	380.	3.10	1.356	1.375	1.380	1.447	1.394 1.463
G02	380.	3.65	1.444	1.464	1.469	1.536	1.481 1.550
G03	380.	6.73	2.285	2.319	2.329	2.465	2.354 2.495
G04	380.	9.76	3.044	3.091	3.106	3.312	3.143 3.357
G05	380.	17.26	5.041	5.129	5.162	5.639	5.244 5.748
G06	380.	42.61	15.589	15.992	16.200	19.843	16.742 20.922
G07	380.	100.00	35.548	37.014	37.935	100.000	40.573 100.000
G08	380.	28.97	12.417	12.711	12.852	15.221	13.222 15.866
H01	380.	2.52	0.537	0.543	0.544	0.554	0.546 0.556
H02	380.	4.90	0.682	0.690	0.691	0.705	0.694 0.708



TABLE D14 (CONT.)  
MEASURED AND PREDICTED FRACTIONAL CONVERSIONS  
INTEGRAL BED REACTOR

RUN	TEMP	FRACTIONAL CONVERSIONS					
		MEA- SURED	ISO- THERMAL	HOMOGENOUS (HW*10**3)	NONISOTHERMAL HOMOGENOUS (HW*10**3)	HETEROGENOUS (HW*10**3)	
				15.0	8.234	1.115	8.234 1.115
H03	380.	2.65	1.081	1.094	1.096	1.125	1.102 1.131
H04	380.	4.39	1.803	1.827	1.832	1.898	1.844 1.912
H05	380.	4.76	2.381	2.413	2.420	2.519	2.438 2.540
H06	380.	9.68	4.132	4.193	4.210	4.450	4.253 4.501
H07	380.	19.60	10.438	10.628	10.700	11.773	10.883 12.021
H08	380.	48.98	23.290	23.860	24.130	28.684	24.834 29.954
H09	380.	100.00	100.000	100.000	100.000	100.000	100.000 100.000
H10	380.	100.00	100.000	100.000	100.000	100.000	100.000 100.000
H11	380.	17.04	15.563	15.886	16.023	18.191	16.380 18.723
H12	380.	4.99	4.771	4.844	4.865	5.165	4.918 5.230
H13	380.	2.81	1.541	1.560	1.563	1.608	1.571 1.617
H14	380.	40.79	55.481	58.287	60.104	100.000	65.926 100.000
H15	390.	6.89	2.565	2.604	2.616	2.791	2.648 2.829
H16	390.	13.35	6.322	6.442	6.492	7.255	6.620 7.436
I01	375.	1.41	0.271	0.275	0.275	0.280	0.276 0.281
I02	375.	0.94	0.216	0.219	0.219	0.222	0.220 0.223
I03	375.	0.87	0.164	0.166	0.166	0.168	0.167 0.169
I04	375.	0.71	0.091	0.092	0.092	0.093	0.093 0.093
I05	380.	3.54	0.563	0.571	0.572	0.596	0.577 0.601
I06	380.	2.56	0.506	0.512	0.514	0.529	0.516 0.532
I07	380.	1.15	0.307	0.310	0.311	0.317	0.312 0.318
I08	390.	8.20	1.475	1.504	1.516	1.692	1.547 1.736





TABLE D14 (CONT.)  
MEASURED AND PREDICTED FRACTIONAL CONVERSIONS  
INTEGRAL BED REACTOR

RUN	TEMP	FRACTIONAL CONVERSIONS					
		MEA- SURED	ISO- THERMAL	NONISOTHERMAL			
				HOMOGENOUS (HW*10**3)	HETEROGENOUS (HW*10**3)		
				15.0	8.234	1.115	8.234
							1.115
I09	390.	4.35	1.100	1.118	1.124	1.209	1.139
I11	375.	1.74	0.460	0.465	0.466	0.477	0.468
I12	375.	1.36	0.316	0.320	0.320	0.325	0.321
I13	400.	15.32	4.593	4.733	4.815	6.487	5.037
I14	400.	7.81	3.092	3.164	3.200	3.807	3.295
I15	400.	5.02	2.186	2.227	2.245	2.518	2.291
I16	400.	3.74	1.436	1.458	1.465	1.573	1.484
I17	400.	1.21	0.723	0.732	0.734	0.760	0.739
I18	400.	10.85	3.336	3.418	3.460	4.197	3.572
I19	400.	19.34	4.359	4.502	4.590	6.450	4.831
I20	400.	9.56	3.204	3.281	3.321	4.002	3.426
I21	420.	42.35	23.031	25.803	28.668	100.000	100.000
I22	420.	26.85	15.259	16.397	17.372	100.000	20.786
I23	420.	10.91	7.570	7.860	8.057	14.302	8.608
I24	420.	55.96	32.457	37.429	43.364	100.000	100.000
I25	420.	100.00	100.000	100.000	100.000	100.000	100.000
I26	375.	0.38	0.055	0.055	0.055	0.055	0.055
I27	375.	0.12	0.158	0.160	0.160	0.161	0.161
I28	375.	0.63	0.235	0.238	0.238	0.240	0.238
I29	375.	1.26	0.285	0.288	0.289	0.292	0.289
I30	375.	0.71	0.478	0.483	0.484	0.493	0.486





TABLE D14 (CONT.)  
MEASURED AND PREDICTED FRACTIONAL CONVERSIONS  
INTEGRAL BED REACTOR

RUN	TEMP	FRACTIONAL CONVERSIONS				
		MEAS- URED	ISO- THERMAL	HOMOGENOUS (HW*10**3)	NONISOTHERMAL HOMOGENOUS (HW*10**3)	HETEROGENOUS (HW*10**3)
				15.0	8.234	1.115
					8.234	1.115
I31	375.	1.61	0.539	0.545	0.546	0.549
I32	375.	2.16	0.667	0.675	0.676	0.680
I33	375.	4.88	0.970	0.983	0.986	0.995
I34	375.	5.14	1.262	1.282	1.288	1.302
I35	375.	100.00	5.394	5.543	5.625	5.840
I36	375.	100.00	44.102	48.300	52.160	100.000
I37	375.	100.00	19.009	19.913	20.542	22.398
I38	375.	92.02	7.930	8.177	8.321	8.708
I39	375.	32.21	5.560	5.711	5.791	6.006
I40	375.	100.00	7.937	8.185	8.329	8.718
I41	375.	19.77	3.889	3.983	4.029	4.151
I42	375.	29.46	6.958	7.152	7.260	7.554
I43	375.	1.67	0.451	0.456	0.456	0.458
I44	375.	1.15	0.590	0.598	0.600	0.603
I45	400.	18.13	5.930	6.124	6.243	6.568
I46	400.	15.65	5.325	5.485	5.580	5.832
I47	400.	15.24	4.296	4.408	4.468	4.629
I48	400.	10.42	2.976	3.040	3.071	3.151
I49	400.	7.09	2.000	2.034	2.047	2.078
I50	400.	2.06	1.207	1.224	1.228	1.239



TABLE D14 (CONT.)

MEASURED AND PREDICTED FRACTIONAL CONVERSIONS  
INTEGRAL BED REACTOR

RUN	TEMP	FRACTIONAL CONVERSIONS							
		MEA- SURED	ISO- THERMAL	NONISOTHERMAL				HETEROGENOUS (HW*10**3)	
				HOMOGENOUS (HW*10**3)					
				15.0	8.234	1.115	8.234	1.115	
I51	400.	23.13	7.857	8.205	8.447	21.208	9.151	100.000	
I52	400.	16.21	5.957	6.151	6.271	8.917	6.596	10.111	
I53	400.	100.00	15.463	16.481	17.302	100.000	20.039	100.000	
I54	420.	0.66	1.335	1.352	1.357	1.424	1.369	1.439	
I55	420.	5.74	5.038	5.161	5.231	6.470	5.411	6.821	
I56	420.	12.69	10.320	10.759	11.072	28.857	11.961	100.000	
I56	420.	19.05	11.596	12.147	12.556	100.000	13.747	100.000	
I57	420.	30.56	17.695	18.942	19.990	53.223	23.527	100.000	
I58	420.	44.90	23.128	25.351	27.436	100.000	36.450	100.000	
I59	420.	58.76	31.793	36.456	41.858	100.000	100.000	100.000	
I60	420.	100.00	42.944	56.474	100.000	100.000	100.000	100.000	
I61	420.	42.26	25.691	28.639	31.620	100.000	50.094	100.000	
I62	420.	20.98	14.403	15.258	15.938	100.000	18.066	100.000	
I63	440.	12.82	18.403	19.160	19.732	100.000	21.255	100.000	
I64	440.	33.95	42.122	45.921	49.067	100.000	100.000	100.000	
I65	440.	100.00	100.000	100.000	100.000	27.435	100.000	100.000	
I66	440.	33.73	41.967	45.540	48.460	100.000	100.000	100.000	



TABLE D15  
DISPERSION EXPERIMENTS  
RAW AND CALCULATED DATA

---

Q2 TREATED RUNS    P,Q,T,V,W  
H2 TREATED RUNS    R,S,U  
UNTREATED RUNS    0

---

RUN	TEMP	DISP	OX/ETH	RATE ETH	RATE CO2	AVE CONV
Q01	385.	0.220	1.734	0.630E-07	0.109E-06	0.0392
Q02	385.	0.220	1.625	0.102E-06	0.747E-07	0.0389
Q03	385.	0.220	2.713	0.971E-07	0.102E-06	0.0441
Q04	385.	0.220	3.777	0.974E-07	0.114E-06	0.0476
Q05	385.	0.220	0.924	0.000E 00	0.282E-07	0.0079
Q06	410.	0.220	0.973	0.908E-07	0.758E-07	0.0373
Q07	410.	0.220	1.450	0.929E-07	0.952E-07	0.0426
Q08	410.	0.220	2.022	0.133E-06	0.123E-06	0.0583
Q09	410.	0.220	2.802	0.126E-06	0.166E-06	0.0678
Q10	410.	0.220	3.942	0.176E-06	0.207E-06	0.0965
P03	410.	0.036	2.051	0.272E-07	0.359E-07	0.0124
P04	425.	0.036	2.028	0.370E-07	0.481E-07	0.0164
P05	425.	0.036	3.393	0.760E-07	0.895E-07	0.0319
Q01	410.	0.115	1.965	0.223E-07	0.701E-07	0.0190
Q02	410.	0.115	3.309	0.815E-07	0.785E-07	0.0320
Q03	410.	0.115	1.387	0.000E 00	0.378E-07	0.0075
Q04	410.	0.115	0.700	0.648E-07	0.618E-08	0.0013
Q05	425.	0.115	1.898	0.697E-07	0.891E-07	0.0307
Q06	425.	0.115	2.184	0.174E-07	0.637E-07	0.0188

---





TABLE D15 (CONT)  
DISPERSION EXPERIMENTS  
RAW AND CALCULATED DATA

O2 TREATED RUNS P,Q,T,V,W  
H2 TREATED RUNS R,S,U  
UNTREATED RUNS O

RUN	TEMP	DISP	OX/ETH	RATE ETH	RATE CO2	AVE CONV
R06	385.	0.120	1.595	0.111E-07	0.000E 00	0.0028
R07	385.	0.120	4.405	0.454E-07	0.506E-07	0.0279
R08	385.	0.120	10.635	0.165E-06	0.889E-07	0.0782
R09	410.	0.120	0.822	0.438E-07	0.183E-06	0.0153
R10	410.	0.120	2.087	0.385E-07	0.582E-07	0.0240
R11	410.	0.120	3.480	0.127E-06	0.110E-06	0.0579
R15	425.	0.120	2.338	0.168E-06	0.770E-07	0.0677
R16	425.	0.120	4.517	0.250E-06	0.243E-06	0.1407
S01	425.	0.155	1.461	0.790E-07	0.662E-07	0.0402
S02	425.	0.155	2.217	0.143E-06	0.118E-06	0.0698
S03	425.	0.155	3.055	0.235E-06	0.199E-06	0.1102
S06	425.	0.155	1.977	0.647E-07	0.117E-06	0.0469
S07	425.	0.155	1.457	0.740E-07	0.767E-07	0.0384
S13	410.	0.155	4.246	0.125E-06	0.864E-07	0.0601
S14	385.	0.155	4.101	0.000E 00	0.182E-07	0.0052
S18	410.	0.155	2.146	0.000E 00	0.472E-07	0.0127
T01	410.	0.170	2.071	0.409E-07	0.428E-07	0.0199
T02	410.	0.170	1.749	0.628E-07	0.268E-07	0.0239
T03	410.	0.170	0.844	0.277E-07	0.181E-07	0.0118
T04	410.	0.170	4.007	0.712E-07	0.183E-07	0.0254
T13	425.	0.170	2.243	0.115E-06	0.407E-07	0.0254
T14	425.	0.170	3.783	0.969E-07	0.649E-07	0.0278
T15	425.	0.170	3.582	0.986E-07	0.988E-07	0.0325





TABLE D15 (CONT)  
DISPERSION EXPERIMENTS  
RAW AND CALCULATED DATA

---

O2 TREATED RUNS    P,Q,T,V,W  
H2 TREATED RUNS    R,S,U  
UNTREATED RUNS    O

---

RUN	TEMP	DISP	OX/ETH	RATE ETH	RATE CO2	AVE CONV
<hr/>						
U01	385.	0.220	1.368	0.355E-07	0.264E-07	0.0096
U02	385.	0.220	2.852	0.460E-07	0.298E-07	0.0131
U03	385.	0.220	4.936	0.943E-07	0.696E-07	0.0300
U05	410.	0.220	0.873	0.000E 00	0.327E-07	0.0052
U06	410.	0.220	1.628	0.000E 00	0.439E-07	0.0074
U07	410.	0.220	2.702	0.344E-07	0.104E-06	0.0243
U08	410.	0.220	4.288	0.217E-06	0.153E-06	0.0623
U09	410.	0.220	2.374	0.566E-07	0.818E-07	0.0257
U10	425.	0.220	1.264	0.112E-06	0.973E-07	0.0332
U11	425.	0.220	2.168	0.201E-06	0.178E-06	0.0652
U13	425.	0.220	2.361	0.164E-06	0.169E-06	0.0586
V01	410.	0.260	2.145	0.000E 00	0.589E-07	0.0099
V02	410.	0.260	1.485	0.776E-07	0.442E-07	0.0200
V03	410.	0.260	3.960	0.750E-07	0.799E-07	0.0271
V09	425.	0.260	9.347	0.179E-06	0.139E-06	0.4353
V10	385.	0.260	8.205	0.391E-07	0.238E-07	0.0126
W03	410.	0.320	2.223	0.793E-07	0.547E-07	0.0267
W04	410.	0.320	4.510	0.128E-06	0.111E-06	0.0492
W06	425.	0.320	3.184	0.250E-06	0.156E-06	0.0797
W07	425.	0.320	2.126	0.112E-06	0.111E-06	0.0450
W08	425.	0.320	1.680	0.815E-07	0.726E-07	0.0307

---



TABLE D16  
TEMPERATURE NORMALIZED RATE CONSTANTS

---

SERIES	DISPERSION	RATE CONSTANTS *10**8 (MOL/G CAT-S)			ACTIVATION ENERGIES (KJ/MOL)
		385 K	410 K	425 K	

---

D	(0.22)	3.427	5.7049		26.75
P	0.036		1.7504	2.568	37.00
Q	0.155		2.3646	3.6818	42.74
R	0.12	1.1787	3.0214	5.0087	49.20
S	0.155	0.4438	2.0683	5.8417	86.79
T	0.17		1.8153	2.7818	41.21
U	0.22	1.3519	3.5447	5.9132	50.21
V	0.26	0.4765	2.2605		81.69
W	0.32	0.5185	2.4611	4.8893	76.93
AVERAGE ACTIVATION ENERGY					54.72

---



## APPENDIX E

### ERROR ANALYSIS AND DATA REPRODUCIBILITY

In this Appendix, the significance of the experimental errors on the measured rates of reaction will be considered. In most cases, the precision and accuracy of physical measurements is considerably greater than the reproducibility of the measured rates of reaction. The reproducibility of the measured rates was at times excellent and at times very poor (compared with the errors estimated in the measurements).

#### E.1 Errors in Temperature Measurement

Errors in the temperature used for each run arise from a number of sources. There is an error inherent in the thermocouple and recorder, a difference between the catalyst bed temperature and the bath temperature, a difference between the temperature recorded by the thermocouple in the middle of the bed and the one near the top of the bed and a difference between the temperature of the bulk gas in the reactor and the temperature on the catalyst surface.

Errors attributable to inaccuracies in the thermocouple and recorder are certainly small. For the iron-constantan thermocouples the difference between the measured and actual temperature was probably less than  $0.1^{\circ}\text{C}$ . The strip chart recorder was regularly calibrated and adjusted, and the error in the voltage measurement was less than  $0.05\text{ mv}$ . The strip chart could be read to an accuracy of  $\pm 0.03\text{ mv}$ . The voltage differences were converted to Kelvins using standard conversion tables. Considering all of these factors, the temperatures measured were probably in error by no more than  $0.5^{\circ}\text{C}$ .





The measured temperatures were then corrected using the calibration curves shown in Appendix B.1.

The possibility that heat transfer limitations could affect the study were discussed previously in Appendix A. The maximum difference between the pellet surface and the bulk gas was calculated at 6 K, however the upper limit on this temperature difference for most of the runs was likely around 1.6 K. As well, since the exact position of the thermocouple tips could not be determined, (i.e. they could be touching a glass bead, a catalyst pellet, or in the bulk gas) the upper bound on the difference between the temperature measured and the temperature of the reaction may well be less than 1.6 K.

Errors which were occasionally appreciable arose due to differences between the temperatures measured by the two thermocouples inside the reactor and the one in the lead-bismuth bath. After the introduction of the reactants into the reactor, the two reactor thermocouples would record transient temperature rises from 0.1°C to 40°C depending on the conditions of the run. In a few cases, reactor heat transfer limitations would result in a steady state offset in the temperature of up to 30°C. That is, the rate at which heat was generated by the reaction was greater than the rate at which it was transferred to the bath. In these cases, the transient offset was maintained throughout the run. These situations usually occurred during high conversion runs which were discarded from the analysis. However, for all runs there was some difference between the bed and the bath temperature.

Perhaps more important though were differences between the temperatures recorded by the two bed thermocouples. If the reactor





was to be a pseudo -CSTR, then the temperature of the entire catalyst bed must be constant. Unfortunately, this was not always the case. Occasionally, for the higher conversion runs, a temperature gradient along the catalyst bed was noticed. This gradient varied from less than a degree up to four degrees. In this case, the reaction zone would not all be at the same temperature, so that the assumption of perfect mixing was not valid.

In every case, the temperature used for the analysis was the temperature measured by the mid - bed thermocouple. The measurement was accurate to  $\pm 0.5^{\circ}\text{C}$ , this measured temperature was within  $1.6^{\circ}\text{C}$  of the pellet surface temperature, and the pellet surface temperature was within  $4^{\circ}\text{C}$  of the temperature anywhere else in the catalyst bed. This means that the temperature, in the worst case, may have been in error by up to  $6.1^{\circ}\text{C}$ . At 400 K, this  $6.1^{\circ}\text{C}$  error in the temperature would result in a 67% error in the rate constant,  $k$ , according to Equation (4.9).

## E.2 Errors in the Flow Measurement

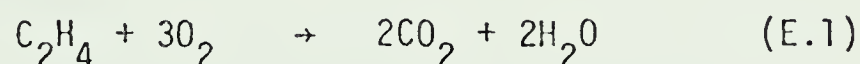
The flow meter readings were made from the strip chart recorder which continuously recorded the output of the mass flowmeters. The meters and the recorder were each zeroed every day, but only rarely was adjustment required. The low range flowmeter (0 -100 SCCM) was believed to be accurate to  $\pm 0.5$  SCCM and the high range flowmeter (0 - 5000 SCCM) was believed to be accurate to  $\pm 5$  SCCM. The measured flow rates were compared against the calibration curves in Figures B.7, B.8, and B.9 to determine the actual flow rates. The calibrations were done at laboratory conditions using a stop watch



(relative error less than 0.5%) and a bubble flowmeter (relative error less than 1%). The error in these calibrations should be less than 1%, so that the total error in the flow measurements is 1.5% for the low range and 2% for the high range meter. The flow rates were generally less than 100 SCCM for the low range and 500 SCCM for the high range meter.

### E.3 Errors in Composition

An indication of the errors in the composition analysis is provided by the percent error entry on each page of the Chromatographic Output in the data book. In Appendix F, Table F.1, the data sheet for Run M 54 (the run used for sample calculations in Appendix A) is reproduced. For most of the entries, the individual entries differ from the average value by less than 1%. The error incurred in the mass balance is of the same order. Since the reaction



is equi-molar, then the carbon balance can be calculated as was done in Section A.3 if the flow rate remains constant, i.e.,

$$E_c = \frac{(2y_{\text{CO}_2} + y_{\text{C}_2\text{H}_4})_{\text{in}} - (2y_{\text{CO}_2} + y_{\text{C}_2\text{H}_4})_{\text{out}}}{(2y_{\text{CO}_2} + y_{\text{C}_2\text{H}_4})_{\text{in}}} \times 100\% \quad (\text{E.2})$$



The apparatus was frequently leak tested at pressures up to 27 psig (about 2 times the reaction pressure) and any detected leaks were eliminated so that the flow rate was indeed constant. For Run M 54 the percentage error in the carbon balance was +1.66%. This was, if anything, a higher than usual value. Mass balance errors of less than 1% were not atypical.

There were some problems with the CO<sub>2</sub> analysis at the beginning of a run. The PoraPak column, used to separate the CO<sub>2</sub> tended to irreversibly adsorb CO<sub>2</sub> at the start of each day, causing some of the early feed analyses of CO<sub>2</sub> to have errors greater than 5%. After a dozen or so injections, the CO<sub>2</sub> peak was reproducible however. During the period between series of runs, the CO<sub>2</sub> on the packing apparently desorbed, so that a conditioning period was required each day.

Since the molar flow rate was constant, the fractional conversions were calculated from the inlet and exit mole fractions using Equations (E.3) and (E.4).

$$X_{\text{ETH}} = \frac{Y_{\text{C}_2\text{H}_4\text{in}} - Y_{\text{C}_2\text{H}_4, \text{out}}}{Y_{\text{C}_2\text{H}_4\text{in}}} \quad (\text{E.3})$$

$$X_{\text{CO}_2} = \frac{Y_{\text{CO}_2 \text{out}} - Y_{\text{CO}_2, \text{in}}}{Y_{\text{C}_2\text{H}_4, \text{in}} \times 2} \quad (\text{E.4})$$



Consider first the case in which the fractional conversion is based on ethylene depletion then, in Equation (E.3),

$$X = \frac{Y_i - Y_o}{Y_i}$$

$$dX = \left(\frac{\partial X}{\partial Y_i}\right) dY_i + \left(\frac{\partial X}{\partial Y_o}\right) dY_o$$

$$dX = \left(\frac{Y_o}{Y_i^2}\right) dY_i - \left(\frac{1}{Y_i}\right) dY_o$$

$$\frac{dX}{X} = \left(\frac{Y_o}{Y_i^2}\right) \left(\frac{Y_i}{Y_i - Y_o}\right) dY_i - \left(\frac{1}{Y_i}\right) \left(\frac{Y_i}{Y_i - Y_o}\right) dY_o$$

$$\frac{dX}{X} = \left(\frac{Y_o}{Y_i - Y_o}\right) \frac{dY_i}{Y_i} - \frac{Y_o}{Y_i - Y_o} \frac{dY_o}{Y_o}$$

$$\text{or, } \frac{dX}{X} = \frac{1-X}{X} \frac{dY_i}{Y_i} - \frac{1-X}{X} \frac{dY_o}{Y_o} \quad (\text{E.5})$$

For the maximum error, assume that the relative errors in  $Y_i$  and  $Y_o$  are additive, i.e.,

$$\frac{dY_i}{Y_i} > 0$$

$$\text{and } \frac{dY_o}{Y_o} < 0$$

If the relative error in the ethylene mole fraction in the inlet stream is the same as in the exit stream, then,





$$\left| \frac{dY_i}{Y_i} \right| = \left| \frac{dY_0}{Y_0} \right|$$

Then, converting (E.5) into finite differences,

$$\frac{\delta X}{X} = 2 \frac{(1-X)}{X} \frac{\delta Y_i}{Y_i} \quad (\text{E.6})$$

On the other hand, if the fractional conversion is based on the amount of  $\text{CO}_2$  produced, then Equation (E.4) should be used.

Substituting

$$Y_1 = Y_{\text{CO}_2, \text{ out}}$$

$$Y_2 = Y_{\text{CO}_2, \text{ in}}$$

$$Y_3 = Y_{\text{C}_2\text{H}_4, \text{ in}}$$

$$X = \frac{Y_1 - Y_2}{2 Y_3} \quad (\text{E.7})$$

$$dX = \left( \frac{\partial X}{\partial Y_1} \right) dY_1 + \left( \frac{\partial X}{\partial Y_2} \right) dY_2 + \left( \frac{\partial X}{\partial Y_3} \right) dY_3$$

$$dX = \left( \frac{1}{2Y_3} \right) dY_1 - \left( \frac{1}{2Y_3} \right) dY_2 - \left( \frac{Y_1 - Y_2}{2Y_3^2} \right) dY_3$$

$$\frac{dX}{X} = \frac{Y_1}{2Y_3} \frac{1}{X} \left( \frac{dY_1}{Y_1} \right) - \frac{Y_2}{2Y_3} \frac{1}{X} \left( \frac{dY_2}{Y_2} \right) - \left( \frac{dY_3}{Y_3} \right)$$

If the relative error in all the compositions is the same,

$$\left| \frac{dY_1}{Y_1} \right| = \left| \frac{dY_2}{Y_2} \right| = \left| \frac{dY_3}{Y_3} \right|$$



For the maximum error, set

$$dY_1 > 0$$

$$dY_2 < 0$$

$$dY_3 < 0$$

then,

$$\frac{dX}{X} = \left[ \frac{Y_1 + Y_2}{2Y_3} - \frac{1}{X} + 1 \right] \left( \frac{dY_1}{Y_1} \right) \quad (\text{E.8})$$

Substituting (E.7) into (E.8) and rearranging in finite difference form,

$$\frac{\delta X}{X} = \left[ 2 + \frac{1}{X} \frac{Y_2}{Y_3} \right] \left( \frac{\delta Y_1}{Y_1} \right) \quad (\text{E.9})$$

Equations (E.6) and (E.9) can be used to evaluate the relative error in the fractional conversion. A generous estimate of the error in the in the compositions is about 2%.

i.e.

$$\frac{\delta Y_i}{Y_i} = 0.02$$

$$\frac{\delta Y_i}{Y_i} = \frac{\delta Y_{\text{CO}_2, \text{ in}}}{Y_{\text{CO}_2, \text{ in}}} = 0.02$$

For most runs,

$$\frac{Y_2}{Y_3} = \frac{Y_{\text{CO}_2, \text{ in}}}{Y_{\text{C}_2\text{H}_4, \text{ in}}} \sim \frac{0.03}{1.00} = 0.03$$

Table E.1 shows the results of substituting these values into Equations (E.6) and (E.9)



TABLE E.1  
RELATIVE ERRORS IN THE FRACTIONAL CONVERSION

Fractional Conversion		Relative Error in Fractional Conversion	
X	$\frac{\delta X}{X}$		
	Based on C <sub>2</sub> H <sub>4</sub>	Based on CO <sub>2</sub>	
1.00	0.00	0.040	
0.75	0.013	0.040	
0.50	0.04	0.041	
0.20	0.16	0.043	
0.10	0.36	0.046	
0.05	0.76	0.052	
0.01	3.96	0.10	
0.005	7.96	0.16	

Table E.1 is the justification for the decision to base the fractional conversions, and hence the rates on the CO<sub>2</sub> value for conversions less than 10%. At a conversion level of 10%, the relative error in the ethylene based conversion is 36% while it is only 4.6% for the CO<sub>2</sub> based conversion. Since the calculations here were for the maximum errors, the error in the reported fractional conversion should not exceed 10%.

A systematic, rather than random error could influence the measurements if the G.C. calibrations were in error. An error in the individual fractional conversions would not be apparent since



the fractional conversions are independent of the calibration.

$$X_E = \frac{RF_E A_{E,in} - RF_E A_{E,out}}{RF_E A_{E,in}}$$

$$\text{OR } X_E = \frac{A_{E,in} - A_{E,out}}{A_{E,out}}$$

where

$A_E$  = peak area of the ethylene peaks

$RF_E$  = response factor of ethylene evaluated from  
the calibration (See Appendix C)

Since the mole fractions were calculated on a normalized basis though, an error in the calibration would result in different values for the fractional conversions. Were there a sizeable error in the response factors, a systematic error in the carbon balance would be noticed. Since the carbon balance was in error both positively and negatively, with no discernable bias, the calibrations are not significantly in error.

#### E.4 Errors in Catalyst Weight and Reactor Pressure

The catalyst samples were weighed on a calibrated balance. The error in the measurements was  $\pm 0.005$  g so that the relative error in these measurements was 0.5%. The reactor pressure was measured with a Bourdon gauge. The uncertainty in the pressure measurements was  $\pm 0.3$  psi or 1.5%. Accurate pressure measurement was not required for this work. The runs were all done at same pressure, and the curve fitting algebra eliminated the pressure from the calculations.





### E.5 Effect of Measurement Errors on Calculated Rates

The measured rates in the recycle reactor were calculated using Equation (A.1)

$$-r_E = \frac{F_{E,in} X_1}{W} \quad (E.10)$$

The relative error in the rate is given by the expression

$$\frac{dr}{r} = \frac{dF_E}{F_E} + \frac{dX}{X} - \frac{dW}{W}$$

or

$$\frac{dr}{r} = \frac{dF_T}{F_T} + \frac{dY_E}{Y_E} + \frac{dX}{X} - \frac{dW}{W} \quad -(E.11)$$

For the maximum error, assume all errors are additive. Then, using the uncertainties estimated for 10% conversion run from Table E.1,

$$\frac{\delta r}{r} = 2\% + 2\% + 4.6\% + 0.5\%$$

$$\frac{\delta r}{r} = 9.1\%$$

The error in the rates attributable to uncertainties in the measurements should be less than 10%. As will be shown in the following section, the reproducibility of the rate measurements must have been affected by variables other than those used to calculate the rate.



In Chapter 4, the measured rates, determined from Equation (E.10) were compared with a rate equation, Equation (4.6).

$$-r = \frac{k[O_2]}{[C_2H_4]} \quad (E.12)$$

The rate constant,  $k$ , was determined for a variety of temperatures.

$$k = \frac{(-r)[C_2H_4]}{[O_2]}$$

The relative error in the calculated rate constants can be estimated from the error in the rates.

$$\frac{dk}{k} = \frac{dr}{r} + \frac{d[C_2H_4]}{[C_2H_4]} - \frac{d[O_2]}{[O_2]} \quad (E.13)$$

The total concentrations were calculated from Equation (A.8).

$$C_i = \frac{P_T Y_{i,out}}{R_T} \quad (E.14)$$

$$\text{So } \frac{dC_i}{C_i} = \frac{dP_T}{P_T} + \frac{dY_i}{Y_i} - \frac{dR}{R} - \frac{dT}{T} \quad \text{---(E.14)}$$

Substituting into (E.13) for  $i = C_2H_4, O_2$ ; and assuming that all errors are additive,

$$\frac{\delta k}{k} = \frac{\delta r}{r} + \frac{\delta Y_{C_2H_4}}{Y_{C_2H_4}} + \frac{\delta Y_{O_2}}{Y_{O_2}}$$

$$\frac{\delta k}{k} = 9.1\% + 2\% + 2\% = 13.1\%$$



Since this was a worst case analysis, the relative uncertainty in the rate constants should be less than 15%.

### E.6 Reproducibility of the Data

One of the tests applied to experimental data involves a demonstration that the results can be duplicated. The reproducibility of experimental data is often regarded as the factor of paramount importance in judging its significance. In some cases however, the very fact that the data are irreproducible is in itself significant. In the previous sections in this Appendix, the errors which could be expected to appear in the rates and rate constants as a result of errors in the measured variables were estimated. In this work, the rates were both well below and well above the estimated errors.

In Table E.2, the results of a number of runs from the DRR are tabulated. These runs illustrate the reproducibility and the irreproducibility of the kinetic data. The first four pairs, (K04, K12), (K15, K23), (L37, L39), and (M23, M33) exhibit good reproducibility. The inlet and exit conditions are comparable, and the rates are within the estimated error bounds. The slight variation in the rates of the pairs is likely due to the slight differences in the total flow rates,  $F_T$ . The next set, (L08, L11, L17) and (M22, M32, M36) show that for some runs, there is both good reproducibility and irreproducibility in activity. The increase in activity was usually linked with an unstable or high conversion run. For example, Run L10 was a complete conversion run, and the rate for Run L11 was in (L08, L11, L17) triplet is more than one and a half



TABLE E.2  
REPRODUCIBILITY OF REPEATED RUNS - DRR

Run	Temp (K)	F <sub>T</sub> (sccm)	Feed Composition (mole %)		Product Composition (mole %)		Rate $\times 10^8$ (mol/g-s)
			C <sub>2</sub> H <sub>4</sub>	O <sub>2</sub>	C <sub>2</sub> H <sub>4</sub>	O <sub>2</sub>	
K04	361	588	0.776	17.3	0.753	17.3	1.2
K12	361	600	0.763	17.3	0.754	17.3	1.0
K15	388	593	0.801	17.1	0.765	17.0	5.0
K23	388	591	0.810	17.1	0.768	17.0	5.2
L37	400	555	0.594	18.6	0.461	18.2	11.4
L39	400	563	0.604	18.5	0.467	18.2	11.6
M23	438	534	2.212	2.242	2.108	1.871	8.5
M33	438	553	2.176	2.207	2.039	1.808	9.4
L08	388	561	0.653	17.9	0.621	17.9	2.6
L11	388	580	0.701	17.9	0.664	17.9	4.1
L17	388	565	0.691	17.9	0.662	17.9	2.5
M22	438	561	2.116	2.908	1.981	2.493	12.0
M33	438	562	2.163	3.065	2.024	2.563	15.5
M36	438	562	2.172	3.306	1.850	2.512	28.0
M11	438	581	1.158	3.123	0.945	2.490	20.5
M31	438	561	1.128	3.123	0.731	2.027	36.1
M13	438	556	1.232	2.179	1.103	1.871	10.7
M14	438	545	1.209	2.086	2.086	1.033	13.6
M16	438	518	1.278	0.794	1.257	0.686	2.3
M17	438	519	1.274	0.838	1.222	0.654	3.8
M39	455	527	2.413	1.519	2.299	1.125	11.3
M41	455	555	2.391	1.535	2.198	1.129	17.1





times larger than the rates in Runs L08 or L17. The final series, (M11, M31), (M13, M14), (M16, M17), and (M39, M41), the results are simply not comparable. As was the case in the previous series, the higher conversion run usually followed a high conversion run or a complete conversion run. As well, the reactor and the catalyst was occasionally left at a high temperature over a weekend, and the first runs following this exposure to a long period at elevated temperatures sometimes resulted in runs with slightly higher rates than would normally be expected.

In Chapter 4, the measured rates were plotted against the ratio of the oxygen to ethylene concentrations in the exit streams. By examining runs (M17, M34), (M30, M32) and (M14, M21), in Table D2, it is clear that the ratio of concentrations is a reasonable variable to use for the fitting. In those three pairs, the inlet and exit concentrations vary considerably, but the concentration ratios in the exit stream are similar. In each case the calculated rate is within the predicted uncertainties.

The integral bed reactor results suffered from the same irreproducibilities as well. Often similar inlet conditions would result in dissimilar exit conversions. Two examples taken from Table D7 (F19, F30) and (F18, F32) are located in Table E.3.

In these two cases, the differences between the two runs at similar inlet conditions is much larger than would be predicted from the error analysis. In other cases though, the reproducibility was very good, but the marked irreproducibility of some of the data presented a considerable problem. The irreproducibility was usually due to a change in the catalyst activity rather than any random or systematic errors in the analysis or experimental



TABLE E.3

## IRREPRODUCIBILITY OF REPEATED RUNS - IBR

Run	Temp (K)	Inlet Concentrations (mole %)		Fractional Conversions (%)
		C <sub>2</sub> H <sub>4</sub>	O <sub>2</sub>	
F18	380	0.426	8.35	100.00
F32	380	0.422	8.35	45.41
F19	380	0.517	8.35	100.00
F30	380	0.572	8.35	24.90

technique. Runs F15 to F19 were characterized by instabilities and high conversions. A comparison of the catalyst activity before these instabilities, Runs F11 to F15 and after the instabilities, Runs F20 to F34, (see Table D7) is pictured in Figure E.1. The runs were all at 380K and excess oxygen (8.35 mol/m<sup>3</sup>). Except for Run F22, all of the runs after the instabilities have conversions higher than corresponding runs before the instabilities. This instability in the catalyst activity was primarily responsible for the irreproducibility of both the DRR and IBR runs. Many of the runs listed in the Data book were excluded from the DRR analyses (both kinetic and dispersion runs) for this reason. All of the IBR runs undertaken are listed in both the Data book and Table D7, and all of the IBR runs were used to evaluate the three reactor models.



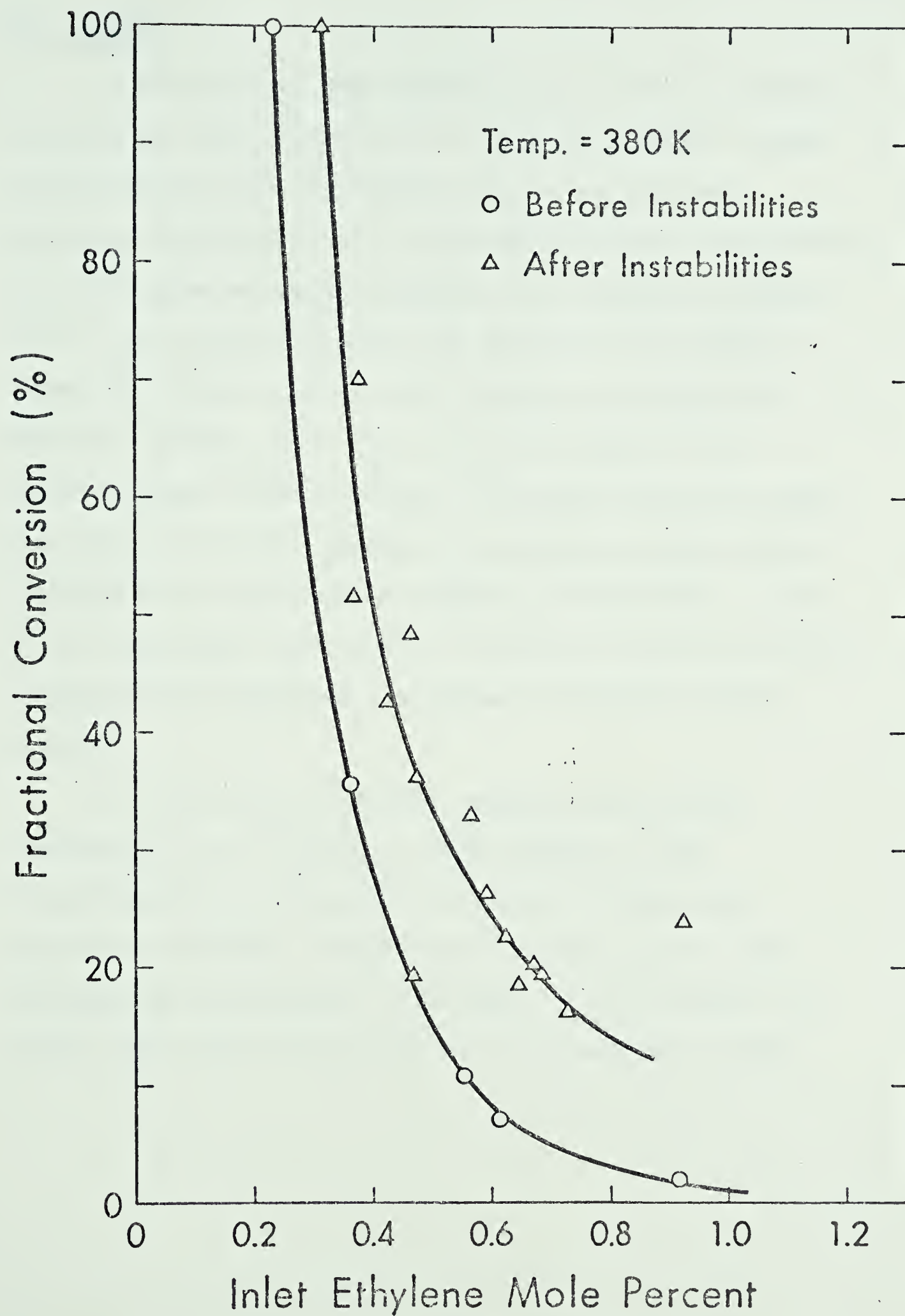


Figure E.1 : Effect of instabilities on ethylene conversion in subsequent runs.





### E.7 Summary

In this Appendix, the uncertainties in the measured variables affecting the rate calculation for the DRR were estimated. Based on these calculations, the relative error in the fractional conversion should be 4.6% if the conversion is based on CO<sub>2</sub> formation, and 36% if based on ethylene depletion for a fractional conversion of 0.10. For conversions below 0.10, the error in the ethylene conversion increases rapidly, while the error in the CO<sub>2</sub> based conversion increases more slowly. For this reason, if the conversions were less than 10%, the CO<sub>2</sub> based conversion was used. From this, the error in the DRR ratio should be less than 10% and the error in the rate constants should be less than 15%. As well, at high conversions, heat transfer limitations, which are difficult to quantify, may also affect the accuracy of the rates and rate constants.

In both the DRR and the IBR, repeated runs exhibited irreproducibilities in excess of these estimates. These irreproducibilities could usually be linked to previous high temperature conditions. Changes in the catalyst activity often influenced the uncertainties in the rates and rate constants to a greater extent than did uncertainties in the measured variables.





APPENDIX FEXAMPLES FROM DATA BOOK

The computer programs used to model the integral bed reactor, analyse the kinetic data, and calculate fractional conversions, along with the outputs are too lengthy to include in this volume. Instead, they are contained in a separate Data Book. The Data Book is available from the Department of Chemical Engineering, The University of Alberta, upon request. In this Appendix, the Table of Contents from the Data Book, and a reproduction of the output from Run M 54, the run used for sample calculations in Appendix A are presented.



TABLE OF CONTENTS  
\*\*\*\*\*

PROGRAM BSOLVE	NON-LINEAR, MULTI-VARIABLE REGRESSION ANALYSIS
PROGRAM IBED	RUNGE-KUTTA INTEGRATION HOMOGENOUS REACTOR MODEL
PROGRAM IBEDHTL	RUNGE-KUTTA INTEGRATION REACTOR MODEL WITH HEAT TRANSFER LIMITATIONS
PROGRAM ROOTS	NEWTON'S ROOT FINDING ISOTHERMAL REACTOR MODEL
PROGRAM KARIN	ANALYSIS OF CHROMATOGRAPHIC DATA
CHROMATOGRAPHIC DATA	ANALYSIS OF ALL CHROMATOGRAPHIC DATA FROM SERIES A TO SERIES W



RUN M 54

## DIFFERENTIAL RECYCLE REACTOR

TEMP =	472.0	K	CATALYST CHARGE
PRESS =	144.789	KPA	4.73 GRAMS
FLOWA =	500.0	SCCM	ENGELHARD 0.3 PCT PT.
FLOWE =	108.0	SCCM	

## FEED COMPOSITIONS

AIR	CO2	ETHENE	N2	O2
98.2000	0.0000	1.7890	0.9641	0.0359
98.2400	0.0000	1.7650	0.9640	0.0360
98.2400	0.0000	1.7620	0.9639	0.0361
98.2200	0.0000	1.7790	0.9644	0.0355

AVERAGES	-----	(MOLE PERCENT)		
98.2249	0.0000	1.7737	94.6987	3.5275

## PRODUCT COMPOSITIONS

AIR	CO2	ETHENE	N2	O2
97.3900	1.7360	0.8760	0.9894	0.0106
97.3900	1.7260	0.8840	0.9884	0.0115
97.3800	1.7290	0.8841	0.9883	0.0117
97.3900	1.7250	0.8870	0.9886	0.0113
97.3900	1.7270	0.8872	0.9885	0.0114
97.4200	1.7070	0.8780	0.9885	0.0114
97.4000	1.7130	0.8818		

AVERAGES	-----	(MOLE PERCENT)		
97.3942	1.7232	0.8825	96.2855	1.1070

## FRACTIONAL CONVERSIONS

-----

## MASS BALANCE

-----  
PERCENT ERROR (G-ATOM BASIS)

ETHENE	0.5024		
CO2	0.4857	CARBON	1.66

## RATES OF REACTION

-----

ETHENE DEPLETION	0.8517E-06 MOL/G-CAT/S
CO2 PRODUCTION	0.8235E-06 MOL/G-CAT/S

EXIT ETHENE CONCENTRATION =	0.3255 MOL/CU. M
EXIT OXYGEN CONCENTRATION =	0.4083 MOL/CU. M
TOTAL MOLAR CONCENTRATION =	36.8845 MOL/CU. M

-----













**B30193**